Development and Application of Heterogeneous Catalysts for Direct Cracking of Triglycerides for Biodiesel Production

ETERIGHO, ELIZABETH JUMOKE

A thesis submitted for the degree of Doctor of Philosophy (PhD) at Newcastle University

School of Chemical Engineering and Advanced Materials, Newcastle University

Abstract

Interest in biodiesel has been growing due to its potential role in moderating global climate change by lowering net CO_2 emissions from fuels used for transportation. Most biodiesel fuels are currently synthesized by transesterification using alkaline catalysts and methanol. Heterogeneous transesterification catalysts have begun to be considered as alternatives, but many drawbacks remain. The costs of production and environmental concerns resulting from the ester washing step: neutralization of residual catalyst, removal of soap, glycerol, methanol and absorbent in some cases have prompted the search for more environmentally friendly processes and solid catalysts. Therefore, it is desirable to replace homogeneous or heterogeneous transesterification with the use of heterogeneous catalysts in direct thermocatalytic cracking. In principle, this could reduce the cost of biodiesel production, as it removes the need for alcohol and numerous downstream processing steps which add to the substantial running costs of transesterification. In addition the problem of glycerol in the product is eliminated.

Four sulphated zirconia catalysts were synthesized via conventional wet-precipitation and solvent-free methods with different molar ratios of the sulphating agent. Their activity for direct thermocatalytic cracking of rapeseed oil was evaluated at a temperature of 270^{o}C and atmospheric pressure. The nature and concentration of the active Brønsted and Lewis acid sites on the catalysts were examined. Brønsted acid sites were found to be important in the catalytic reaction. The catalysts at this temperature exhibited different selectivities towards formation of saturated and unsaturated methyl esters. The solvent-free catalysts were more active with a conversion of 78% in $2^{1}/_{2}$ hours, while the wet-precipitated catalysts had a maximum of 66% conversion after two hours. The catalysts prepared by the solvent-free method had 59% yield for methyl ester, with 75% of these being unsaturated. The wet-precipitated catalysts exhibited a lower yield for methyl esters (maximum: 32%), but within this a greater proportion (68%) were saturated. After regeneration, the solvent-free catalysts regained their catalytic properties, whereas the conventional catalysts did not. Three of the catalysts exhibited substantial leaching, with one of the conventional catalysts losing 100% of the sulphate responsible for its activity. Thus, to improve their properties the catalysts were supported with meta-kaolin which resulted in higher Brønsted acidity and better stability.

Dedication

This Ph.D. dissertation work is dedicated to my late parents for their love, encouragement, support, prayers and most importantly my mother for dreaming this for me long before I could. Any achievement in my life is a direct result of her sacrifices and a testimony to her excellent parenting. Maami Mary Sherifat Anike (nee Ajiga) and Chief Baale Jethro Ogayemi sun re o.

Acknowledgments

First and foremost, I would like to express my sincere thanks and appreciation to God Almighty for giving me the strength and dedication to achieve and complete this degree programme. Special thanks to my phenomenal supervisor Prof. Adam P. Harvey for his advice and guidance, continued support, tremendous help, encouragements, and insight and sharp criticism. Despite his busy schedule, he would always find the time to discuss anything on experimental results. His questions and mentorship inspired the series of experiments described in this dissertation. Sincerely I have learnt lots of things from his way of thinking and his research methodology. I can honestly say that this Ph.D. dissertation would not have been accomplished without his outstanding supervision, scientific knowledge and experience.

I would like to thank Prof. Allen Wright for his permission for the use of his laboratory facilities and Julie parker for the training on the use of the facilities.

Special thanks also go to Dr Karen Wilson and her group members at the Department of Chemistry, University of Cardiff for performing the X-ray photoelectron spectroscopy and the pyridine adsorption analyses.

I would like to thank all the members of the Process Intensification (PI) group who directly or indirectly provided invaluable discussion and comments during our meetings.

I like to acknowledge all my colleagues both in the office (C500, SCEAM Newcastle University, UK) and 2008 Ph.D. PTDF scholars.

Furthermore, I wish to extend my warm thanks to Rob Dixon and Paul Sterling, and all the staff in the general workshop and the school general office, for their help and support during my research period. You all made my stay in Newcastle a home away from home.

I would also like to express many thanks to the following people: Danai Poulidi and Alan Thursfield for their help on the BET equipment, Pauline Carrick for doing the

SEM morphological images, digital mappings and the elemental analysis, Maggie White for her readiness in performing the X-ray diffractogram.

I wish to acknowledge the URCCIP for the travel grants for attendance at conferences. The IChemE for the award and prize of second best post graduate presenter at the 2010 conference on 'catalyst preparation 4 the 21st century'.

I am deeply indebted to my husband, my children, my maternal siblings and my friends for their love, patience, care, and sacrifice during my study. Thank you so much for continuous assistance.

I am also grateful to the Nigerian government for their financial support through the Petroleum Trust Development Fund (PTDF) during my study.

Finally and humbly, I would like to express my sincere thanks and appreciation to all members of Life Transformation Church, Newcastle particularly; Pastor (Dr) and Pastor (Mrs) Julius Fashanu words are inadequate to express my truthful and profound thanks.

THANK YOU ALL

Table of Contents

List of Figures

List of Tables

Nomenclature and Abbreviations

BET	Brunauer Emmett Taylor
CM	conventional method
DG	diglycerides
(ε_R)	random error
ε_S	systematic error
ESEM	environmental scanning electron microscopy
FAME	fatty acid methyl ester
FFA	free fatty acid
FTIR	Fourier Transform Infrared Spectroscopy
FWHM	full width half measurement
GC	gas chromatography
GCMS	gas chromatography and mass spectroscopy
ICDD	lnternational Centre of Diffraction Data
IEA	International Energy Agency
IR	infrared
IS	internal standard
MG	monoglycerides
MSTFA	N-methyl-N-trimethylsilylfluoroacetamide
RTFO	Renewable Transport Fuels Obligation
SFM	solvent-free method
TG	triglyceride
TGA	thermogravimetric analysis
USDA	U.S. Department of Agriculture
VGO	Vacuum gas oil
XPS	x-ray photo spectroscopy
XRD	x-ray diffraction

Chapter 1: Introduction

1 Introduction

Fossil fuels are the primary source of energy worldwide with global demand presently standing at about 12 million tonnes per day (84 million barrels oil equivalent a day) Pickett *et al*. (2008). Petroleum fuels have been a key factor in the growth of industry, transportation, the agricultural sector and many other areas serving basic human needs. The World's energy is mainly supplied by fossil fuels estimated at about 35.3% of the total in 2008 (see
Figure 1.1).

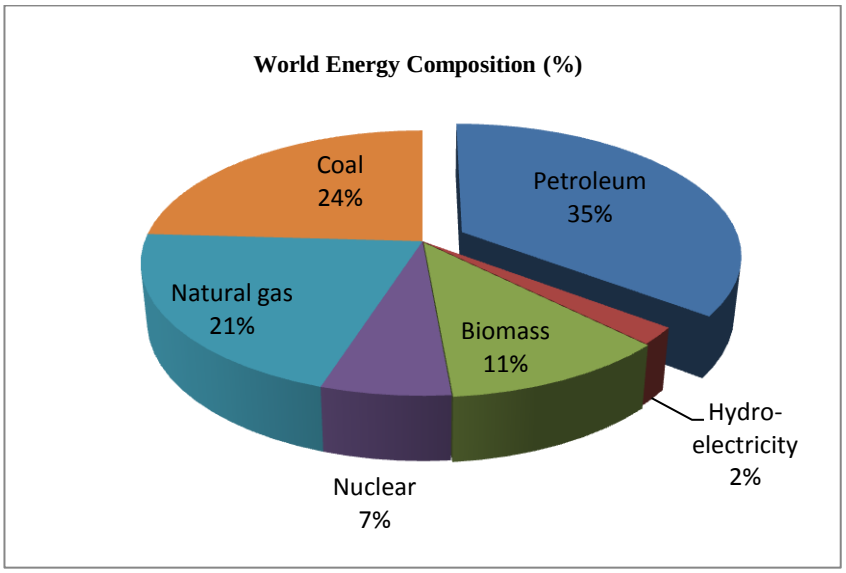

Figure 1.1: World Energy Matrix in Percentage (IEA, 2008)

Present projections suggest an increased demand to 16 million tonnes per day (116 million barrels a day) by 2030. However, a global peak in oil production before 2035 has been predicted. Currently 30% of global oil consumption is used for transport, but a report by the International Energy Agency (IEA, 2007) indicates that 60% of the rise in demand expected by 2030 will be mainly for transportation (Figure 1.2 below). With the expansion of the transport sector in most developed countries, as well as the industrialisation of emerging economies such as China and India, these figures may be an underestimate.

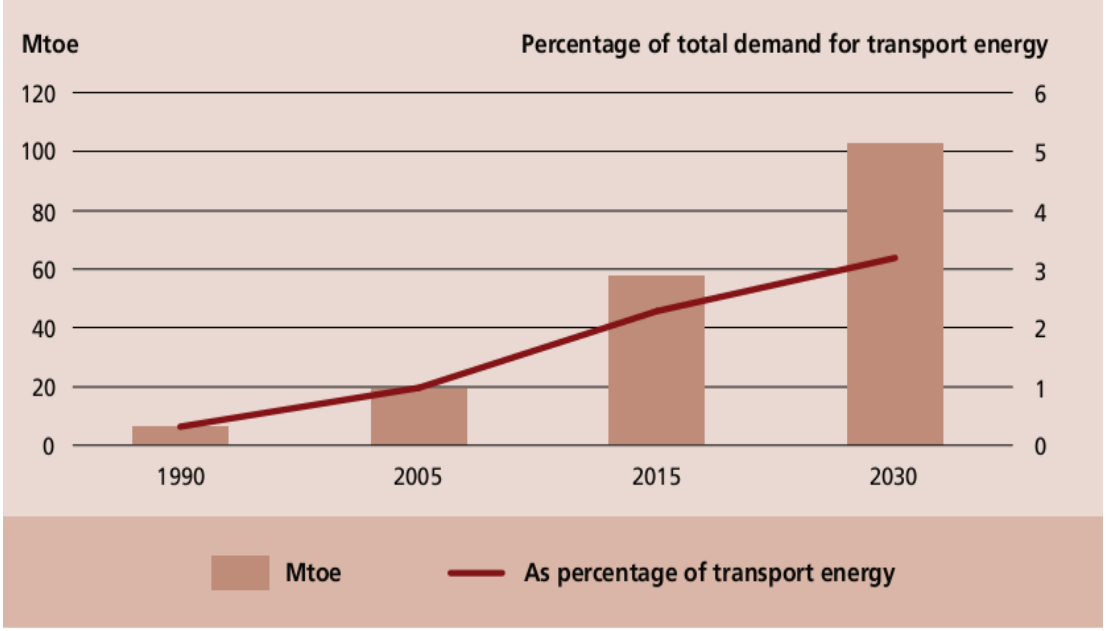

Figure 1.2: Trends in Consumption of Transport fuel Worldwide

As sources of fossil fuel are finite, coupled with growing problems of environmental pollution problems owing to their use, there is a need for alternative sources that are technically feasible, economically competitive, environmentally acceptable, and readily available in order to meet the rising demand. Several alternatives are currently being explored, amongst which crop-based fuels (biofuels) such as biodiesel and bioethanol have emerged as promising alternatives to the use of gasoline and conventional diesel in transportation. This study focuses on the advantages of biodiesel over other biofuels and survey various production processes, with emphasis on economic viability

1.1 Background

Biodiesel is a mixture of mono-alkyl esters of fatty acids derived from vegetable oils or animal fats which conforms to the ASTM D6751 requirements (see Table 1.1). It is the product of the reaction of vegetable oils or animal fats and an alcohol in the presence of an alkali catalyst, with glycerol as a co-product. Biodiesel is biodegradable, has a lower life cycle emission profile than petro-fuels and is non-toxic (Taufiqurrahmi and Bhatia, 2011)

.

Table 1.1: American Society for Testing and Materials (ASTM) Standards of Diesel and Biodiesel Properties (Kiss *et al*., 2008)

Property	Diesel	Biodiesel
Standard	ASTM D975	ASTM D6751
Composition	HC[a] (C_{10}-C_{21})	FAME[b] (C_{12}-C_{22})
Kinematic viscosity (mm2/s) at 40^{o}C	1.9-4.1	1.9 – 6.0
Boiling point(^{o}C)	188 - 343	182 - 338
Carbon weight (wt %)	87	77
Pour point (^{o}C)	-35 to -15	-15 to 16
Flash point (^{o}C)	60 - 80	100 - 170
Hydrogen (wt %)	13	12
Water (vol %)	0.05	0.05
Sulphur (wt %)	0.05	0.05
Cloud point (^{o}C)	-15 to 5	-3 to 12
Oxygen (wt %)	0	11
Stoichiometric air/fuel ratio (AFR)	15	13.8
(HFRR), High frequency reciprocating Rig (μm)	685	314
Ball-on-Cylinder Lubricity Evaluator (g) (BOCLE),	3600	>7000
Life-cycle energy balance (energy units produced per unit energy consumed)	0.83/1	3.2/1
Ignition quality (cetane no)	40 - 55	48 - 60

[a] *Hydrocarbon,* [b] *Fatty Acid Methyl Esters*

Biodiesel has similar physical properties to petro-diesel, for instance, with canola oil. Biodiesel has attracted tremendous attention in recent years due to its environmental and technological advantages. Its technical advantages over petroleum-based fuels include: 1) a higher cetane number and flash point, which results in better and safer performance; 2) higher lubricity, which prolongs engine life; and 3) the presence of oxygen (~10%), which improves combustion and reduces carbon monoxide and greenhouse gas emissions. It also has various additional societal benefits, for instance, rural revitalization, the creation of new jobs, and less risk of contributing to global warming. Given the energy crisis during an era of growing energy consumption,

combined with an increase in greenhouse gas (i.e. CO_2) concentrations from burning petroleum-based fuels, alternative fuels are being increasingly researched. Generally, biodiesel derived from crops, including sugar, starch and oil (edible feedstocks), using conventional technologies is referred to as first generation biofuels, the most common examples being biodiesel and bioethanol. Biodiesel produced from non-edible feedstocks, including algae, waste vegetable oils and fats, non-food crops and biomass sources are regarded as second generation biofuels as shown in Figure 1.3 (Luque *et al*., 2010, Dupont *et al*., 2009). They are developing partly in an attempt to overcome the major shortcomings of the first generation biofuels feedstock. These include: competition between food security and energy and they are less costly to procure.

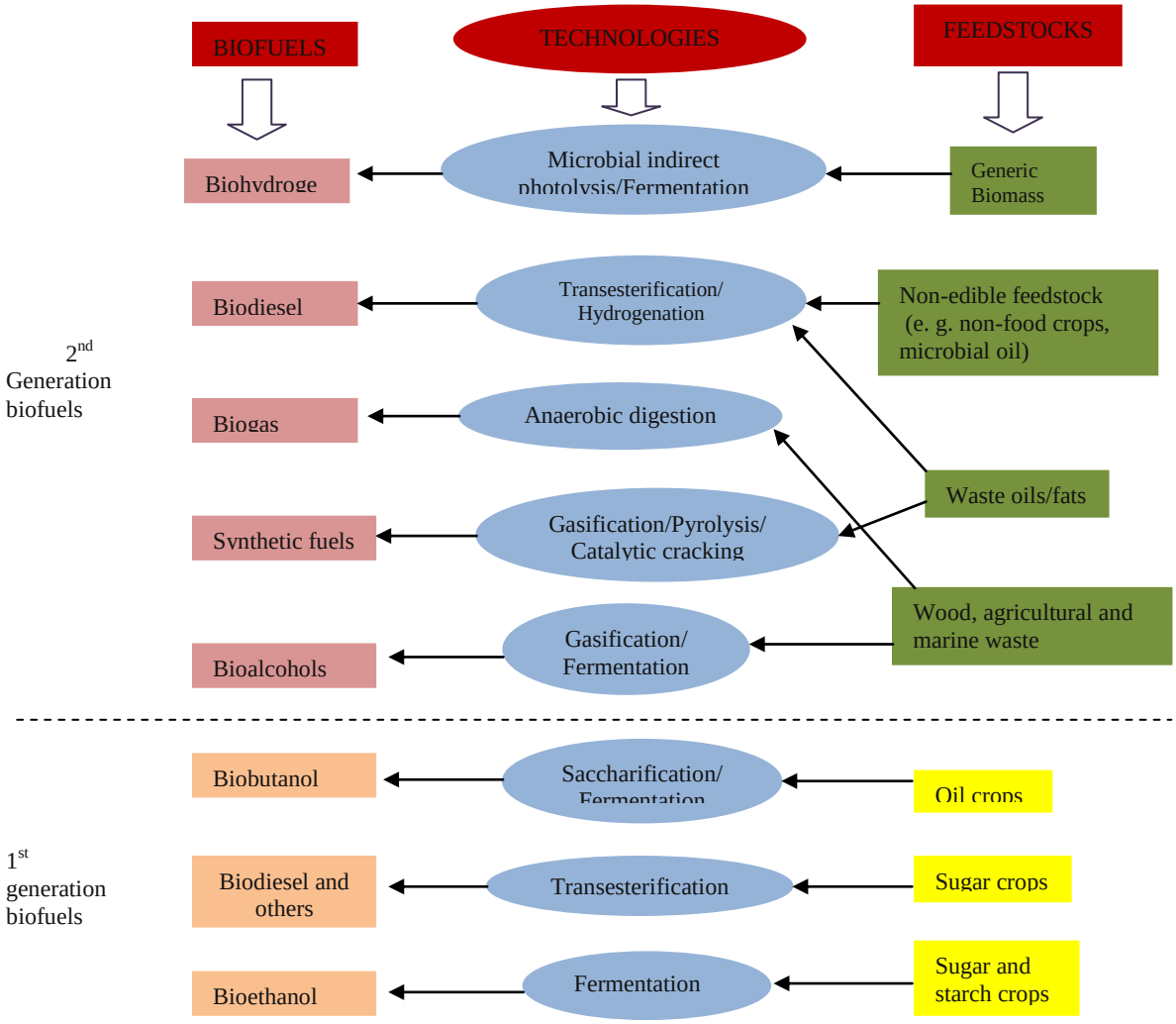

Figure 1.3: The Biofuels Production from Different Feedstocks and Technologies (Luque *et al*., 2010)

Biodiesel combustion in engines results in a "closed carbon cycle", since the amount of CO_2 emitted is equivalent to that the plant absorbed during its vegetative phase (Puppan, 2002). Concern in society about the impact of greenhouse gases (GHG) led to the development of the United Nations Framework Convention on Climate Change (1992), which later resulted in the 1997 Kyoto Protocol to tackle the problem of greenhouse gases. In 2002 the European Union ratified the Kyoto Protocol, and the emphasis shifted to scientific innovation as a means of countering greenhouse gases emissions; however this is yet to be realised. Transportation has contributed immensely to GHG emissions over the last ten years accounting for 20% of global CO_2 emissions, and 25% of UK emissions, with a predicted increase of about 80% in higher energy usage and carbon emissions by 2030 (Rogner *et al*., 2007). A major aim behind biodiesel production is to help mitigate climate change and to reduce the levels of CO, SO_x, NO_x and particulate matter being emitted into the atmosphere. Over the past few years many governments have put in place policies to support the switch from a petrol-based to a bio-based industry, so that in general a more secure energy supply can be guaranteed (Demirbas and Balat, 2006). The United States and several European Union (EU) member states already have biofuel policies (Puppan, 2002). The United Kingdom (UK) government initially set a target of 5% biofuel by volume of total road transport fuel sales by 2010 (Smith *et al*., 2009) which has now been revised to 10% by 2020 as shown in Figure 1.4.

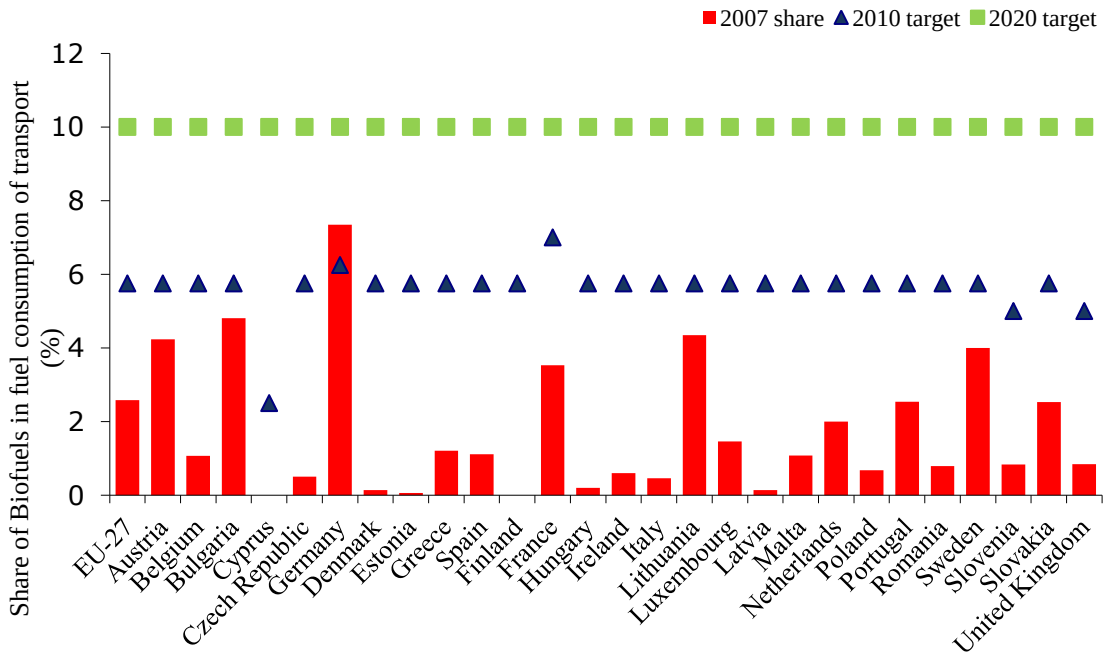

Figure 1.4: Targets for Biofuel Consumption in Transportation (%) in 2007, 2010 and 2020 (Source: http://www.eea.europa.eu/data-and-maps/figures/)

In 2005, biodiesel was the leading biofuel used in the EU, representing 81.5% of a total of 3,184Mte produced. Among the EU member states, Germany had the highest proportion of production of 52.4% (Zinoviev *et al*., 2007). Presently, biodiesel production can be found in over 28 counties, of which Germany and France are the world largest producers; however some countries are yet to meet their 2010 targets for reasons such as inadequate production processes, government policy, or feedstock availability.

Traditionally, biodiesel is produced from a chemical reaction called transesterification. The most used feedstocks are virgin vegetable oils such as soybean oil, rapeseed oil, palm oil and linseed (Srivastava and Prasad, 2000). Non-edible oils waste vegetable oil and waste animal fat can be used, but the feedstock would need to undergo a pre-treatment esterification before it could be used successfully in transesterification. This is due to their high free fatty acid (FFA) levels, which result in the formation of soap instead of the desired biodiesel in transesterification. Various drawbacks have contributed to high production costs, and so other approaches have been investigated such as the use of acid catalysts in transesterification (Lotero *et al*., 2005). Though these methods have been found to be useful for feedstocks with high level of free fatty acid, the rates of conversion are very slow and higher reaction temperatures and methanol to oil molar ratios are required. Enzymes as catalysts have been shown to exhibit good tolerance for free fatty acid, but they are expensive and unable to provide the degree of reaction completion required to meet the ASTM fuel specifications. This is because of the inhibitory effect of alcohols like methanol (Ranganathan *et al*., 2008). However, research dealing with the use of immobilize enzymes is presently in focus (Tan *et al*., 2010). Despite the problems encountered, the consumption of biodiesel has increased exponentially in the last few years, as reported by Luque *et al*. (2010) (see Figure 1.5).

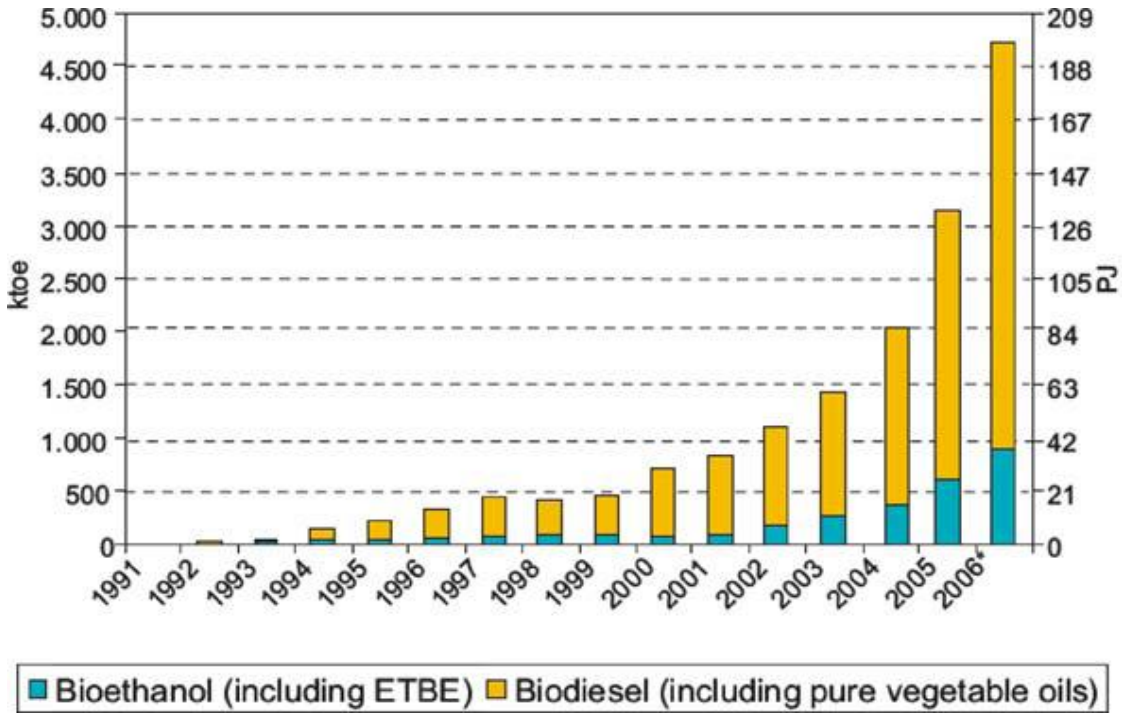

Figure 1.5: Biofuels Consumption in the EU27 (Source: Luque *et al.*, 2010)

The research frontier in the biodiesel field has now shifted from a situation where selling the product was the primary challenge. The present need is to identify suitable and appropriate catalysts that could facilitate the highly selective conversion of economically viable feedstocks into desired products in the existing infrastructure. This is the main concern of bio-based fuels: to solve ever-growing global energy concerns (Chew and Bhatia, 2008).

1.2 Vegetable Oils as fuel

Vegetable oils, also known as triglycerides comprise of 98% triglycerides and small amounts of mono- and di-glycerides. Triglycerides are esters made up of three molecules of fatty acids and one of glycerol and contain substantial amounts of oxygen. The fatty acids in triglycerides vary in their carbon chain length and in the number of double bonds.(Taufiqurrahmi and Bhatia, 2011; Barnwal and Sharma, 2005). Triglycerides are suitable for use as fuel because of their molecular structure (Figure 1.6), containing sustainable carbon with high energy that can be converted into fuels (see Table 1.2) (Ma and Hanna, 1999; Ali and Hanna, 1994).

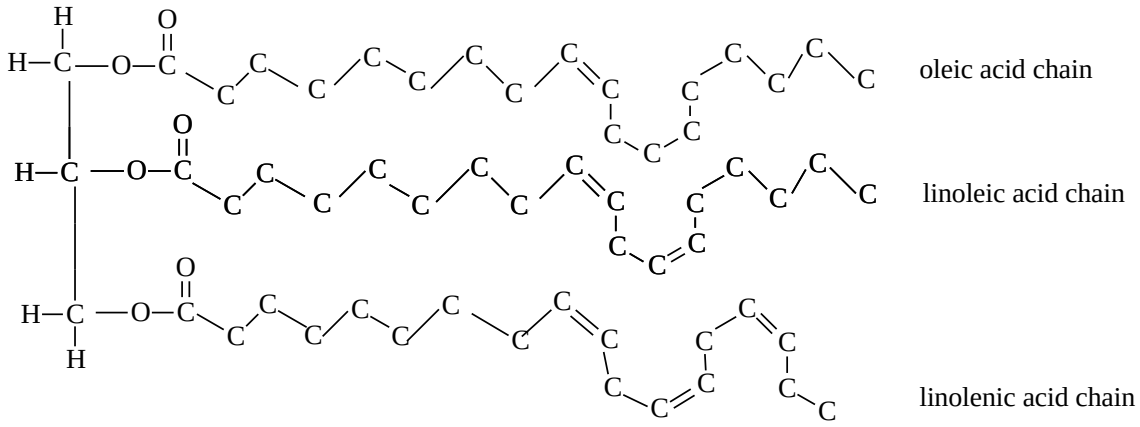

Figure 1.6: Molecular Structure of Vegetable Oil (e.g. Rapeseed Oil). (Dupain *et al*., 2007)

The use of vegetable oils as alternative fuels began over a hundred years ago when Rudolph Diesel first tested peanut oil in his compression ignition engine. He concluded that: "The use of vegetable oils for engine fuels may seem insignificant today. But such oils may in the course of time be as important as petroleum and the coal tar products of the present time" (Meher *et al*., 2006).

Table 1.2: Physical and thermal properties of some vegetable oil (Dutta, 2007)

Vegetable oil	Kinematic viscosity (40°C)	Cetane no	Heating value (MJ/kg)	Cloud point (°C)	Pour point (°C)	Flash point (°C)	Density (Kg/l)	Carbon residue (wt %)	Sulphur (wt %)
Corn	34.9	37.6	39.5	-1.1	-40.0	277	0.9095	0.24	0.01
Cotton seed	33.5	41.7	39.5	1.7	-15.0	234	0.9148	0.24	0.01
Cramble	53.6	44.6	40.5	10.0	-12.2	274	0.9044	0.23	0.01
Linseed	22.2	34.6	39.3	1.7	-15.0	241	0.9236	0.22	0.01
Peanut	39.6	41.8	49.8	12.8	-6.7	271	0.9026	0.24	0.01
Rapeseed	37.0	37.6	39.7	-3.9	-31.7	246	0.9115	0.30	0.01
Salflower	31.3	41.3	39.5	18.3	-6.7	260	0.9144	0.25	0.01
Sesame	35.5	40.2	39.3	-3.9	-9.4	260	0.9133	0.25	0.01
Soyabean	32.6	37.9	39.6	-3.9	-12.2	254	0.9138	0.27	0.01
Sunflower	33.9	37.1	39.6	7.2	-15.0	274	0.9161	0.23	0.01
Palm	39.6	42.0	-	31.0	-	267	0.9180	-	-
Bahussa	30.3	38.0	-	20.0	-	150	0.9460	-	-
Tallow	-	-	40.0	-	-	201	-	6.21	-

However there are many problems associated with the direct use of vegetable oil in diesel engines, especially direct injection engines, including: carbon deposition, lubrication difficulties and piston ring sticking (Knothe *et al*., 2005). Other disadvantages are a high viscosity of 35–60 cSt at 40°C, compared to 4 cSt for petrol diesel fuel, which is about 11-17 times less viscous. Vegetable oils have lower volatilities, which causes formation of deposits in engines due to incomplete combustion and vaporization problems (Ali and Hanna, 1994), (Agarwal, 2007), (Demirbas, 2008). At high temperatures there could also be problems with the polymerisation of unsaturated fatty acid, which may result in cross-linking between molecules. This could cause agglomerations and gumming if the oils are used directly in engines. This may not be the case with fats, as they have a very low concentration of unsaturated fatty acids; however, they are known to have high melting points. The degree of saturation determines the boiling point of triglycerides. This is because most oils and fats contain at least some unsaturated fatty acids. The degree of saturation of a fatty acid can be determined from a simple formula, $C_{n:\,b}$, where 'n' refers to the carbon length and 'b' the number of double bonds (see Table 1.3). Modern direct injection engines are more vulnerable to vegetable oils of poor fuel quality. Therefore neat vegetable oils are not suitable for direct use as fuel in diesel engines. Instead they have to be modified under the right processing conditions in order to bring their combustion-related properties closer to those of petroleum fuel. To date considerable effort has been devoted to upgrading vegetable oils and fats and their derivatives into bio-fuels that can be used in the existing transport infrastructure. The American standard ASTM D6751 requires a kinematic viscosity of 1.9-6.0 mm^2/s, and the European standard EN 14214 is 3.5-5.0. To achieve these standards and reduce the operational problems associated with the direct use of vegetable oils, two main types of process are employed: thermo-chemical processes and bio-chemical processes (Goyal *et al.*, 2008).

Table 1.3: Typical Chemical Compositions of Some Vegetable Oils (wt %) (Ali and Hanna, 1994)

Vegetable oil	Myristic	Palmitic	Stearic	Behenic	Oleic	Erucic	Linoleic	Linolenic
$C_{n:b}$	14:0	16:0	18:0	22:0	18:1	22:1	18:2	18:3
Corn	0.3	11.67	1.85	0.00	25.16	0.00	60.60	0.48
Cottonseed	1.5	28.33	0.89	0.00	13.27	0.00	57.51	-
Rapeseed	1.5	3.49	0.85	0.00	64.40	0.00	22.30	8.23
Soybean	-	11.75	3.15	0.00	23.26	0.00	55.53	6.31
Peanut	-	11.38	2.39	2.52	48.28	0.00	31.95	0.93
Crambe	-	2.70	0.70	0.80	18.86	58.51	9.00	6.85
Sunflower	-	6.08	3.26	-	16.93	0.00	73.73	-
canola		6.00	2.50	-	66.90	-	-	14.1
palm	47.50	6.30	53.00	-	12.00	-	31.00	-
linseed	-	7.0	5.0	-	37.0	-	23.0	60.0

'n' refers to the carbon length; 'b' the number of double bonds

Various vegetable oils have been reported as being used as feedstocks. European biodiesel is typically made from rapeseed oil, whereas soybean oil is predominantly used in the US and palm oil in tropical countries. This is a reflection of natural agricultural practices as shown in Figure 1.7 and Figure 1.8.

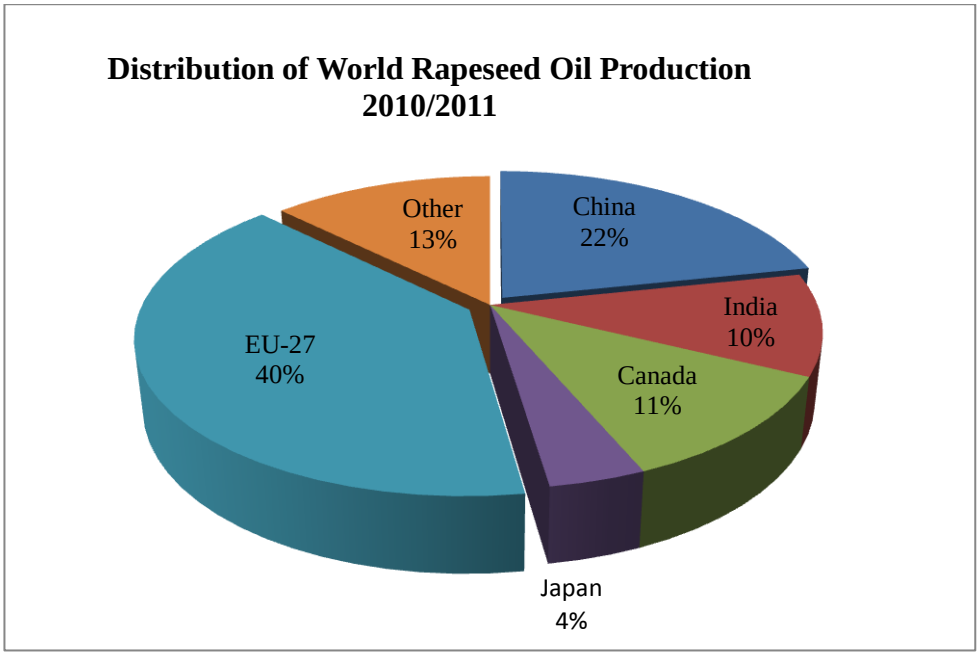

Figure 1.7: World Production of Rapeseed Oil. *Source of Data:(USDA, 2011)*

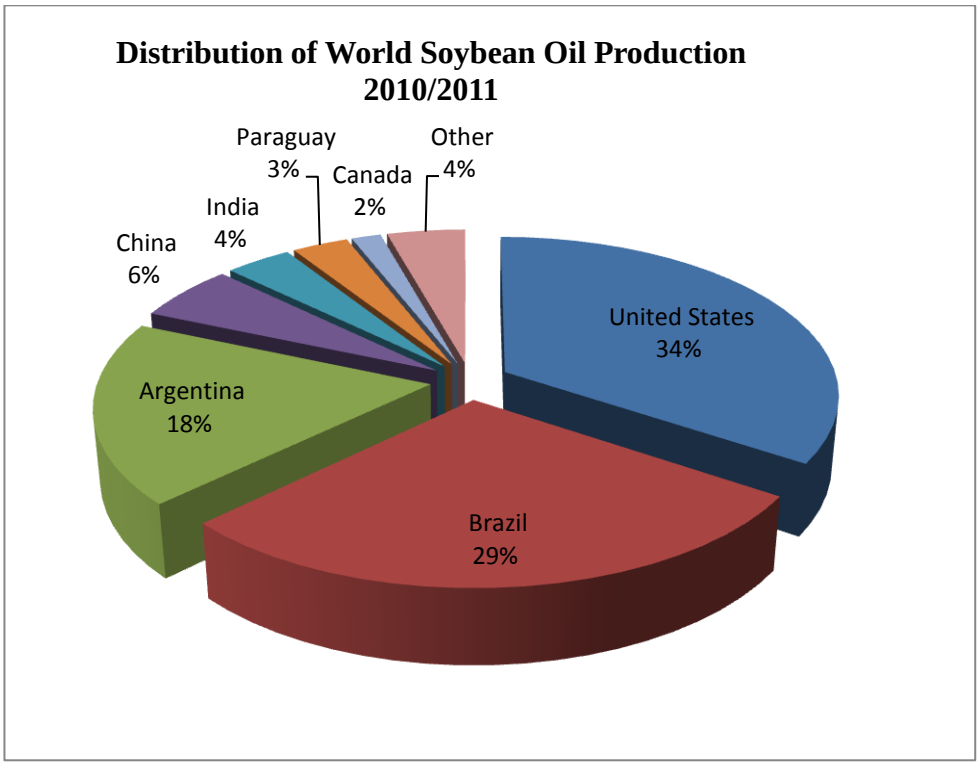

Figure 1.8: World Production of Soybean Oil. *Source of Data:(USDA, 2011)*

With the first documented commercial production of biodiesel from rapeseed oil reported to have occurred in 1988 (Rbitz, 2001), two prominent conversion methods have been used: a low temperature liquid phase catalytic process (transesterification), and a high temperature solid-catalysed cracking process. Recently, there has been increased interest in the latter, which can produce a wide range of liquid hydrocarbon fuels (Tian *et al*., 2008a; Huber and Corma, 2007; Meher *et al*., 2006). Vegetable oils used as feedstock have been characterised and found to consist of different compositions of triglycerides, as earlier shown in Table 1.2.

1.3 Biodiesel Processing

Several production methods are available, which employ the use of homogeneous, heterogeneous, or bio-catalysts. The most commonly used commercial technology for biodiesel production is the transesterification reaction of triglycerides of fatty acids with low molecular weight alcohols in the presence of homogeneous alkaline catalysts (usually sodium hydroxide). Its reaction is shown in Figure 1.9, which in practice is usually conducted at 60^{o}C in the presence of excess methanol in order to push the equilibrium towards the reaction products (Ma and Hanna, 1999). Although biodiesel has been accepted worldwide as a solution to the heavily reliance on petroleum-derived

diesel oil, its current commercial production technology via homogenous transesterification has a lot of limitations.

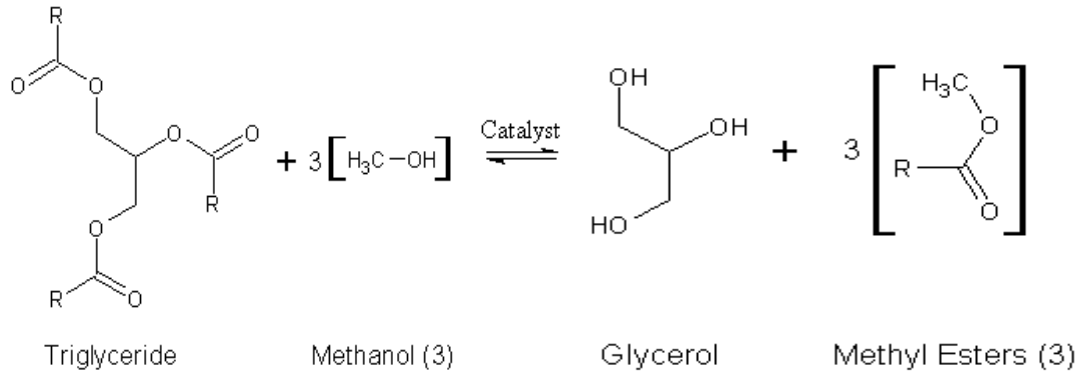

Figure 1.9: Transesterification Reaction for Biodiesel Production

In transesterification the feedstocks must be highly refined vegetable oils, otherwise undesirable products such as soap would be formed due to side reactions as a result of the presence of free fatty acids (FFAs) and water. A tolerable free fatty acid level in feedstock for the transesterification reaction is reported to be less than 1.0% (Haas, 2004); otherwise a pre-treatment of the feed would be necessary. On the other hand, heterogeneous transesterification process appears to be less problematic with easy operations compared to homogenous and non-catalytic transesterification processes. However, reactivity of the heterogeneous catalysts has become a concern. Not many heterogeneous catalysts could produce high yield of fatty acid methyl esters (FAME) in the transesterification process. The production of large quantity of glycerol, a by-product from transesterification process has presently become an issue. With these limitations the cost of biodiesel production is not economical. Hence, it becomes a challenge to design a durable and highly reactive heterogeneous catalyst which can be used in an alternative process other than transesterification.

1.4 Advantages of Thermocatalytic Cracking for Biodiesel (FAME) Production

The thermocatalytic cracking process achieves the direct cracking of oils or fats irrespective of the free fatty acid (FFA) level in the presence of solid catalysts, forming biodiesel without the use of alcohol. The process has been used to upgrade bio-oils from other processes (e.g. pyrolysis) to higher quality fuels and chemicals in the presence of hydrogen. The glycerol is catalytically cracked to value-added chemicals, thereby

eliminating the challenge posed by its large-scale production from the transesterification of triglycerides. In a recent review by Taufiqurrahmi and Bhatia (2011), thermocatalytic cracking of vegetable oils or fats has been described as an effective alternative to either transesterification or pyrolysis. Fundamentally, cracking of triglyceride mechanism during the thermocatalytic process, have not yet been fully explored. However, Maher and Bressler (2007) reported some mechanisms based on the type of feedstock, catalyst and operating conditions. These mechanisms were similar to the Gusmao *et al*. (1989) mechanism. They proposed two pathways depending on the operating conditions. Little is known about direct thermocatalytic cracking of vegetable oils to methyl ester (biodiesel) in the absence of hydrogen. Hence, its application in cracking triglycerides creates an exciting and promising research opportunity in biofuels catalysis and production. An additional advantage is that fewer process operations are required in the heterogeneously catalysed process (see Figure 1.10) compared to transesterification, thus reducing its capital costs.

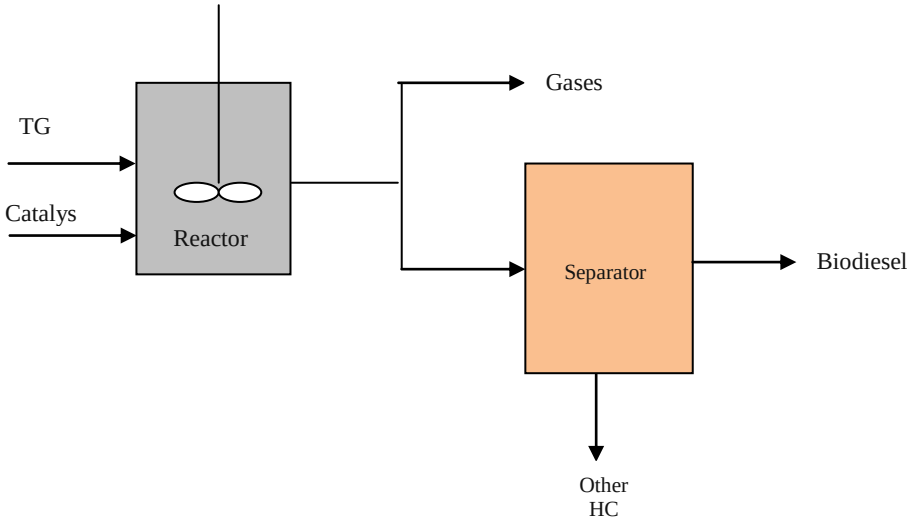

Figure 1.10. Thermocatalytic Cracking Process for Biodiesel Production

1.5 Sulphated Zirconia Catalyst

Sulphated zirconia among other solid acid catalysts has been found to be a promising catalyst for organic reactions**.** It is conventionally synthesized by hydrolysing zirconium salt using aqueous ammonium hydroxide solution. The resulting zirconium hydroxide is impregnated with a suitable sulphating agent before calcination. However, the process

involves the use of aqueous medium at different stages as shown in Figure 1.11 and it takes 72 hours for completion.

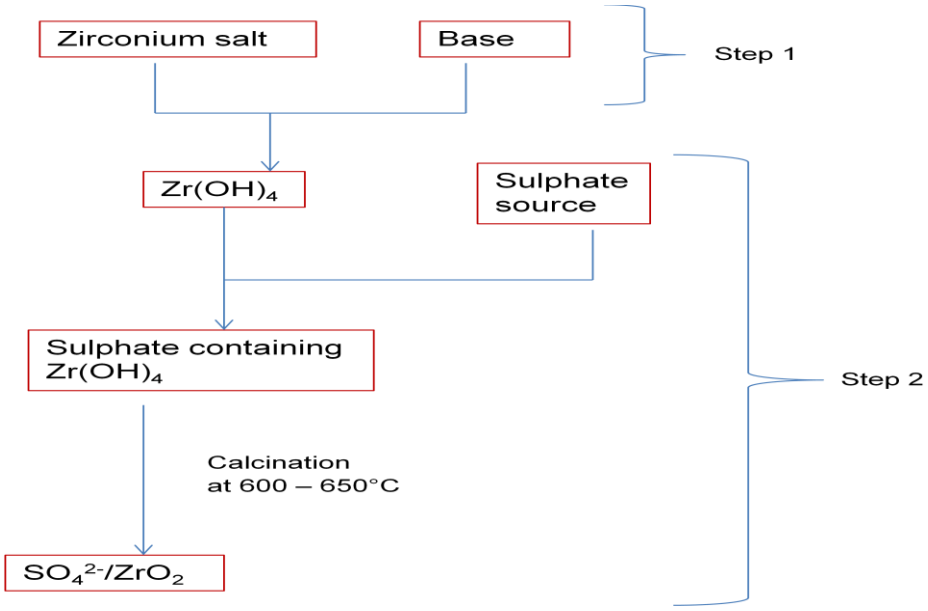

Figure 1.11: Conventional Wet-Precipitation Process of Sulphated Zirconia

Other techniques such as co-precipitation, sol-gel processes, and hydrothermal synthesis have been used to synthesize sulphated zirconia. The multiple steps involved in these methods pose the possibility of scarce reproducibility of the textural and, consequently, of the catalytic properties of the synthesized sulphated catalyst (Melada *et al*., 2004). The drawback with sol–gel processes is that several parameters intervene in imposing the features of the catalyst, both concerning the ‘‘chemical’’ composition of the reacting mixture and also the temperature and time length of the hydrolysis-condensation steps involved (Melada *et al*., 2004).

1.6 Research Objectives

Extensive research has been performed on heterogeneous acid catalysts. However, there are few publications on the use of heterogeneous acid catalysts in thermocatalytic cracking for biodiesel production compared to transesterification. Likewise, the production of biodiesel using solid acids catalysts by thermocatalytic cracking is not yet established in industry. Showing a similar trend, the use of sulphated zirconia in cracking has been widely studied, but there are few reports on its use in the thermocatalytic cracking of triglycerides. New catalytic routes are consequently under

investigation to improve its competitiveness in different applications. However, less is known about directly synthesised sulphated zirconia in the thermocatalytic cracking of triglycerides for biodiesel/biofuel production. Hence, the overall goal of this research is to develop a heterogeneous catalyst; sulphated zirconia, with improved catalytic properties for biodiesel production in a thermocatalytic reaction. The specific objectives are as follows:

1. To use an environmentally friendly method to synthesise sulphated zirconia catalysts, by completely eliminating the use of any aqueous medium
2. To optimize the sulphated zirconia catalyst design to achieve improved overall activity compared to the conventional catalyst.
3. To develop zirconium sulphated heterogeneous catalysts that can convert triglycerides to fatty acid methyl esters (FAMEs) in the absence of alcohol
4. To investigate the kinetics of the reaction
5. To look for other products of this reaction, this might have added value to the process.

.

Chapter 2: Literature Review

2 Scope

This chapter discusses the benefits of biodiesel as an alternative to petro-diesel, and considers current manufacturing techniques used for biodiesel production as well as various new technologies that are being developed. It primarily focuses on the development and application of catalysts, the problems associated with them and the benefits of different catalyst systems. The use of heterogeneous catalysts in transesterification for the production of biodiesel is reviewed. The need for and advantages of replacing the homogeneous catalyst-based transesterification process with heterogeneous catalysts in thermocatalytic cracking is explained. Details of some of the analytic methods available and those implemented in this work are also discussed. Finally, areas in this field of study which require further research are highlighted.

2.1 Biodiesel Production

The methods used to produce biodiesel can be categorised into three types: these are chemical catalytic (base- or acid catalysis), bio-catalytic (enzyme catalysis) and non-catalytic processes. Several reviews of the different methods of biodiesel production from different feedstocks can be found in the literature (Marchetti *et al*., 2007; Mittelbach and Remschmidt, 2006). A very good overview comparing such technologies was given by Balat (2008) in Figure 2.1. Each of these processes gives a different range of products under different operating conditions. The choice of conversion process depends on the type and the desired form of energy, while the product range is a function of the catalyst used, the nature of the feed, pressure, reactor geometry, temperature and residence time. The most common biofuels used in Europe today are of the first generation of biodiesel. To date, most biodiesel processes use a soluble base as the catalyst in transesterification process, but the use of this type of catalyst complicates product recovery and purification. In 2007, around 19 biodiesel plants in EU member states were starting operations, or were under construction and in the planning stage. Currently, relatively large plants are found in Poland, Lithuania and Romania in addition to Germany and France (Luque *et al*., 2010)**.** Solid or liquid catalysts are predominantly used in the two chemical catalytic processes (transesterification and pyrolysis) and in the case of the biological conversion the use of enzyme catalysis is employed.

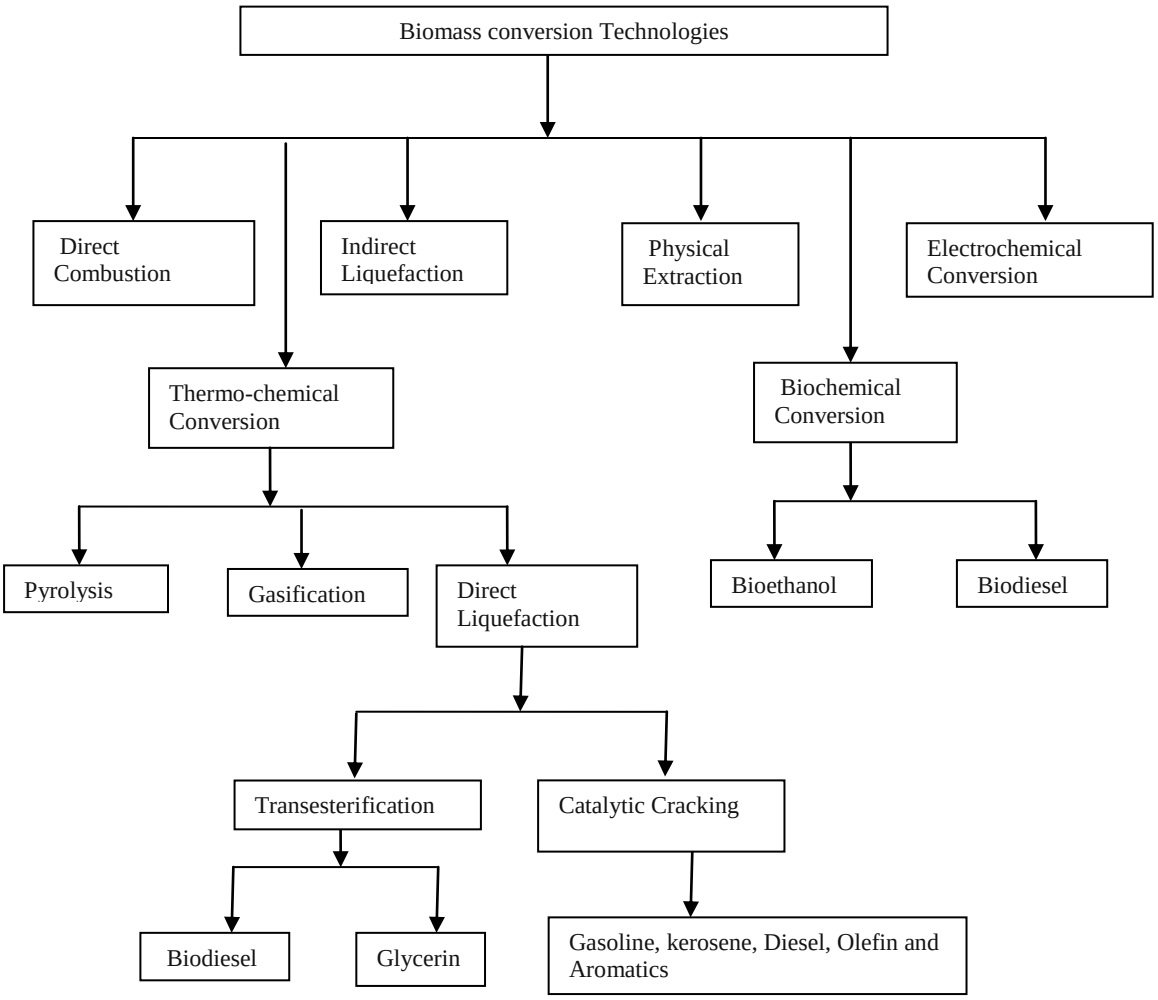

Figure 2.1: Main Biomass Conversion Processes (Balat, 2008)

2.1.1 Transesterification

Transesterification, also known as alcoholysis, is the conventional methodology for the production of biodiesel. It involves the displacement of alcohol from an ester by another alcohol in a process similar to hydrolysis, except that an alcohol is used instead of water as shown in Figure 2.2. The product of the reaction is a mixture of methyl esters which are known as biodiesel and glycerol. This process has been widely used to reduce the viscosity of triglycerides. It is a reversible reaction and proceeds essentially via the mixing of triglycerides and alcohols (primary or secondary monohydric aliphatic alcohols with C_1 to C_8 atoms) in the presence of a catalyst. Methanol is the most commonly used alcohol due to its low cost.

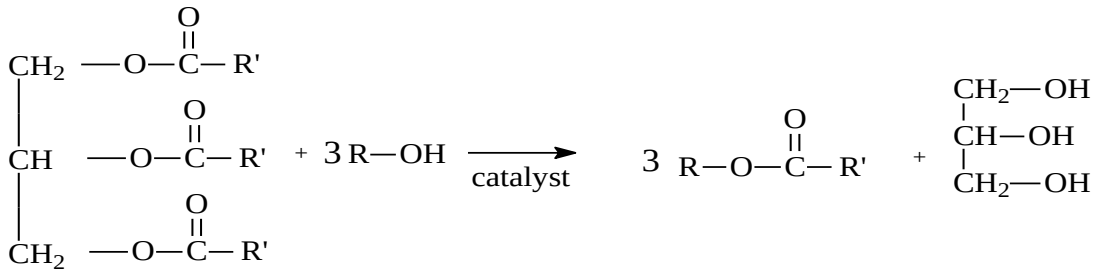

Figure 2.2: A Simple Transesterification Reaction

where:

R^1, R^2, and R^3 are long-chain hydrocarbon (alkyl group),

R is where any two of the 'R' could be the same

As a reversible reaction, excess alcohol is used to shift the equilibrium towards the formation of the esters. The stoichiometic ratio of alcohol to glycerides is 3:1; however in practice it is commonly 6:1–30:1 (Demirbas, 2003; Ma and Hanna, 1999). Homogeneous base catalysts such as NaOH, KOH, CH_3ONa or CH_3OK are used in the process. However, when these catalysts are used, feedstock selection is crucial to the success and economic feasibility of biodiesel production. This is because the catalysts require anhydrous conditions and level of free fatty acids (FFA) below 20% in the feedstocks. However, if the level of free fatty acid (FFA) in the feedstock is greater than 20%, liquid acids such as H_2SO_4, HCl or H_3PO_4 are employed as catalysts in a process called esterification. The liquid acid catalysts tend to show tolerance towards FFA, but the reaction may be very slow. The reaction is carried out at temperatures above 100°C and it takes more than three hours to complete the conversion process (Meher *et al*., 2006; Demirbas, 2005; Schuchardt *et al*., 1998). The water content in the feed is another issue of concern and should be kept below 0.06% (Demirbas, 2009b). It is important that the water and FFA content of the feedstock be at minimum since the presence of FFA can result in additional unwanted products such as soap as shown in Figure 2.3, while water reacts with the ester (see Figure 2.4) to form a primary alcohol in addition to soap. Therefore the presence of water and FFA increase the formation of by-products, making downstream processing much more difficult and leading to reduced product yield (Demirbas, 2009a; Vasudevan and Briggs, 2008; Ma and Hanna, 1999). The

negative effect of the presence of water have been reported at levels as low as 0.1% by Canakci and Van Gerpen (1999).

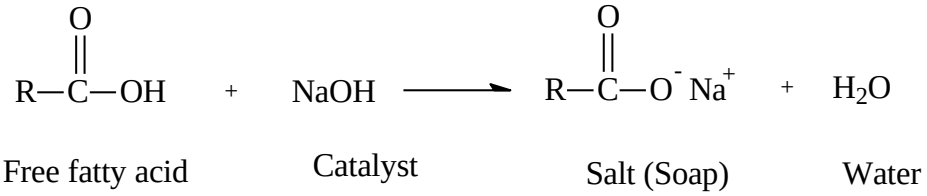

Figure 2.3: Saponification of Free Fatty Acid

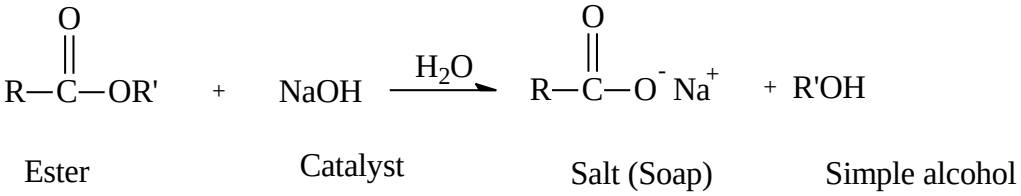

Figure 2.4: Saponification of Ester

In order to boost the efficiency of the transesterification process and to eliminate some of its drawbacks, heterogeneous catalysts have been investigated on the basis that their use does not lead to the formation of soaps through the neutralization of FFAs or saponification of triglycerides and methyl esters. Furthermore, solid acid catalysts are particularly attractive, having the potential to simplify downstream operations and decrease overall production costs. The aim here is to improve the sustainability of the biodiesel production process by eliminating the corrosion problems associated with the use of and consequent environmental hazards posed by their liquid counterparts. Rattanaphra *et al*. (2010) recently reported the use of a heterogeneous solid acid catalyst in the simultaneous esterification of free fatty acids and transesterification of triglycerides, leading to high fatty acid methyl esters (FAME) yield. However, there still appear to be some major limitations of this technique due to downstream separation, as shown in a simple schematic diagram of the transesterification process in Figure 2.4

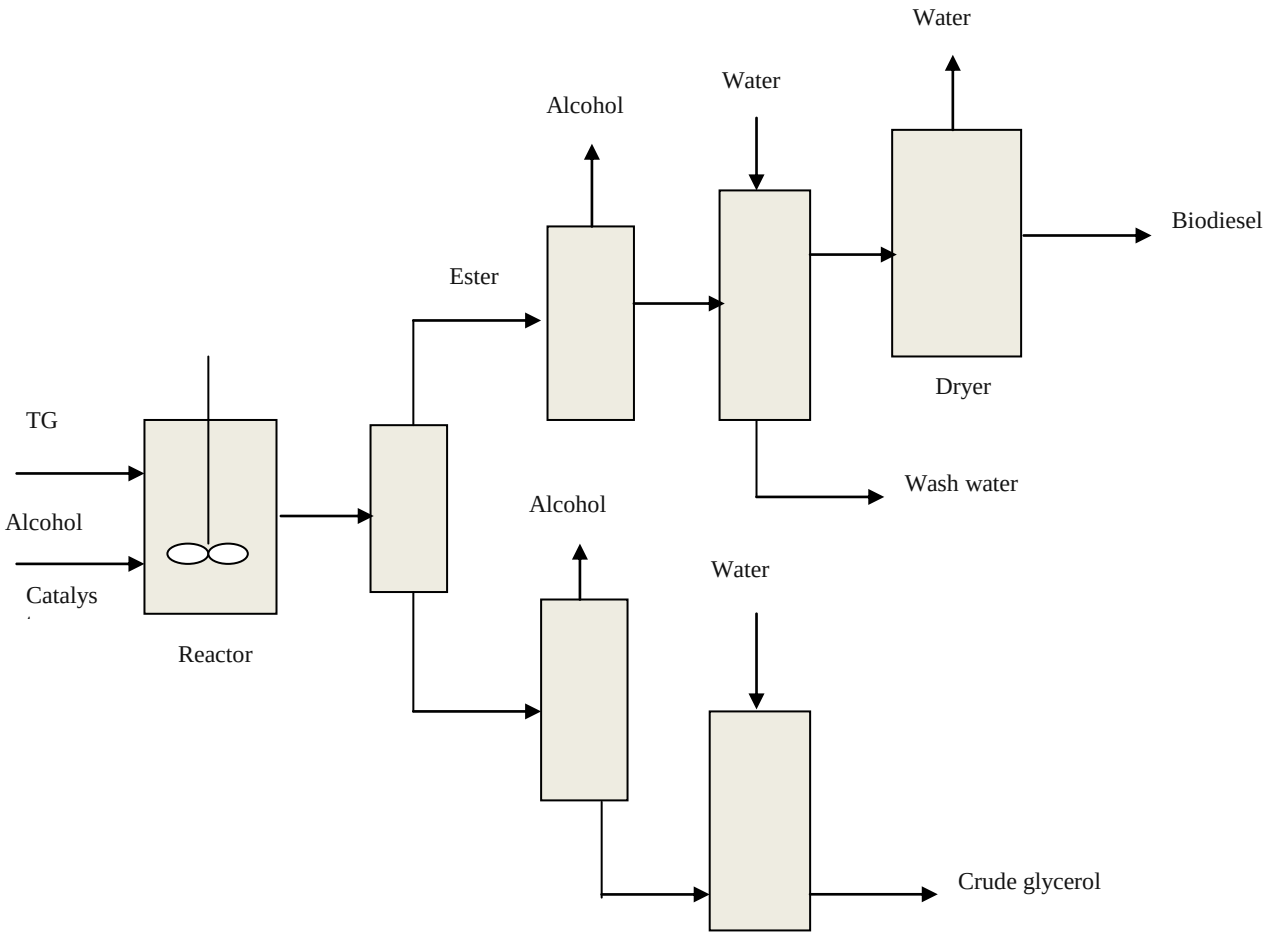

Figure 2.5: A Simple Schematic Diagram of the Transesterification Process

For a bio-refinery to thrive, a diverse range of processing catalysts must be available, in particularly those with the ability to selectively transform biomass feedstocks into specific products using chemical catalytic routes. With its versatility and robustness, heterogeneous catalysis can play a key role in the conversion of feedstocks into high-value methyl esters and other chemical products. Heterogeneous catalysts and catalytic processes need to be developed in order to provide bio-refineries with the capability and flexibility to adjust and optimize performance in response to feedstock changes and market demand. One example is the Neste Oil Corporation, a producer of renewable diesel oil. Up to 2010, the Corporation used edible oil for approximately 87% of its feedstock, but hopes to move to 100% non-edible oil by 2020 as shown in Figure 2.6. In fact the company is currently conducting research into the potential of using algae oil, which has high levels of FFA, as a feedstock for producing biodiesel. If this is to be viable, then a stable and effective heterogeneous acid catalyst for the effective conversion of the free fatty acid in the feedstock is required.

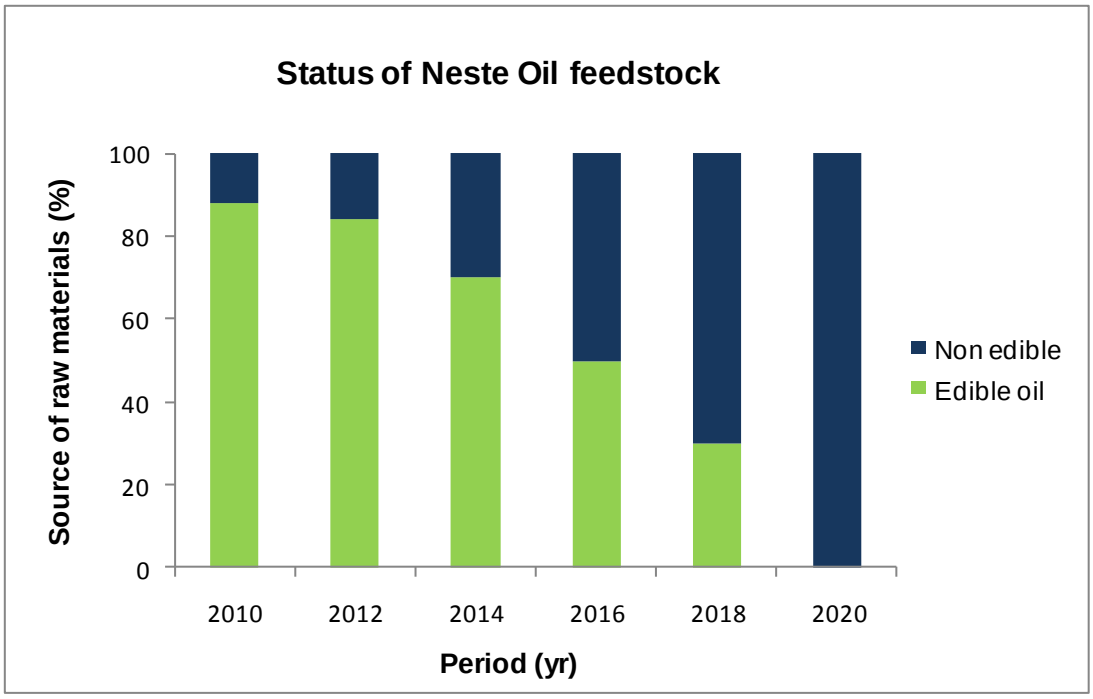

Figure 2.6 Neste Oil Corporation Feedstock. Source: Neste Oil (2010)

2.1.2 Pyrolysis

Another method of chemical conversion is pyrolysis. This technique is used to convert biomass in the absence of oxygen or nitrogen into a valuable liquid derivative, known as bio-oil (Fukuda *et al*., 2001). Ali and Hanna (1994) defined this method as a severe form of thermal cracking, with a subsequent rearrangement of fragments which other authors have described as a "destructive" distillation of biomass. This is due to the high temperature that is usually employed (Goyal *et al*., 2008). Pyrolysis can be classified as slow, fast or flash depending on the operating conditions. Several studies on the pyrolysis of vegetable oils and animal fats have been reported (Adebanjo *et al*., 2007). Billaud *et al*.(1995) studied the pyrolysis of rapeseed oil diluted with nitrogen in a tubular reactor between 550 and 850°C. The principal products observed were linear 1-olefins (C_{10}-C_{14}), n-paraffins, and short-chain unsaturated methyl esters, with a gas fraction containing CO, CO_2, and H_2. However, it should be noted that the product of pyrolysis, bio-oil, must be upgraded or blended before it can be used as fuel. The most significant problems with bio-oil are poor volatility, high viscosity, coking, corrosiveness, and cold flow problems (Czernik and Bridgwater, 2004).

2.1.3 Non-catalyzed Systems and Bio-chemical Methods

The most common, non-catalysed process of biodiesel production process uses supercritical methanol via the simultaneous transesterification of triglycerides and esterification of fatty acids (Demirbas, 2006). High temperatures and pressures (350 to 400°C and > 80 atm. or 1200 psi) are essential to obtain the desired products. The procedure has been claimed to be very effective, yielding high FAME within a very short reaction time (typically less than 30 minutes). Nevertheless, the supercritical method is capital-intensive, and requires a very large excess of methanol to oil ratio of (42:1) (Gerpen *et al*., 2004). Furthermore, the reaction must be quenched very rapidly so that the products do not decompose. Clearly, while the results are very interesting, scale-up to a commercially useful process may be quite difficult. On the other hand Balat (2008) described bio-chemical conversion to bioethanol as slow to embrace due to the following reasons: (1) the high cost of the collection and storage of low density biomass feedstocks; (2) the resistance of the biomass to being broken down; (3) the variety of sugars that are released when the hemicellulose and cellulose polymers are broken down; and (4) the need to find or genetically engineer organisms to efficiently ferment these sugars. Another problem with bioethanol as a fuel is that it absorbs water and is very volatile, making it difficult to store and transport (Smith *et al*., 2009).

These disadvantages have led the attention of researchers to thermocatalytic cracking of triglycerides as an easier and more feasible process. The technology involved is very similar to that of conventional petroleum refining, yet research in this area is nowhere near as advanced as it is in the transesterification of oil to biodiesel (Maher and Bressler, 2007). In addition, the thermocatalytic process can be used to upgrade the primary products from other processes such as pyrolysis so as to produce higher quality fuels and chemicals.

2.2 Current Challenges for Biodiesel Production

Although transesterification has the advantages of high conversion rates and short reaction times, the future potential of the process is controversial due to several associated drawbacks. The presence of free fatty acids and water in the feedstock causes soap formation, thereby restricting the range of potential feedstocks and leading to reduced yields of biodiesel. Secondly, the neutralization of the alkaline also forms soap, making it difficult to wash the glycerol. Moreover the transesterification process is far from being environmentally benign. The product stream needs careful separation,

neutralization and thorough washing. This generates a lot of waste water which needs to be further purified or treated and furthermore the homogeneous catalyst cannot be recycled. These factors certainly increase the total production costs of biodiesel even as the quality of its main by-product, glycerol, is reduced. The biodiesel itself must be subjected to further washing and at times drying to remove the traces of glycerol in order to meet EU quality standards (EN 14214) which prescribe 0.02% or lower glycerol content in the biodiesel. In some cases, however, homogeneous acid catalysts as an alternative to alkalis have been reported which achieve simultaneous esterification and transesterification conversion with up to 78% (Sharma *et al*., 2008). It is also usually a slow two-step process at high temperatures above 100°C and taking more than three hours to complete the conversion (Demirbas, 2007; Schuchardt *et al*., 1998). Another limitation of the transesterification process is its production of glycerol. This is a valuable primary by-product, but has now become a subject of concern, because it is expected to become difficult to find suitable applications for large amounts of it in the near future (Dupain *et al*., 2007; Huber *et al*., 2006). Although transesterification is presently conducted on a large scale using crude feedstock in order to cut costs, the problems of energy and water consumption still face the industry (Dupont *et al*., 2009). Therefore, with the growing environmental concern about the use of homogeneous catalysts, heterogeneous catalysts have recently been introduced in transesterification. This is because their usage offers various advantages:

- The catalyst may be recycled and subsequently employed again in the reaction,
- The biodiesel product is assumed to have improved properties compared to those from the homogeneously catalysed process.
- Pre-treatment steps in the case of feedstock with high level of free fatty acids are eliminated,
- Waste is minimised

However, the process has the removal of glycerol from the biodiesel as a major limitation, in order to meet the EEC regulations. For pyrolysis the challenge is that its liquid product cannot be used directly for transportation fuel because of unacceptable levels of carbon residues, ash, and poor pour points (Sharma *et al*., 2008; Fukuda *et al*., 2001). Products are also less stable and less miscible with conventional fuels, and

usually need upgrading in order to improve their quality (Goyal *et al*., 2008). Therefore recent research has focused on ways to minimise or eliminate the above constraints, yet still achieve desired product of high quality.

In summary, the greatest hurdle in commercializing biodiesel is the cost of production resulting from the cost of raw material, as well as costs incurred in the transesterification production method. The cost of production is still keeping the retail price of biodiesel too high for it to be an option for many users, and until these problems are resolved the cost of production will remain relatively high. To sustain biodiesel commercially and competitive with petroleum-based diesel, heterogeneous catalysts needs to replace the transesterification, which is time-consuming, high in capital costs and labour intensive. In a recent review by Taufiqurrahmi and Bhatia (2011), the thermocatalytic cracking of vegetable oils and fats has been reported as an ideal alternative to transesterification and pyrolysis. The process could significantly enhance the economic viability of biofuel production in general. Since replacing the liquid catalysts minimizes the separation process required, better quality biodiesel, easy catalyst recovery and reusability are all achieved.

2.3 Catalytic Cracking of Vegetable Oil

Catalytic cracking of vegetable oil entails the breaking down of the molecular structures of renewable feedstock in the presence of solid catalyst. This technology is similar to that of conventional petroleum refining and can be used in upgrading bio-oil produced by other processes to higher quality fuels and chemicals (Smith *et al*., 2009; Meng *et al*., 2005), at a lower temperature (300-450^{o}C) than pyrolysis. Large molecules are degraded to smaller compounds by operations such as dehydration, dehydrogenation, deoxygenation, and decarboxylation. In addition, the process can be used to improve the thermal stability of cellulosic molecules as well as reducing their oxygen content. Compared with the hydrotreating process, catalytic cracking does not require the use of hydrogen, which is another advantage. Furthermore, it is a process that can use any form of biomass to produce variety of biofuels in the existing oil-refineries as reported by (Huber and Corma, 2007).

Besides, non-edible and used cooking oils have also received considerable attention recently in connection with this process. At present, catalytic cracking is considered to be the most convenient method of producing biofuels and chemicals from vegetable oils and fats. It does not only reduce costs but, compared to pyrolytic cracking, allows

flexibility in the adjustment of product distribution (Tian *et al*., 2008b; Meng *et al*., 2005). The attempt is to replace both homogeneous catalysts and transesterification with heterogeneous catalysts in catalytic cracking process in order to minimize waste and sustain biofuel production and the environment in general. The use of acidic heterogeneous catalysts in organic reactions has long been well-documented, as indicated in an extensive review by Weisz *et al* (1979) and Corma (1995). However, such heterogeneous catalysts have only recently been used in biodiesel (FAMEs) production by catalytic cracking. Thereby creating exciting and promising research opportunities in biodiesel catalysis (Zabeti *et al*., 2009; Lotero *et al*., 2005)**.** This has led to growing interest in the cracking of triglycerides into biofuels using different heterogeneous catalysts. Several heterogeneous catalysts have been used and compared for their activity in the catalytic cracking of triglycerides from various sources as reported in a review by Taufiqurrahmi and Bhatia (2011) and shown in Table 2.1. Katikaneni *et al*. (1996) performed catalytic cracking on canola oil at a temperature range of 400–500^{o}C and reaction time of 1.8–3.6h^{-1}. Their product spectrum contained organic liquid product (OLP), gas, water, and coke. The authors observed that the catalytic cracking of the canola oil resulted in 95wt% aromatics in the OLP mainly benzene, toluene, and xylenes.

Table 2.1: Feedstocks, Catalysts and Operating Conditions used in the Study of Catalytic Cracking of Vegetable Oil (Taufiqurrahmi and Bhatia, 2011)

Feed	Catalyst	Temperature (K)
Palm/soy beans oil	FCC equilibrium catalyst	838
Cottonseed oil	FCC equilibrium catalyst	713-783
Rapeseed oil	FCC equilibrium catalyst(REUSY coated with ZSM5)	823
woody oil	Al_2O_3/MCM-4l/CaO	723-773
Calotropis procera oil	Equilibrium FCC catalyst	733-793
Soybean oil	Na_2CO_3/K_2CO_3/Al_2O_3/MCM-4l	623-673
Soybean oil	HZSM-5/MCM-41/impregnated MCM-41	693 & 723
Cottonseed oil	FCC equilibrium	653-833
Soybean oil	Bauxite	653-673
Fresh & used sunflower oil	Hydro-cracking catalyst	653, 643 & 663
Canola oil	HZSM-5, H-mordenite, H-Y, silicate, AL-PILC, $SiO_2Al_2O_3$	473-873
Sunflower oil	Alkali treated (NaOH) aluminium oxide (Al_2O_3)	460-630
Soybean oil	Alumina doped with tin and zinc	623-673
Olive oil	KOH, Na2CO3	540-630
Palm/soybean oil	CORH (main component USY zeolite) & LTB-2 (main component ZSM-5 zeolite)	773 & 793
Waste olive oil	Dolomite	773-1073
Rapeseed	Equilibrium FCC catalyst/ZSM-5	758-858
Glycerol from biomass	FCC equilibrium catalyst/USY/ Al_2O_3/HZSM-5	773-973
Used vegetable oil	HZSM-5/sulphated zirconia/HZSM-5 & sulphated zirconia	653-703
Used vegetable oil	Sulphated zirconia	673-703
Soybeans/palm/castor oil	HZSM-5	623-673
Fatty acid(ocatanoid acid	Activated alumina	623, 648 & 673
Used sun flower oil	HZSM-5	673-693
Used sunflower oil	Na_2CO_3	673 & 693
Canola oil	HZSM-5/SiAl2O3/HS mix	673-773
Canola oil	HZSM-5, silicate, silica alumina, γ- alumina, CaO, MgO	673 & 773
Canola oil	Potassium-impregnated HZSM-5	673-773
Canola oil	HZSM-5, H-mordenite, H-Y, silicate, AL-PILC, $SiO_2Al_2O_3$	648-773

Similar Tian *et al*. (2008) studied the cracking of oils and fats on a mixture of solid acid catalysts in a two-stage riser fluid catalytic cracking (TSRFCC) reactor. The catalyst mixture comprised mainly of Ultra-Y (USY) zeolite and ZSM-5 (Zeolite Socony Mobil-Five). The oils and fats tested were pure vegetable oils (palm oil and soybean oil), animal fats (chicken fat), and blends with vacuum gas oil (VGO). The reaction was

conducted at atmospheric pressure and two different temperatures. The first stage riser was operated at 500^{o}C, catalyst to feed ratio of 6 and residence time of 1.4 sec. The second stage riser was at a temperature of 520^{o}C for a residence time of 1.7sec and mass ratio of catalysts/feed of 8. They reported palm oil had the highest yield of LPG and light olefins among the three feeds with 97% conversion. The total liquid yield form the palm oil was 77.6%, 45% LPG and 23% propylene. Blending the palm oil with VGO resulted into a higher yield (79.2%) of liquid product but lower LPG (39.1%) and propylene (18.1%) yield. Oxygen content of the liquid products was very low (about 0.5%), and were removed mostly as H_2O and partly as oxides. Furthermore, vegetable oil and animal fat gave the sum of 83.6% aromatics and olefins; comprising of C_5, C_6 olefins and C_7, C_8, C_9 aromatics. On the other hand the palm oil yielded higher aromatics of 82.7% and only 6.3% olefins. The cracking of gasoline to olefin was mainly during the secondary cracking in the second stage in the reactor. However, nothing was reported on the comparison of the catalysts activity. The overall conversions of feed and product distribution are presented in Table 2.2 and Table 2.3.

Table 2.2: Overall Product Distribution of TSRFCC Reactor (%, by mass) Tian *et al*. (2008)

Feed	Conversion	LOP	Product distribution					
			Dry gas	LPG	Gasoline	Diesel oil	Heavy oil	Coke
Chicken fat	97.1	78.5	4.5	34.3	32.8	11.4	3.0	2.3
Palm oil	98.3	77.6	7.2	45.0	28.1	8.9	2.0	2.2
Soybean oil	95.5	76.9	4.6	29.2	32.4	15.3	4.5	4.0
PO/VGO (50/50)	93.9	79.2	6.1	39.1	20.9	19.3	6.1	4.0

Table 2.3: Product Distribution of Light oil and Olefin (%, by mass) Tian *et al*. (2008)

		Yield of C_2-C_4 olefins		
Feed	Light oil	Ethylene	Propylene	Butylenes
Chicken fat	45.2	3.7	16.4	15.2
Palm oil	37.0	5.6	21.0	16.6
Soybean oil	47.7	3.6	14.7	12.4
PO/VGO (50/50)	40.2	4.9	18.1	15.7

In another study, Charusiri *et al.* (2006) studied the catalytic conversion of used vegetable oil to liquid fuel over some catalysts; HZSM-5, sulphated zirconia and hybrid of HZSM-5/sulphated zirconia. The reaction was performed in a batch microreactor over a temperature range of 380-430^{o}C, in the presence of hydrogen gas at a pressure range of 10-20 bars, and reaction time range of 45-90min. Analysing the LOP in a simulated distillation gas chromatograph, revealed the highest yield of gasoline (26.57wt%) was by HZSM-5/sulphated zirconia (0.3: 0.7) at a temperature of 430^{o}C, a pressure at 10 bars, and 90min reaction time. The addition of HZSM-5 to sulphated zirconia enhanced its activity by increasing acidity and the pore structure for effective aromatization. Leng *et al* (1999) showed that similar reaction can be carried out under atmospheric pressure. Calcined and uncalcined HZSM-5 catalysts were used in a fixed bed micro-reactor. The calcined catalyst showed a higher rate of cracking at a conversion of 70wt% after 2 h^{-1} (WHSV) at 400°C and atmospheric pressure. They showed that both temperature and space velocity affected the palm oil conversion. The highest conversion was at 390^{o}C and a space velocity between 3 to 4 h^{-1}, after which there was a decrease in conversion and liquid product. The catalyst was selective for aromatics and hydrocarbons in the gasoline, diesel and kerosene range. Other products include light gases, coke and water. They attributed the decrease in conversion to coke formation on the catalyst which reduced the acid sites available for cracking. Using different types of zeolite and its hybrid in a fixed bed microreactor at a reaction temperature of 350-450^{o}C and atmospheric pressure, Twaiq *et al*. (1999) produce gasoline, kerosene, and diesel fuel in different yields of 28%, 9%, and 5%, respectively, from a palm oil feed. HZSM-5 catalyst gave the highest conversion of 99 wt% and a gasoline yield of 28wt% after 1h under a reaction temperature of 350^{o}C. From Table 2.1, above, many of the research have been performed on FCC catalysts, zeolites, silica-alumina and their hybrids at high temperatures. However, the issue of catalyst choice is paramount for the effectiveness of the process. Therefore, there is need for more research into other types of potential catalysts for biofuel production by catalytic cracking at lower temperatures.

2.3.1 Mechanism of the Catalytic Cracking of Triglycerides

The catalytic cracking of triglyceride is a technique that involves the breaking of chemical bonds at various points within the molecule. Several publications are available that describe the successful catalytic cracking of vegetable oils into liquid bio-fuels (Kirszensztejn *et al*., 2009; Ooi *et al*., 2005; Idem *et al*., 1997; Katikaneni *et al*., 1996)

at high temperature. The detailed mechanism of the process is not well-established, however, various authors (Taufiqurrahmi and Bhatia, 2011; Dupont *et al*., 2009; Huber and Corma, 2007; Maher and Bressler, 2007; Idem *et al*., 1996) reported similar pathway for catalytic cracking of triglyceride molecule. Generally, it is initiated with a thermal cracking process by means of free radicals before catalytic conversion to oxygenated compounds. Depending on the reaction conditions; in the presence of a catalyst with active acid sites accessible for triglyceride molecules, the triglyceride decomposes by means of interaction of the oxygen bonding of the ester carbonyl groups with an acid site. In an earlier study, Gusmao *et al*. (1989) summarised the mechanism of catalytic cracking of vegetable oil to diesel-like fuel over Ni/SiO_2 and sulphated Ni-MO/γ-Al_2O_3 catalysts as shown in Figure 2.7. They reported the catalytic cracking reaction occurs via two steps: (i) decomposition of triglycerides to carboxylic acids, acrolein and ketenes. Acrolein (propenal) is the simplest unsaturated aldehydes, both acrolein and ketenes are unstable and very reactive. These compounds recombine at the reaction conditions to form esters, carboxylic acids and hydrocarbons; (ii) the carboxylic acids are decarbonylated or decarboxylated, producing, respectively, carbon monoxide, olefins and water or carbon dioxide and paraffins.

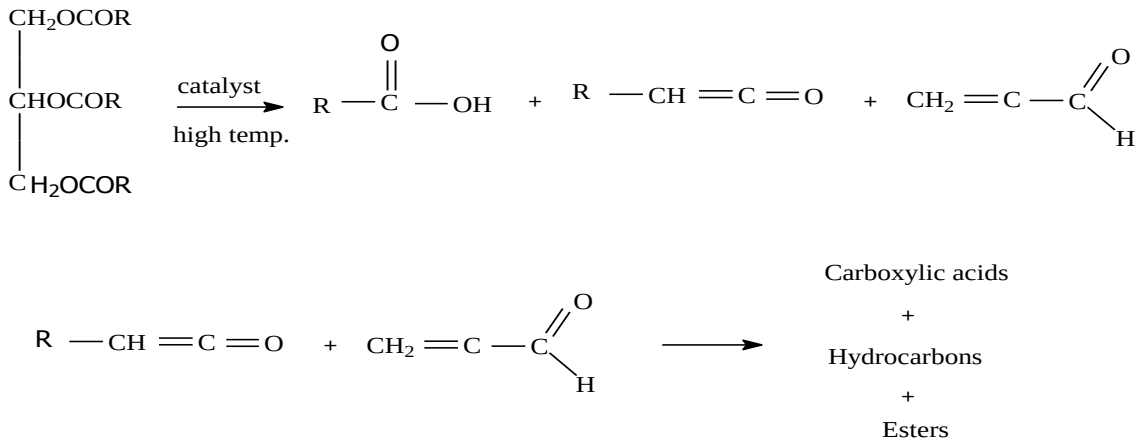

Figure 2.7: Catalytic Cracking of Triglycerides (Gusmao *et al*., 1989)

The occurrence of the different reaction routes and other hydrocarbon products depend on the double bonds in the initial oxygenated hydrocarbon (Osmont *et al*., 2007). Similarly, Maher and Bressler (2007) reported the production of free radicals during triglycerides cracking. Although the positions at which cracking occurs along the chain length is not established, Suarez (2006) proposed the possibility of some positions where cracking could occur during primary or secondary cracking (see Figure 2.8).

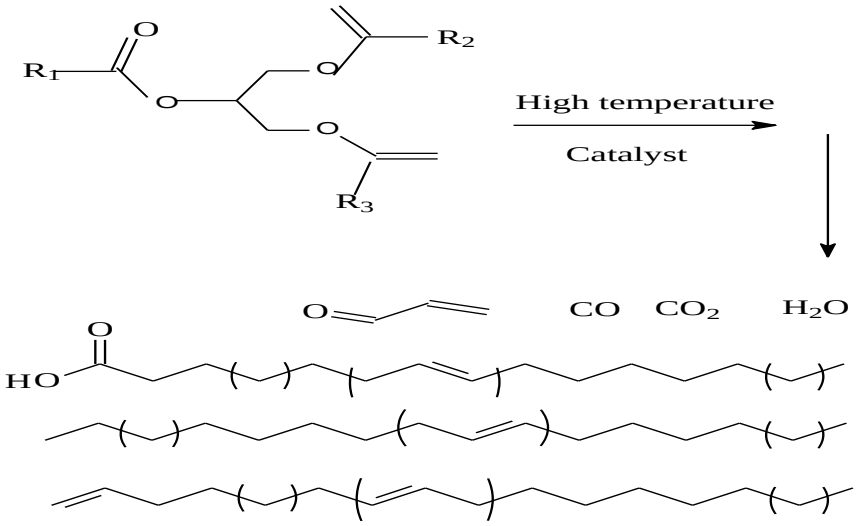

Figure 2.8: Proposed Cracking Positions on Triglycerides (Suarez, 2006)

In a review, Maher and Bressler (2007) reported carboxylic acids, ketones, esters, acrolein and hydrocarbons as typical reaction products of triglyceride cracking. The organic liquid products (OLP) from the reaction is a mixture of oxygenated and heavy oxygenated hydrocarbons consisting of compounds like olefins, paraffins, alcohols, acids, ketones, aldehydes, C_6^+ aliphatic hydrocarbons, C_9^+ aromatic hydrocarbons, and gases as reported by Idem *et al*. (1996). Other processes such as aromatization, alkylation, isomerisation, oligomerization, polymerization and condensation may occur. Similar reaction mechanism was reported by Melero *et al*. (2009) in catalytic cracking of mixtures of crude vegetable oils and non-edible animal fats with vacuum gas oil. They reported that once the triglyceride molecule has been primarily cracked to heavy oxygenated hydrocarbons such as fatty acids, ketones, esters, and aldehydes, further reactions to reach other products start by means of the breaking of the C-O and C-C bonds by β-scission reactions. A beta scission is characterized by the scission of a bond beta (connected to an adjacent atom) to the atom bearing a radical. In another study Katikaneni *et al*. (1995a) proposed a reaction scheme from cracking of canola oil over zeolite as shown in Figure 2.9. They also reported that the heavy oxygenated hydrocarbons and oxygenates undergo further catalytic cracking to produce esters.

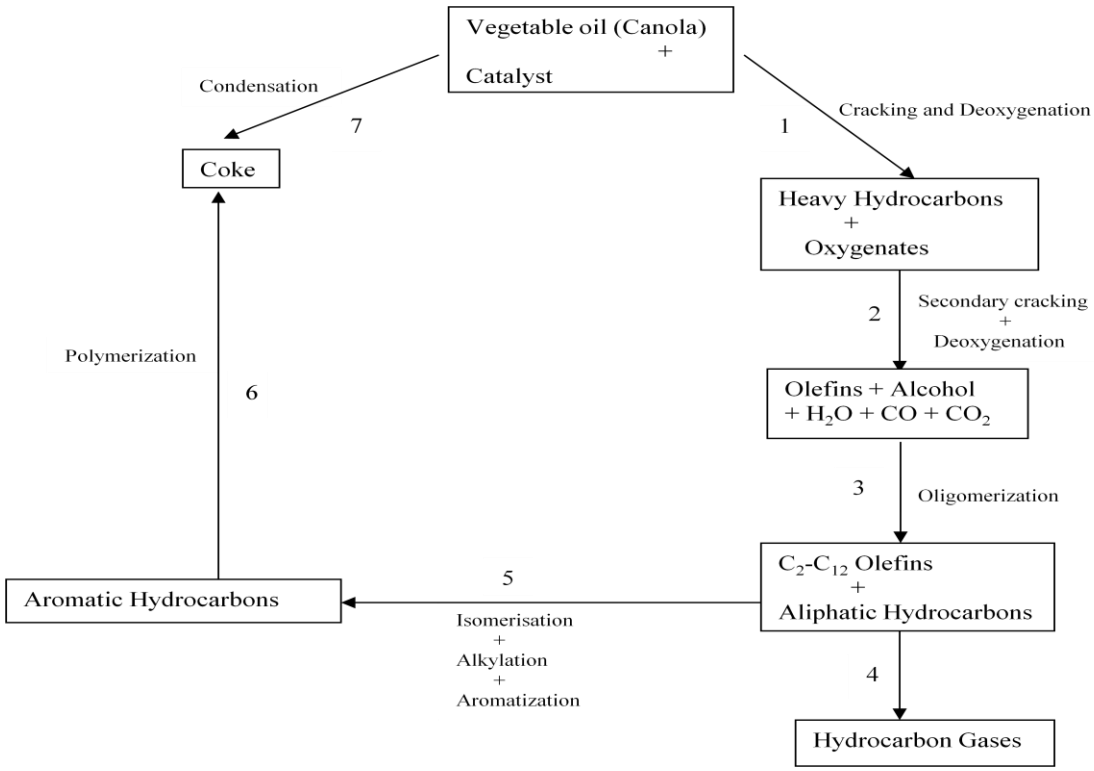

Figure 2.9: Proposed Reaction Pathway for Catalytic Cracking of Canola over Zeolite Catalyst (Katikaneni *et al*., 1995a)

Dupain *et al*. (2007) studied the catalytic cracking of rapeseed oil (pure and blended with conventional FCC feedstock) on commercial equilibrium catalyst (E_{cat}). They varied the process variables, reactor temperature and reactor length. The operating temperature was also varied from 480 to 585^{o}C at reaction time between 8sec to 50min and a catalyst/oil ratio of 4: 1.The liquid product was subjected to GC/MS analysis; interestingly there was no evidence of ketones or aldehydes in the product mixture but the spectrum showed oxygenates (acid) and methyl ester (FAMEs). Not only was gasoline in large amounts (57 wt%) of aromatics and olefins formed, but also higher boiling-ranges of di-aromatics and tri-aromatics were distinctively present. The triglycerides were predominately converted within 50min between 485–585^{o}C into fatty acids through radical cracking reactions. They reported that the formation of radicals was enhanced by the presence of catalyst external surface as compared to thermal cracking. They therefore proposed a cracking mechanism for the conversion of the rapeseed oil to gasoline and diesel boiling-range as shown in Figure 2.10.

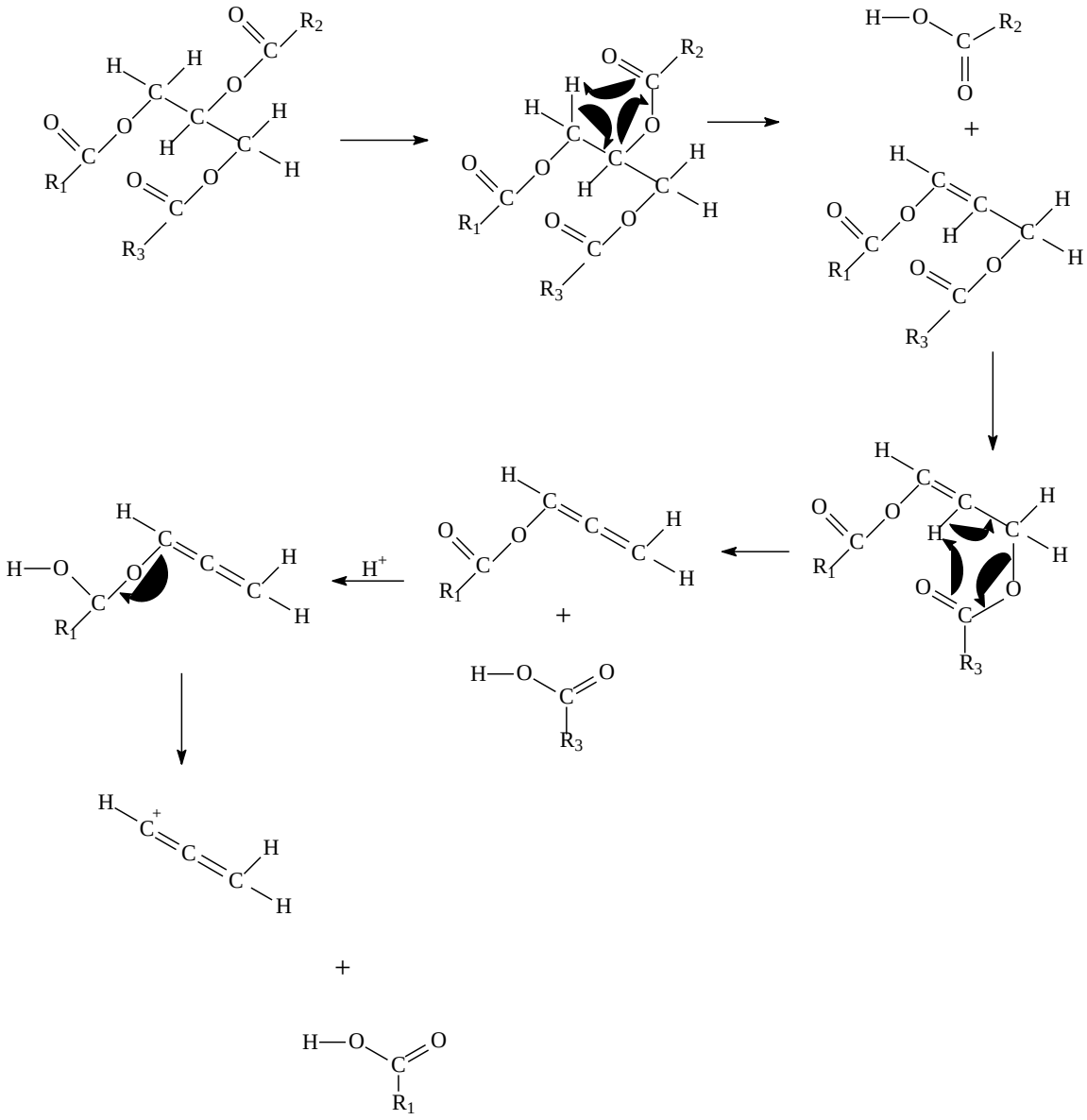

Figure 2.10: Proposed Mechanism for Catalytic Cracking of Rapeseed Oil (Dupain *et al.*, 2007)

In another study, Vonghia *et al*. (1995a) reported that triglyceride deoxygenation occurs via two mechanisms: γ-hydrogen transfer to produce alkenes and β-elimination to produce carboxylic acids and unsaturated glycol difatty acid esters (UGDEs). Their detailed mechanism of triglyceride deoxygenation is shown in Figure 2.11.

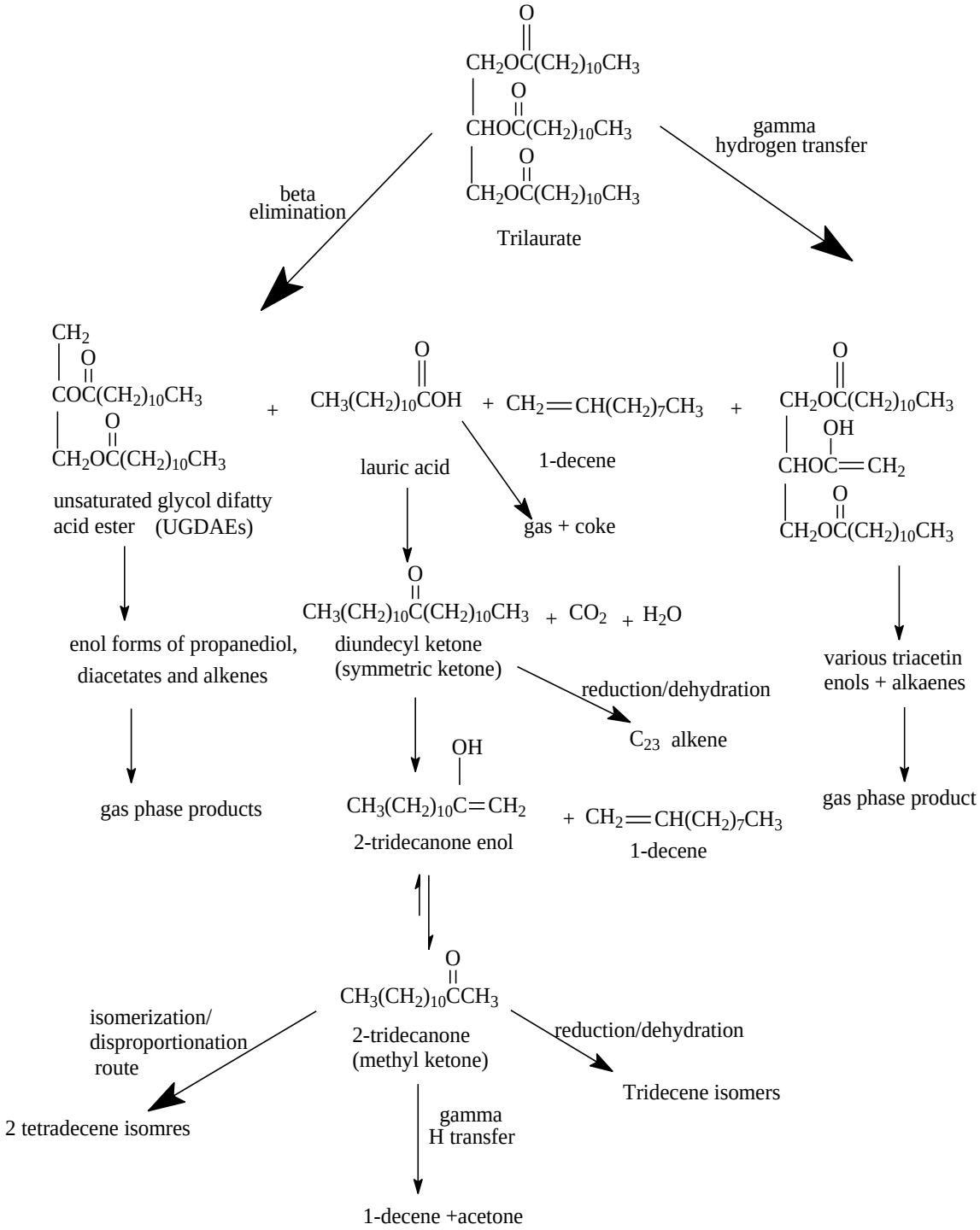

Figure 2.11: Proposed Pathway for Triglyceride Conversion

The radical conversion of the triglyceride into the fatty acid, which is a relatively fast and stepwise process, is reported as temperature dependent. Depending on the operating condition and catalyst acidity the six-membered transition-state can either crack or interact further into other products. However, they concluded that it is not known whether radicals are formed directly from the triglyceride molecule or from the formed

intermediate free fatty acids. Dandik and Aksoy (1998) reported that during catalytic pyrolysis, the decomposition of triglycerides to heavy oxygenated hydrocarbons as carboxylic acids (RCOOH), ketones (RCOR), aldehydes (RCHO) and esters (RCOOR) are dominant steps in the cracking reactions and begins at 240–300^{o}C.

Generally, in solid acid catalysis, the reactions often proceed via a carbocation intermediate. However, the presence of an acid site is required to form a carbocation intermediate. They are very reactive intermediates that rearrange to form more stable species. The order of their stability usually follows the trend below (Bartholomew and Farrauto, 2006):

- tertiary > secondary> primary
- allyl > alkyl

However, different feedstocks and catalysts may require different operating conditions, which could affect product quality and distribution. Therefore, when strong solid acids react with organic compounds, many different products can be created as a result of the type of intermediate formed. Hence, to produce the desired product in the highest possible yield, the catalyst properties need to be tuned for the specific reaction.

It is possible to control the product spectrum of catalytic cracking of vegetable oils to yield desired products if the chemistry, together with factors such as the choice of catalyst and reactor performance, are better understood (Huber *et al*., 2006). In order words, with the proper design of cracking catalysts, temperature and suitable oils, a desired biofuel can be produced. This is especially relevant for biodiesel, since the reaction temperature with the assistance of a catalyst determines product distribution (Taufiqurrahmi and Bhatia, 2011). Therefore, to produce the desired product at the highest possible yield, the catalyst must be designed in such a way so as to tune its catalytic properties to a specific reaction.

2.4 Catalysis

A catalyst is a chemical compound that increases the rate of chemical reactions which are thermodynamically feasible, yet the catalyst itself is not altered in any way at the end of the reaction. It can be defined simply as a reaction accelerant, which affects reaction products by enhancing the speed of one reaction pathway in favour of another.

Catalyst can be either a homogeneous base or acid or a heterogeneous base or acid. Heterogeneous catalysts provide a physical surface for reactants to come together. The following factors should be considered when choosing a catalyst for a particular task:

- Acid or base sites or both
- Acid/base site strength.
- Acid/base site concentration.
- Catalyst chemical composition.
- Catalyst morphology.
- Physical durability of the catalyst.
- Shape selectivity of the catalyst.
- Catalyst interaction with potential sources of de-activation.

The universal requirements for a catalyst in bio-renewable conversion to fuels, according to Miller and Jackson (2004), are the abilities to selectively remove excess oxygenate functionality from feedstocks, and form products with liquid or gas properties suitable for fuel utilization. The most commonly used catalysts for transesterification are homogeneous (NaOH and KOH). Homogeneous catalysts are said to be more active because their active sites are in the liquid phase and are capable of moving freely among the reactants. Meanwhile, the active sites of heterogeneous catalysts are confined to their surface, limiting the reactions according to the effect of internal mass transfer resistance (Nijhuis *et al*., 2002). Given the limitations associated with homogeneous catalysis, suitable heterogeneous catalysts are a matter of urgency for green chemistry, as emphasised by Corma and Garcia, (2003). The use of solid catalysts in industrial transesterification is generally preferable because they are more environmentally benign. Ideally, the chemical composition of the catalyst should remain unchanged subsequent to reactions that it has catalysed, and thus stable and effective heterogeneous acid catalysts are needed for the production of biodiesel.
However, physical or chemical changes may occur when either the protons or electrons used for catalytic action are removed.

2.4.1 Heterogeneous Cracking Catalysts

Heterogeneous catalysts provide significant advantages over their homogeneous counterparts mainly in terms of environmental, handling and disposal problems. Other

advantages include the reduced corrosion of equipment, catalyst regeneration, easier product separation, and a lower likelihood of the contamination of waste streams released into the environment. However, mass transfer resistance becomes critical when micro-porous catalysts are employed in organic reactions. Maher and Bressler (2007) reviewed the various catalysts used in the catalytic cracking of biomass and grouped them into four categories: transition metals, molecular sieves, activated alumina and sodium carbonate. Heterogeneous acid catalysts typically contain acid sites with different strengths of Brønsted and/or Lewis acidity. It is generally difficult to evaluate the relative importance of a given site in a reaction (Zhao *et al*., 1999). Several variables should be considered when choosing a catalyst for a particular task. A good catalyst must possess both high activity and long-term stability, but its single most important attribute is its selectivity. This is a reflection of its ability to direct the conversion of the reactant along one specific pathway.

2.4.1.1 Transition Metal Catalysts

Their catalytic properties are easily modified by sulphate loading, the addition of other supporting metal oxides, and other methods of preparation. This has made them of great interest in catalysis. They are traditionally used for hydro-processing in the heavy oil industry at high temperatures (350-500°C). Depending on the metal involved, when used in conventional refining processes the products include gases, alkanes, aromatics and diesel (Charusiri *et al*., 2006; Yadav and Nair, 1999b). They have also found wide application in the cracking of vegetable oil and animal fats (Thomas and Thomas, 2005).

2.4.1.2 Molecular Sieves

These are highly reactive and crystalline, porous, and exhibit size selectivity. They can be classified as micro-, meso- and macro- depending on the size of the pores which can be altered to obtain specific reaction products. One molecular sieve with wide application is zeolite, whose crystalline structure and tetrahedral shape offers significant advantages over amorphous silica–alumina catalysts. A typical example is HZSM-5, and a large number of studies have used this catalyst for the conversion of triglyceride oils and fats to hydrocarbons fuels (Twaiq *et al*., 2004; Twaiq *et al*., 1999; Katikaneni *et al*., 1996; Katikaneni *et al*., 1995b; Weisz *et al*., 1979). One of the first studies using HZSM-5 catalyst was by Weisz *et al*. (1979) to convert vegetable oils (corn and peanut oil) to hydrocarbons. The products were reported as: C_1 and C_2 gas, liquefied petroleum

gas (C_3 and C_4), gasoline, and light distillate (jet fuel, kerosene, or light diesel and heating oil). Tian *et al*. (2008a) monitored the catalytic cracking of palm oil and animal fats over a Co-Rh catalyst containing ultra-stable Y (USY) zeolite and LTB-2 with the ZSM-5 zeolite as the active component. The authors achieved 47% yields of olefins, 21% gasoline and high yields of liquid petroleum gas. When comparing molecular sieve catalysts, particularly zeolites, to metal oxides the former were found to give better product distribution and yield than metals because of their catalytic activity, which is a function of shape selectivity, acidity, porosity and surface area (Charusiri *et al*., 2006). However, they are quite expensive.

2.4.1.3 Activated Alumina

When pure these catalysts are not acidic and their main activity is dehydration. Alumina can exist in different forms depending on the method of preparation and treatment used. When activated, they are acidic and show high catalytic activity. A common example is activated γ-alumina, which is an effective catalyst for the decarboxylation of fatty acids at 450°C in atmospheric pressure. It has also been used in the production of alkanes and alkenes from sewage sludge containing triglycerides (Maher and Bressler, 2007; Billaud et al., 2001; Vonghia et al., 1995a). Kirszensztejn *et al*. (2009) investigated the use of alumina modified with boron oxide in the cracking of rapeseed oil. A mixture of water, carbon dioxide, hydrogen, aliphatic and aromatic hydrocarbons and a little liquefied natural gas (C_2-C_5) were produced. The major disadvantages of this catalyst are that: (i) the further treatment of the product via fractional distillation is required in order for the product to be suitable as fuel; (ii) it must be at moderate strength because most sites are buried in inaccessible locations; (iii) there is no shape selectivity and (iv) pore size is variable (Katikaneni *et al*., 1995a). Vonghia (1995b) studied the deoxygenation of triglycerides to aliphatic hydrocarbons (mainly monoalkenes) over activated alumina at 450^{o}C in a fixed bed tubular reactor. The intermediate products of the pyrolysis included methyl ketones, dodecyl aldehyde, and dodecanol. They concluded that the triglycerides can split out carboxylic acids by β-elimination or yield alkenes by a γ-hydrogen transfer mechanism.

2.4.1.4 Sodium Carbonate

Several studies have reported the use of sodium carbonate in cracking vegetable oil into liquid organic products (Dandik and Aksoy, 1998; Zaher and Taman, 1993; Konwer *et al*., 1989). Pyrolysis of used sunflower oil was studied by Dandik and Aksoy (1998) in a

packed column reactor of different lengths: 180, 360 and 540mm at temperature range of 400 to 420^{o}C in the presence of sodium carbonate catalyst with different percent (1, 5, 10 and 20) based on the oil weight. They had as high as 83% conversion with 10% catalyst in 180mm column reactor at 420^{o}C. The products of used oil consisted of gas and liquid hydrocarbons, carboxylic acids, CO, CO_2, H_2, and water. Increasing the catalyst and the temperature resulted in increased liquid hydrocarbon and gas products and decreased coke–residual oil. The major hydrocarbons in the liquid phase were C_5 – C_{11} with 36.4% yield. Konwer *et al* (1989) examined the effect of sodium carbonate on the pyrolytic conversion of fatty acids that are the principal constituents of Mesua-ferrea seed oil to hydrocarbons at 650^{o}C. The samples were collected at various boiling range fractions of petroleum hydrocarbon and analysed. Depending on the temperature the liquid product comprised of gasoline, kerosene and diesel fuel, but a possible concern with the use of sodium carbonate is that traces of sodium may be present in the product (Maher and Bressler, 2007).

2.4.1.5 Combined Catalysts

In some cases a mixture of different types of these catalysts are used to enhance product selectivity. Dupain *et al*. (2007) studied the catalytic cracking of rapeseed oil using a commercial equilibrium FCC catalyst (silica–alumina matrix with zeolite crystals). The catalysts were found to be effective. The presence of double bonds in the molecular structure of the feedstock enhanced the formation of aromatics in gasoline and light cycle oil (LCO).

Modified transition metal oxides have been found to be potentially active catalysts that could allow the same hydrocarbon conversion at lower temperatures than zeolites, when other operating conditions are similar (Charusiri *et al*., 2006; Idem *et al*., 1997). Despite this, current challenges include maximizing their efficiency by improving the pore size and stability.

2.5 Solid Acid Catalysts

These are of fundamental industrial importance because of their vital role in the petroleum industry where they are employed in various reactions to upgrade oil quality and chemical production. Over three hundred solid acid catalysts have been developed within the last 40 years (Tanabe and Yamaguchi, 1994). Silica-alumina gels were among the first kinds of solid acid catalyst to be used industrially for cracking hydrocarbons (Corma, 1997). Furthermore, they can be designed to give higher activity,

selectivity, and longer catalyst life. A review by Yamaguchi (1990) classified solid acid catalysts in three groups: (a) mounted acid, involving the fixation of a liquid acid such as SbF_5 on supports of high surface area; (b) combined acids of metal halides with metal salts; and (c) sulphate-promoted metal oxides. Solid acid catalysts can be designed to give increased activity and selectivity in terms of site type and concentration available for reaction. Thermal stability is another characteristic that must be considered in choosing a solid acid catalyst for catalytic cracking. In recent years there has been keen interest in using heterogeneous catalysts such as sulphated metal oxide catalysts.

2.5.1 Nature of Acid Sites:

To design a solid acid catalyst for optimum performance for a specific reaction, important features are the concentration, strength, and accessibility of the acid sites. The concentration of acid sites on the surface of a solid acid plays a vital role in controlling its catalytic activity and is commonly expressed as the number of mmol of acid sites per unit weight or per unit of surface area of the solid (Mikhail and Robens, 1983). It is, however, important that the acid sites should be accessible rather than necessarily being high in strength. This is because the rate of reaction depends on the rate of desorption of products from the acid sites on the catalyst, and in some cases increased acid site strength can produce unwanted side reactions (Rosenberg and Anderson, 2002). Solid acid catalysts are easily characterised by the presence of Brønsted and/or Lewis acid sites. The formation of Brønsted acid is given in Equation 2.1.

a) Brønsted Acidity

A Brønsted acid is a proton donor, which donates a proton to a Brønsted base to generate the conjugate acid.

$$H - A + : B \leftrightarrow A^- + HB^+ \qquad \text{Equation 2.1}$$

where:

A^- is the conjugate base of the acid HA and BH^+ is the conjugate acid of base B. For example, the Brønsted acid of HCl in water is H_3O^+, as shown in Equation 2.2. A polar hydrogen chloride molecule donates a proton and a water molecule accepts it.

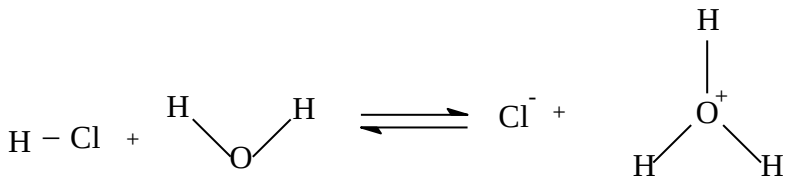

Equation 2.2

Acid Base Conjugate base Conjugate acid

When HCl loses/donates a proton a chloride ion is left which is regarded as the conjugate base. The water (H_2O) accepts/gains the proton to produce what is called the conjugate acid, H_3O^+. Typically Brønsted acidity can be formed in solid acids through: 1) exchangeable H^+ ions; and 2) exchangeable high charge-to-radius metal cations, as in Equation 2.3, which under conditions of limited hydration can hydrolyse water to H^{+4}.

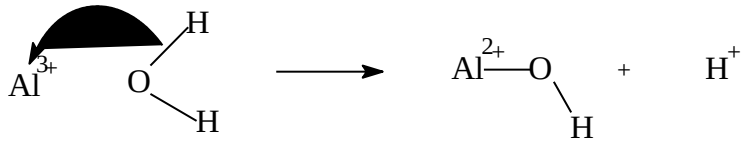

Equation 2.3

In this case the H^+ can further react with H_2O to form H_3O^+

b) Lewis Acid

A Lewis acid accepts an electron pair; that is, it must have a vacant, low-energy orbital. Most metal cations are Lewis acids since they can accept a pair of electrons when they form a bond with a base (see Equation 2.4).

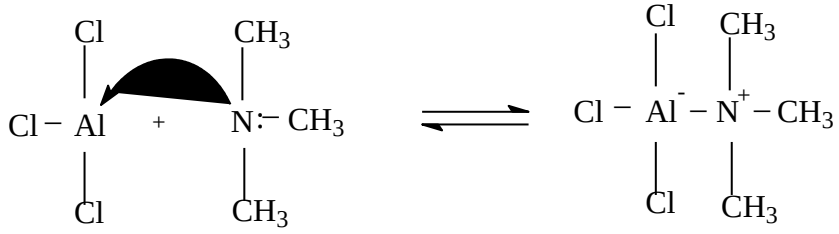

Equation 2.4

Lewis acid Lewis base

Given the acidic properties of heterogeneous solid acid catalysts, selectivity for any desired product can be achieved. Although many studies of different solid acid catalysts have been carried out, only a small number present data on their thermal stability. Among the few that do, sulphated zirconia has been found to be thermally stable for organic reactions, and it is well known for its super-acidity. However, the design of active solid acid catalysts which are environmentally benign in usage is a major challenge.

2.5.2 Surface Area of Heterogeneous Catalyst

The surface area of a catalyst is the only physical property which determines the extent of adsorption and catalytic reaction (Thomas and Thomas, 2005). The rate of product formation is a function of the available surface area of the catalyst. Support or promoter may be used to increase the surface area. The larger the surface area of a catalyst that is accessible to the reactants the greater the throughput. That is the amount of reactant converted to product per unit time per unit catalyst mass. If, on continuous use, the activity of a catalyst declines rapidly than any decrease in the surface area the catalyst is said to be poisoned (i. e. blockage of active sites). On the contrary, if the surface area reduces with reduced activity, then the catalyst is thermally deactivated. The pore structure is also important because it contributes to the total surface area; however, narrow pore structure limits reaction rate. The surface and pores of a catalyst are responsible for the catalytic reactions, and they must not be blocked so that the catalytic sites will be accessible to reactants.

2.6 Sulphated Zirconia

Zirconium (IV) oxide is a well known oxide with an extensive number of applications in industrial ceramics, and particularly in the catalysis area. Zirconia can exhibit difference phase transformation from one structure to another depending on temperature and pressure (Srinivasan *et al*., 1995). Addition of sulphate anions to zirconia plays an important role in stabilizing its structure by retarding the formation of oxo bonds between zirconium atoms and oxygen atoms. This prevents sintering at high temperature, and hence, prevents rapid phase transformation. Sulphated zirconia is zirconium oxide impregnated with sulphate from sulphuric acid or any sulphate source in order to enhance its acidity and thus its reactivity. Holm and Baily (1962) were the first to report that, when modified in the presence of sulphate groups and platinum crystallites, zirconia exhibited superior acidity (Song and Sayari, 1996). However,

detailed studies were not conducted until about twenty years later when it was discovered that sulphated zirconia (SZ) catalysts possessed acid sites that were stronger than those in zeolites as well as being stronger than 100% sulphuric acid. As a result they have frequently been defined as solid super-acids. Hino *et al*. (1979) found that sulphated zirconia can be an active solid acid catalyst for organic reactions at temperatures as low as room temperature. According to these authors, if properly treated with sulphuric acid or ammonium sulphate, sulphated zirconia exhibits an acidity of H_0 =16, which is 10^4 greater than that of 100% sulphuric acid by Hammet's indicator. However it is also reported to have a relatively small surface area, which tends to limit its application.

Efforts are being made to improve its catalytic and structural properties, one of which involves using it in its modified, sulphated form and preparation method. The presence of sulphates increases the thermal stability, as well as the active phase, of zirconia (Katada *et al*., 2000; Davis *et al*., 1994). Parvulescu *et al*. (1999) reported a direct correlation between sulphate loading and the chemical properties of sulphated zirconia catalyst. They also argued that strong acidity can be generated if the support is amorphous rather than crystalline. Parvulescu *et al*. (1999) and his group also identified that the pH and ammonia concentration under which its precursors are hydrolyzed determine the textural properties of the sulphated zirconia. This is in line with the findings of Davis *et al*. (1994), amongst other authors, who investigated and reported that the catalytic properties of sulphated zirconia are a strong function of its preparation method. Though sulphated zirconia was first reported by Hino *et al*. (1979) for isomerisation of n-butane at room temperature, it has been shown to be active in several other reactions including hydrocracking, alkylation, and isomerisation (Song and Sayari, 1996). It is also a reactive catalyst for long-chain hydrocarbons under mild conditions where other solid acid catalysts like zeolite will not be active (Permsubscul *et al.*, 2007; Charusiri and Vitidsant, 2005; Reddy *et al.*, 2005; Katada *et al.*, 2000; Davis *et al.*, 1994). Since its discovery as a strong solid acid catalyst, sulphated zirconia and its modified forms have found wide application in cracking (Dias *et al*., 2007; Sun *et al*., 2004; Zhou *et al*., 2003). It is known to possess the highest acidity amongst all known solid super-acids, though not all authors agree on its super acidic properties. Some claim that it is a Brønsted acid (Permsubscul *et al.*, 2007; Parvulescu *et al.*, 1999), while others claim it is a Lewis acid (Morterra *et al*., 1993a; Yamaguchi *et al*., 1987). Interestingly, Lunsford *et al*. (1994) and Waqif *et al*. (1992) reported evidence of the

existence of both Lewis and Brønsted acid sites on the surface of their prepared sulphated zirconia. Most recent studies agreed on the presence of Lewis as well as Brønsted acidity, especially for samples with high sulphate loading (Song and Sayari, 1996; Chen *et al*., 1993; Nascimento *et al*., 1993).

2.6.1 Acid sites on sulphated zirconia catalyst

Series of models have been postulated in order to resolve the controversy surrounding how sulphation enhances the surface acidity and the nature of the active sites. The first model of sulphated zirconia was proposed by Yamaguchi *et al*. (1986), where they claimed that only Lewis sites existed on the surface of the catalyst. Clearfield *et al*. (1994) proposed a dual Brønsted and Lewis model. Their model suggested that the uncalcined sulphated zirconia contains protons as bisulphate and a hydroxyl groups bridging the two zirconium ions. According to them, during calcination the water lost could result into two species (I and II), as shown in Figure 2.12. The Brønsted acid sites are formed as a result of the reaction of two adjacent hydroxyl groups. In both cases Lewis acid sites are formed as indicated by the asterisks. However in model I, the bisulphate remains intact.

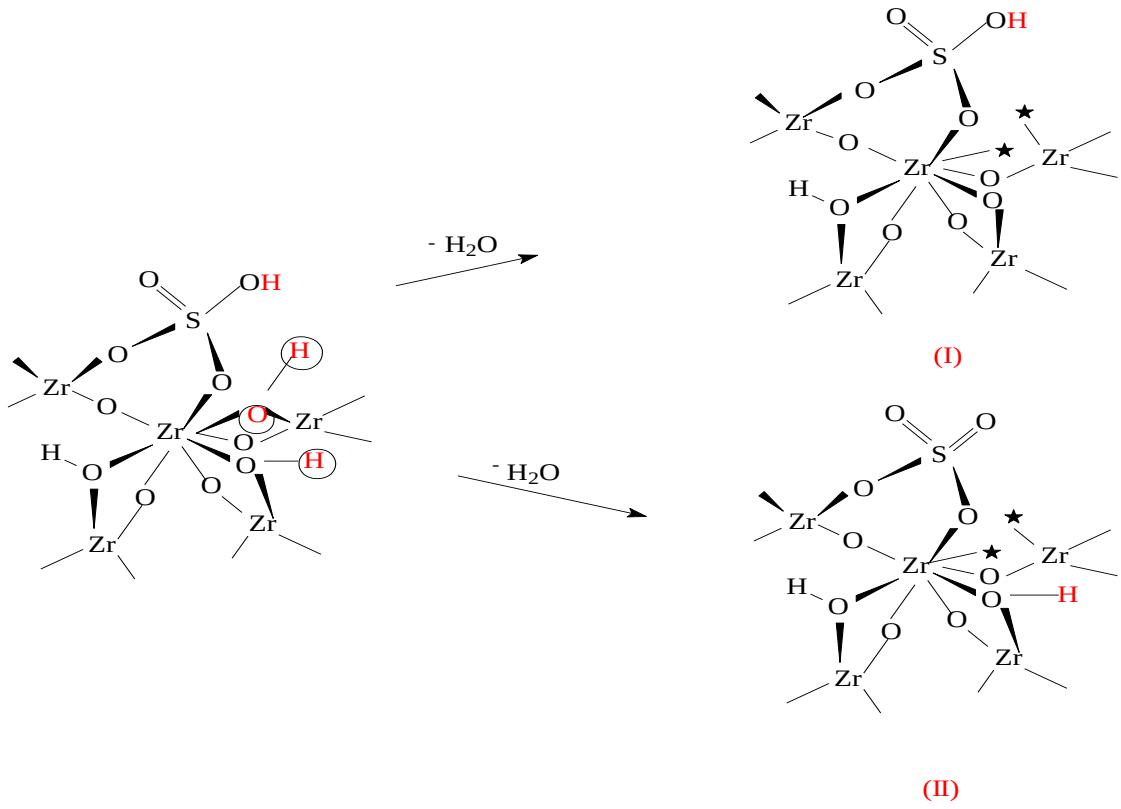

Figure 2.12: Postulated Structures of Acid Sites in Sulphated Zirconia (Clearfield *et al*., 1994)

Their assumption of Brønsted sites was based on the displacement of the bridge hydroxyl groups of hydrated zirconia as indicated by the circles. The Lewis acid sites are formed due to the reaction of the bisulphate ions with an adjacent hydroxyl group. These bisulphate groups act as highly acidic Brønsted sites since the neighbouring Lewis acid sites tend to withdraw electrons from the bisulphate group, thereby weakening the SO-H bond. The authors reported that the combination of the bisulphate with the adjacent Lewis acid sites is responsible for the strong acidity of sulphated zirconia. Many other models have been proposed including tridentate and disulphate (S_20_7). A slightly different model was proposed by Babou *et al*. (1995). They suggested that the protons of the sulphuric acid are trapped onto the surface of the zirconium hydroxide to form an ionic surface. The SO_4^{2-} ions are then adsorbed on the positively charged surfaces. According to their report, during drying at temperatures below 200°C the first water molecule is loss and at temperatures further than 200°C the second water molecule is eliminated with formation of a chemisorbed SO_3 group, see Figure 2.13.

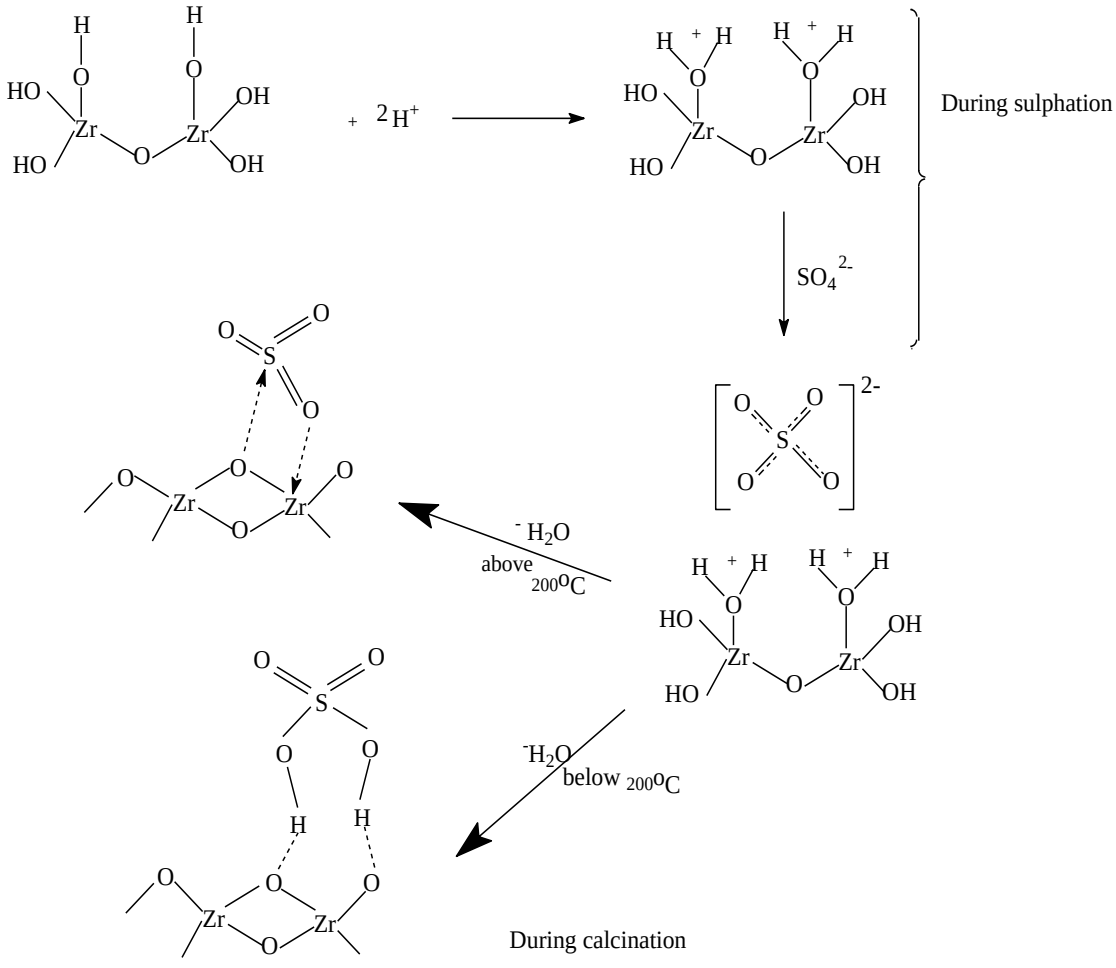

Figure 2.13: Model of Sulphated Zirconia Proposed by Babou *et al*. (1995)

However, Clearfield *et al*. (1994) models have gone a long way to explain the apparently contradictory results in the literature. For instance, concerning the nature of the acid sites, model I accounts for the presence of both Brønsted and Lewis acid sites. The location of the hydroxyl groups has also been an area of interest. Various models have the hydroxyl groups as part of the sulphate structure as shown in the Clearfield *et al.*(1994) model (shown earlier in Figure 2.12). Ward and Ko (1994) on the other hand attached the hydroxyl groups to the zirconia, placing them adjacent to the sulphate groups as shown in see Figure 2.14.

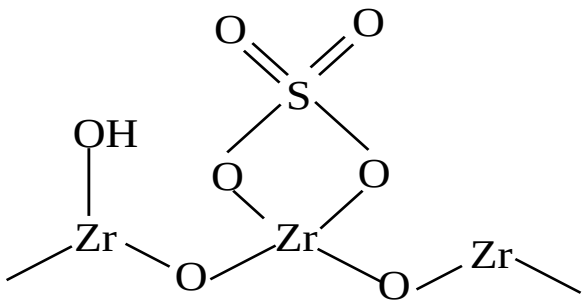

Figure 2.14: Model of Sulphated Zirconia Proposed by Ward and Ko (1994)

It therefore becomes clear that Brønsted and Lewis acid sites must both be present on sulphated zirconia catalyst in order to be regarded as a catalyst with super-acidity properties, as proposed earlier in a similar model by Arata and Hino (1990).

The type of acid site and other catalytic properties however, depend on the preparation method and activation procedure (Sun *et al*., 2005; Corma and Garcia, 1997; Song and Sayari, 1996; Morterra *et al*., 1993b). Therefore, a number of methods have been investigated for the preparation of SZ in terms of precursor type, supports, precipitating agents, type of sulphating agent, method of impregnation, and calcination temperature. Nevertheless, there is still no consensus on the correlation of SZ activity either with its sulphate nature and content, or its textural and structural properties. Therefore many studies have centred on the structural and catalytic properties of sulphated zirconia, as well as attempting to further improve its catalytic activity and stability.

2.6.2 Conventional sulphated zirconia

The preparation of sulphated zirconia has received considerable attention. Even though it has been extensively studied, the search continues for newer preparation methods that will further enhance its characteristics to achieve greater activity and selectivity.

Sulphated zirconia catalysts have typically been synthesized by inorganic wet chemistry techniques, such as precipitation, co-precipitation, sol-gel processes, hydrothermal synthesis or impregnation. The multiple steps involved in precipitation and co-precipitation methods pose the possibility of scarce reproducibility of the textural and, consequently, of the catalytic properties of the synthesized sulphated catalyst (Melada *et al*., 2004). In the case of sol–gel processes several parameters intervene in imposing the features of the catalyst, both concerning the ‘‘chemical’’ composition of the reacting mixture and also the temperature and time length of the hydrolysis-condensation steps involved (Melada *et al*., 2004). Wet impregnation a two-step procedure before calcination is the most common method, perhaps due to its simplicity. However, the catalyst support must meet certain criteria, such as tolerance to synthesis and reaction solvents, high surface area and good catalytic properties. Yadav and Nair (1999b) reported various different procedures that have been used to synthesize sulphated zirconia, as shown in Table 2.4. For example, Arata *et al*. (1990), Nascimiento *et al*. (1993) and Davis *et al*. (1994) reported preparation method, activation temperature, sulphate loading, and the moisture content of the catalyst as important factors in determining the activity of sulphated zirconia catalysts.

Table 2.4: Different conventional procedures for the preparation of SZ (Yadav and Nair, 1999b)

Starting material	Precipitating agent	Sulphating agent	Calcination temperature (°C)	Nature of phases[a]		Surface area (m^2/g)
$ZrOCl_2 \cdot 8H_2O/ZrO(NO_3)_2$	Liq. NH_3	$H_2SO_4/(NH_4)_2SO_4$	350	M	A	-
			650	M	T	-
	Urea	$H_2SO_4/(NH_4)_2SO_4$	850	M	T +M	-
$ZrCl_4$	Liq. NH_3	$H_2SO_4/(NH_4)_2SO_4$	200	A	A	241
			400	M	A +C	115
		SO_2, SO_3, CS_2	600	M +C	A +C	19.6
$ZrOCl_2 \cdot 8H_2O$	Liq. NH_3	H_2SO_4	650	T		34

A: amorphous; M: monoclinic; C: cubic; T: tetragonal.

For instance, at a calcination temperature of 500-650^{o}C in air or oxygen, Tanabe (1994) reported a crystallographic phase change from amorphous to tetragonal. The active

crystalline phase of conventional sulphated zirconia was reported to be the tetragonal phase. It forms when the catalyst was calcined between 500°C and 700°C, while the monoclinic phase appears at 800^{o}C (Song and Sayari, 1996).

2.6.3 Modified sulphated zirconia

Conventional sulphated zirconia catalyst is micro-porous with a relatively small surface area, Lewis acid sites, and prone to sulphate leaching. Hence, various modifications have been investigated to improve these properties. A variety of other novel methods of preparation have also been reported. For instance, Yadav and Murkute (2004) used chlorosulphonic acid dissolved in an organic solvent as a precursor, rather than the conventional sulphuric acid. This resulted in sulphated zirconia with a higher sulphate loading and increased resistance to leaching. It was found to exhibit higher catalytic activity for the esterification of *p-tert*-butylcyclohexanol with acetic acid than the conventionally prepared sulphated zirconia. Structural properties, such as meso-pores and morphology, were also enhanced when Yi *et al*. (2005) used zirconium nitrate and ammonium sulphate in an alcohol medium at a 120^{o}C in a one-step method. The resulting catalyst was tested and found to be much more active in the isomerisation of n-butane.

The properties of catalysts have often been improved by the addition of other metals. Zhu *et al*. (2004) demonstrated this by modifying sulphated zirconia with silica in sol–gel preparation in the presence of a cross-linking agent, triethoxysilane. The catalyst was dried at room temperature for two days, heated at 50°C for 5h, and then to 550°C at a rate of 10°C/h, prior to calcination at 550°C for 3h. The modified catalyst exhibited superior catalytic activity compared to zeolites Y, β, and ZSM-5 in the alkylation of isobutane with 1-butene. Mesoporous sulphated zirconia with 2.0 to 4.0nm pores was prepared by McIntosh and Kydd (2000) using amine templates (neutral templating method). The neutral templating method, involves the use of long-chain primary alkyl amines as the template. The approach was based on hydrogen bonding and self-assembly between the neutral primary amine micelles and neutral inorganic pre-cursors. The template could be removed by ethanol extraction, due to the weaker interactions between it and the inorganic framework. They demonstrated that material with larger pores was significantly more active in the alkylation reaction of *p*-xylene with cyclohexene. Silica has been found to be a good support for sulphated zirconia. Chen *et al*. (2007) synthesized sulphated zirconia on silica SBA-15, and its catalytic

performance in the esterification of long-chain lauric and palmitic free fatty acids was investigated. Their findings on the effect of preparation on conversion agreed with those of Hino *et al*. (2006). In another report, Akkari *et al*. (2008) modified sulphated zirconia by grafting silica onto the surface using the aerogel technique, in order to examine the influence of the preparation parameters on the physicochemical properties of the catalysts in the isomerisation reaction of n-butane. A recent review by Arumugam *et al*. (2009) reported different levels of activity of sulphated zirconia and its modified forms depending on the method of preparations. In general, a significant challenge for studies of the catalytic cracking of renewable feedstocks is the design of solid acid catalysts to selectively alter the functionality at specific molecular sites. This would make the manufacture of a wide variety of products possible, ranging from slightly modified to fully deoxygenated chemicals and fuels based on existing feedstocks and infrastructure.

2.7 Characterization of Catalyst

Numerous techniques are used for characterization. In this research they included: X-ray diffraction (XRD), Fourier transform infrared spectroscopy (FTIR), nitrogen adsorption and desorption for surface area (BET) and Pyridine- DRIFTS (Diffuse Reflectance lnfrared Fourier Transform Spectroscopy) for the measurements of the acidity, X-ray photoelectron spectroscopy (XPS) and EDX (Energy Dispersive X-ray).

2.7.1 X-ray Diffraction (XRDP)

X-ray diffraction is a characterization technique used to obtain the X-ray diffraction pattern of a catalyst. The technique is based on the fact that each compound in the catalyst produces a different diffractogram pattern. When a beam of x-rays comes into contact with a solid they are scattered by the electron clouds. A crystal lattice is usually made up of a regular pattern of atoms and planes which are separated by the same distance. When x-rays are reflected from successive planes of atoms, interference can occur which may be either constructive or destructive. When the interference is constructive a diffracted beam is produced, as shown in Figure 2.15.

.

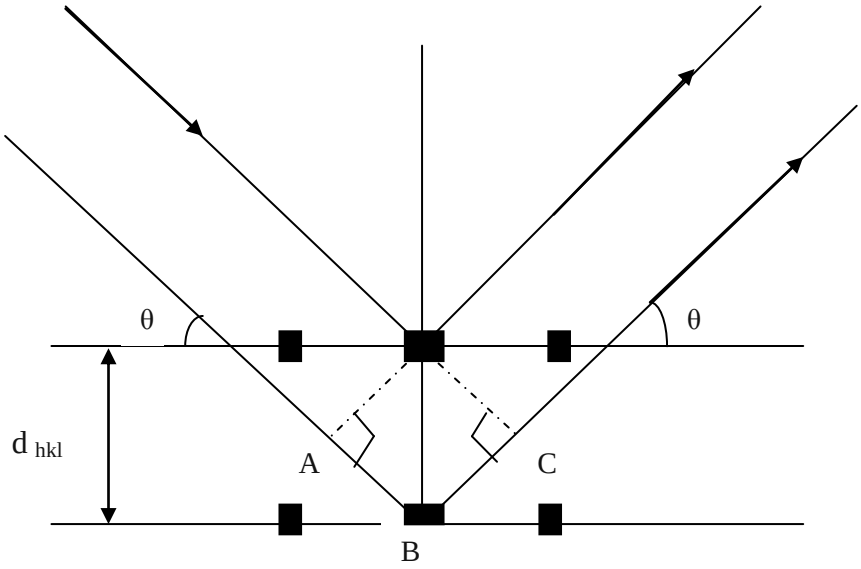

Figure 2.15: Scattering of X-Rays from a Parallel Set of Planes.

In XRPD a powdered sample rather than a single crystal is examined. A powdered sample contains an enormous number of small crystallites which will randomly adopt the whole range of possible orientations. Hence, when an X-ray beam strikes a powdered sample, it is diffracted in all directions (according to Bragg equation) resulting in diffraction cones. Each of these cones is a set of closely spaced dots, and each dot corresponds to the diffraction from a single crystallite within the sample. The catalyst phases can usually be determined by comparing the intensity of a number of particular peaks to the intensity of the same peaks obtained from standard samples or simulated XRD. The overall diffraction pattern is usually a plot of the intensity of reflection versus angle of diffraction, *2θ*, which satisfies the Bragg equation, Equation 2.5, and is characteristic of a particular crystalline material.

$$n\lambda = 2dsin\theta \qquad \text{Equation 2.5}$$

where:

n is an integer number, i. e. the order of diffraction

λ is the wavelength of the beam,

d is the interplanar spacing and

θ is the diffraction angle

When the x-rays interact with the planes of atoms in the three-dimensional lattice, diffraction occurs from parallel sets of equally spaced planes. Each set of the planes is described by the indices h, k, and l. The spacing for the sets of planes (d) differ so that each set gives rise to a reflection at a characteristic angle theta (θ) according to the Bragg equation. The overall diffraction pattern is determined by a plot of intensity of reflection against 2θ, and is characteristic of a particular crystalline material.

2.7.2 Hammett indicators - titration methods

The characterisation of the surface acidity of a catalyst involves measuring the acid site concentration, strength, and accessibility. For homogeneous catalysts this is relatively straightforward, and a simple pH scale can be used. However, this is not the case for solid acid catalysts, as the acid sites are located on the surface. Furthermore the acid strength is not simply a function of proton concentration. The pH scale is based on the assumption that the strength of individual H_3O^+ ions is fixed, as expressed in Equation 2.6:

$$pH = \log [H_3O^+]/[H^+]$$

or

$$pH = -\log a_{H+} \qquad \text{Equation 2.6}$$

where:

a_{H+} is the activity of H^+.

The main limitation of the pH method is that for highly concentrated aqueous acids, the possibility that the acid is fully dissociated and no longer exists in aqueous solution must be considered. There are various methods available for determining the acidity of a catalyst.

The Hammett indicator scale expresses the acidity of concentrated acids or non-aqueous systems. The Hammett acidity function (H_o) is an extension of the pH scale and is related to the degree of transformation of a weakly basic indicator B to its conjugate acid form BH^+, which defines the Brønsted acid strength. The equilibrium for the indicator is given below Equation 2.7:

$$BH^+ \rightleftharpoons H^+ + B$$ Equation 2.7

The equilibrium constant K_{BH+} is given as shown Equation 2.8

$$H_o = pK_{BH+} - \log\frac{C_{BH+}}{C_B}$$ Equation 2.8

where:

C_B is the concentration of the indicator conjugate, (mmol/g)

C_{BH+} is the concentration of the conjugate acid of the indicator (mmol/g)

pK_{BH+} is a measure of the strength of the conjugate acid, BH^+, of base B. It is a measure of the readiness with which BH^+ will lose a proton. Therefore the smaller the numerical value, the stronger the acidity of BH^+ and the weaker B is as a base.

This method has certain limitations, and one difficulty is in visually determining the colour change, especially with dark catalysts. Water can also be a contaminant, as it competes with the indicator for the acid sites. It is also not suitable for solid catalysts with very small pores where the indicator molecules may be unable to penetrate. Furthermore, the method gives only the sum of Brønsted and Lewis acid sites and not separate values for each.

2.7.3 Vibration spectroscopy methods

Raman and Infrared (IR) spectroscopy have often been used to investigate the acidity of solid acids (Katada *et al*., 1997). IR is a powerful technique, especially for revealing the numbers of hydroxyl groups present either directly or through adsorbed probe molecules. The frequencies of molecular vibrations lie within the infrared region of the spectrum (4000-400cm^{-1}). The infrared spectra of solids are usually complex with a large number of peaks, each corresponding to a molecular vibration. However, only vibrations giving rise to a change in dipole moment are observed in infrared spectroscopy . Therefore it is possible to identify species by their infrared spectra.

Furthermore, the acid type on heterogeneous catalyst is best determined by infrared spectroscopy of adsorbed pyridine on the catalyst. This is because the interactions of pyridine can be sensitively detected by monitoring the ring vibration modes. This is via

the nitrogen lone-pair electrons with aprotic (Lewis) and protonic (Brønsted) acid sites. Adeeva *et al.* (1995) proposed a complex surface on which Brønsted and Lewis acid sites are in close proximity, as shown below in Figure 2.16:

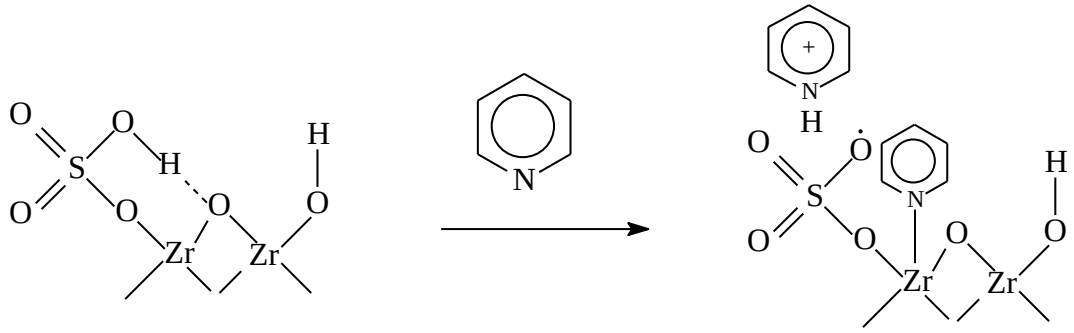

Figure 2.16: Pyridine on Sulphated Zirconia indicating Brønsted and Lewis Sites (Adeeva *et al.,* 1995)

In principle, the concentration of hydroxyl groups is equivalent to the concentration of Brønsted acid sites and can be determined from the corresponding IR bands, where the frequency of -OH bonds is inversely proportional to acid strength. IR bands for adsorbed pyridine are in the region 1400–1700cm^{-1}. Data from this region provide valuable information about the nature of the hydroxyl group. An important feature of IR spectroscopy is that it provides distinct bands for pyridine at Lewis acid and Brønsted acid sites. An estimate of the acid strength distribution profile is possible if IR is combined with temperature programmed desorption (TPD). Pyridine and ammonia have been widely used as probe molecules, but pyridine is preferred because it is weaker than ammonia (pK_b of pyridine is ~9 compared to ~5 for ammonia) so it is less likely to react with weak acid on the catalyst (Rosenberg and Anderson, 2002)**.** However, there must not be an excessive amount of water on the catalyst, because this would pose problems with the infrared spectrum in this region. Therefore the catalysts to be examined must be thoroughly dried and maintained in a dry state throughout the process of spectrum acquisition.

The vibration of the hydroxyl group is associated with Brønsted acidity on the catalyst, and the calculation of the number of Brønsted and/or Lewis acid sites on the catalyst is usually determined using Equation 2.9.

$$Nt = \left[\frac{B(cm-1)\times A\,(cm2)}{\varepsilon b(cm\mu mol-1)\times m(g)} + \frac{L\,(cm-1)\times A\,(cm2)}{\varepsilon l(cm\mu mol-1)\times m\,(g)}\right] \times 1000 \qquad \text{Equation 2.9}$$

where:

N_t is the total number of micromoles of pyridine per gram of the sample adsorbed, (mmol/g)

B and *L* are the integrated absorbance of the IR bands that are due to pyridine adsorbed at Brønsted and Lewis sites respectively

A is the cross sectional area of the pressed disc

m is the mass of the pressed disc

ε_b and ε_l are the molar absorption coefficients for pyridine at Brønsted and Lewis sites respectively.

2.7.4 X-ray Photoelectron Spectroscopy (XPS)

The XPS technique is based on the properties of photoelectrons emitted from a sample on irradiation with X-rays as shown in Figure 2.17. The principle involves the precise measurement of the kinetic energy of these emitted electrons which is characteristic of both the electron energy level from which it originated and the energy of the incident radiation. Photoelectrons can be emitted from valence electrons (those which take part in chemical bonding) and from core energy levels (those not involved in chemical bonding). The basic mechanism behind an XPS instrument is the use of photons of a specific energy to excite the electronic states of atoms below the surface of the sample.

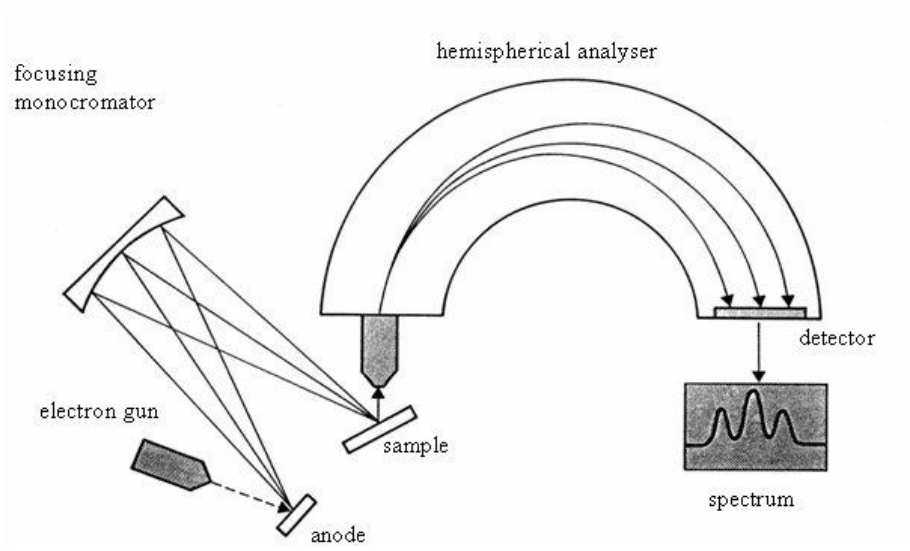

Figure 2.17: Schematic Diagram of an X-ray Photoelectron Spectrometer with Monochromator

Those photoelectrons that are emitted from core levels have kinetic energies which are characteristic of the atoms from which they originated. However, small changes do occur in the detected binding energies (chemical shifts), and these changes depend on the chemical environment of these atoms. Valuable information concerning the chemical characteristics of a sample under investigation can be gathered from the chemical shift data. XPS is used in this research to study the effect of sulphate species on the acidity of the catalyst by measuring the kinetic energy of photoelectrons emitted from the surface atoms after the X-ray irradiation of the uppermost atomic layers of the catalyst. A typical XP spectrometer is shown in Figure 2.18

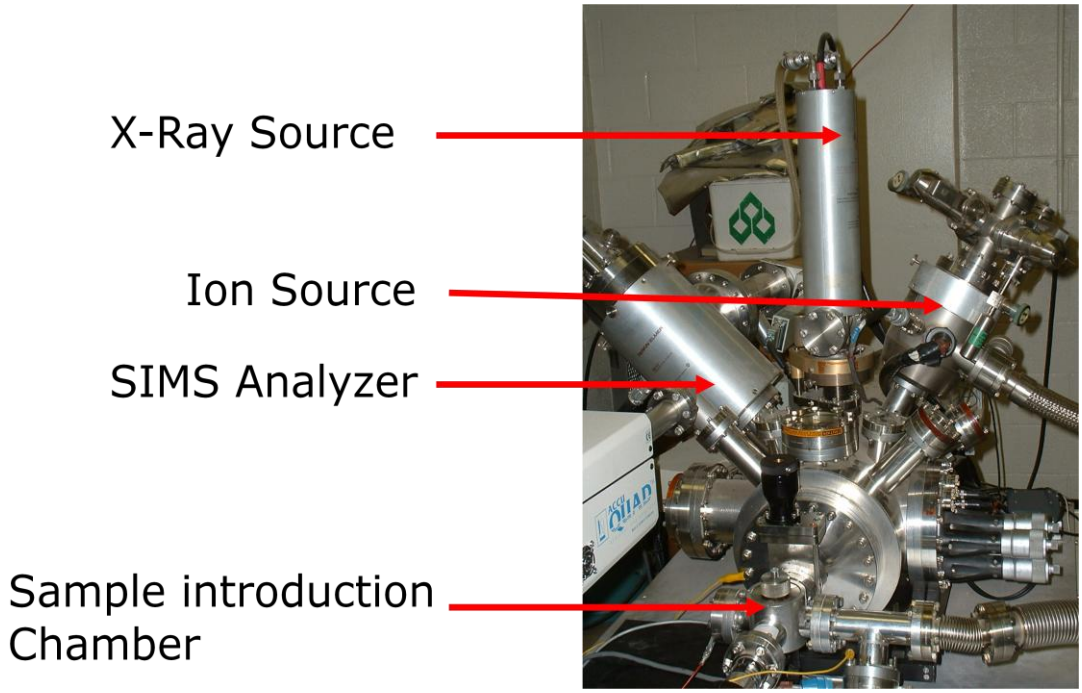

Figure 2.18: Kratos Analytical X-ray Photoelectron Spectrometer (courtesy NEXUS, Newcastle University UK)

XPS can also be used to characterize surface acid sites, particularly for determining the acidity of solid acid catalysts that are opaque to IR irradiation. The only problem with using this technique for acid site determination is the requirement of a vacuum therefore, the technique is best for the determination of sulphate species.

2.7.5 Nitrogen adsorption and adsorption isotherms

The quantity of gas taken up by a solid sample is proportional to the mass (m) of the sample, the temperature (T), the pressure (p) of the gas as well as the nature of both the solid and the gas. The adsorption isotherm is a graph reflecting the amount of adsorbed gas against pressure or relative pressure at constant temperature. It is usually expressed as the amount of adsorbate per gram (or volume) of adsorbent to each equilibrium pressure of the gas at a constant temperature. Adsorption isotherms are used to measure the specific surface area of a solid, the size of pores in a porous solid and their distribution if not uniformly distributed. Liquid nitrogen is most often used rather than other inert gases, so the technique is usually known as nitrogen adsorption. The general principle involves increasing the pressure of nitrogen at equilibrium with the adsorbent from zero to its saturated vapour pressure, which for N_2 is conducted at -196 °C and a saturated vapour pressure of 1.0 atm. The concept involved is an extension of Langmuir theory, it is the simplest, most commonly used model for interpreting

adsorption isotherms, and is based on monolayer molecular adsorption with three hypotheses:

a) Gas adsorption on the solid surface cannot proceed beyond monolayer coverage, and only one adsorbate molecule occupies each surface site.
b) The energy for adsorption and the ability of the molecule to adsorb is independent of the number of the surrounding sites that are occupied, and
c) The surface is uniform and adsorption sites are equivalent

An adsorption isotherm is constructed by plotting the amount of nitrogen adsorbed against relative pressure, (*p/po*), where *po* is the saturated vapour pressure. There are six main types of isotherm known for adsorption systems, as shown in Figure 2.19. Each adsorption system has its own characteristic adsorption isotherm, most of which can be classified into one of six categories.

1. *Type I* isotherms the amount adsorbed increases steadily with pressure until it reaches a plateau at $\theta = 1$. At this point it is believed that all sites are populated by the adsorbate, which is true for micro-porous solids.
2. *Type II* isotherms the monolayer plateau region is reached at point B. However there is a further increase in the amount adsorbed and many layers are ultimately adsorbed as $p/po = 1$ is approached. This type of isotherm is associated mainly with non-porous solids.
3. *Type III* isotherms are characteristic of weak gas-solid interactions usually associated with multilayer formation. The isotherm lies convex to the x-axis (*p/po)* and does not exhibit a point B. An example of this type is the adsorption of nitrogen on polyethylene.
4. A *type IV* isotherm follows the same shape as type II isotherm in the low-pressure region. At a certain point it begins to deviate upwards, until at higher pressures the slope begins to decrease. As the saturation vapour pressure is approached, the amount adsorbed shows little variation. The characteristic feature of type IV isotherm is its hysteresis loop, which is associated with evaporation and condensation in meso-porous material as commonly found in catalysts. The shape of the hysteresis curve often indicates the size and type of pore in the catalyst.
5. The *type V* isotherm is uncommon and has the same shape as a Type III isotherm in that the adsorbent-adsorbate interaction is weak.

6. The *type VI* isotherms represent a stepwise multilayer adsorption on uniform non-porous surfaces, and are indicative of adsorption on homogenous and non-porous surfaces such as graphitised carbon black at liquid nitrogen temperature.

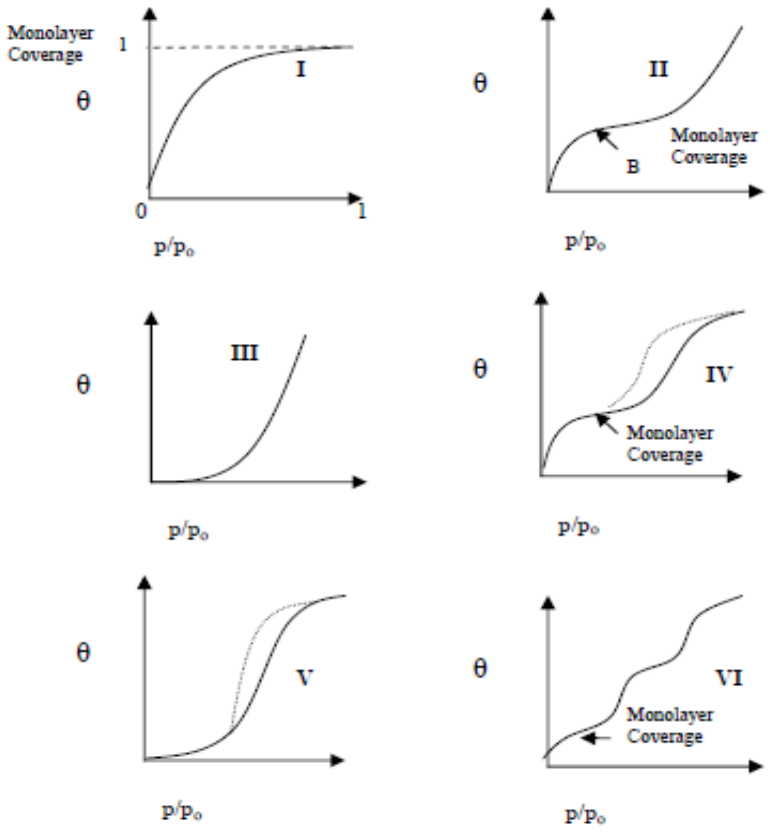

Figure 2.19: Six Main Types of Isotherm Classification according to the IUPAC.

θ = Fraction of surface sites occupied by adsorbate
p = Pressure
po = Standard pressure (equal to saturated vapour pressure of the adsorbate)
——— Adsorption branch
- - - - - - Desorption branch

Calculation of surface area based on the Langmuir equation assumes adsorption is limited to one monolayer of adsorbate. However, in some cases there is need to account for multilayer of adsorbate; as seen in Type II and Type IV isotherms, where instead of the isotherm levelling off to a saturated value at high pressures, it rises beyond it. The most widely used isotherm dealing with multilayer and determination of surface areas of porous materials is the BET adsorption theory. In addition to the Langmuir major assumptions, BET model assumed the following:

1. Unrestricted multilayer formation may take place.
2. Only the uppermost layers of molecules in the multilayer system are in dynamic equilibrium with the vapour.
3. Enthalpies of adsorption of the second and higher layers are equal to the enthalpy of condensation.
4. Desorption can only occur from the uppermost exposed layer

The interpretation of adsorption isotherms is usually based on two main theories, Langmuir adsorption theory (Equation 2.10, below) and Brunauer-Emmett-Teller (BET) adsorption theory (Equation 2.11):

$$\frac{P_a}{V} = \frac{P_a}{V_m} + \frac{1}{KV_m} \qquad \text{Equation 2.10}$$

where:

A plot of P_a/V against P_a gives a straight line of slope $1/V_m$ and an intercept of $1/KV_m$

$$\frac{P}{V\,(Po - P)} = \frac{1}{V_m\, c} + \frac{(c-1)}{V_{mc}} \times \frac{P}{Po} \qquad \text{Equation 2.11}$$

where,

P and *P*o are the equilibrium and saturation pressure of adsorbates at the temperature of adsorption

V is the volume adsorbed at P (cm^3)

V_m is the volume adsorbed at monolayer coverage (cm^3/g)

C is the BET constant.

A plot of *P*/*V*(*P*o-*P*) against *P*/*P*o gives a gradient (*C*-1)/(*Vm*C), and an intercept 1/(*VmC*). From these, V_m can be calculated. The BET isotherm is widely used to determine surface area, at relative pressure of *p/po* = 0.05-0.30 since it does not work at all pressures.

2.7.6 Environmental scanning electron microscope (ESEM) and Energy Dispersive X-ray (EDX)

ESEM is an acronym for Environmental Scanning Electron Microscope. In this technique a gaseous environment can be used, whereas other conventional scanning electron microscope techniques operate in vacuums. Electrically non-conductive specimens do not require preparation techniques (such as the deposition of a thin gold or carbon coating or other treatments) to render the surface conductive, as in SEM. A prototype is shown in Figure 2.20, and its principle of operation is to employ a scanning electron beam, where electromagnetic lenses are used in focusing and directing beams on the specimen surface in the same way as in the conventional scanning electron microscope.

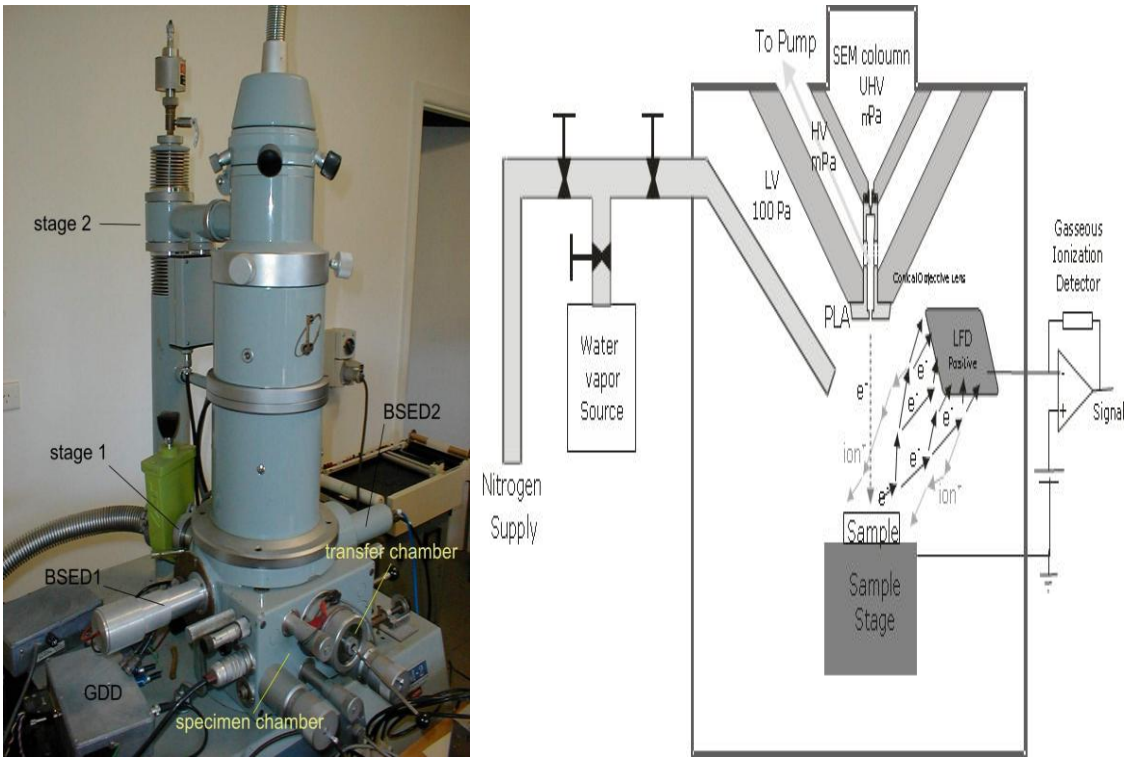

Figure 2.20: A Prototype and Schematic of an ESEM (Stokes, 2008)

The ESEM has specialized electron detectors and differential pumping systems that allow the transfer of the electron beam from high vacuum in the gun area to the high pressures attainable in its specimen chamber. It is suitable for imaging specimens in their natural state. The beam electrons interact with the specimen surface layer to produce various signals which give information about the specimen that is collected with appropriate detectors. The beam electrons interact with the specimen surface layer

to produce various signals which give information about the specimen that is collected with appropriate detectors.

Energy-dispersive X-ray spectroscopy (EDX) is an analytical technique used in conjunction with ESEM, but it is not a surface science technique, but is rather used for the elemental analysis of the chemical composition of the sample. It operates on the interaction of x-ray excitation on the sample. To stimulate the emission of characteristic X-rays from a specimen, a high-energy beam of charged particles such as electrons or protons is focused on the sample. The incident beam could excite an electron in an inner shell, ejecting the electron from the shell and thereby creating an electron hole, which is usually filled by an electron from an outer higher-energy shell. The difference in energy between the higher-energy shell and the lower shell is released in the form of an X-ray photon. The number and energy of the X-rays emitted from the specimen are measured by an energy-dispersive spectrometer, allowing the elemental composition of the specimen to be determined.

2.8 Liquid Product Characterization

Various types of equipment and different methods can be used in analysing biodiesel in the liquid mixture, but only those relevant to this study are discussed here. These include gas chromatography (GC), gas chromatography-mass spectroscopy (GC-MS), and titration. The water content was determined by Karl Fischer Titration.

2.8.1 Gas chromatography (GC)

Gas chromatography is a technique illustrated in Figure 2.21 that is used to separate mixtures of gases or liquid. A small micron (~1µl) of the sample is injected through the injector port onto the column; where it is vaporized and allowed to move slowly through the column by the flow of inert gas. The column itself can be a packed or capillary type which contains a liquid stationary phase which is adsorbed onto the surface of an inert solid. The carrier gas, usually N_2, He, or CO_2, must be chemically inert.

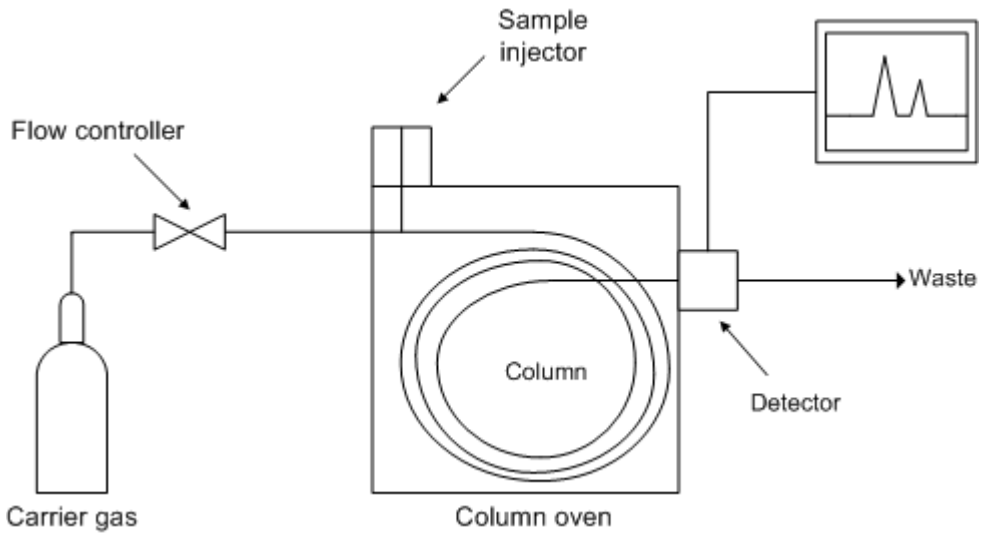

Figure 2.21: Schematic Diagram of Gas Chromatography (extracted from Prichard and Stuart (2003)

There are several types of detectors, but the flame ionization detector is used for most organic samples. The effluent from the column is ignited after having been mixed with hydrogen and air to produce ions and electrons that are capable of conducting electricity through the flame. The resulting current is measured by the recorder. The components of the mixture are recorded as a sequence of peaks as they leave the column. Each component reaches the detector at a characteristic time, known as its "retention time". The area under the peaks is proportional to the amount of each component in the sample.

2.8.2 Gas chromatography-mass spectrometry (GC-MS)

This is a combination of two techniques to form a single method used for analysing mixtures of chemicals, as shown in Figure 2.22. The gas chromatography separates the components in the mixture using the principle explained in section 2.8.1 while the mass spectroscopy characterizes each of the components individually. As the individual compounds elute from the GC column, they enter the electron ionization detector in the mass spectroscopy, from where they are bombarded with a stream of electrons causing them to break apart into fragments.

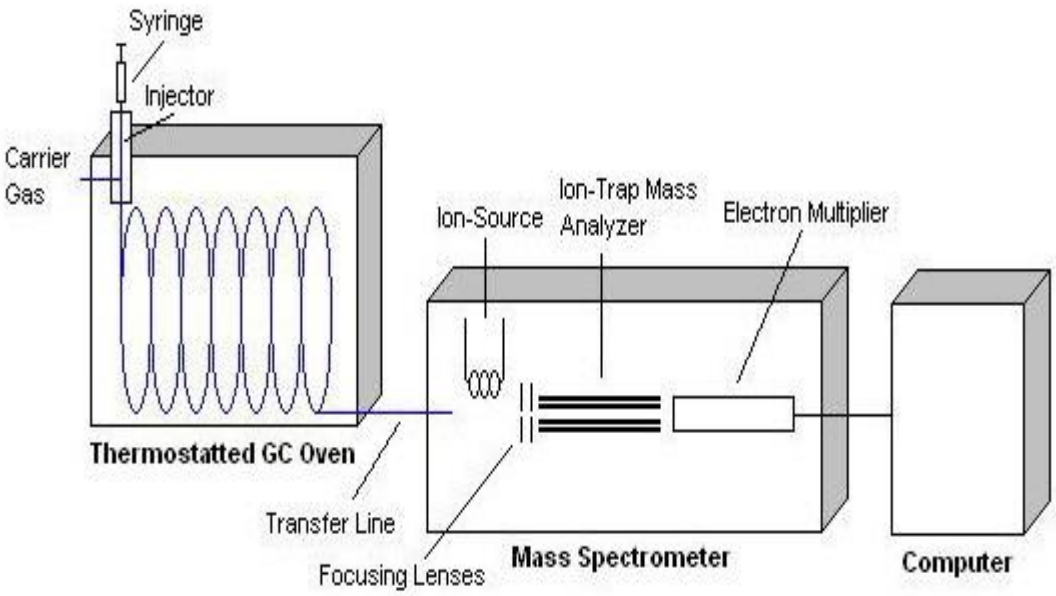

Figure 2.22: Schematic Diagram of a GC-MS (extracted from De Hoffmann and Stroobant (2007)

The fragments are measured in terms of their mass–to-charge ratio (m/z) but most fragments have a charge of 1^+, and therefore m/z usually represents the molecular weight of the fragment.

2.8.3 Karl Fischer titration

Karl Fischer titration is an analytical method widely used to determine trace amounts of water content in substances. Its principle is based on the quantitative reaction of water with iodine and sulphur dioxide in the presence of a lower alcohol such as methanol and an organic base such as pyridine. The popularity of the Karl Fischer titration lies in its several practical advantages over other methods of moisture determination. These include:

- High accuracy and precision
- Selectivity for water
- Small quantity of sample required
- Ease of preparation of sample
- Short duration of analysis
- It can measure a nearly unlimited range of levels of water (from 1ppm to 100%)
- It is suitable for the analysis of solids, liquids and gases
- It operates independently of the presence of other volatile compounds in the sample

The Karl Fischer titration cell consists of an anode solution of alcohol, sulphur dioxide and iodine, and a cathode immersed in the solution. However, the anode and cathode are separated by an ion-permeable membrane. Alcohols such as diethylene glycol monoethyl ether can also be used in place of methanol. The two determination methods are volumetric titration and coulometric titration. In the latter, the sample to be analysed is added to the pyridine-free Karl Fischer reagent, whose principal components are iodine ions and sulphur dioxide. Its fundamental principle is based on the Bunsen reaction between iodine and sulphur dioxide in an aqueous medium shown below in Equation 2.12:

$$I_2 + SO_2 + 2H_2O \rightarrow 2HI + H_2SO_4 \qquad \text{Equation 2.12}$$

The iodine is generated electrolytically at the anode and it reacts with water in the sample. The amount of iodine generated is in direct proportion to the quantity of electricity, according to Faraday's Law. A mole of iodine is said to react quantitatively with one mole of water. Based on this principle, the water content in the sample can be determined directly from the quantity of electricity required for electrolysis. Volumetric titration is based on the same principles, except that the anode solution is used as the titrant solution. In this case the iodine is added mechanically to a solvent by the titrator's burette during titration. The volumetric titrator usually performs three key functions:

1.) Dispensing the KF titrating reagent which contains iodine into the cell using the burette;

2.) Detecting the endpoint of the titration with the aid of the double platinum pin indicator electrode

3.) Calculating the end result using the on-board microprocessor based on the volume of KF reagent dispensed.

The amount of water is quantified on the basis of the volume of Karl Fischer reagent consumed during the titration. For the method to be effective, the water has to be accessible and easily brought into methanol solution, the Karl Fischer reagent. A major disadvantage is in the case of solids where the water is released slowly or with difficulty into the solution. In either volumetric or coulometric titration, the amount of sample

used depends on the anticipated water content and the degree of accuracy that is desired. Table 2.5 shows the relationship between water content and sample size.

Table 2.5: Relationship between water content and proper sample size (Poynter and Barrlos, 1994)

Sample water content (%)	Volumetric sample size (g)	Coulometric sample size (g)
100	0.02 to 0.05	Not recommended
50	0.05 to 0.25	0.01
10 (100,000 PPM)	0.25 to 0.50	0.01 to 0.05
5 (50,000 PPM)	0.50 to 2.50	0.05 to 0.10
1 (10,000 PPM)	2.50 to 5.00	0.10 to 0.50
0.5 (5,000 PPM)	5.00 to 7.25	0.20 to 1.00
0.1 (1,000 PPM)	7.25 to 10.00	1.00 to 2.00
0.01 (100PPM)	10.00 to 15.00	2.00 to 5.00
0.001 (10 PPM)	15.00 to 20.00	5.00 to 10.00
0.0001 (1 PPM)	Not recommended	10.00 or more

2.9 Summary

Heterogeneous catalysis can play a major role in the catalytic conversion of triglycerides into biodiesel. The catalytic cracking of triglycerides using solid acids is not yet well-established in industry, since it is much more difficult to find a solid acid that is suitably active and chemically and thermally stable. The advantages of using heterogeneous acid catalysts compared to their homogeneous counterparts cannot be over-emphasized. Although many studies of different solid acid catalysts have been carried out, only a small number have presented findings relevant to their use in the catalytic cracking of triglycerides for fatty acid methyl esters (FAMEs).

Sulphated zirconia has been found to be thermally stable, but exhibits a high degree of leaching and reduced surface area if prepared by conventional methods. However, a number of studies have proven that its catalytic properties can be enhanced by methods of preparation. With the proper design of parameters such as type of precursor, pH, calcination temperature, amount of sulphating agent and preparation route, an active sulphated zirconia catalyst with both Lewis and Brønsted acid sites can be synthesised for use in catalytic cracking at mild reaction temperatures.

Catalytic cracking using a sulphated zirconia catalyst may conveniently improve the production of biodiesel to meet the 2020 UK RTFO targets, since the process is similar to petro-cracking and can be carried out in existing refineries.

Chapter 3: Materials and Methods

3 Materials and Methods

3.1 Synthesis of Sulphated Zirconia Catalysts (SZ)

The focus of this research is to develop a chemically, thermally stable and most probably commercially viable catalyst for biodiesel production by triglycerides cracking. The first step to achieving this goal was to identify different heterogeneous acid candidates from literature and sulphated zirconia was found to be a super- acid catalyst suitable for organic reactions, whose catalytic activity is a function of its preparation method. Different methods of catalysts preparation were employed but same procedure was followed for testing their activities. Using two main different preparation methods; the conventional wet precipitation method and non-aqueous method, four different sulphated zirconias were synthesized, by varying the molar ratio of sulphating agent. The catalytic activities of the catalysts were tested in a 100 ml batch reactor using triglycerides. In an attempt to further improve the surface area and activity, the catalysts were modified by doping with dealuminated kaolin (i.e. metakolin). The synthesized catalysts can be grouped into three categories depending on preparation and molar ratio of reactants used. The characterization of the catalysts from each of these methods will be discussed.

3.1.1 Non-aqueous Method of Sulphated Zirconia Synthesis (SFM)

This method does not involve the use of any aqueous medium. In preparing the catalyst, Zirconium oxychloride ($ZrOCl_2.8H_2O$) and ammonium sulphate $(NH_4)_2SO_4$ were carefully weighed to achieve a molar ratio of 1: 6 (Sun *et al*., (2005) and 1:15 respectively. The mixture was ground for 20 minutes at room temperature (23°C) and left for 18 hours at room temperature before calcinations for 5 h at 600°C.

3.1.2 Conventional Method of Sulphated Zirconia Synthesis (CM)

The conventional method according to Yadav and Nair (1999a); Zirconium oxychloride ($ZrOCl_2.8H_2O$) was hydrolysed with 25% ammonium hydroxide at pH 9. The resultant gel was stirred for 4 h and filtered. The resultant zirconium hydroxide was thoroughly washed with water to remove all chloride salts before drying at 100^oC for 24 h. 0.5 N $AgNO_3$ was used to test for the presence of chloride. The zirconium hydroxide was

impregnated with 1 M H_2SO_4 (15 ml H_2SO_4 per 1g of $Zr(OH)_4$) under constant stirring for 2 h. The solution was filtered and the residue was dried at 100^oC for 24 h and calcined in air at 650^oC for 3 h. The same procedure was repeated with molar ratio of 1: 6 of zirconium hydroxide and sulphuric acid respectively.

3.1.3 Modified Sulphated Zirconia with Metakaolin

Dealumination of kaolin was according to Colina *et al*., (2002) and Caballero *et al*., (2007). A known weight of uncalcined kaolin was mixed with a standard analytical-grade 36 N sulphuric acid (H_2SO_4) solution at a molar ratio of 1: 5. Aliquot of the mixture was placed in open quartz crucible, which was heated in a furnace at 500^oC, ramped at 5^oC/min for one hour. Once the reaction temperature was reached the crucible was left in the furnace for 6 h. The resulted material (metakaolin) was doped with zirconium oxychloride and sulphated with ammonium sulphate $(NH_4)_2SO_4$ at a molar ratio of 0.5: 1: 6 in the case of non-aqueous synthesis and 0.5: 1: 15 molar ratio for the conventional method of preparation.

3.2 Characterization of Sulphated Zirconia Catalysts

The freshly prepared and spent sulphated zirconia were characterized by X-ray diffraction (XRDP) powder patterns, Infrared (IR) spectroscopy, Scanning Electron Microscopy (SEM), X-ray photoelectron spectroscopy (XPS), Energy Dispersive X-ray (EDX), Fourier Transform Infrared Spectroscopy with pyridine as probe molecule **(**Py-DRIFTS), chloride determination, Thermogravimetric Analysis (TGA) and Brunauer-Emmett-Teller (BET) nitrogen desorption measurements for the surface areas.

3.2.1 Fourier Transform Infra-Red Spectroscopy (FTIR)

FTIR measurements were performed in a Varian 800 (Scimitar series) spectrometer to determine the functional group of the catalyst. The spectra were produced at a resolution of 2 cm^{-I} between 4000cm^{-1} and 400cm^{-1} using a Pike Technologies diamond crystal plate ATR. Catalysts samples were finely ground and approximately 2 mg of each was transferred to a mechanical disk press assembly and subjected to pressure of approximately 10 tons. With this technique, vibrational excitation of bonds as a result of interaction between certain wavelength of infrared radiation and molecules of the catalysts are observed depending on the functional group of the compound. The types of

bond excitation that can occur are stretching (higher energy) and bending (lower energy) vibrations.

3.2.2 X- ray diffraction powder studies (XRDP)

The X- ray Diffraction technique was used to determine the phases and crystallinity of the various catalysts synthesized and compared with the XRDP pattern of zirconia of the database of lnternational Centre of Diffraction Data (ICDD). The XRDP was performed using a Panalytical X'Pert Pro Multipurpose Diffractometer (MPD) fitted with an X'Celerator and a secondary monochromator which accelerates the speed of the scan. The diffractograms were recorded with a divergent slit of 0.38 mm using Cu Kα radiation with a wavelength of λ = 1.54 Å generated at a voltage of 40 kV and 40 mA from 2^oC to 100^oC. The catalyst samples were prepared for analyses in powder form and dispersed on glass slides for continuous scans set to cover a range of 2^o to 70^o. Their crystallite sizes were calculated using data from X-ray diffractogram and X'pert data viewer software in the Scherrer's formula Equation 3.3.1. The X-ray diffraction powder was carried out by Maggi white of Materials and Analytical Unit, Newcastle University.

$$\text{Crystallite size (Å)} = {}^{K\lambda}/_{B\text{Cos}\theta} \qquad \text{Equation 3.3.1}$$

where

K Scherrer's constant

λ is the wave length of X-ray

B is instrument broadening (FWHM)

θ is half of the Bragg angle

The most common values for K are 0.94 for FWHM of spherical crystals with cubic symmetry and 0.89 for integral breadth of spherical crystals or cubic symmetry

3.2.3 Surface area measurements (BET)

The catalytic surface areas of the catalysts were obtained from N_2 adsorption isotherms determined at 77K using the Coulter™ (SA 3100™ series). The samples were outgassed under high vacuum for 2 h at 200°C (Akkari *et al*., 2007) prior to the analysis. The dry weight of the sample was used to obtain the final value of the specific surface area. In the case of the sulphated zirconia modified with metakaolin, they were

degassed at 300^{o}C for 24 h. The equipment could not be used to determine the pore sizes of the catalysts; however an alternative method adopted, the ImageJ software with SEM images.

3.2.4 Scanning electron microscopy and elemental analysis (SEM, EDX)

The size and morphology of the catalyst were obtained by using environmental scanning electron microscope (ESEM Model: XL30) called JEOL 5300 LV fitted with Rontec and energy dispersive X-ray detector (EDX). The advantage of the ESEM is that it can be operated at both low and high vacuum. Both detectors, (i. e. ESEM and EDX) were operated under liquid nitrogen. The SEM was done under high vacuum while the qualitative elemental analysis (Energy Dispersive X-ray; EDX) was run at low vacuum and a voltage of 25 kV. For good images samples were coated with gold. This scanning electron microscopy and energy dispersive X-ray was carried out by Pauline in the Materials Analytical Unit, of Newcastle University.

3.2.5 X-ray photoelectron spectroscopy (XPS)

XPS technique is used to investigate the chemistry of catalysts at the surface. X-ray photoelectron spectroscopy experiments are based upon the properties of photoelectrons emitted from a sample on irradiation with X-rays. The XPS spectra were performed using CasaXPS 2.3.15 software on Kratos analytical system, Figure 3.1 equipped with a monochromator Al$K\alpha_{1,2}$ X-ray sources of 1486.6 eV and 0.85 eV widths. The binding energies were referenced by setting the CHx peak maximum in the resolved C 1 s spectra to 284.6 eV. The samples were loaded into the slab and attached mechanically to the specimen mount. These were left in the system for 48 hours under a high vacuum (10^{-10} mbar). For the purpose of chemical state identification for quantitative analysis and peak de-convolution, processing of the results were on wide and detailed scans. The X-ray photoelectron spectroscopy was performed in chemistry department of Cardiff University, UK.

Figure 3.1: Kratos Analytical X-ray photoelectron spectrometer (courtesy Chemistry Department University of Cardiff, UK)

3.2.6 Chloride determination

The presence of chloride in the non-aqueous catalysts was determined using ion chromatography, a Dionex ICS-1000 with an AS40 autosampler and IonPac AS14A analytical column. 0.5g of each sample was dissolved in 10 ml of deionised water and refrigerated for 24 h before they were filtered using 0.2 micron filters. 5 ml of each sample was used for the analysis. The instrument detects the sample via a conductivity cell that measures the electrical conductance of the sample ions as they emerge from a suppressor thus producing a signal based on specific chemical/physical properties of the analyte of interest. The system is based on measuring negatively charged ions (anions) in samples. The eluent is 8.0 mM Na_2CO_3/1.0 m M $NaHCO_3$ solution at a flow rate of 1ml/min. The concentration of chloride present in the sample was calculated in mg/kg using Equation 3.2.

$$Conc. = \frac{A \times V}{W} \qquad \text{Equation 3.2}$$

where

A is the amount of ion found in sampl in ppm

V is the final volume of sample in ml

W is the weight of dry sample used

3.2.7 Thermogravimetric analysis (TGA)

Thermogravimetric analysis is an analytical technique used to determine the volatile components of a compound by monitoring the weight loss as a function of either time or temperature as the material is heated. The surface sulphate and thermal stability of the catalysts were monitored by thermogravimetric (TG) analysis as a function of mass loss with respect to temperature. The TGA studies were performed on a Pyris STA 6000 Model under flowing helium at constant rate of 30 ml/min with temperature ramped 10^{o}C/min in 30–1000^{o}C range. The TGA consists of an electronic microbalance and a ceramic container suspended with platinum hanged down the centre of the furnace. The sample initial mass, temperature and final mass loss were monitored by computerised control unit.

3.2.8 Fourier Transform Infrared Spectroscopy with pyridine as probe molecule (DRIFTS)

The acid properties of the catalysts were determined by Pyridine- DRIFTs (diffuse reflectance infrared Fourier transform spectroscopy). Pyridine was used instead of ammonia because it is a relatively strong base, it is weaker than ammonia; so might not react with weak acid on the catalyst; therefore it is better probe. According to Rosenberg and Anderson (2002), the use of pyridine as probe gives a narrow width band on spectroscopy, thereby giving a good resolution of the vibrational modes to distinguish between Brønsted and Lewis acid. Prior to measurement the samples were diluted in KBr by 5% dilution. This was done to avoid absorption saturation at low wave numbers and the mixed was thoroughly ground together. Each of the mixed samples (catalysts and KBr) was divided into two equal halves. A portion each of the mixed samples was exposed to pyridine vapour for 24 hour in a desiccator, after which they were outgassed under vacuum of 0.13mPa for 2 hours to remove any unadsorbed pyridine. Measurements were carried out using self-supported wafer. Firstly, the spectra of the samples without pyridine were recorded, followed by samples that were exposed to pyridine. In each case, the sample was referenced against a blank KBr. The X-ray photoelectron spectroscopy was performed in chemistry department of Cardiff University, UK.

3.3 Catalytic Studies

The catalysts screening for activity were tested in a thermocatalytic reaction using a 100 ml batch reactor (Model: 4560) equipped with a magnetic stirrer, auto sampler and an

external heating mantle, Figure 3.2. The process conditions were controlled by WinISO software. The reactions were performed using known weight (67g) of feed (rapeseed oil), different weight percent of catalysts and operating temperature of 270°C and conversion monitored against time as indicated in Table 3.1. However the screening of the catalysts could not be done at higher temperature for safety reasons as the reactor maximum temperature was 320°C. The feed was heated from ambient room temperature to 269°C before each injection of the catalysts. Samples were taken from the reaction mixture at time interval of 60, 30 and 15 minutes.

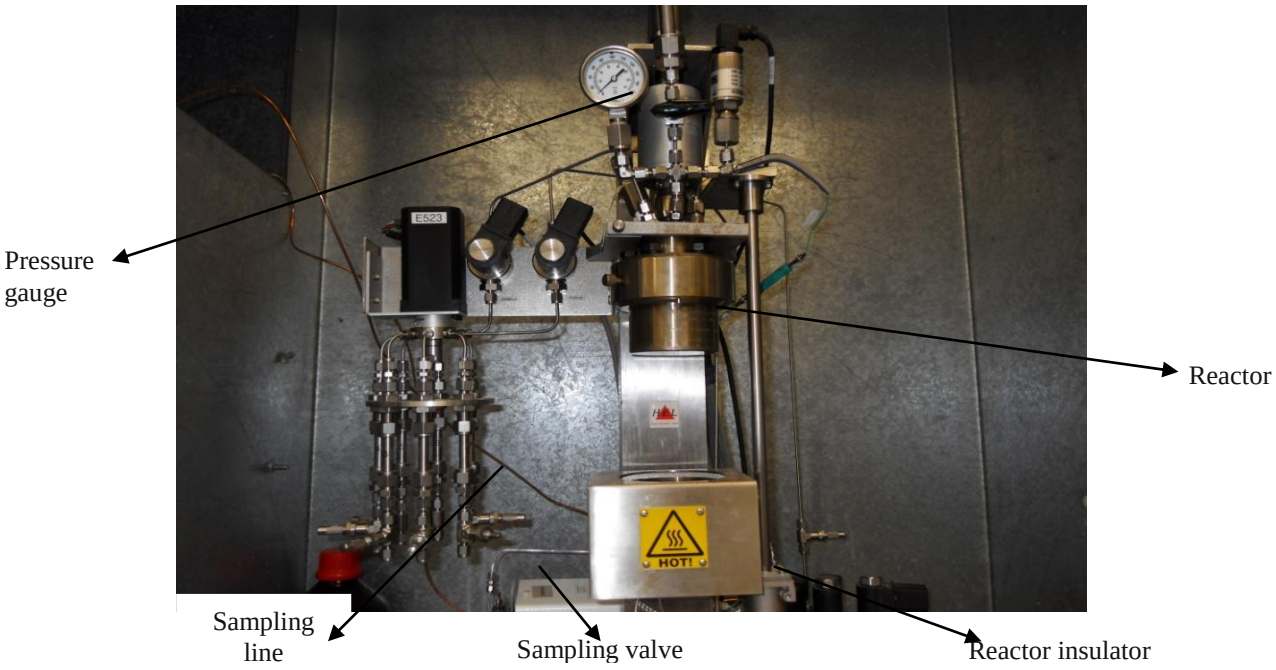

Figure 3.2: Catalytic Reactor (HEL automate system)

After these the products were subjected to analytical methods to determine Methyl esters, diglycerides, monoglycerides, free fatty acids and glycerol. Another set of experiments was carried out at higher temperature of 300^{o}C in a different reactor (Figure 3.3) without a sampling port, while some were also performed at a lower temperature range of 210-240^{o}C in another reactor. All experiments were repeated at least three times.

Figure 3.3: Parr High Temperature Reactor (Model, 5500)

3.3.1 Experimental set

The following experimental matrices were performed to determine the activities of the catalyst using triglycerides, and their effectiveness was compared with respect to the method of preparation.

Table 3.1 Experimental Matrix for Catalysts Testing in the Batch Reactor (A-F)

	Catalyst type	Reaction temp. (^{o}C)	Sampling time (min)	Amount of catalyst used (wt % feed)
A	SFM	270	60	2
	CM	270	60	2

SFM is solvent-free method;
CM conventional method

	Catalyst type	Reaction temp. (^{o}C)	Sampling time (min)	Amount of catalyst used (wt % feed)
B	SFM	270	15	2
	CM	270	15	2
	SFM*	270	15	2
	CM*	270	15	2

SFM is solvent-free method; CM conventional method
SFM is same ratio as CM; CM*same ratio as SFM*

	Catalyst type	Reaction temp. (^oC)	Sampling time (min)	Amount of catalyst used (wt % feed)
C	SFMM	270	15	2
	CMM	270	15	2

SFMM is non-aqueous method doped with metakaolin;
CMM conventional method doped with metakaolin

	Catalyst type	Reaction temp. (^oC)	Sampling time (min)	Amount of catalyst used (wt % feed)
D	SFM	300	60	2
	CM	300	60	2
	SFM*	300	60	2
	CM*	300	60	2

SFM is solvent-free method; CM conventional method
SFM is same ratio as CM; CM*same ratio as SFM*

	Catalyst type	Reaction temp. (^oC)	Sampling time (min)	Amount of catalyst used (wt % feed)
E	SFM	240	15	2
	CM	240	15	2
	SFM*	240	15	2
	CM*	240	15	2

SFM is solvent-free method; CM conventional method
SFM is same ratio as CM; CM*same ratio as SFM*

	Catalyst type	Reaction temp. (^oC)	Sampling time (min)	Amount of catalyst used (wt % feed)
F	SFM	210	15	2
	CM	210	15	2
	SFM*	210	15	2
	CM*	210	15	2

SFM is solvent-free method; CM conventional method
SFM is same ratio as CM; CM*same ratio as SFM*

3.3.2 Thermogravimetric analysis for gas determination

It was difficult to collect gaseous samples from the batch reactor; however this was done using Teflon bag on a TGA, Pyris STA 6000 Model at reaction temperature reported above. The gas mixture was identified on a gas chromatography. The thermogravimetric (TGA) studies were performed on a Pyris STA 6000 Model under flowing helium at constant rate of 30 ml/min with temperature ramped 10^oC/min in 30–1000^oC range.

3.4 Analysis of Products from the Reactions

The reaction product was subjected to standard analytical method for biodiesel defined in BS EN 14103:2003. The presence of free glycerol and residual mono-, di- and triglycerides contents in the fatty acid methyl esters (FAMEs) was determined as indicated in EN 14105: 2003. The free fatty acid in the liquid products was evaluated by simple titration method as reported by Rattanaphra *et al*. (2010). Karl Fischer titration was used to measure the water content in the sample. Coke deposited on the spent catalysts was determined using Katikaneni *et al*. (2002) protocol. The products were also examined using Fourier Transform Infrared Spectroscopy (FTIR) to determine the presence of hydrocarbons in addition to fatty acid methyl esters (FAMEs).

3.4.1 Determination of Fatty Acid Methyl Esters (FAMEs) by Gas chromatography

The approach used was based on the standard method defined in BS EN 14103:2003. The BS EN 14103:2003 is a standard for determination of the ester content of fatty acid methyl esters intended for use as pure biofuel. In preparing the internal standard by this method, 500 mg of methyl heptadecanoate was dissolved in 50ml volumetric flask. Sample preparation was 250 mg of the sample and 5 ml of the stock solution of the internal standard in a 10 ml sample vial. 0.1µl of the prepared sample mixture was manually injected into the gas chromatography (GC). The gas chromatography was Hewlett Packard 5890 Series II gas chromatography with an FID detector and forte BPX70 column (SGE analytical science) with dimensions 0.32 mm i.d. and 50 m length. The temperature of the FID and injector was maintained at 250^{o}C each. The carrier gas was helium at a flow rate of 18.75 ml/min and the column temperature was maintained at 210^{o}C. Equation 3.3 and Equation 3.4 were used to evaluate the concentration of total and individual esters content respectively; expressed as a mass fraction in percentage. The experiment was performed at least three times.

$$C = \frac{(\sum A) - A_{E1}}{A_{E1}} \times \frac{C_{E1}V_{E1}}{M} \times 100\% \qquad \text{Equation 3.3}$$

$$L = \frac{A_L}{(\sum A) - A_{E1}} \times 100\% \qquad \text{Equation 3.4}$$

where

ΣA is the total peak area on the chromatogram (C_{14} to $C_{24:1)}$

A_{E1} is the peak area corresponding to methyl heptadecanoate (IS)

C_{E1} is the concentration in milligram per millilitre of the methyl heptadecanoate solution used.

V_{E1} is the volume, in millilitre of the methyl heptadecanoate used.

A_L is the peak area corresponding to the individual ester of interest.

m is the mass, in milligram of the sample

3.4.2 Glyceride Analysis by Gas Chromatography and Mass Spectrometer (GC-MS)

The reaction product was analysed by gas chromatography-mass spectrometer using EN 14105: 2003 method. The method specifies a procedure for determination of free glycerol and residual mono-, di- and triglycerides contents in fatty acid methyl esters (FAMEs). Two internal standards were prepared and used to quantify the peak sizes. The first internal standard IS1 (1 mg/ml) was prepared by weighing 50 mg of 1, 2, 4 butanetriol into a 50 ml volumetric flask with pyridine. Secondly, 80 mg of 1, 2, 3 tricaproylglycerol (tricaprin) was weighed into a 10 ml volumetric flask with pyridine (8 mg/ml) as internal standard (IS2). Prior to sample injection, calibration curves of 1-monooleoylglycerol (monoolein), 1,3-didoleoylglycerol (diolein) and 1,2,3-trioleoylglycerol (triolein) were constructed using standard stock solutions. Preparing the samples for analysis approximately 100 mg of each sample from the reaction product was accurately weighed into a 10 ml vial, 80 µl of IS1 and 100µI of IS2 were added. To this mixture 100 µI of MSTFA (Nmethyl-N-trimethylsilylfluoroacetamide) was added to silylate the OH bonds in the presence of pyridine thereby increasing the volatility of the sample. The mixture was shaken and left for 15 minutes at room temperature, after which 8 ml of heptane was added. 10 µl of each sample was put into sampling vials of an auto-sampler GC-MS equipped with capillary column (15 m × 0.25 mm i.d. and 0.25 µm film thickness). The GC column temperature was ramped up linearly at 50°C per min from 180°C (hold 4 min) to 230°C (hold 4 min) to 370°C. The carrier gas was helium at a flow rate 1 ml/min, inlet line and source temperatures at 270°C and 250°C respectively. The mass percent of the mono, di and triglycerides present in the sample can be calculated using Equation 3.5.

$$M_i = \left\lfloor a_i \left(\sum A_i / A_{ei2} \right) + b_i \right\rfloor \times \left(\frac{M_{ei2}}{m} \right) \times 100 \qquad \text{Equation 3.5}$$

where:

M_i is the mass percent of mono, do or triglycerides in the sample;

a_i and b_i are the slope and intercept from the regression of the calibration curve;

m is the mass of sample used for the analysis in milligrams;

$\sum A_i$ is the sum of the peak area of the mono, di- and triglycerides;

A_{ei2} is the peak area of internal standard (IS1 or IS2);

M_{ei2} is the mass of internal standard used (IS1 or IS2) in milligram

3.4.3 Determination of free fatty acids (FFA)

A simple method of titration by Rattanaphra *et al*. (2010) was used to determine the fatty acid present in the product. The base NaOH was prepared by dissolving 0.5g in 500 ml volumetric flask of distilled water to prepare 0.025N solution. 0.1g of each sample (from the reaction) was measured into a conical flask and 1ml of propan-2-ol was added as solvent, 2-3 drops of 0.2% of phenolphthalein indicator were added to each sample mixture and titrated with the prepared sodium hydroxide solution until the appearance of the first permanent pink colour which lasted for at least 30 seconds indicating completion of the reaction and the volume of the titre was recorded. Equation 3.6 was used to evaluate the free fatty acid concentration in the samples from average titre.

$$\mathrm{FFA}(\%) = \frac{\mathrm{V} \times \mathrm{N} \times \mathrm{MW_{acid}}}{\mathrm{w} \times 1000} \times 100 \qquad \text{Equation 3.6}$$

where:

V is the volume of titre in ml

N is the normality of the standard NaOH solution

w is the weight of the sample of oil in grams

282.52 is the molecular weight of oleic acid (MW_{acid})

3.4.4 Determination of water content by Karl Fischer Titration

The presence of water in the liquid product was determined by Karl Fischer Titration (Metrohm, model 701 Titrino), Figure 3.4. This equipment was used because of its effectiveness in determining micro amount of water in products, amongst other advantages such as accuracy, short analysis duration and small sample requirement. The Karl Fischer Titration kit was set up by adding 30 ml of solvent (methanol dry) into the

reaction vessel to cover the platinum electrode. The reagent was then introduced until the end point of 20µl/min was reached as indicated on the instrument.

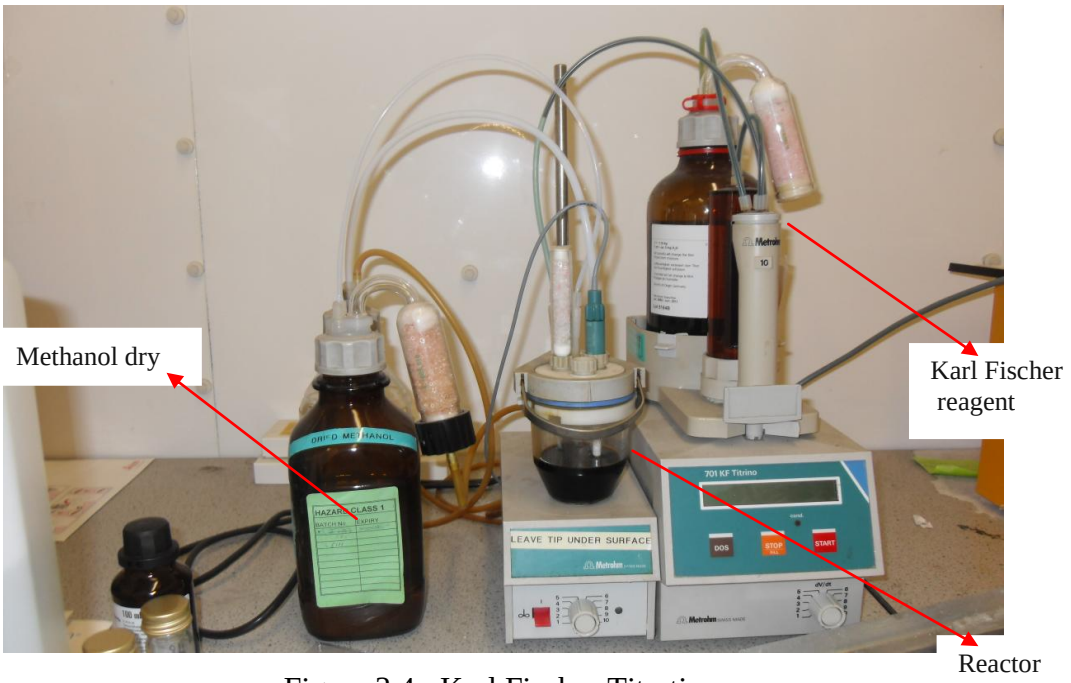

Figure 3.4: Karl Fischer Titration

At this point the sample 0.2g (approximately 0.16 ml) was injected into the reaction vessel with the aid of a 1 ml syringe and titrated with the Karl Fischer reagent under constant magnetic stirrer until a stable endpoint was achieved. The water content, in percentage by mass was calculated using Equation 3.7.

$$Water\ content\ = \frac{V \times D}{1000 \times m} 100 \qquad \text{Equation 3.7}$$

where:

V is the volume (ml) of the Karl Fischer reagent used;

D is the water equivalent (mg water/ml) of the Karl Fischer reagent, which is 5mg/ml;

m is the mass (g) of the sample injected.

3.4.5 Kinetic data of the reaction

The kinetics of the reaction for each of the catalysts were calculated using isothermal data from the cracking of triglycerides with the catalysts on a TGA (Pyris STA 6000 Model) at different reaction temperatures (210^{o}C, 240^{o}C, 270^{o}C and 300^{o}C) in the rate equation and the Arrhenius equation. In each reaction, the temperature was ramped. For

instance, at 270^{o}C the temperature was ramped up linearly from 30^{o}C to 270^{o}C at 50°C/min and was held for 180 minutes at 270^{o}C (a typical reaction temperature in the batch reactor) followed by cooling at 50°C/min. The rate of heating and the hold time were same for all the reactions at different temperatures. Using the isothermal data generated from the TGA, conversions at different time, t from each reaction were calculated using Equation 3.8.

$$x = \frac{m_o - m_t}{m_o - m_f} \qquad \text{Equation 3.8}$$

where:

m_o is the initial mass of the sample

m_t is the mass of the sample at time, t and

m_f is the final mass of the sample in that reaction

Assuming a first order reaction, the rate in terms of conversion is given by:

$$\frac{dx}{dt} = k\,(1 - x) \qquad \text{Equation 3.9}$$

Integrating the rate Equation 3.9 at the initial condition x = 0 at t=0, gives Equation 3.10

$$-\ln(1 - x) = kt \qquad \text{Equation 3. 10}$$

The rate constant, k can be determined graphically from the gradient of a plot of In$(1 - x)$ vs. time t) which should give a straight line with slope = $-k$. For each catalyst this value (k) was determined at four different temperatures. Subsequently, the values of the activation energy (E_a) and the pre-exponential factor (A) can be estimated from the slope and intercept of an Arrhenius plot. Taking the natural logarithm of the Arrhenius Equation 3.11, it gives Equation 3.12 similar to a straight line equation

$$k = A\,exp\left(-\frac{E_a}{RT}\right) \qquad \text{Equation 3.11}$$

where:

A is the pre-exponential factor (the unit depends on the order of the reaction)

k is the rate constant (the unit depends on the order of the reaction)

E_a is the activation energy (kJ/mol)

R is the gas constant ($JK^{-1}mol^{-1}$)

T is the temperature of reaction (K)

$$ln(k) = \frac{-E_a}{R}\frac{1}{T} + \ln(A) \qquad \text{Equation 3.12}$$

Plotting ln(*k*) versus T^{-1} gives a straight line, the activation energy is given as (-*R*) multiplied by the slope of the plot and *A* is the exponential of the intercept.

3.5 Other Analyses

The catalysts were further subjected to more characterization and analyses to determine their reusability and leaching during the reactions.

3.5.1 Determination of Coke on the Catalyst

The amount of coke deposited on the catalysts was investigated by simple method as described by Katikneni *et al*. (2002). Spent catalysts were weighed after which they were washed with hexane to remove any triglycerides, thereafter they were weighed again. The washed catalyst were regenerated by calcinations in the furnace at 600^{o}C for 1 hour and weighed. The difference in weights of the washed and regenerated catalyst was calculated as the coke deposited on the catalysts for each reaction with respect to time.

3.5.2 Test for Catalyst Leaching

To investigate the sulphated zirconia catalyst for any leaching, Garcia *et al*. (2008) protocol was used. The spent catalysts were thoroughly washed with hexane to remove any tryglyceride and dried at 60^{o}C for 1 hour. About 300 mg of the sample was stirred in 50 ml of distilled water and left for 24 h. the same procedure was repeated for flesh (un-used) catalyst, the suspension was filtered and reacted with barium chloride ($BaCl_2$) solution. Samples from both suspensions were subjected to FTIR analysis to determine the presence of sulphate.

3.5.3 Regeneration and Characterization of the Regenerated Catalysts

The washed catalysts from session 3.5.1 were regenerated by calcinations in the furnace at 600^{o}C for 1 hour as described by Katikneni *et al*. (2002). The regenerated catalysts were subjected to XRPD, XPS, EDX, pyridine- DRIFTs analyses in order to validate their possible reusability.

3.5.4 Error Analysis

Error analysis was performed for the analytic methods used for the product mixture from the reaction. There are two types of error: the random error (ε_R) and the systematic error (ε_S). The measured values during an experiment are always subject to fluctuations; therefore the error due to this fluctuation is called the random error. It is calculated from the mean of the set of numbers of measured values during the experiment (see equation 3.13 and 3.14). It is simply the standard deviation of the measured values. Whereas the systematic error is due to experimental equipment used such as inaccuracy of the equipment performance or the measuring device.

$$\varepsilon_R = \sqrt{\frac{1}{n}\sum_{i=1}^{n}(T_i - \overline{T})^2} \qquad \text{Equation 3.13}$$

and

$$\overline{T} = \frac{1}{n}\sum_{i=1}^{n} T_i \qquad \text{Equation 3.14}$$

This is usually calculated from the scale resolution of the measuring device; mostly taken as ± half the scale resolution. The combination of both errors gives the overall error of the experiment; however, they cannot be added together since they are not the same. The overall error is calculated as the root mean square of the random and systematic errors as given in equation 3.15.

$$\varepsilon = \sqrt{\varepsilon_R^2 + \varepsilon_S^2} \qquad \text{Equation 3.15}$$

Chapter 4: Results and Discussion

4 Introduction

The chapter comprises two sections; the first concerns the characterization of the catalysts produced by the two methods. The second evaluates the activity of the catalysts and their selectivity for methyl esters in the thermocatalytic cracking of triglycerides.

4.1 Characterization of Catalysts

The different preparation methods tested can be divided into two main categories: conventional and solvent-free methods. Six catalysts were synthesized, varying in sulphating agent, precursor and molar ratio used. The characteristics of the catalysts obtained from each method and preparation factors are discussed below. The catalysts were characterized by X-ray powder diffraction (XRPD) patterns, Infrared (IR) spectroscopy, energy dispersive X-ray (EDX), pyridine-DRIFTS (Diffuse Reflectance Infrared Fourier Transform Spectroscopy), X-ray photoelectron spectroscopy (XPS), thermogravimetric analysis (TGA) and nitrogen adsorption measurement. These characterizations yielded information about the morphology, sulphate content, elemental composition, acid type and surface areas of the catalysts.

In the conventional preparation method, ammonium hydroxide (NH_4OH) was the hydrolysing agent and sulphuric acid (H_2SO_4) the sulphating agent (see section 3.1.2). The procedure used in the solvent-free method is described in section 3.1.1. Here two different molar ratios were used. For convenience, the catalysts prepared using the conventional method are designated as "CM" (1:15) and "CM*" (1:6), and those synthesized using the solvent-free method are "SFM" (1:6) and "SFM*" (1:15). The CM* means the method of preparation is same as CM but with same ratio of reactants as SFM while the SFM* is the same as method as SFM but same ratio of reactants as the CM.

4.1.1 X-ray diffraction pattern (XRPD)

The X-ray diffraction patterns of the catalysts derived from the conventional method (CM and CM*) and the solvent-free method (SFM and SFM*) calcined at 650^{o}C and 600^{o}C respectively as reported in section 3.2.2 are discussed below.

4.1.1.1 Conventional method

The X-ray patterns of non-calcined sulphated zirconia catalyst samples from both ratios (1:15 and 1:6) of zirconium hydroxide to sulphuric acid using the conventional method exhibit no peak of crystallinity. The X-ray pattern of non-calcined sample is amorphous with a broad peak between 25^{o} and 35^{o} (2θ), also typical of an amorphous material. When the sample was calcined in air at 650^{o}C, there was a phase transformation from amorphous to tetragonal crystalline phase indicated by the change in various peak intensities at 30^{o}, 35^{o}, 52^{o}, 60^{o}, 82^{o} and 95^{o}. The peaks at the mid-angle are of higher intensities, as shown in Figure 4.1 and Figure 4.2.

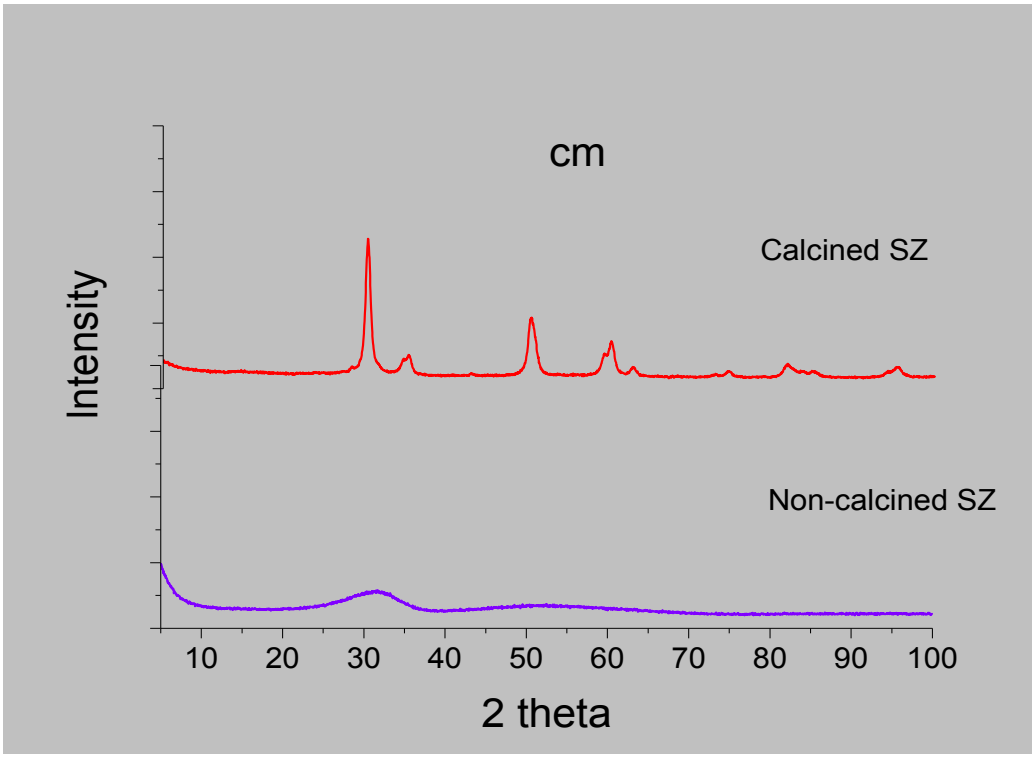

Figure 4.1: XRPD Patterns for CM Sulphated Zirconia by Conventional Method compared with its Non-calcined Sample

The intensity of the peaks tends to decrease along the angle. In the CM and CM* samples the peaks observed at 30^{o}, 35^{o}, 52^{o} and 60^{o} are common peaks that can be indexed as (1 0 1), (1 1 0), (1 1 2) and (2 1 1), assuming a tetragonal unit cell and are similar to zirconia (see appendix A).

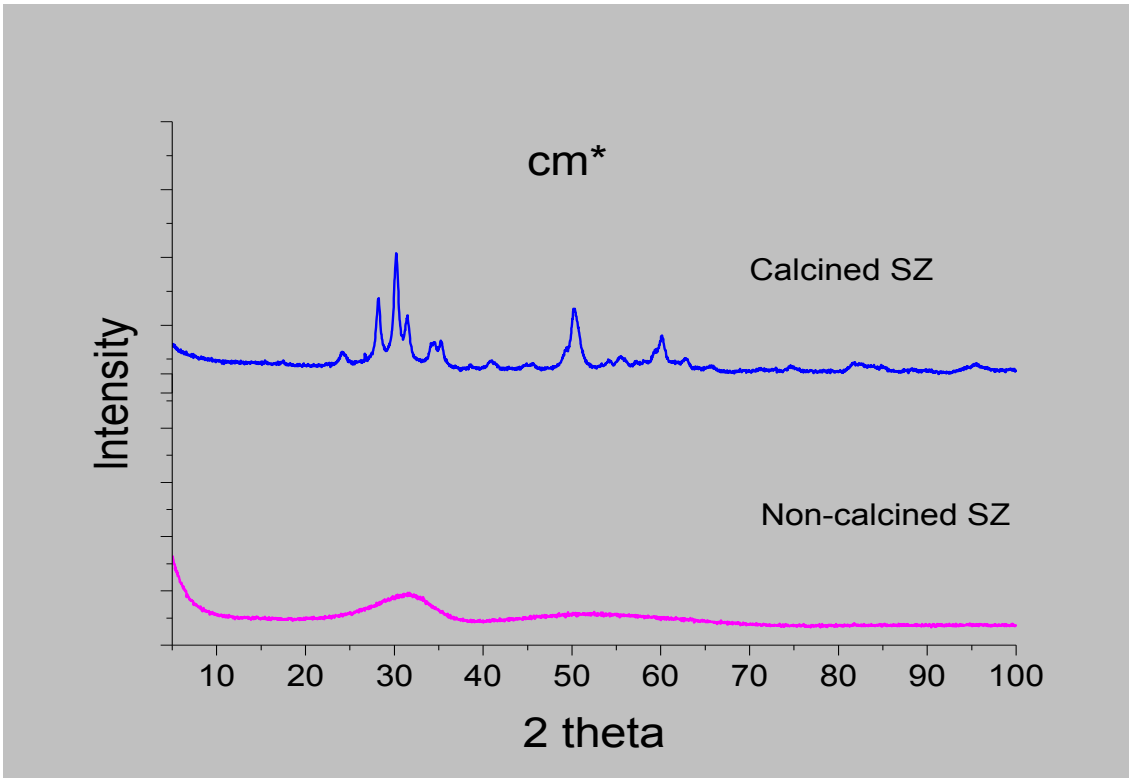

Figure 4.2: XRPD Patterns for CM* Sulphated Zirconia by Conventional Method compared with its Non-calcined Sample

Comparing the diffractograms in Figure 4.3, additional peaks were observed at a low-angle X-ray diffraction pattern in the CM* sample (ratio 1:6), indication of monoclinic phase of zirconium oxide (see appendix B). These peaks at 28^{o} 24^{o} and 31^{o} can be indexed as (-1 1 1), (0 1 1) and (1 1 1) respectively. When the ratio of sulphating agent was reduced from 1:15 to 1:6, the intensities of the tetragonal reflections were reduced by 50% as seen with CM*, but the width of the peaks are much narrower than that of CM. This suggests that zirconia particles in CM are much smaller than those in CM*. The monoclinic peaks were much larger in size (based on by Scherrer's equation). The diffractograms indicate that reducing the amount of sulphate during preparation causes a different crystalline phase of zirconia to form, as both tetragonal *and* monoclinic forms begin to be observed. The appearance of the monoclinic phase at this calcination temperature of 650^{o}C agrees with the findings of Li *et al.* (2001)

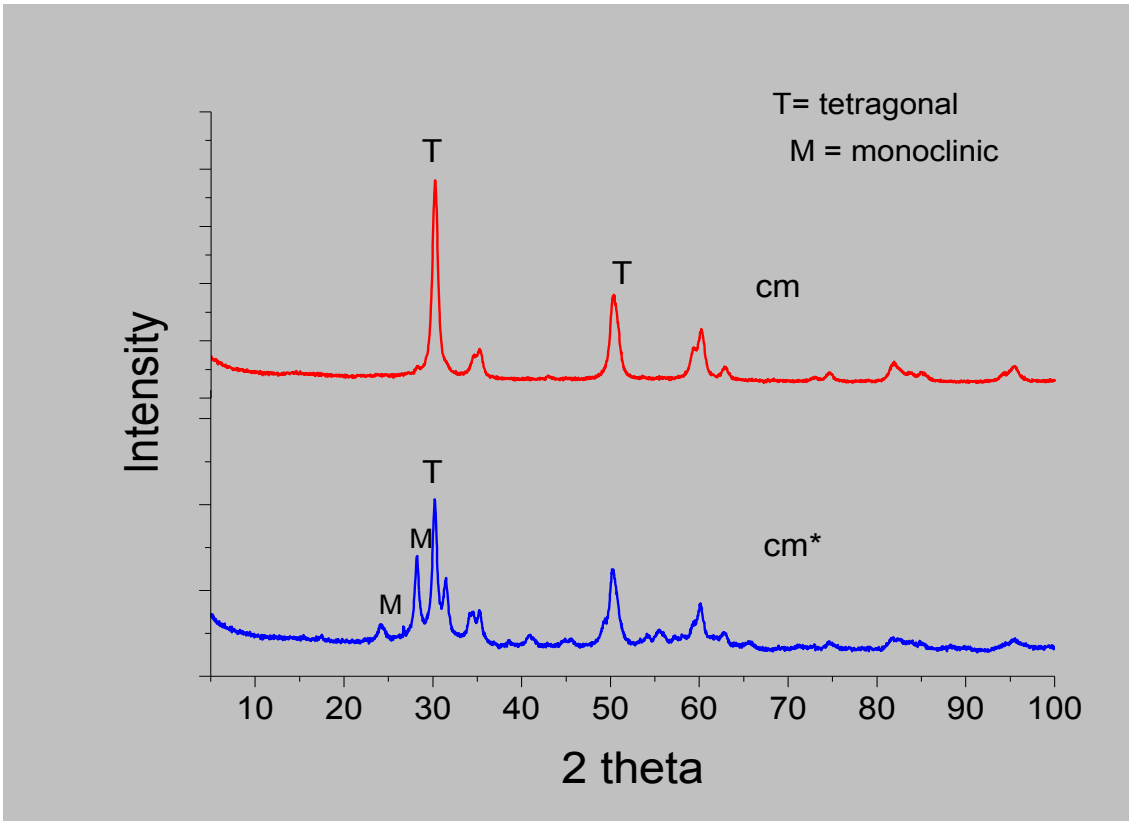

Figure 4.3: XRPD Patterns for CM (1:15) and CM* (1:6) by Conventional Method

Li *et al.* (2001) observed the transformation of amorphous to tetragonal zirconia at a calcination temperature range of 300-400^{o}C, and tetragonal to monoclinic phase between 400-500^{o}C. Although, Comelli *et al.* (1995) had earlier reported that the calcination temperature for the transformation of the tetragonal to the monoclinic phase is slightly higher than 500^{o}C for zirconia that contains sulphate.

4.1.1.2 Solvent-free Preparation Method

In contrast to the conventionally prepared catalysts, the X-ray diffraction pattern of the non-calcined sulphated zirconia from the solvent-free method was crystalline, as shown in Figure 4.4 and Figure 4.5, below. The crystallinity observed on the diffractogram is due to the presence of $(NH_4)_2SO_4$ and NH_4Cl in the non-calcined catalyst. The X-ray diffraction patterns of the calcined samples SFM and SFM* at 600^{o}C exhibited similar XRD patterns, indicating that neither the monoclinic nor tetragonal phases were present, but a completely amorphous zirconia phase, as shown in Figure 4.4. This indicates that

the method of preparation reduced the appearance of monoclinic or tetragonal phase of the zirconia.

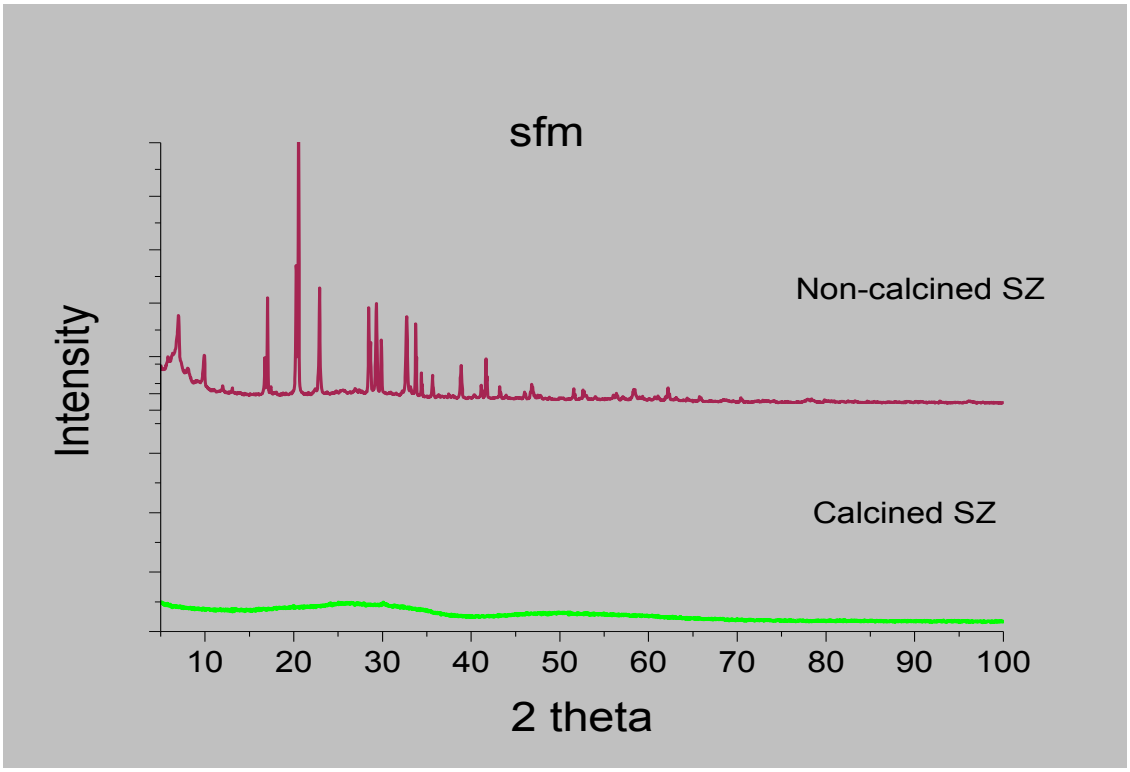

Figure 4.4: XRPD Patterns for SFM Sulphated Zirconia by Solvent-Free Method Compared with its Non-calcined form

The direct method of sulphation allowed for increased sulphate content on the precursor, which tends to hinder the crystalline phase of the zirconia. It was expected that, during calcination, the NH_4Cl would have decomposed. Ammonium chloride sublimes at temperature above 200^{o}C and after sublimation it dissociates into the gaseous phase of ammonia and hydrochloric acid (Olszak-Humienik, 2001). Hence, it is clear that the sintering of zirconia crystallites during the calcination process using the solvent-free method is delayed by the presence of sulphate ions on the surface of the catalyst. The XRD pattern of the non-calcined and the calcined SFM* are shown in Figure 4.5.

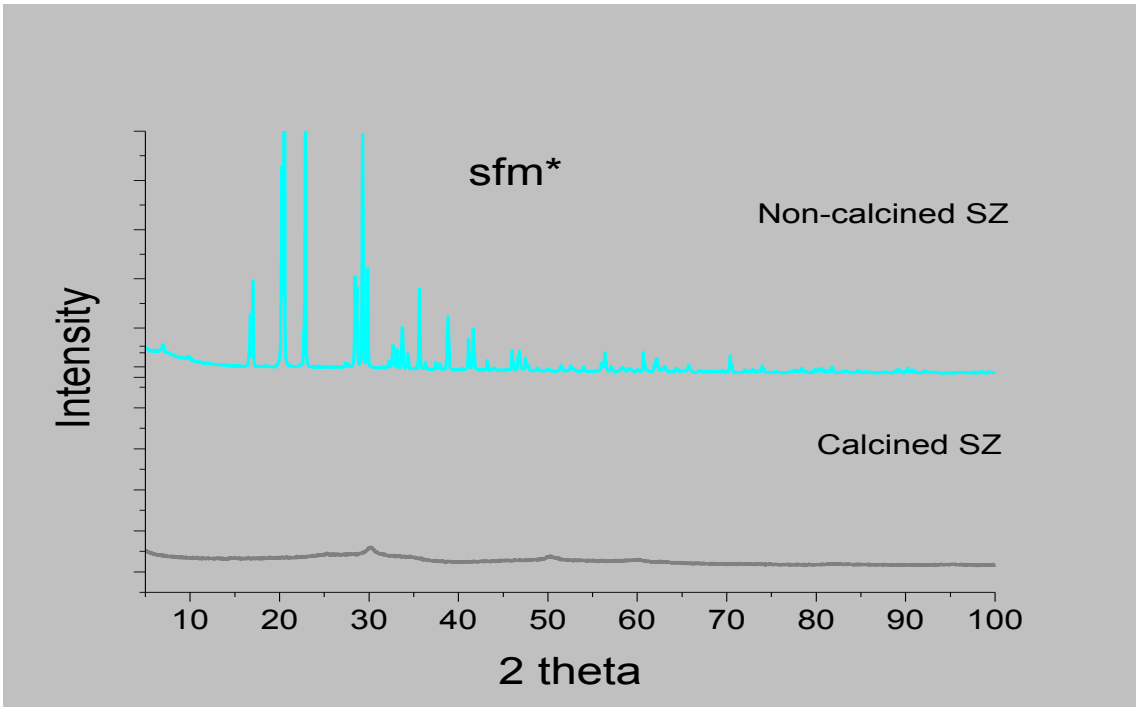

Figure 4.5: XRPD Patterns for SFM* Sulphated Zirconia by Solvent-Free Method compared with Non-calcined Sulphated Zirconia

The phases observed were identified by matching the peaks on the XRPD trace with the known diffraction patterns contained in the database published by the lnternational Centre of Diffraction Data (ICDD). The solvent-free catalysts' XRD patterns did not change due to calcination (Figure 4.6). The presence of zirconium oxide and zirconium sulphate oxide were identified using the database.

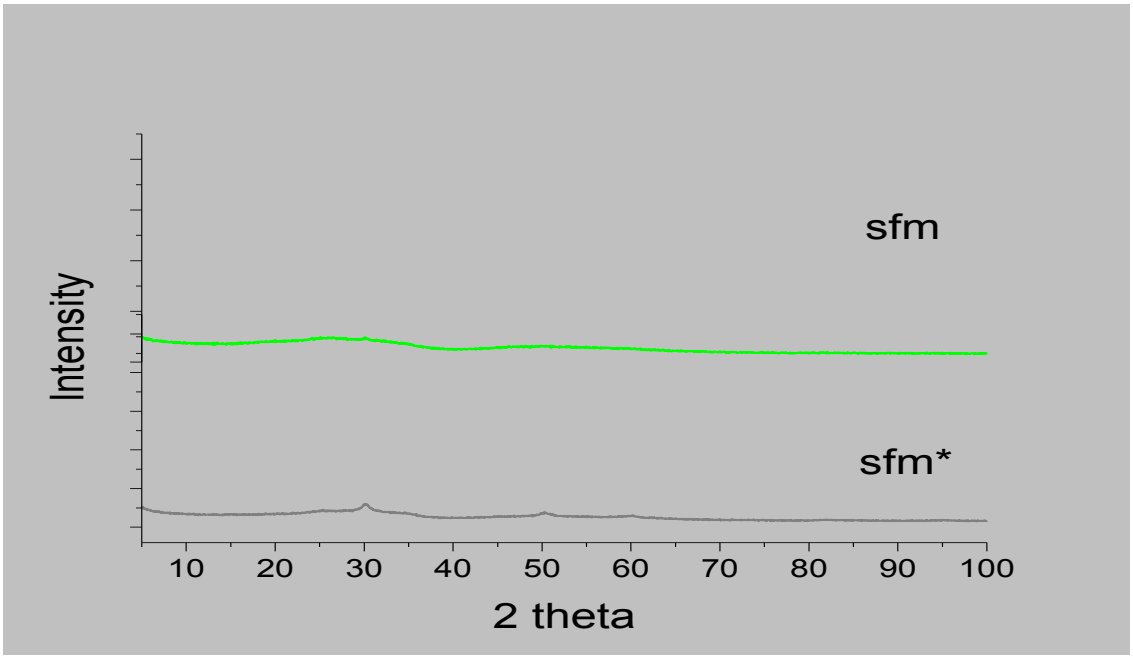

Figure 4.6: XRPD Powder Patterns for Solvent-free Sulphated Zirconias

The BET surface area, crystallite size, scanning electron microscopy (SEM) and elemental analysis (EDX) were performed according to sections 3.2.3 and 3.2.4. A sample of the BET data analysis from the BET equipment (Coulter^{TM}, SA 3100^{TM} series) is in Appendix C and the EDX spectra in Appendix D. The elemental analysis revealed that the solvent-free catalysts had higher percentages by weight of sulphur than the conventionally prepared catalysts. In addition the solvent-free method was found to increase the surface area of the catalysts. The crystallite size measurements obtained from the X-ray diffraction for the conventionally treated sulphated zirconia are shown in Table 4.1. In order to verify the reproducibility of the catalysts, they were synthesized at least five times throughout the period of the research and characterized. Their percentage errors were calculated from their elemental analysis (EDX) for the major components in the catalysts.

Table 4.1: Textural Properties and Elemental Analysis of the Synthesized Catalysts

Catalyst	BET (m^2/g)	Crystallite size (nm)	Elemental analysis (wt%)			
			Zr	O	S	Zr/S
CM	65	10.5^T	49.9±0.4	43.1±0.1	7.0±0.9	7.13
CM*	79	17.3^T	48.2±0.3	47.4±0.3	4.5±0.6	10.71
SFM	168	A	35.5±0.1	51.6±0.3	12.9±0.4	2.75
SFM*	108	A	42.1±0.4	49.2±0.4	8.7±0.1	4.84

T = tetragonal phase, A= amorphous

The SFM and CM* catalysts were synthesized using the same ratio of sulphating agent but the SFM catalyst retained more (> 170%) sulphur species on the surface than CM*. Likewise the CM and SFM* with SFM* having approximately 24% more than the CM. With the solvent-free method more sulphur was retained on the catalysts. It can be observed also that changes in the method of preparation increased the surface area, while change in molar ratio of sulphating agent affected the crystallite size of the catalysts. The scanning electron micrographs of the CM and CM* shown in Figure 4.7 and 4.8, below revealed several particles stacked together to form agglomerates. It can be deduce from the percentage errors (see Table 4.1) that these catalysts can be reproduced without any major change in their properties.

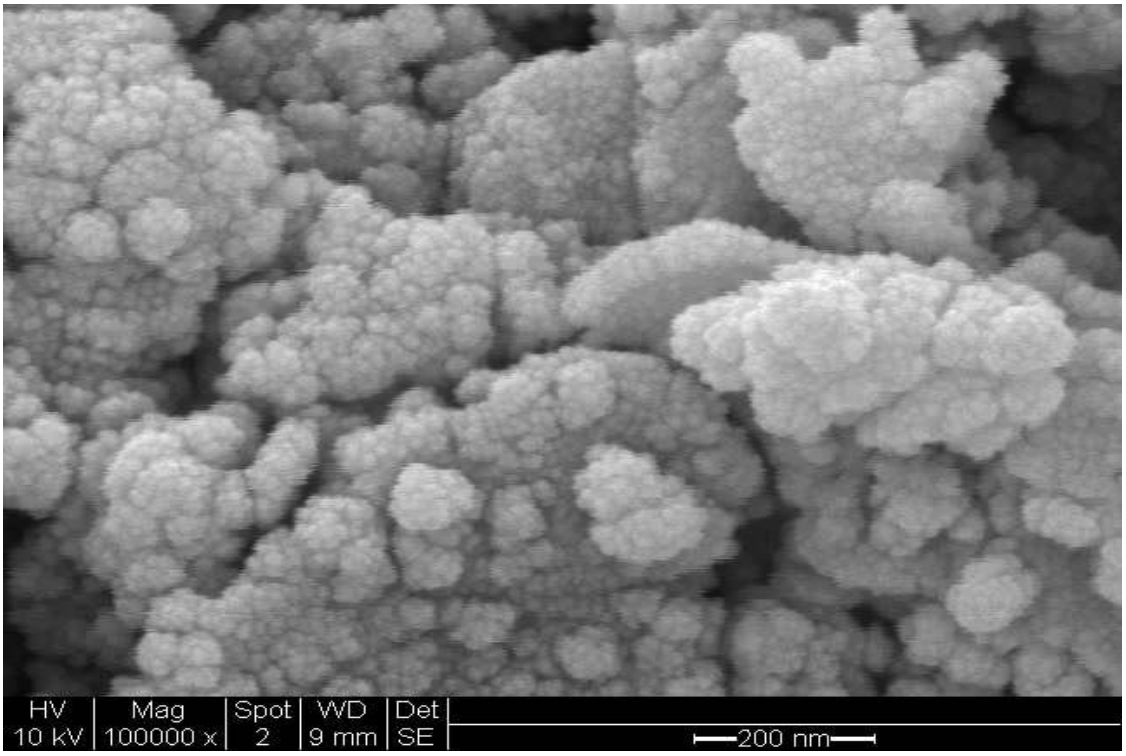

Figure 4.7: SEM Micrograph of the CM Catalyst

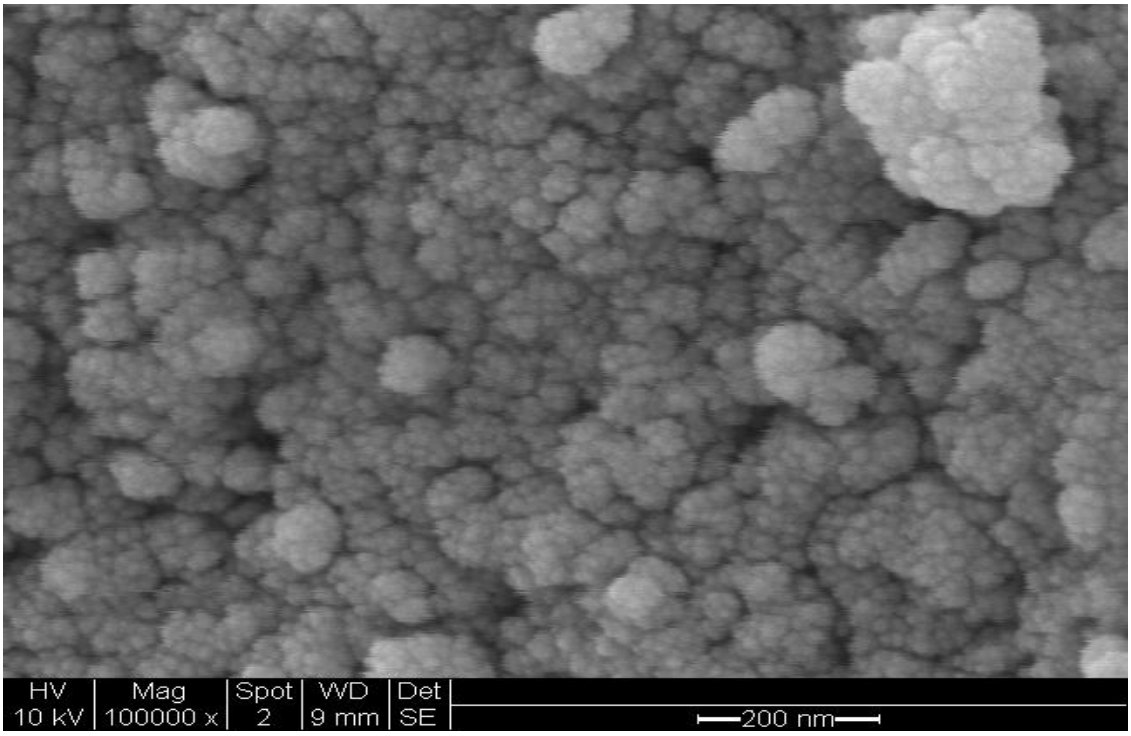

Figure 4.8: SEM Micrograph of the CM* Catalyst

The SEM images of solvent-free catalysts (Figures 4.9 and 4.10) exhibited a substantially different morphology, of well-bonded aggregates rather than the detached particles of the conventional method catalysts.

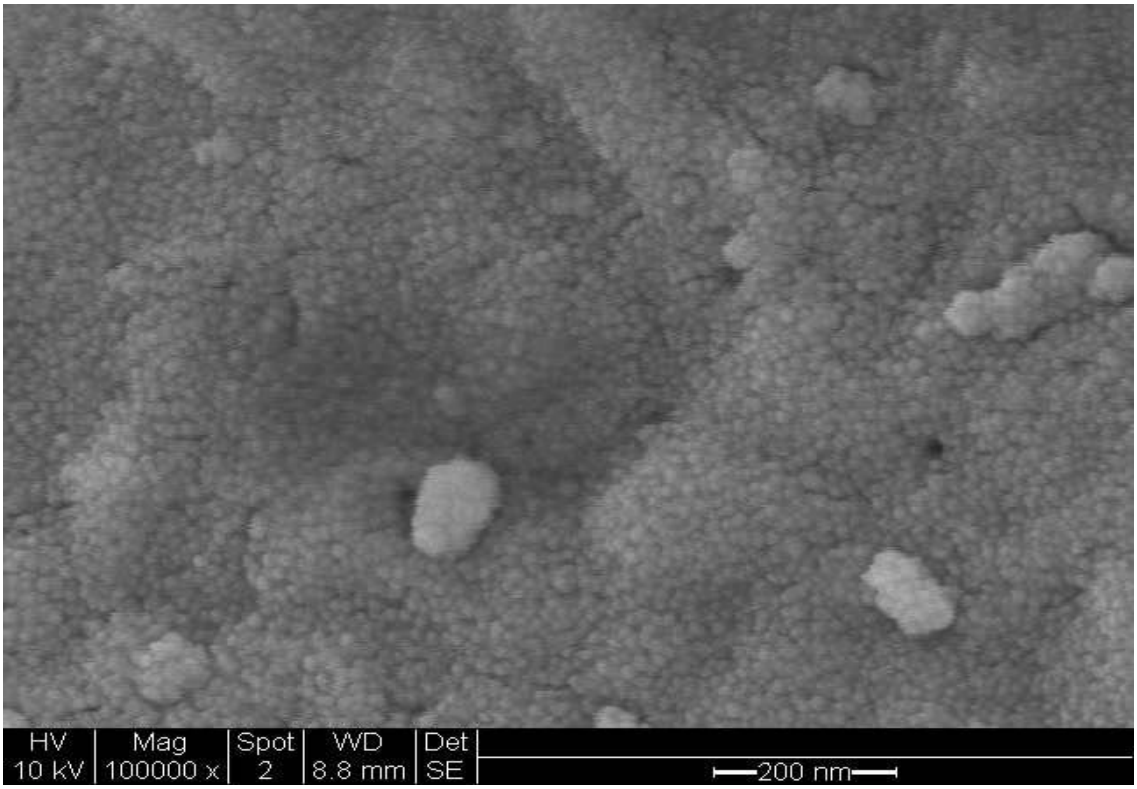

Figure 4.9: SEM Micrograph of the SFM Catalyst

However, the particles appeared denser in SFM* than the SFM as shown in Figure 4.10

Figure 4.10: SEM Micrograph of the SFM* Catalyst

The SEM digital maps of the catalysts confirmed the presence of more oxygen and sulphur on the solvent-free catalysts than the conventional, see section 4.2.1.5.

4.1.2 Infrared Spectroscopy

The sulphate content of the catalysts after calcination at 650^{o}C and 600^{o}C for conventionally prepared and solvent-free catalysts respectively was estimated using Infrared (IR) spectroscopy as described in section 3.2.1. The spectra were produced at a resolution of 2cm^{-1} between 4000cm^{-1} and 400cm^{-1}.

4.1.2.1 Conventional samples

The IR spectra of CM and CM* are shown in Figure 4.11. The CM spectrum exhibited a broad peak in the region 3750–2750cm^{-1}, corresponding to the O-H bond vibration of the adsorbed water on the surface of the zirconia. The intensity of this peak reduced with the decrease in the amount of sulphate used during CM* catalyst preparation, as seen in the IR profile in Figure 4.11. This is followed by weaker absorption at 1580-1640cm^{-1}, which is assigned to the bending mode (δ-OH) of coordinated water. The sulphate content present on the catalysts is evidenced by the sulphate stretches in the spectra in the range 1300-900cm^{-1}.

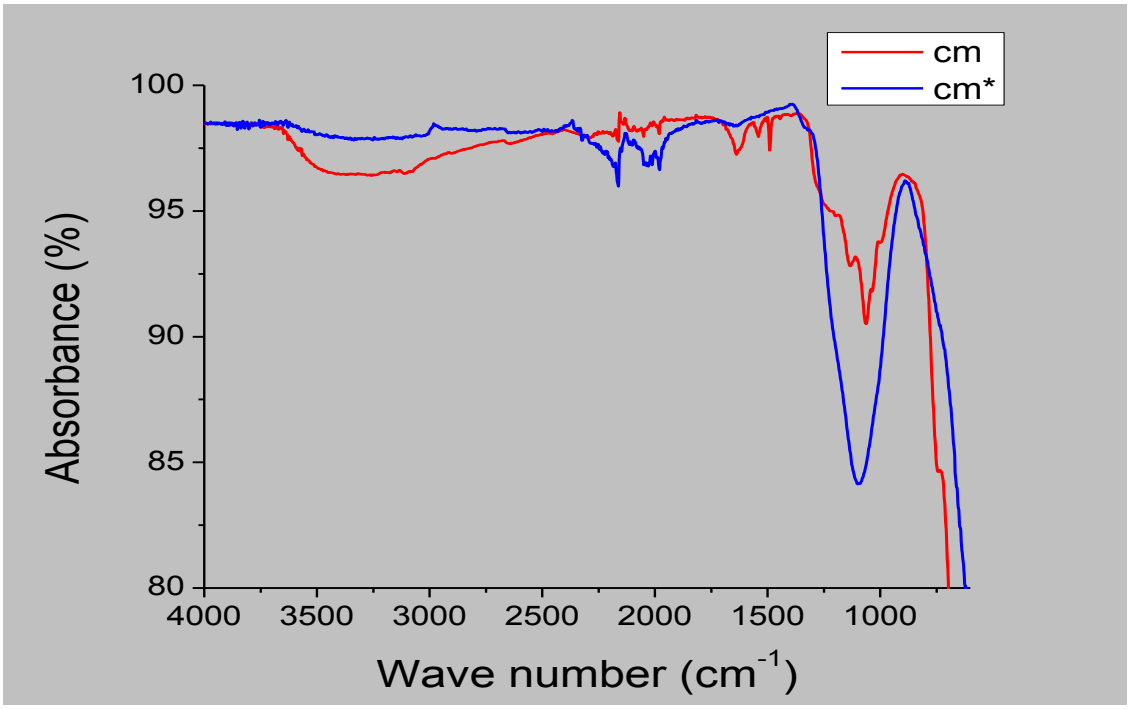

Figure 4.11: IR Spectra of Catalysts from the Same Method of Preparation (conventional wet-precipitation)

4.1.2.2 Solvent-free samples

The same trend as the conventional catalysts was observed in the IR spectra for the solvent-free catalysts (see Figure 4.12). They exhibited similar intensities of O-H bond vibration at wave numbers 3750–2750cm^{-1} whereas the conventional had different intensities. The sulphate absorptions are very similar, indicating the same sulphur species.

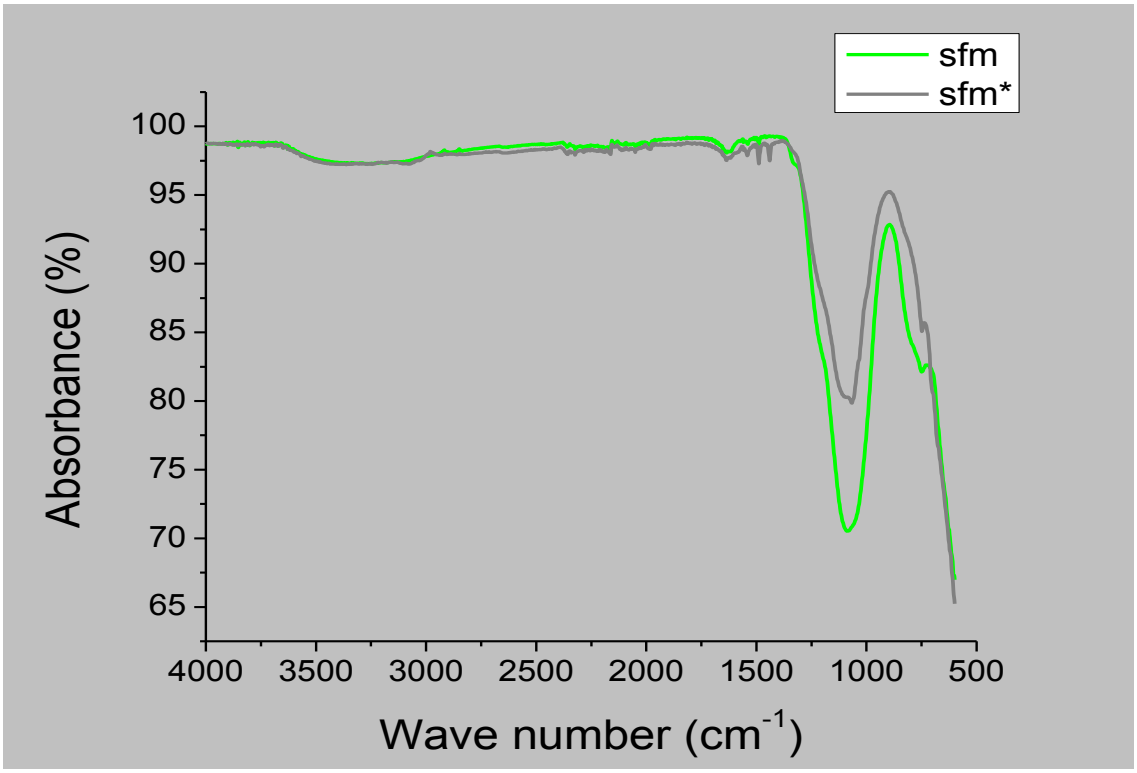

Figure 4.12: IR Spectra of Catalysts from Solvent-free Method of Preparation

4.1.2.3 IR of samples with the same ratio

The intensities of absorbance within the sulphate region for catalysts with the same ratio of sulphating agent (1:15), CM and SFM* are compared in Figure 4.13, below. A closer look at the spectrum of the CM sample within the wave numbers 980cm^{-1} and 1250cm^{-1} shows five IR absorption dips at 1250, 1140, 1060, 1030 and 1000cm^{-1}, whereas for SFM*, a single dip is indicated. This change is presumably due to the formation of polynuclear sulphate compounds on the CM sample. However, they are the characteristic peaks for the S=O and S-O stretching modes of the vibration of the coordinated SO_4^{2-} species on the surface of the catalysts. According to Parvulescu *et al.* (1999), the peaks at 1250cm^{-1} and 1140cm^{-1} are typical of S=O stretching modes in chelating bidentate sulphate species coordinated to the zirconium cation.

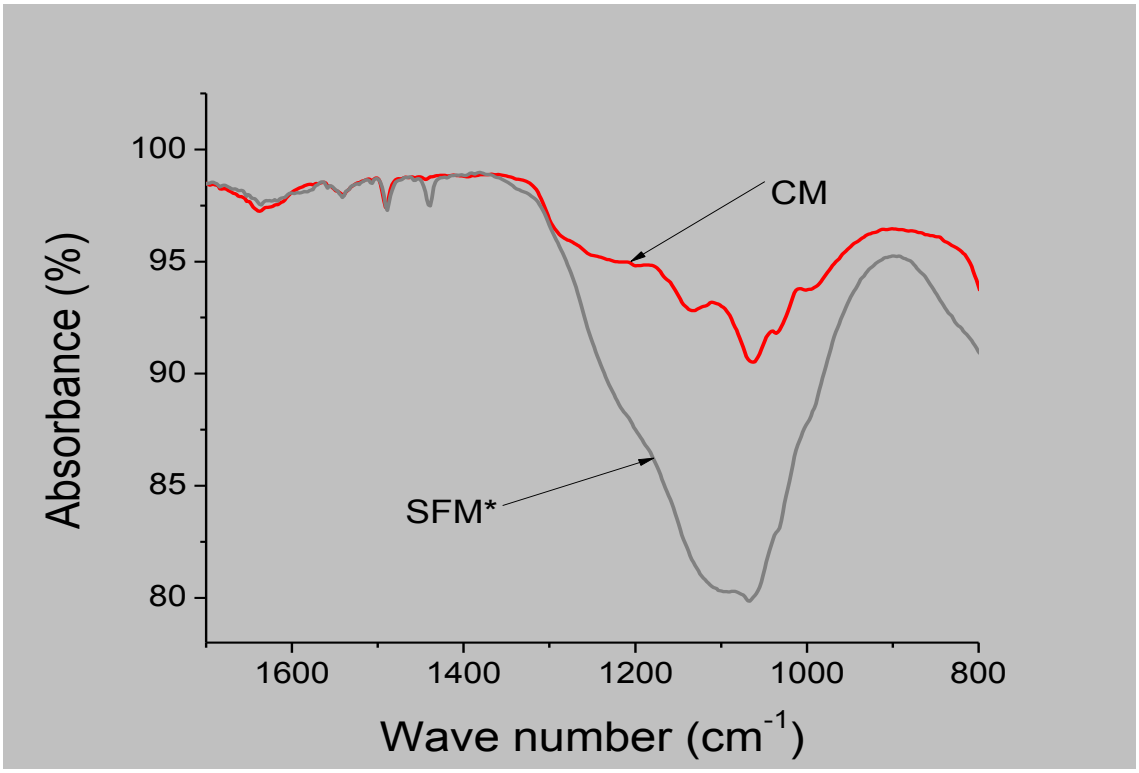

Figure 4.13: IR Spectra in the Sulphate Region of the Sulphated Zirconias with the same ratio of $Zr(OH)_4/SO_4^{2-}$ (1:15)

The bands at 1060, 1030 and 1000cm^{-1} correspond to the S-O stretching frequency in bridged bidentate sulphate species. Furthermore the SFM* catalyst revealed a higher absorbance of 20%, whereas for CM it was 7.5% even though the same ratio of sulphate agent was used. This difference in the retained sulphate on the SFM* catalyst and the CM is due to the synthesis method. These results are in agreement with those of thermal analysis described in section 4.1.3.

In the case of samples with the ratio of 1:6 (shown in Figure 4.14), the sulphate-stretching frequencies are very similar but have different intensities. The intensity of the absorbance of the SFM sample was 30% and that of CM* 15%. The solvent-free method ageing period of 18h appears to allow a sufficient time for contact between the zirconium source and the sulphate ions for enhanced sulphate retention on the catalysts.

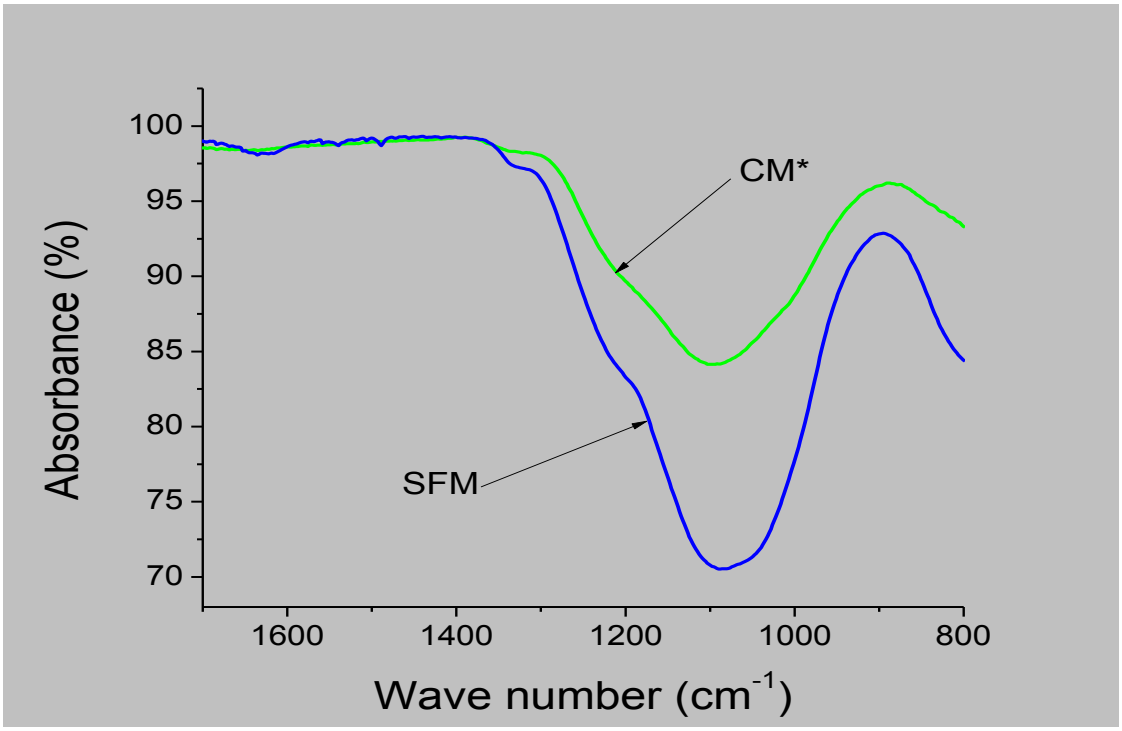

Figure 4.14: Infrared Spectra in The Sulphate Region of the Sulphated Zirconias with the same ratio of $Zr(OH)_4/SO_4^{2-}$ (1:6)

Furthermore, another characteristic peak for the vibration mode S=O was observed at a frequency of 1310cm^{-1} on the SFM catalyst, but this was not evident for the SFM*. This band presumably occurred due to the increase in the concentration of the surface sulphate group. It is worth mentioning that the conventional catalyst, CM*, with reduced sulphate during preparation retained more sulphate on the precursor than its counterpart, CM. Based on the IR analysis, it seems that the solvent-free method enhanced the retention of sulphate on the catalysts irrespective of the ratio of sulphate used or its source as shown in Figure 4.15.

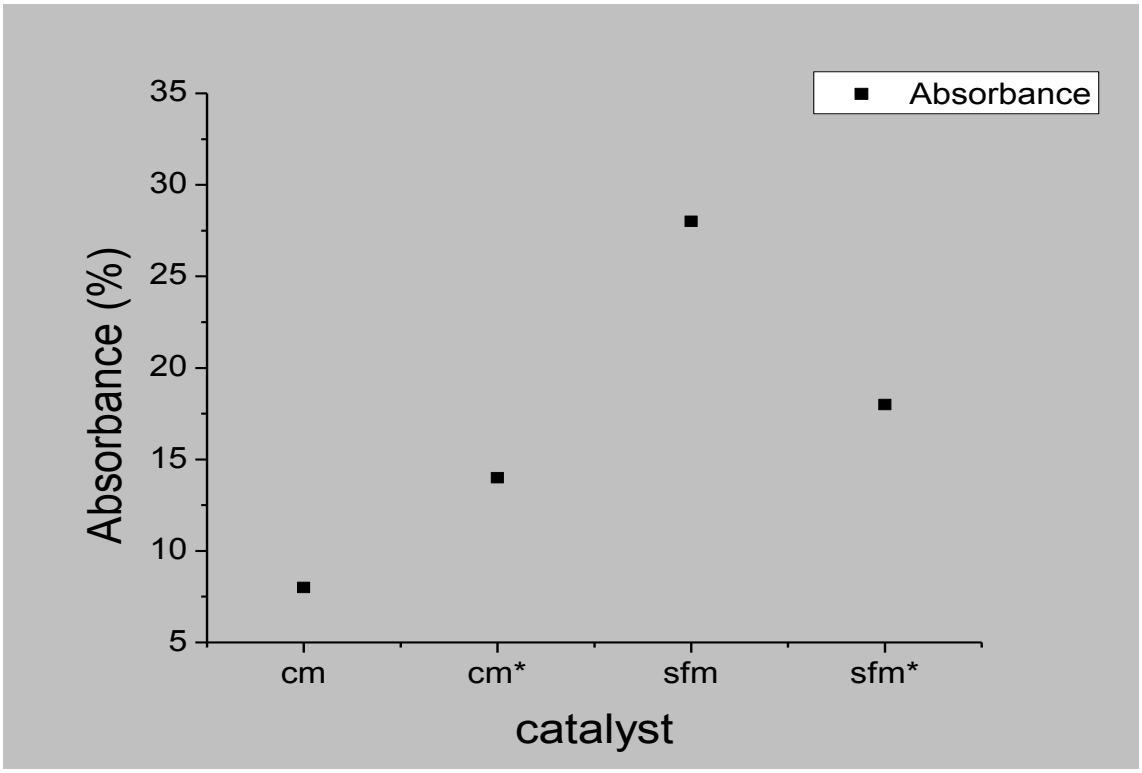

Figure 4.15: Absorbance of Infrared Spectra of the Catalysts (%)

4.1.3 Thermal gravimetric analysis (TGA)

Thermal gravimetric analysis was performed on the catalyst samples, as described in section 3.2.7, in order to confirm the calcination temperatures and to monitor sulphate decomposition. Figure 4.16 shows the TGA profiles for the non-calcined samples. These suggest that the samples thermally decomposed in a stepwise manner. In the first step, the weakly bonded water molecules were lost (100-200^{o}C), and with further heating (300-600^{o}C) excess sulphate was lost until at higher temperature (> 600^{o}C), the decomposition of the sulphated metal oxide occurred to give zirconium oxide and the volatile by-products sulphur dioxide and oxygen. The phenomena observed are in accordance with the findings of Strydom and Pretorius (1993) on thermal decomposition of zirconium sulphate hydrate.

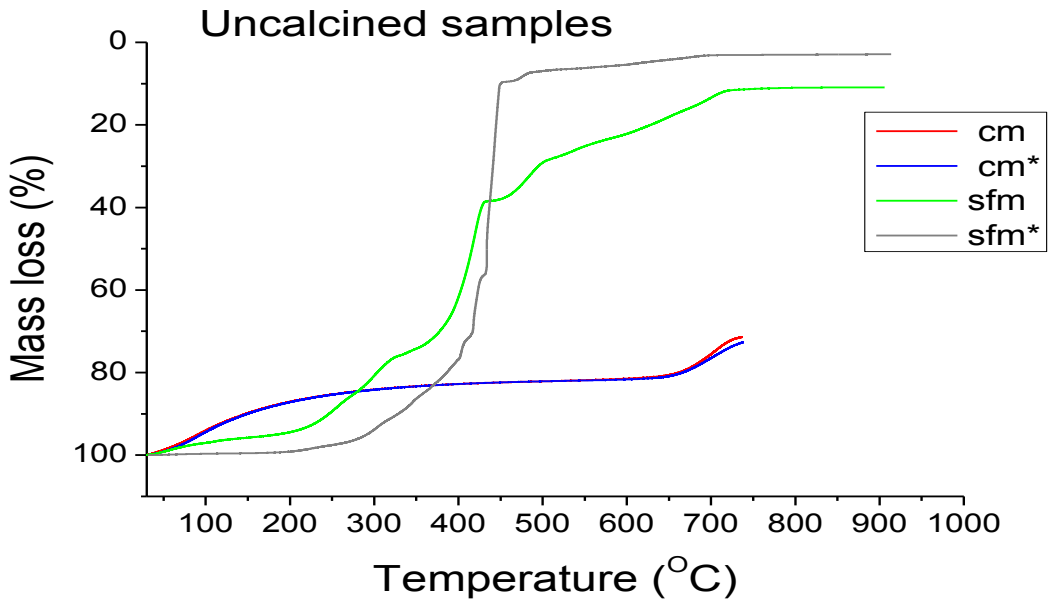

Figure 4.16: Thermogravimetric Analysis Profiles for the Non-calcined Sulphated Zirconias

However additional weight loss was noticed with the solvent-free catalysts. Weight losses within the temperature range of 200-250°C and 300-400°C as seen in Figure 4.17 can be attributed to the loss of water molecules and the loss of ammonia and chloride ions, probably as HCl due to the decomposition of NH_4Cl on the samples.

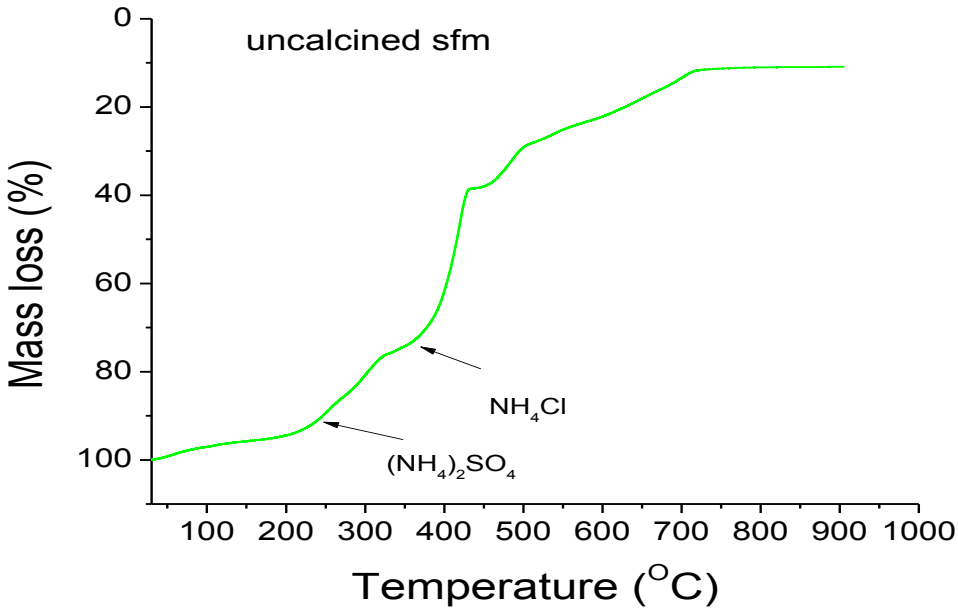

Figure 4.17: Thermogravimetric Analysis of Non-calcined Solvent-free Sulphated Zirconia

This is on the basis that Olszak-Humienik (2001) had reported that ammonium chloride decomposes between 300-400^{o}C. The unreacted $(NH_4)_2SO_4$ on the surface of the catalyst could also decompose to gaseous NH_3, SO_3 and H_2O because ammonium sulphate decomposes between 200-280^{o}C (Yilmaz *et al*., 1994). The presence of NH_4Cl on the solvent-free catalysts was revealed earlier by the X-ray diffraction patterns of the non-calcined solvent-free samples shown in Figure 4.4 and Figure 4.5.

The amounts of sulphate on the calcined catalyst samples were also monitored by thermogravimetric analysis. The profiles are similar to those of non-calcined samples, but with different weight losses. The mass losses corresponded to the amount of sulphate on the catalysts with the highest being from the solvent-free catalysts (see Figure 4.18). The SFM* catalyst showed higher losses of weakly bonded water molecules than SFM between 100^{o}C to 200^{o}C. In the region of 600-900°C, the weight losses of samples CM and CM* were 1.4% and 13% respectively. These percentages show that CM* had more sulphate on the catalyst than CM. The weight losses due to the decomposition of zirconium sulphate with SFM and SFM* were 40% and 28% respectively.

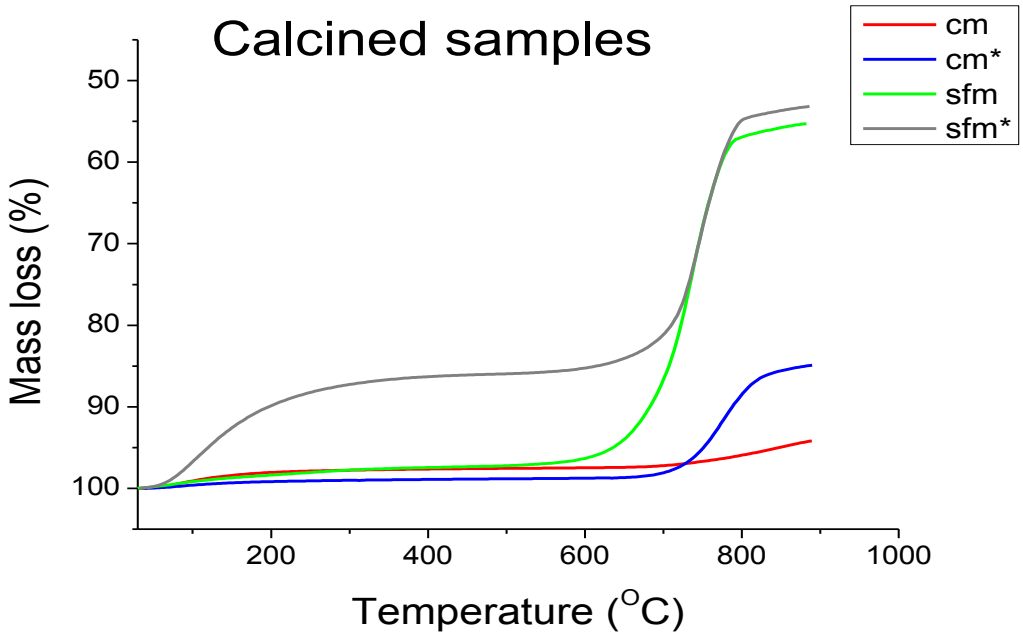

Figure 4.18: Thermogravimetric Analysis of Calcined Sulphated Zirconia

A comparison based on the same ratio of sulphating revealed that 35wt% of the catalyst was sulphate on SFM* whereas CM had only 7wt% of sulphate in the total weight of the catalyst (see Figure 4.19).

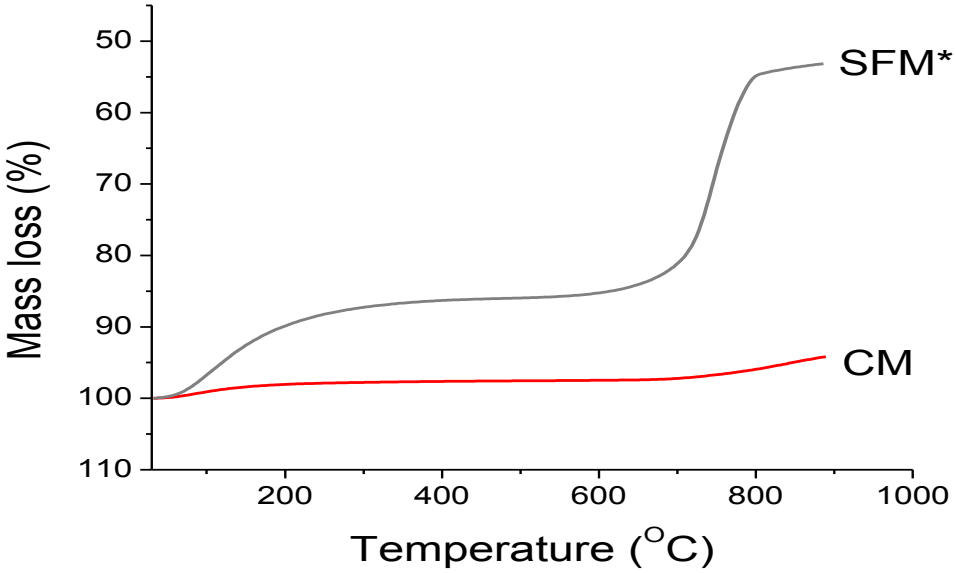

Figure 4.19: TGA Profiles for Samples with the Same Ratio (1:15) of Sulphating Agent

Figure 4.20 compares samples SFM and CM* (same ratio 1:6), showing that a total weight loss of 41% was sulphate on the SFM catalyst sample whereas for CM* it was 13wt%.

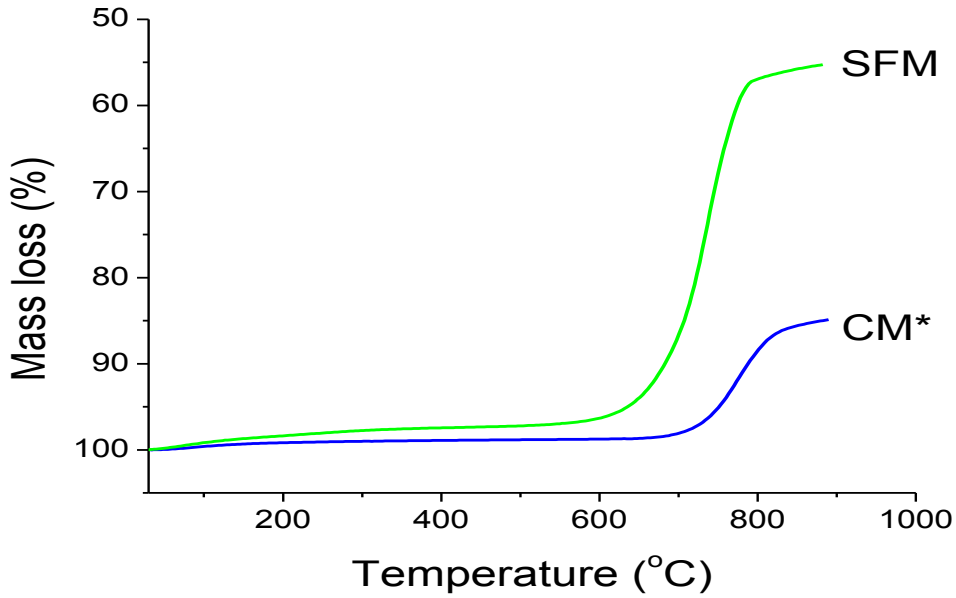

Figure 4.20: TGA Profiles of Samples with Same Ratio (1:6) of Sulphating Agent

Based on the chemical composition of the catalysts and decomposition temperature of sulphate which was reported as 600^{o}C by Bear and Mumme (1970); the only element responsible for the weight loss at the temperature of the thermal decomposition (900^{o}C) is sulphate decomposition. Generally, the results of the thermogravimetric analysis revealed higher weight loss on the solvent-free method. Therefore it is a more effective method than the conventional method in terms of sulphate retention on the surface of the catalysts.

4.1.4 Pyridine-DRIFTS (Diffuse Reflectance Infrared Fourier Transform Spectroscopy)

Measurements of the acidity of the synthesized sulphated zirconia catalysts were conducted using pyridine-DRIFTS in accordance with the procedure described in section 3.2.8. The spectra of adsorbed pyridine on the samples at room temperature revealed characteristic bands in the region 1400 to 1600cm^{-1} on the different catalyst samples prepared by the conventional method (CM and CM*) and the solvent-free method (SFM and SFM*) (see Figure 4.21).

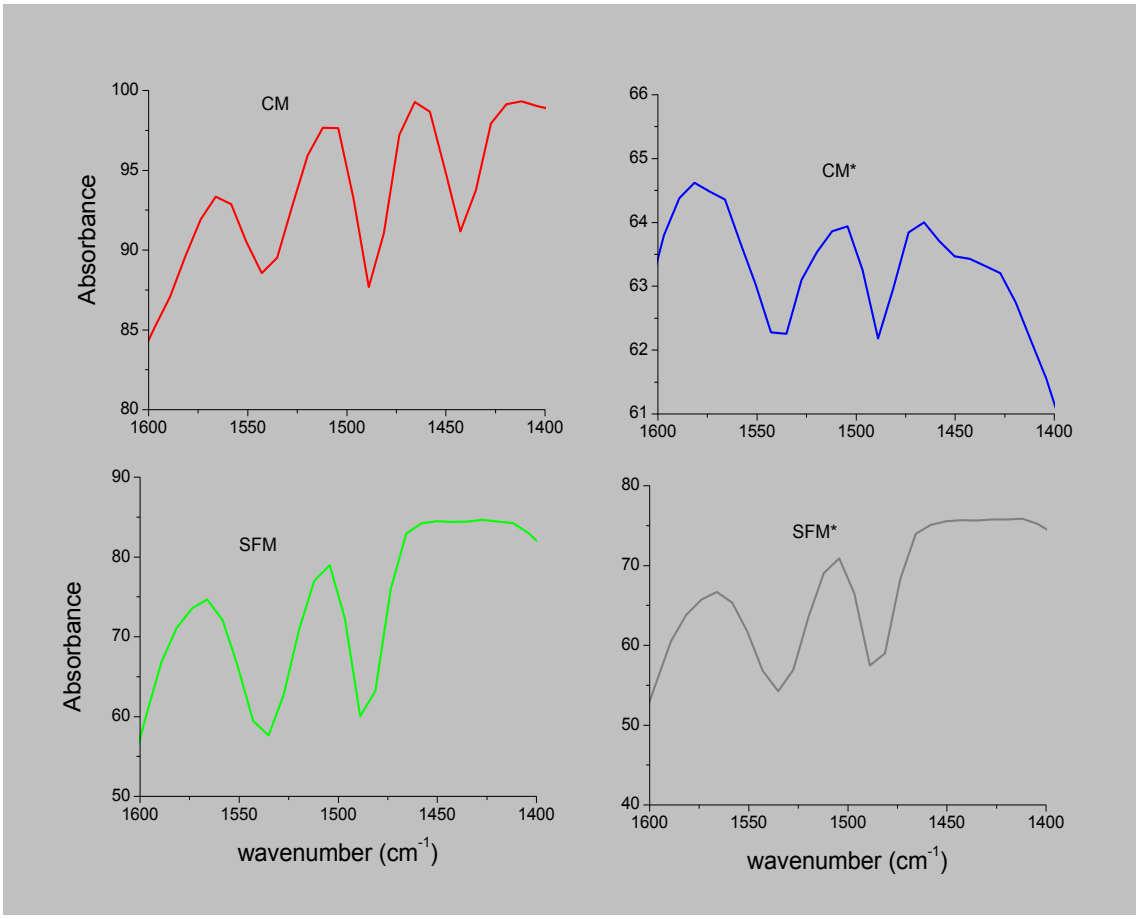

Figure 4.21: FT-IR Spectra of Adsorbed Pyridine on the different Catalysts

Generally the spectra showed typical pyridine-IR absorption bands for sulphated metal oxides (Sun *et al*., 2005; Morterra *et al*., 1993a). Bands at 1545cm^{-1} are due to adsorbed pyridine interacting with Brønsted acid sites (Song and Sayari, 1996). There were also well-defined adsorption bands around 1445 and 1488cm^{-1} of Lewis acid sites and pyridinium ions **(**Parvulescu *et al*., 1999). However, the intensity of the bands changed from one catalyst to another according to the preparation method and the molar ratio of the sulphating agent used for sample preparation. The band at 1488cm^{-1} is a weak band which is assigned to pyridine adsorbed on Lewis acid sites.

Comparison of the spectra revealed a strong Lewis acid sites band at 1445cm^{-1} on the conventional catalyst samples (see Figure 4.22). This band is more well-defined on the CM sample than on the CM*, and it shifted to a higher wave number of 1450cm^{-1} on the CM* catalyst. This shift in band is probably due to a weakening of the S=O bonds, which may be induced by the increase in electron density as a result of the pyridine molecule interacting directly with the sulphated species on the surface of the CM catalyst (Babou *et al*., 1994). However, the band was not pronounced on CM* and was completely absent from the solvent-free samples. The band at 1488cm^{-1} is a weak Lewis band and is common to all the catalyst samples.

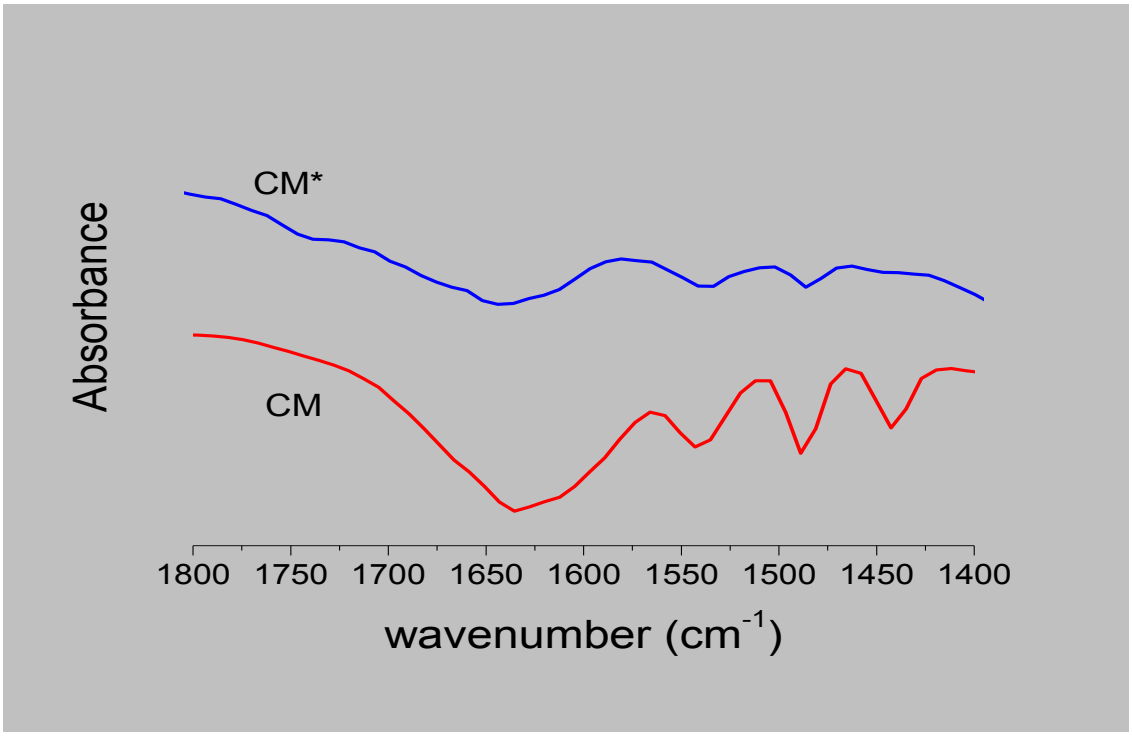

Figure 4.22: IR-py Spectra of Conventionally Prepared Catalysts

The difference in sulphate ratio between samples CM and CM* did not result in any shift of wave number. It seems the increase in the overall amount of sulphate used in CM preparation resulted in enhanced S=O stretching modes in chelating bidentate sulphate species coordinated to the zirconium cation. The second band at 1488cm^{-1} corresponding to Lewis acid sites was common to both samples, although its absorbance varied. The CM sample's absorbance is 10% for band at 1488cm^{-1} and 2% for CM*. The intensity of the Brønsted acid sites band at 1545cm^{-1} was 6% for the CM sample and 2% for the CM* sample , as the Lewis acid site**.** Catalyst samples prepared by the solvent-free method SFM and SFM* showed similar wave numbers (as shown earlier in Figure 4.21) irrespective of the molar ratio of the sulphate used during preparation. Therefore there was no effect of the ratio of sulphating agent on the type of acid sites on the catalysts. Generally, solvent-free catalyst samples did not exhibit a band at 1445cm^{-1}, indicating the absence of strong Lewis acid sites. Furthermore, the solvent-free samples had higher band intensities at 1545cm^{-1}, compared to the conventional catalysts. The intensities of the bands at 1488cm^{-1} and 1545cm^{-1} were 15% and 14% respectively for SFM whereas for SFM* they were 14% and 13%. However, the areas of the bands varied: SFM had the highest for both bands, followed by the SFM*, whereas CM* had the least. This means that higher concentrations of the acid sites were present on the SFM catalyst despite the lower ratio of sulphate used for its synthesis, indicating that the solvent-free method of preparation has a better atom efficiency.

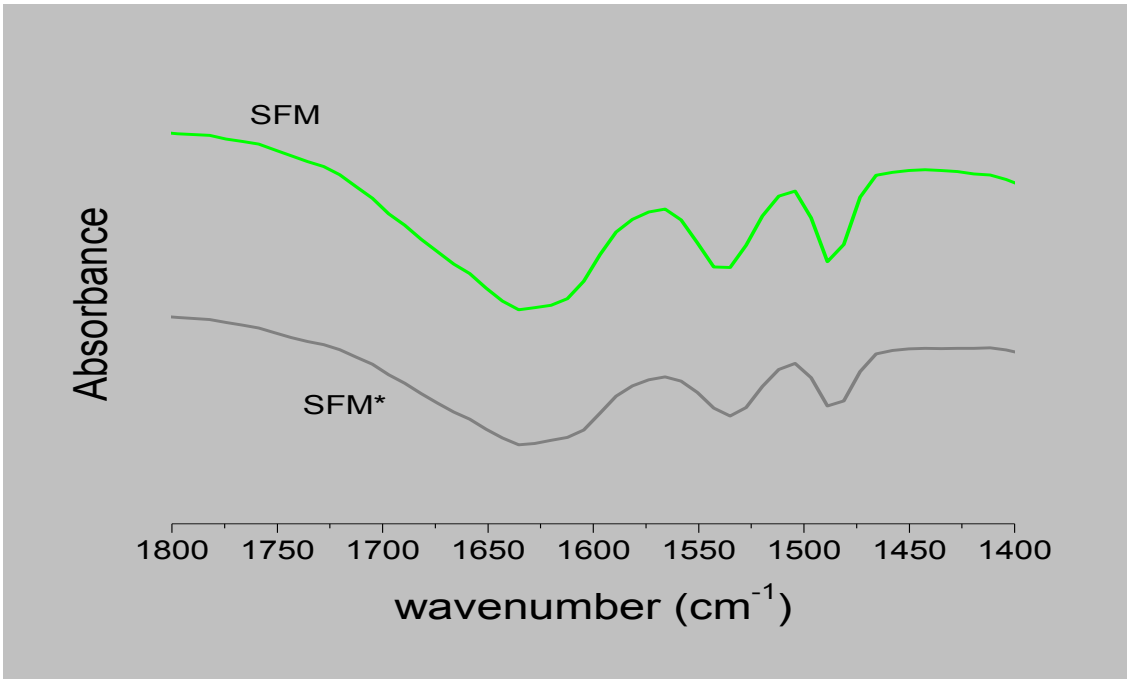

Figure 4.23: IR-py Spectra of Solvent-free Prepared Catalysts

Another interesting finding is the sizeable difference in the percentage of Brønsted acid sites on the CM sample to about 13% that of the SFM* sample, despite the same amount of sulphate being used for both catalysts. The percentage of integrated area of Brønsted acidic was 46% for SFM* and 33% for CM. (see Figure 4.24). The percentage for Lewis acid site was 67% on CM catalyst. This implies that the double bond in S=O in CM is much stronger than a simple metal sulphate bond and has contributed to the increased Lewis acid by its inductive effect in the structure of the catalyst. The presence of polynuclear sulphates observed in Figure 4.13 under section 4.1.2.3 is another reason for increased Lewis acid sites on the CM catalyst Parvulescu *et al*. (1999).

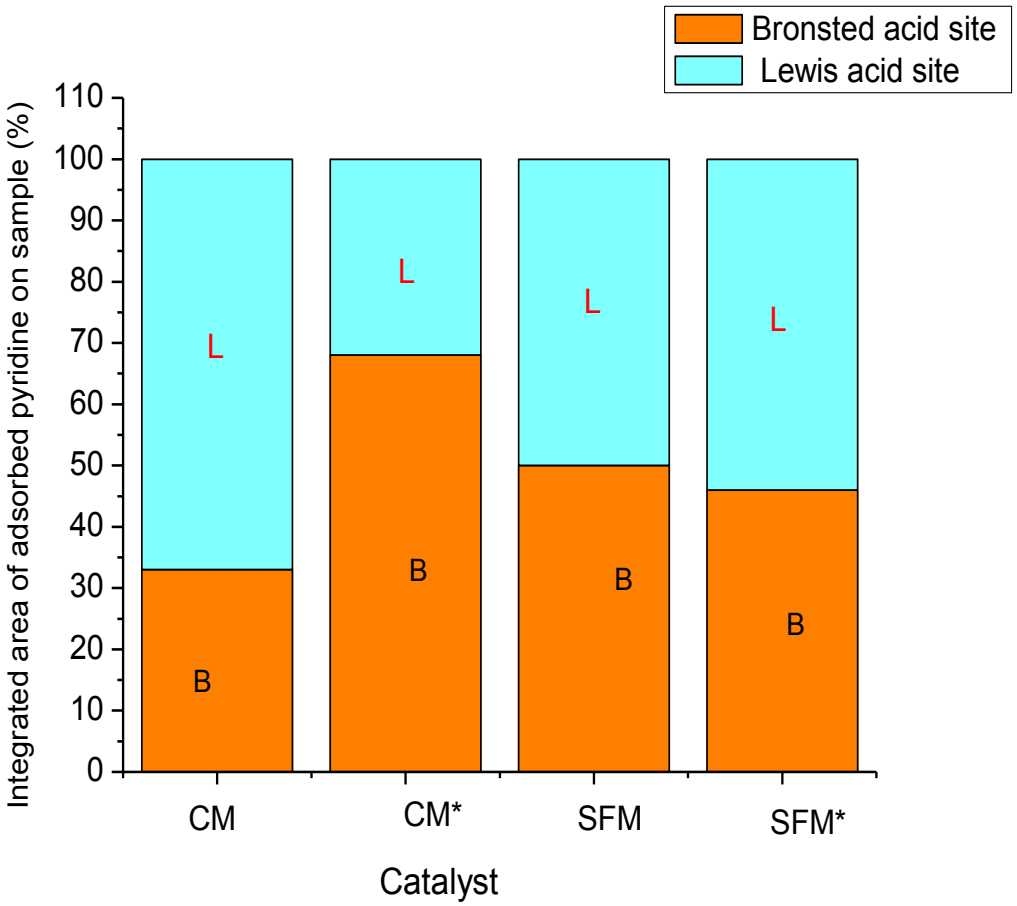

Figure 4.24: Percentages of Integrated Area of Brønsted and Lewis Acid on each of the Catalysts

Although CM* tends to have more percentage of Brønsted acid sites (~ 70%) than SFM; the peak area and the acid site concentrations was much smaller. Generally, therefore, comparing the decrease in the band intensity with the amount of sulphate used, such a

reduction could suggest that the solvent-free method facilitates a stronger interaction between the sulphate groups with the zirconia cations. The samples prepared by the solvent-free technique (SFM and SFM*) exhibited higher concentrations of Brønsted rather than Lewis acid sites. The reverse was the case in the CM catalyst, but CM* had more Brønsted acid sites than the CM, as shown in Figure 4.25 compared with their total acid site concentrations.

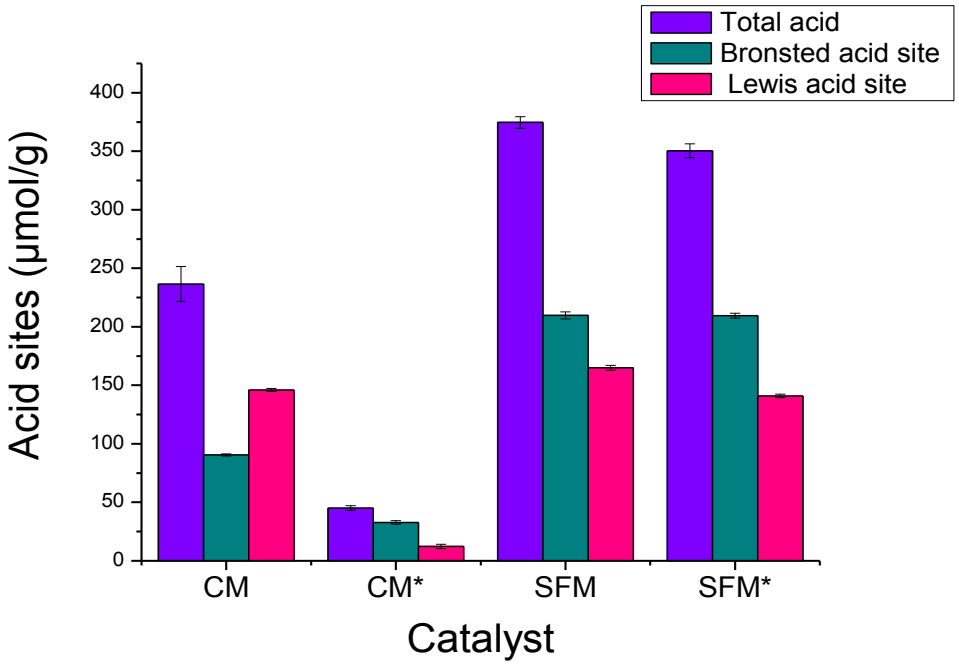

Figure 4.25: The Figure Indicating the Amount of the Total Acid and its corresponding Brønsted and Lewis acid sites on the Catalysts

In all the samples it is evident that the method of preparation had a more direct effect on the total and individual concentrations of the various types of acid sites. In other words the amount of sulphate retained on the catalyst is not only determined by the amount of sulphate used but much more the method of preparation. Secondly the type of acid site depends on the displacement of the bridge hydroxyl groups of hydrated zirconia and bisulphate ions with an adjacent hydroxyl group, as reported by Clearfield *et al*. (1994). From the characterization results, particularly the FTIR and the IR-py, the S=O bond was predominant and stronger in CM whereas it was S-O bond in solvent-free catalysts. Based on these the dominant bonding structure in the solvent-free catalysts as well as in the CM* sample can be represented as shown in Figure 4.26 (a) and Figure 4.26 (b) for the CM catalyst.

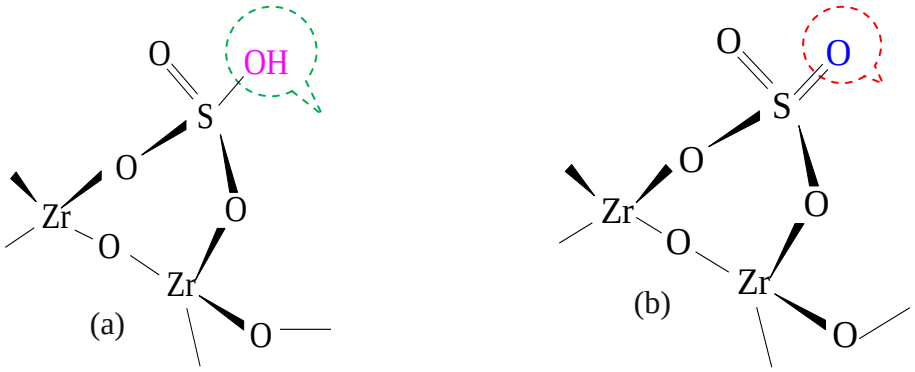

Figure 4.26: Showing the S-O and S=O bonds responsible for the Brønsted (a) and Lewis (b) Acid Sites respectively on the catalysts

With the solvent-free method, it seems reasonable to suspect that the bridge hydroxyl groups on the hydrated zirconia were displaced while the bisulphate remains intact during calcination. In the case of conventional method most of the hydroxyl groups on the bisulphate were involved in the reaction during calcination; resulted into Lewis acidity. These resulted structures agreed very much with the models described by Clearfield *et al*. (1994) and Babou *et al*. (1995).

4.1.5 X-ray photoelectron spectroscopy (XPS) spectra

The X-ray photoelectron spectroscopy data were generated using the procedure reported in section 3.2.5. The characteristic peaks for sulphur, oxygen and zirconium were found in the XPS Handbook; Moulder *et al*. (1995) and Wagner *et al*. (2000). The relative sensitivity factors were used to scale the measured peak areas and the accuracy of the reported binding energies (BE) can be estimated to be ±0.2eV.

4.1.5.1 Zirconium

Figure 4.27 shows doublet pairs spectra for both $3d^5$ and $3d^3$ corresponding to zirconium in the IV oxidation state. Doublet pairs are due to the splitting of energy levels as a result of the presence of an electron sub-shell with unpaired electrons in the final state of the electronic system.

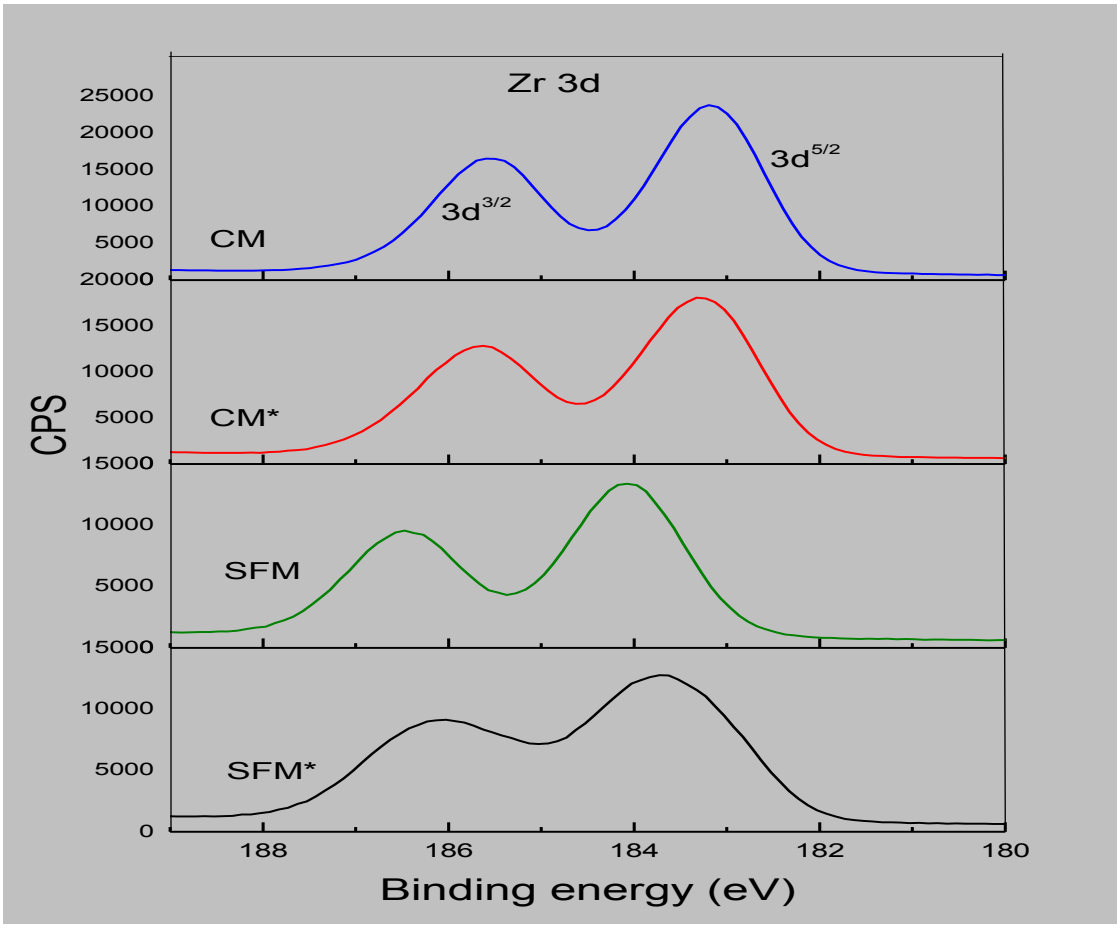

Figure 4.27: XPS Zr 3d Spectra of the Various Catalysts

The binding energies for CM and CM* were similar at 182.9eV and 185.3eV for $3d^5$ and $3d^3$, respectively. The same energy of 2.40eV was recorded between the split of each doublet for all the catalysts. The binding energies for $3d^5$ and $3d^3$ were 183.1eV and 185.5eV for the solvent-free samples SFM and SFM*. Interestingly, the only shift observed in the binding energy of the catalysts at the $3d^5$ and $3d^3$ bands is based on the different method used for the catalysts preparation. The conventional method catalysts (CM and CM*) exhibited similar Zr 3d Spectra and the solvent-free catalysts (SFM and SFM*) exhibited the same pattern. The reason for the observed shift is attributed to the weakening of the S=O bonds which may be induced by electron transfer from the pyridine molecule (strong base) towards a Zr4+ cation (Lewis site). It could also be attributed to direct interaction of the pyridine molecule with the sulphated species as reported by Babou *et al*. (1995). These data, suggest that CM and CM* catalyst samples are very similar, while the Zr in SFM sample is electron deficient in-line with the higher sulphate content in this sample. The SFM* Sample has an intermediate sulphate content

giving rise to the Zr 3d being comprised of two zirconium environments. The various samples showed the same acidic zirconium species.

The method of preparation seems to have had minimal effect on the Zr states. However, although, the oxidation states of the zirconium ion in the four samples were the same, the quantitative areas under the peaks varied in the following order: SFM < SFM* < CM* < CM for both $3d^5$ and $3d^3$. This implies that the conventional samples had more zirconium oxide on their catalysts.

4.1.5.2 Sulphur

The binding energies of sulphur were recorded in the region of 2p energies, as presented in Figure 4.28. The peak corresponding to the S2p species exhibited a pronounced asymmetry. Processing and quantification of the spectra was performed on CasaXPS software. The deconvolution of these peaks using the software led to two different peaks, one located around 169.8eV and another at 170.8eV irrespective of the method and the amount of sulphating agent used for preparation. These peaks are attributed to the S $2p_{1/2}$ and $2p_{3/2}$ respectively.

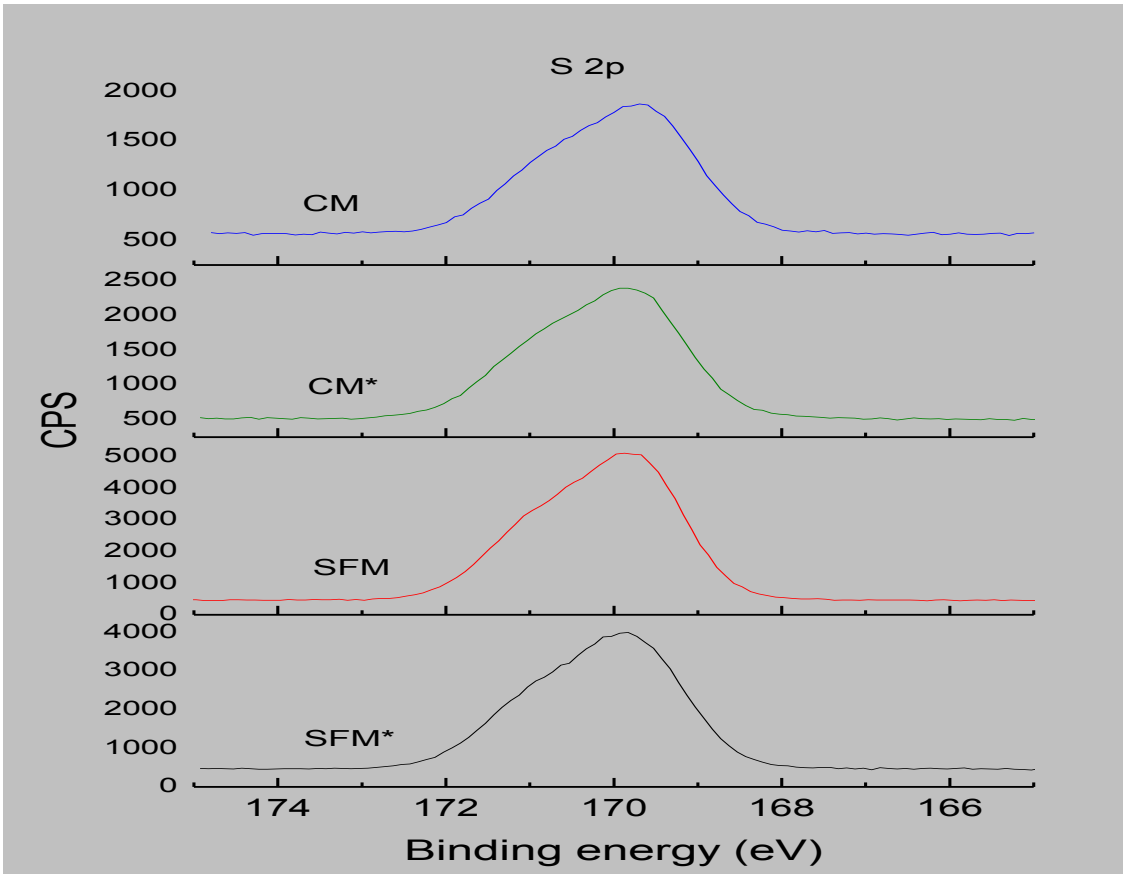

Figure 4.28: XPS S2p Spectra of the Various Catalysts

These binding energies correspond to the sulphur in sulphate species on the sample, which agrees with the findings of other authors (Melada *et al*., 2004). From the deconvolution of the S2p spectra and Parvulescu *et al*. (1999) findings, it is assumed that the sulphur species located around 169.8eV may correspond to the protonated sulphated species, whereas those around 170.8eV would correspond to the deprotonated species. From such assumption, the protonated sulphate groups tend to dominate the samples prepared using the solvent-free method. This could be a consequence of a more interaction of sulphate groups with the zirconium species (Marcus *et al*., 2003). Thus, the solvent-free catalysts exhibited higher intensities at 169.8eV, which correspond to increases in the protonated species population, as shown in Figure 4.29. This was due to the enhanced interaction of sulphate groups with the zirconium oxide support that was possible because of the method of preparation.

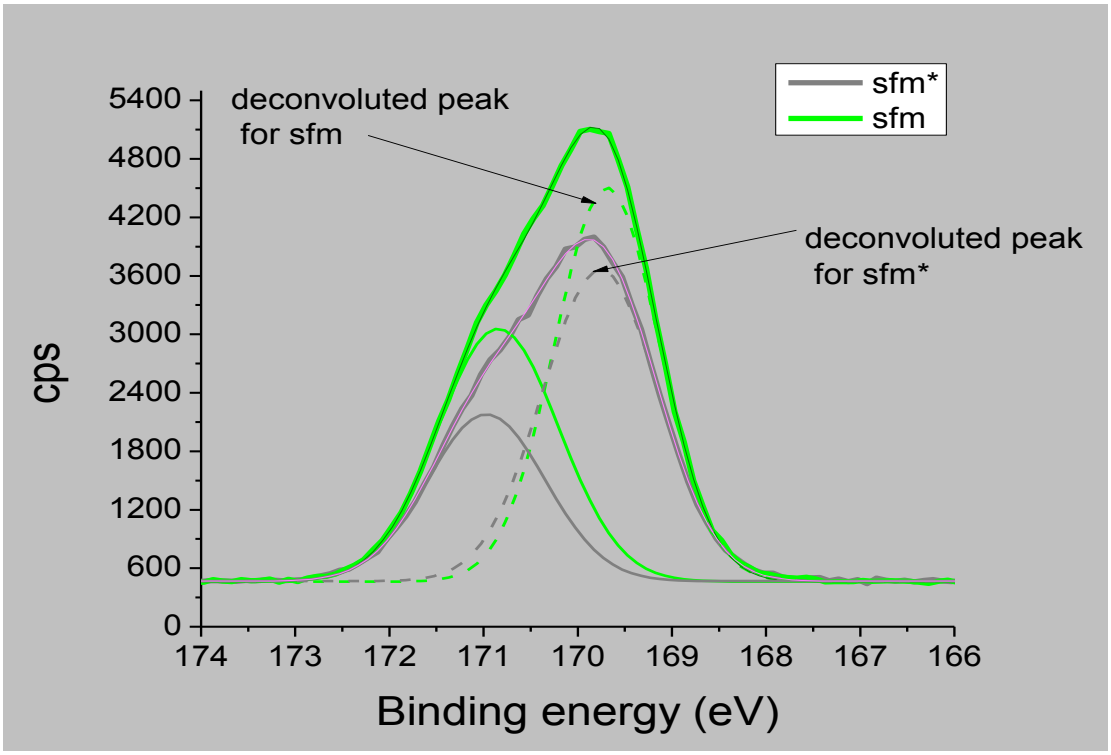

Figure 4.29: XPS S2p Spectra of Solvent-free Catalysts showing the Protonated (----) and Deprotonated (-) Species

On the contrary, deprotonated species exist to a large extent in the catalysts prepared via impregnation of zirconium hydroxide, particularly the CM. That this assumption is correct is clearly demonstrated in Figure 4.30, which compares the moles of sulphur

used during preparation and those retained on the catalysts after calcination at 600^{o}C for solvent-free catalysts and 650^{o}C for conventional catalysts.

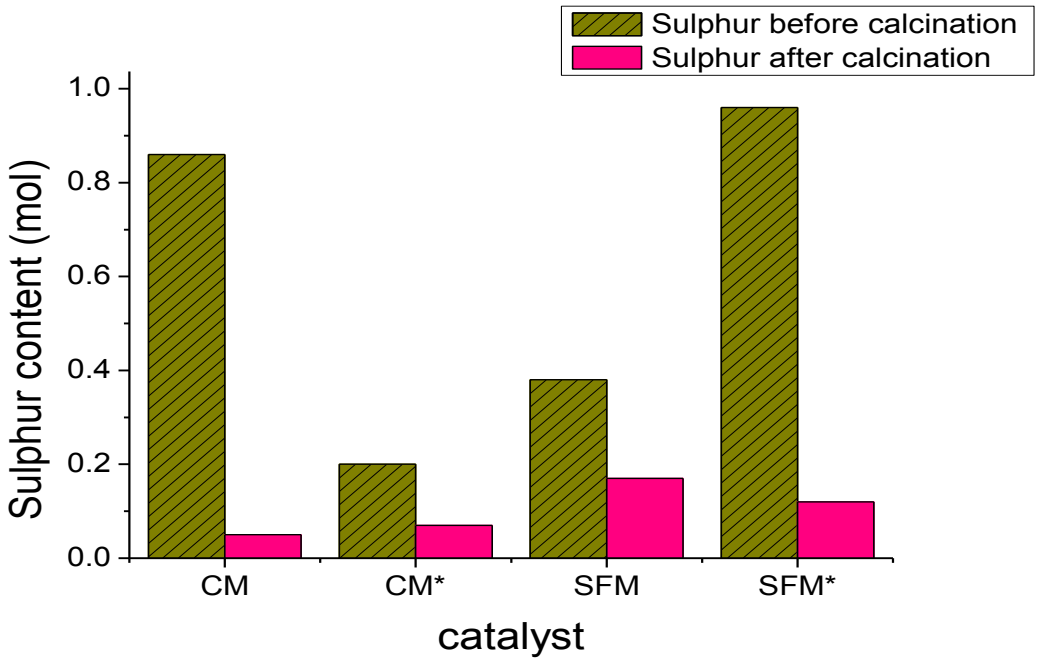

Figure 4.30: Comparing Number of Moles of Sulphate used during Preparation and Sulphur retained on the Catalysts after Preparation.

The calculated values of sulphur on the calcined catalysts agreed with the intensity of the sulphate reported by the IR spectra in section 4.1.2.

4.1.5.3 Oxygen

The binding energies of oxide and sulphate oxygen for all samples were consistent, as shown in Figure 4.31 however, the spectra are different in intensities. The binding energy indicating the oxide oxygen of the zirconia is evident at 530.5eV and the shoulder peak at binding energy 532.5eV is assigned to sulphate oxygen on the surface of the catalysts. According to the XPS Handbook (Hino *et al*., 2006; Moulder *et al*., 1995) the O1s spectra indicated the sulphur is in the SO_4^{2-} form.

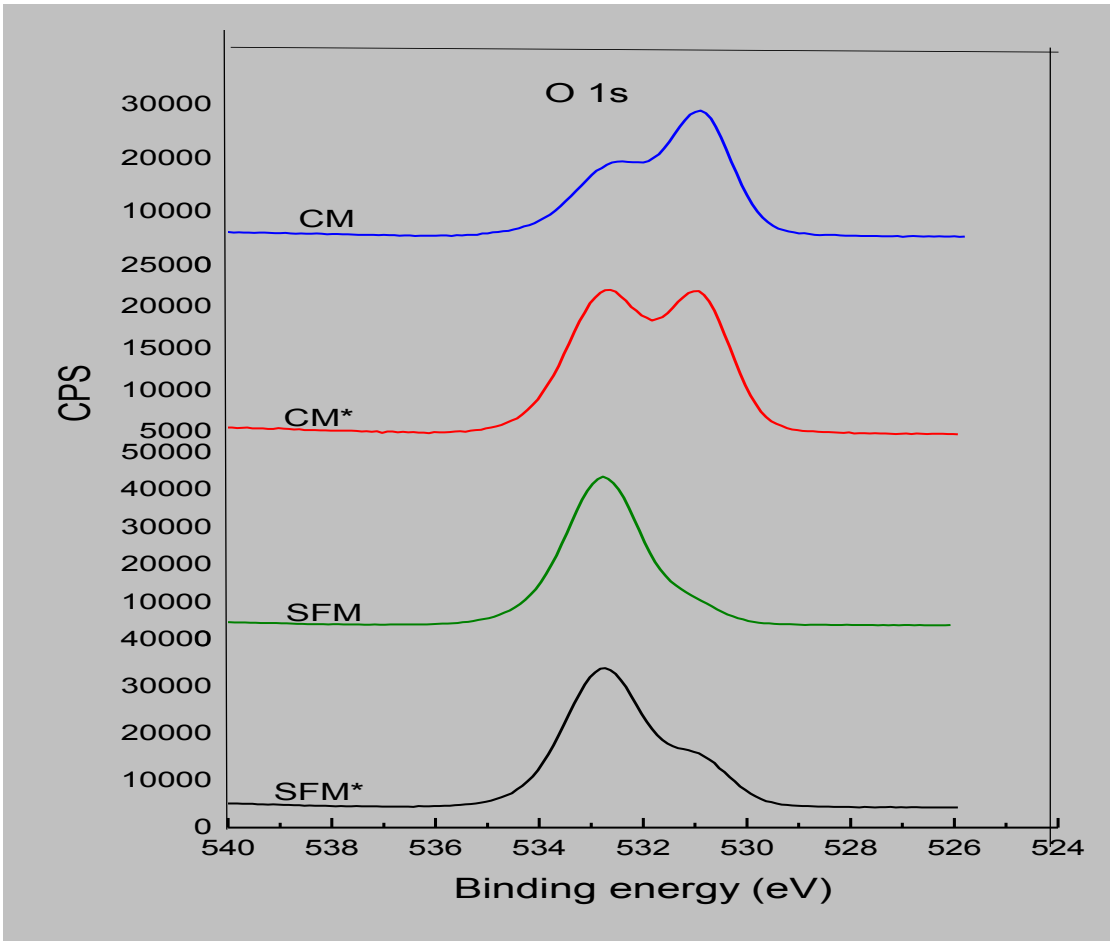

Figure 4.31: XPS O1s Spectra of the Various Catalysts

The peak at 530.5eV is higher for samples prepared by the conventional method, with CM catalyst having the highest. Also, samples produced by the solvent-free method exhibited higher peaks at binding energy 532.5eV, with SFM sample being the highest. This is better illustrated in Figure 4.32 and Figure 4.33 below. The de-convoluted oxide oxygen peak was highest for samples prepared by the conventional method, with the CM catalyst showing the higher peak as demonstrated in Figure 4.32.

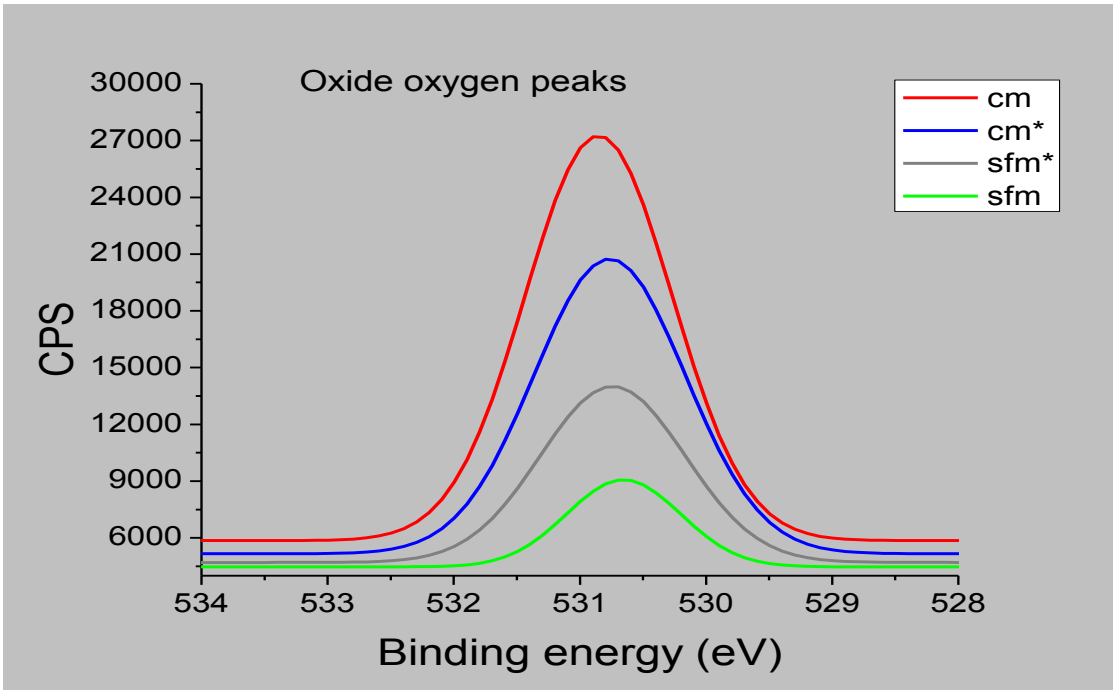

Figure 4.32: Deconvoluted Peaks of O1s showing the Oxide Oxygen Peaks of the Catalysts

On the other hand, the highest peak at a binding energy of 532.5eV, which is sulphate oxygen, was more pronounced in the samples prepared by the solvent-free method.

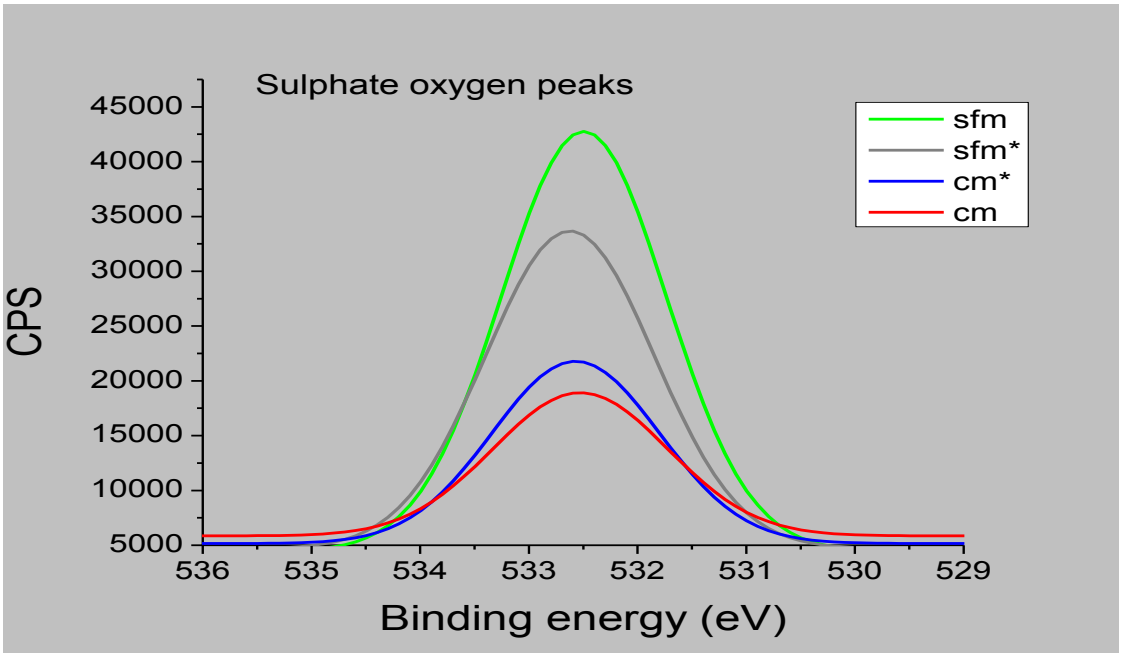

Figure 4.33: Deconvoluted Peaks of O1s showing the Sulphate Oxygen Peaks of the Catalysts

The percentage of sulphate oxygen was higher in solvent-free catalysts; SFM had 93% and SFM*, 81% as shown in Figure 4.34. The high percentages of sulphate explain why the highest number of Brønsted acid sites are found on the solvent-free catalysts, as was evident from the pyridine-DRIFTS analysis in section 4.1.4.

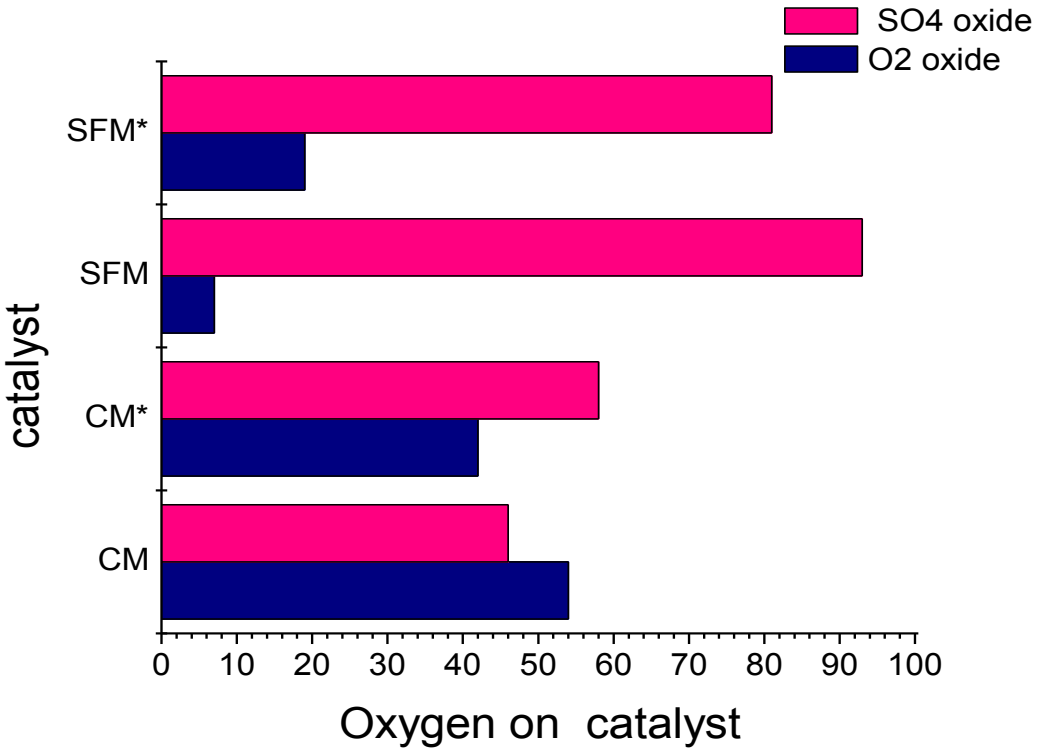

Figure 4.34: Percentages of Oxide Oxygen and Sulphate Oxygen on the Catalysts from the Deconvolution of the O1s Spectra

Although, the conventional catalysts had lower percentages of sulphate oxygen but notably the CM* had higher sulphate oxygen (58%) than the CM (46%). This could be the reason for the high Brønsted acid site on the CM* catalyst whereas, the CM is higher in Lewis acidity. This is probably due to the difference in the volume of sulphating agent used in the preparation rather than the method itself. The 15ml of H_2SO_4 used per gram of zirconium hydroxide for CM resulted into more zirconia than zirconium sulphate on the catalyst, while the 3ml of H_2SO_4 used for the CM* was enough to produce more sulphate oxygen than the oxide oxygen. These observation were further demonstrated by relating the sulphate oxygen on the catalysts and their corresponding protonated species as shown in Figure 4.35, which caused the high levels of Brønsted acidity exhibited by the solvent-free catalysts, relative to the CM and CM* samples.

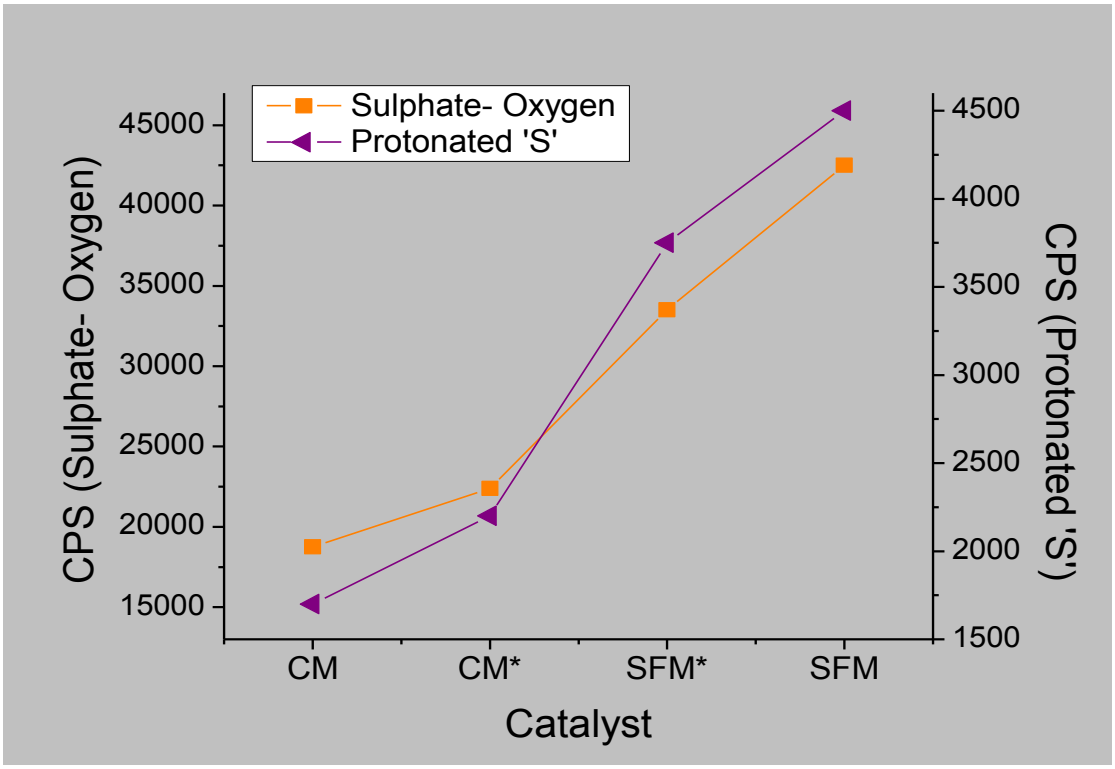

Figure 4.35: Sulphate Oxygen and Protonated Species of the Sulphur on the Catalysts (Note: scales are not the same)

4.1.5.4 Sulphur-to-Zirconium Ratios

The sulphur to zirconium ratios of the catalysts prepared by the solvent-free method was higher than those from the conventional method (see Table 4.2). Obviously the conventional method causes a diminution of this ratio, this being evident in samples with the same sulphate ratio but different methods of preparation. Solvent-free catalysts reflected values higher than 1.0 with a higher ratio observed in the SFM catalyst. These mean that the conventional catalysts have more zirconia on their surfaces. Also the ratio of the protonated to deprotonated sulphur indicted higher S-O bond than S=O bond on the solvent-free catalysts. The values of the ratios buttress the proposed catalysts' structures earlier proposed in Figure 4.26.

.

Table 4.2: XPS Parameters of the Various Catalysts Samples

Sample	Binding energy (eV) Zr		Binding energy (eV) S_{2p}		Binding energy (eV) O1s		
	Zr $3d^5$	Zr $3d^3$	S_{2p}	cps of 169/170	O1s	cps of O_2 of SO_4^{2-}/ O_2 of Zr	XPS
CM	183.4	185.5	169.7/170.7	1.3	530.5/532.5	0.6	0.3
CM*	183.4	185.7	169.7/170.9	1.5	531.0/532.5	1.1	0.6
SFM	184.0	186.5	169.8/170.8	2.2	531.0/532.5	10.5	2.0
SFM*	183.5	186.0	169.8/170.9	1.8	531.0/532.5	3.2	1.3

The same trend is evident in Figure 4.36. Irrespective of the preparation variant, the values obtained from XPS measurements have the same trend as those determined from chemical analysis by EDX.

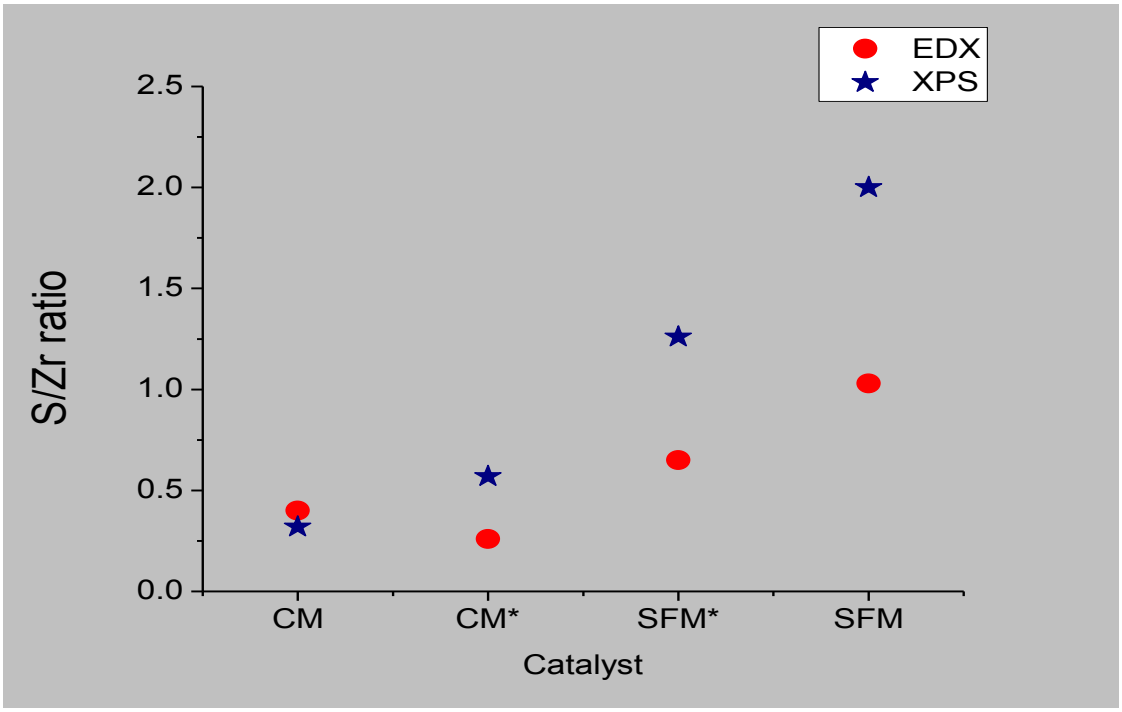

Figure 4.36: S/Zr Ratios of the Catalysts determined by XPS and EDX

Interestingly, the XPS and the EDX elemental results differed by only 0.1%. The SEM digital maps of all the catalysts revealed the density of each of the major elements of interest in the various catalysts. The SFM digital maps confirmed the presence of more sulphur on the solvent-free catalysts than the conventional (see Appendix F). The same trend of increased oxygen (SFM > CM > CM*) is observed on the digital maps for oxygen on the surface of the catalysts as shown in Appendix G. However, the zirconia on the catalysts did not follow the same trend. There was more zirconia on the solvent-free catalyst, followed by the CM* and the least was on the CM catalyst as revealed in Appendix H.

Based on the two sulphate ratios used in preparing the catalyst samples in this work, the presence of excess sulphating agent had no enhancement effect on the nature of the acid sites. One could conclude that the amount of sulphate used for CM and SFM* was greater than the threshold value of H_2SO_4 needed per gram of $Zr(OH)_4$ as reported by Farcasiu *et al.* (1997), hence the lower retention of sulphate on the catalyst. The authors reported that at higher sulphate loading the sulphate moves into the bulk phase of the catalyst rather than remaining on the surface. From the XPS and elemental analyses the formulae for the species on the catalysts surface are given as follows (see Table 4.3 below):

Table 4.3: Proposed Formulae for the Various Catalysts

Catalyst	Formula
CM	$ZrSO_4.4ZrO_2$
CM*	$ZrSO_4.3ZrO_2$
SFM	$Zr.SO_4$
SFM*	$ZrSO_4.ZrO_2$

Deducing from the formulae it is evident why the solvent-free catalysts were higher in both acid concentrations and Brønsted acidity particularly the SFM catalyst. The surface of the SFM catalyst was purely sulphate bonded to zirconia whereas zirconium oxide was present on other catalysts in the following order: SFM*< CM* < CM. It is observed from the formulae that the difference in the chemical composition between catalysts with same amount of sulphation is three ZrO_2 species (see CM and SFM*; SFM and CM*).

4.2 Meta-kaolin-supported Sulphated Zirconia Catalysts

The sulphated zirconia catalyst was supported on meta-kaolin in an attempt improve the properties of the catalyst. Supporting the catalyst appropriately should prevent the sintering of the zirconia particles and provide a higher surface area. Meta-kaolin was prepared from kaolin by a process known as "dealumination", described in section 3.1.3.

4.2.1 Characterization of kaolin and dealuminated kaolin (meta-kaolin)

Kaolin was used because it is inexpensive, so could be an economically viable support, and because and the ratio of aluminium to silicon can easily be modified by the process of dealumination. The textural properties and elemental analysis of the kaolin and the dealuminated kaolin (meta-kaolin) are given in Table 4.4. For convenience kaolin is designated as 'K' and meta-kaolin as 'MK'.

Table 4.4: Textural and Elemental Composition of Kaolin and Meta-Kaolin

Catalyst	Crystallite size (nm)	Elemental analysis (EDX) (wt%)					
		O	Si	Al	P	Fe	S
K (kaolin)	42.06	57.8	21.5	18.0	1.9	0.9	-
MK (meta-kaolin)	-	57.3	36.5	2.4	2.9	-	0.9

The elemental analysis shows that the aluminium content was reduced by 86% and the silicon increased by 74%. However, the level of oxygen remained relatively constant. The presence of 0.9 wt% sulphur in the meta-kaolin is due to the sulphuric acid that was used during the dealumination of the kaolin. The dealumination was clearly successful, as the SiO_2/Al_2O_3 ratio of the kaolin, which was initially 1:2 increased to 15.0 (see EDX analysis in Table 4.5 below and spectra in Appendix D). The meta-kaolin has more silica and less alumina than the kaolin.

Table 4.5: Elemental Analysis and Textural Properties of Support

Sample	Si/Al (wt%)	S/Zr (wt%)	XRD pattern
K (kaolin)	1.2	N/A	Crystalline
MK (meta-kaolin)	15.0	0.9 (S^{6+})	Amorphous

N/A implies not applicable

The XRPD pattern of the kaolin was crystalline with three phases identified (kaolinite, quartz and mica) however the quartz and mica were minor (see appendix E). In the X-ray diffraction pattern of meta-kaolin, there were no kaolinite crystalline peaks. The disappearance of these major peaks gave way to amorphous material with a very broad band within the low-range angle 15-35^{o} 2θ as in shown in Figure 4.37. Belver *et al*. (2002) described the broad band as an amorphous phase of silica (SiO_2).

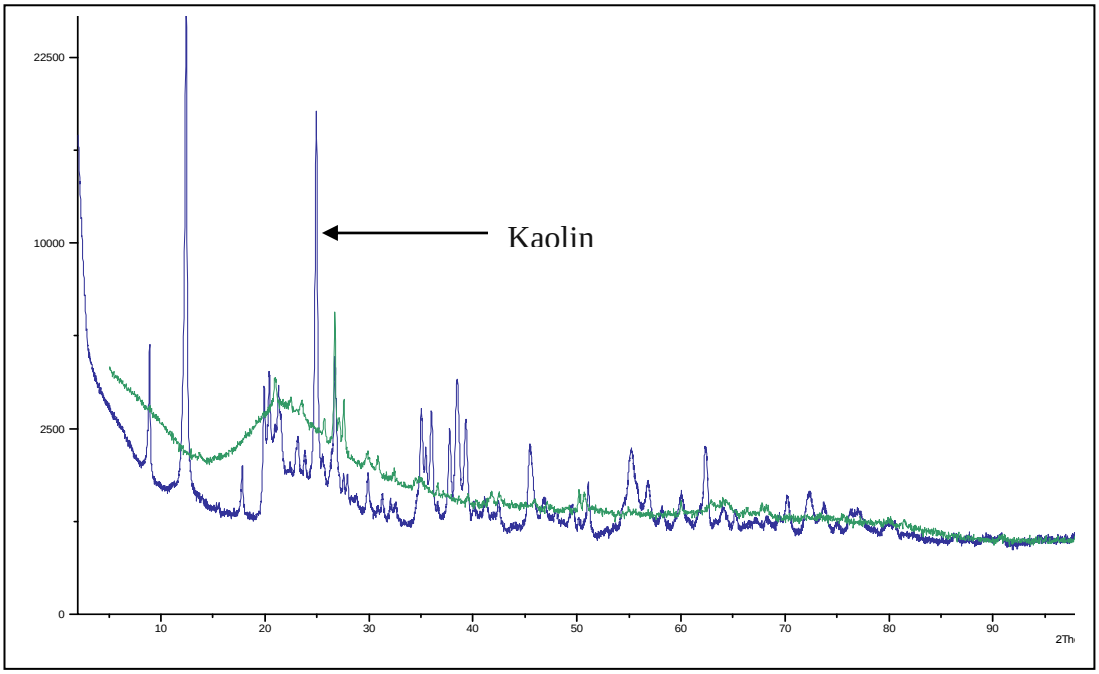

Figure 4.37: XRPD patterns of kaolin (blue) and meta-kaolin (green)

The effect of dealumination on percentage composition of the Si/Al ratio is also shown by XPS analysis. The Al 2p spectra for kaolin and the meta-kaolin at the same binding energy of 74.5eV (see Figure 4.38), correspond to aluminium (III) oxide.

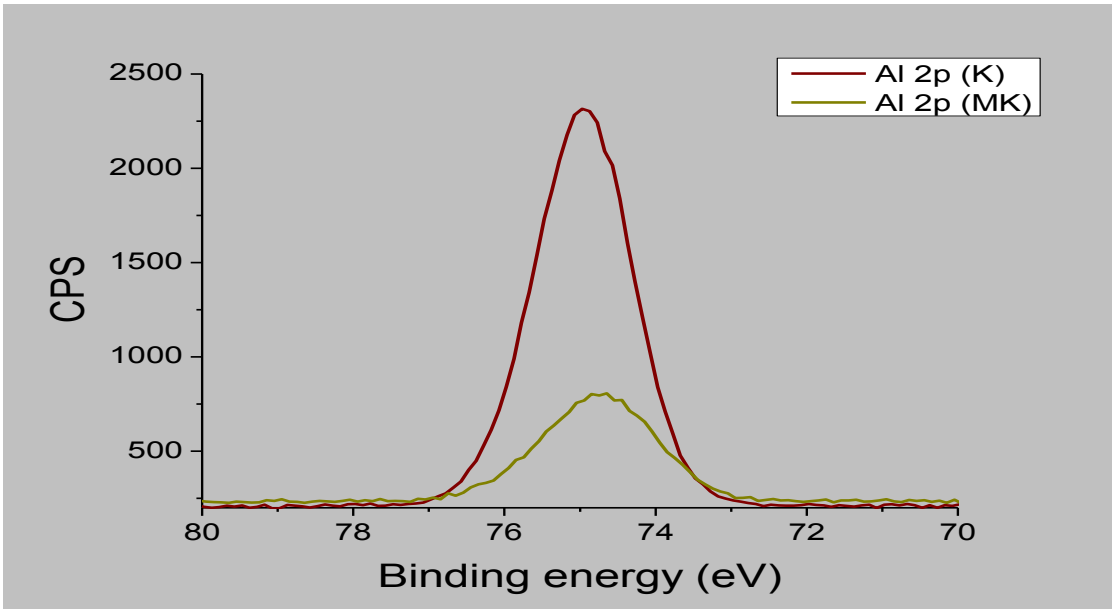

Figure 4.38: XPS Spectra of Al 2p of Kaolin and the dealuminated kaolin (meta-kaolin)

The silicon (Si2p) spectra of kaolin and meta-kaolin were very similar around 103.3eV (the binding energy of silicon), as shown in Figure 4.39. This indicated that it was Si^{4+} in silicon oxide.

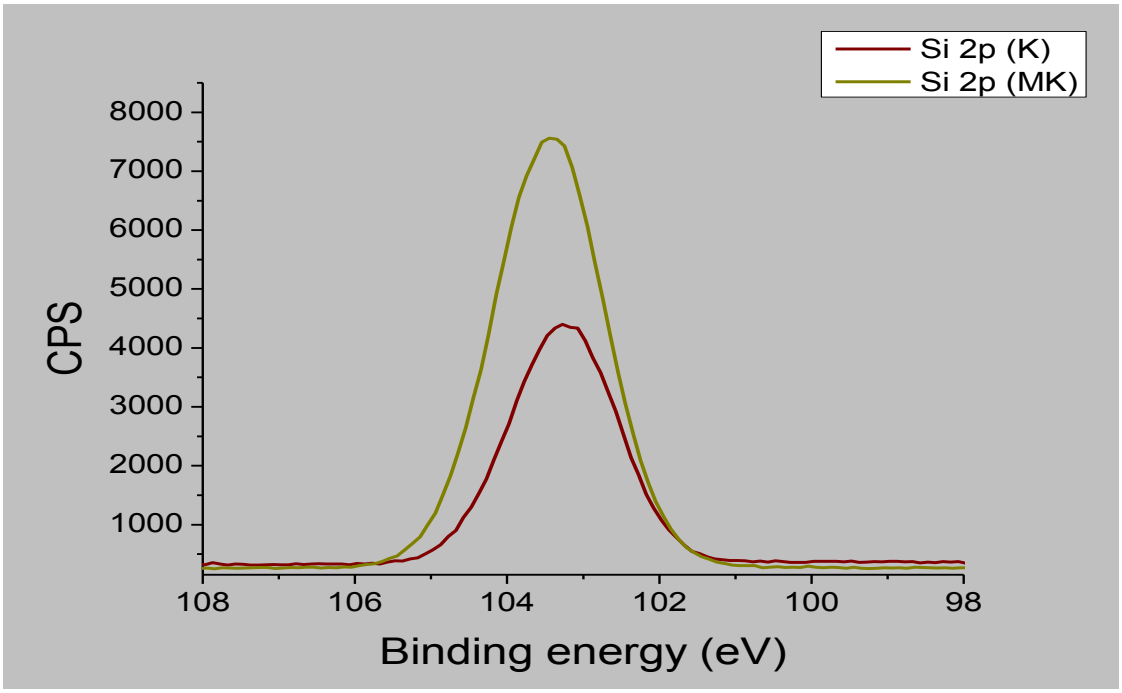

Figure 4.39: XPS Spectra of Si 2p of Kaolin and the dealuminated Kaolin (Meta-kaolin)

With meta-kaolin as the support, two new sulphated silica-zirconia catalysts were synthesized by the conventional and solvent-free methods. The sample from the

conventional method is now designated as 'CMM' and 'SFMM' is the sample from the solvent-free method.

4.2.2 Preparation of modified catalyst samples (CMM and SFMM)

In synthesising the catalyst samples, the ratios of zirconium to sulphate in both conventional and solvent-free methods were the same as in the previously prepared SFM and CM, but the ratio of meta-kaolin to zirconia was 0.5:1 in both cases. The catalysts were then prepared by the same procedures as used for CM and SFM, and then characterised.

4.2.1.2 Infrared Spectroscopy

The infrared spectrum of the CMM sample shows similar bands to that of the CM catalyst between 4000cm^{-1} and 400cm^{-1}. The sulphate spectrum on the CMM sample corresponded to that of the CM sulphate within the same wave number of 900-1200cm^{-1}, but with a significant increase in its absorbance as shown in Figure 4.40.

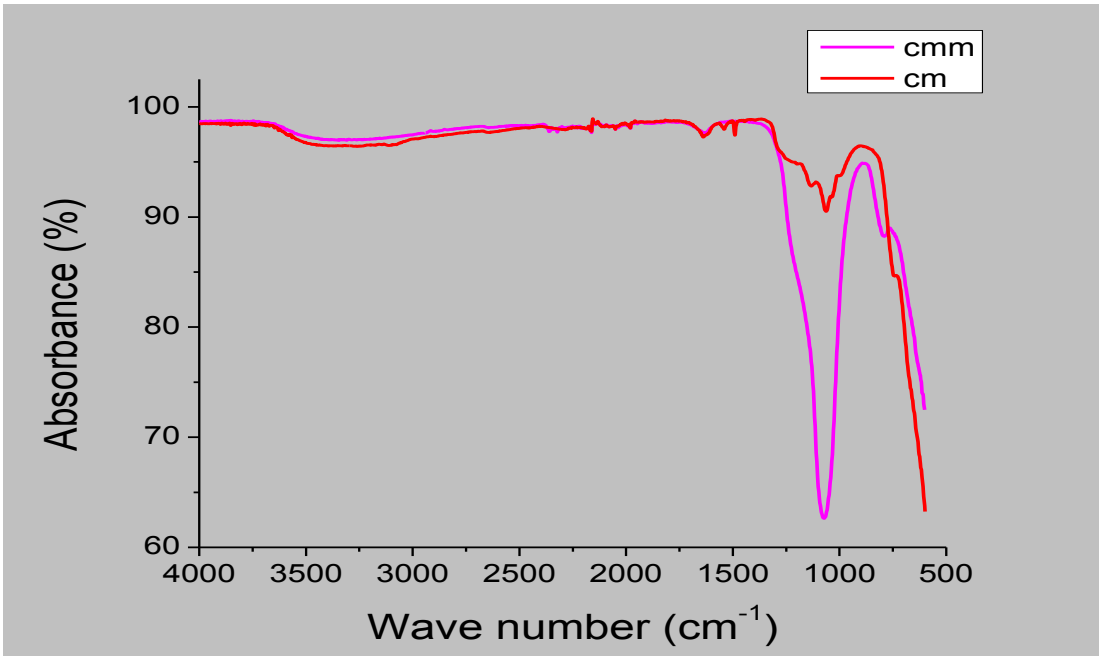

Figure 4.40: IR Spectra of CMM and CM Catalysts

This implies that the addition of meta-kaolin enhanced the retention of sulphate on the catalyst. A similar trend was found with the SFMM and SFM catalyst samples (see Figure 4.41). The band for the SFMM sample has an absorbance of 46% as against 30% for the SFM.

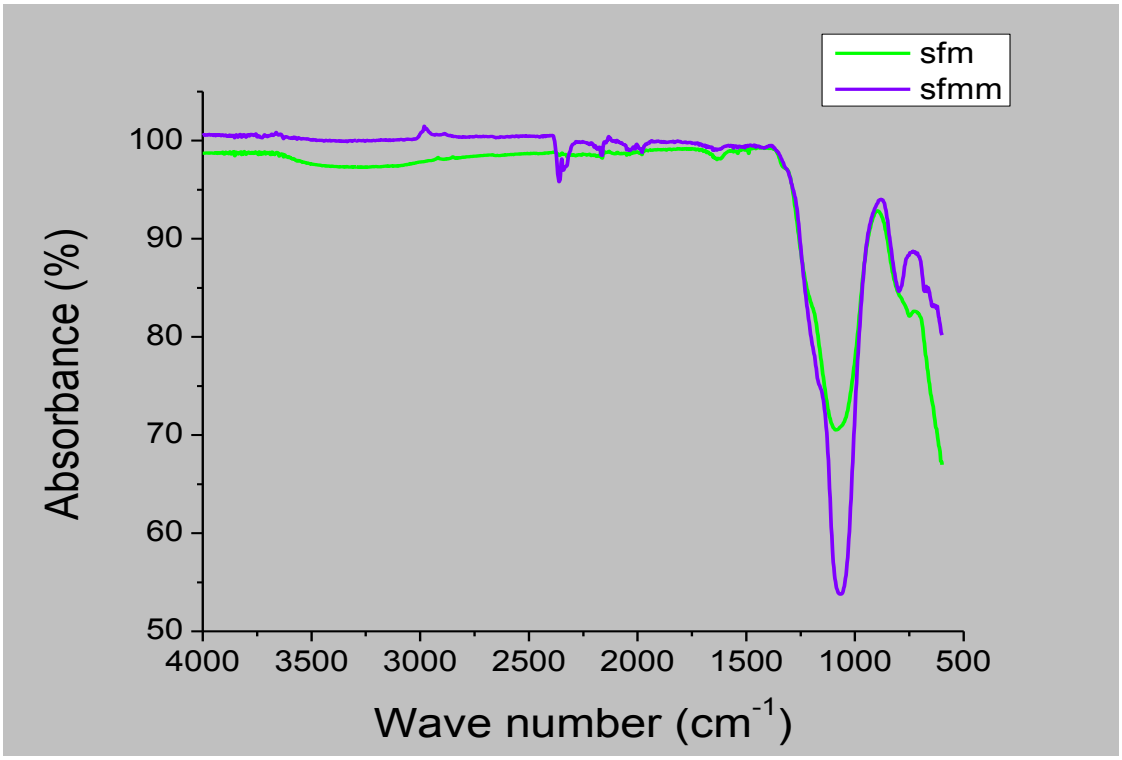

Figure 4.41: IR Spectra of SFM and SFMM Catalysts

In addition, a small but conspicuous band at 800cm^{-1} was observed for the SFMM sample. According to Rosenberg *et al.* (2003), the band is due to S-O single bond vibration sulphite bound to a metal through oxygen. The SFM sample does exhibit this band, but at a lower wave number with a very weak absorbance. Generally, the addition of meta-kaolin enhanced the physicochemical properties of the catalysts irrespective of synthesis method, and an improved retention of sulphate on the catalysts was indicated by the infrared analysis. This is much clearer in Figure 4.42 and Figure 4.43, which show the comparison in percentages of sulphate retained on the six catalysts according to method of preparation.

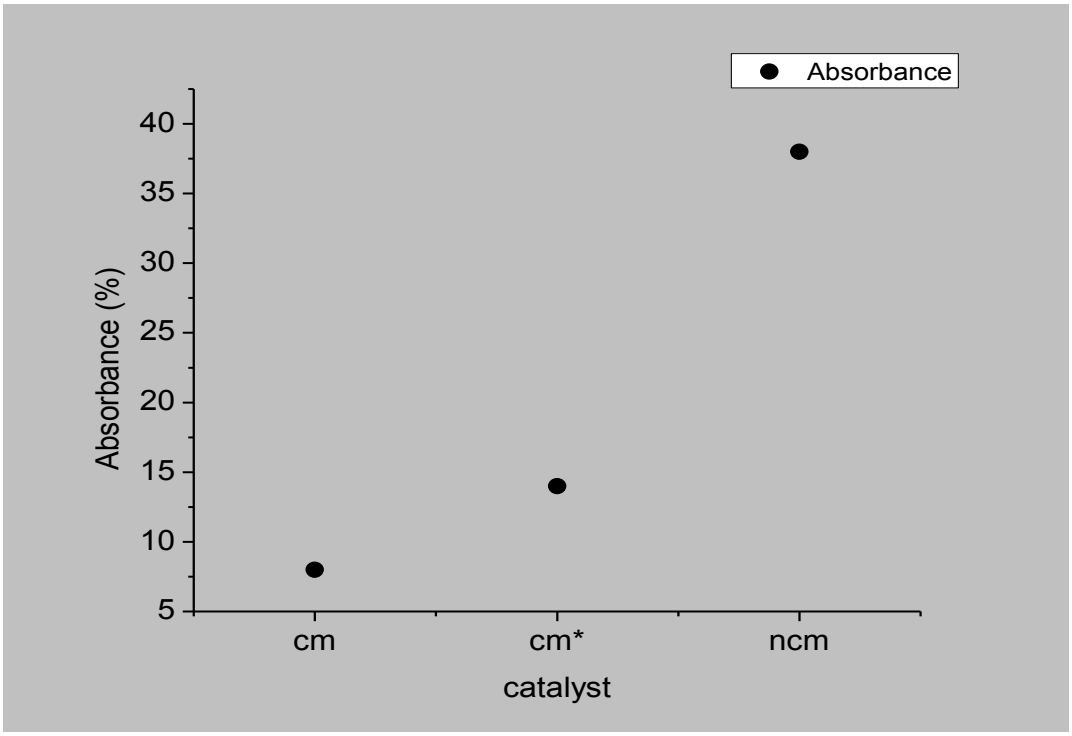

Figure 4.42: Percentage of Sulphate Present on the Conventional Catalysts (from FTIR)

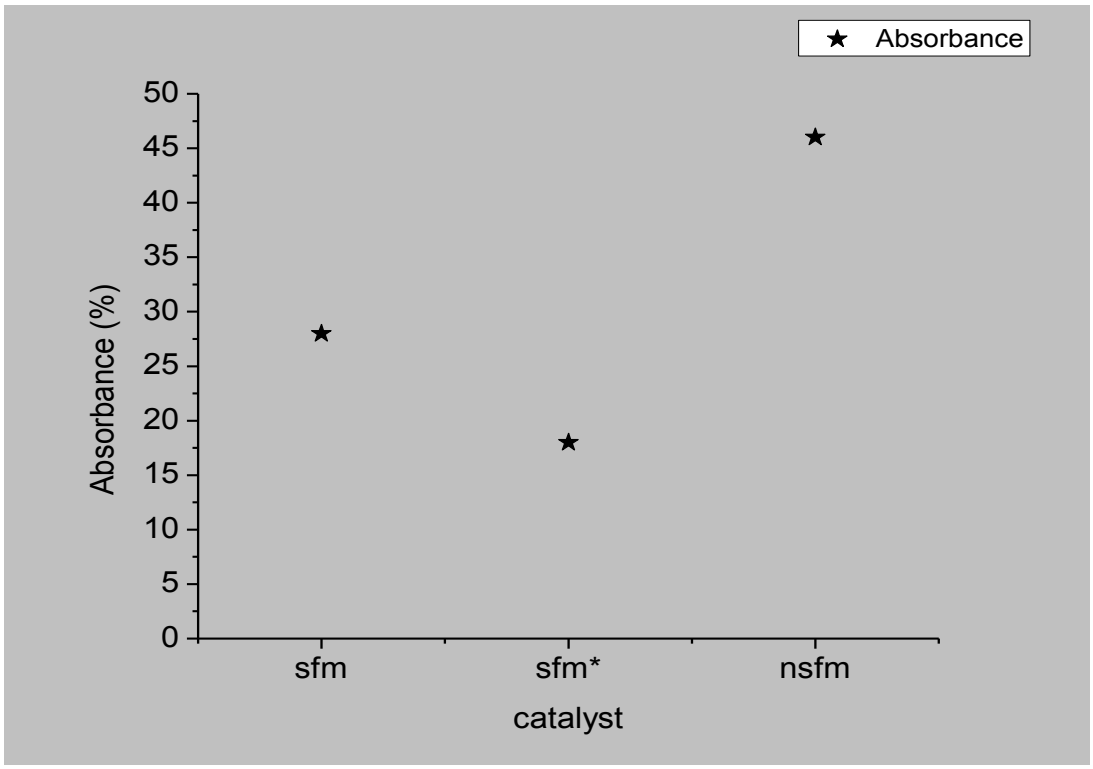

Figure 4.43: Percentage Sulphate Present on the Solvent-free Catalysts (from FTIR)

The SFM* probably lost some of its sulphate during calcination. The lost of sulphate on the CM was during the preparation and calcination.

4.2.1.3 *Pyridine-DRIFTS (Diffuse Reflectance Infrared Fourier Transform Spectroscopy)*

The spectra of adsorbed pyridine on the modified samples had characteristic bands in the region of 1445cm^{-1}, 1488cm^{-1} and 1545cm^{-1}, as shown in Figure 4.44. The bands at 1488cm^{-1} and 1545cm^{-1} are common to both CMM and SFMM and correspond to adsorbed pyridine on Brønsted acid and Lewis acid sites respectively. The band at 1445cm^{-1} on the CMM catalyst is similar to that on the CM sample, indicating strong Lewis acid sites.

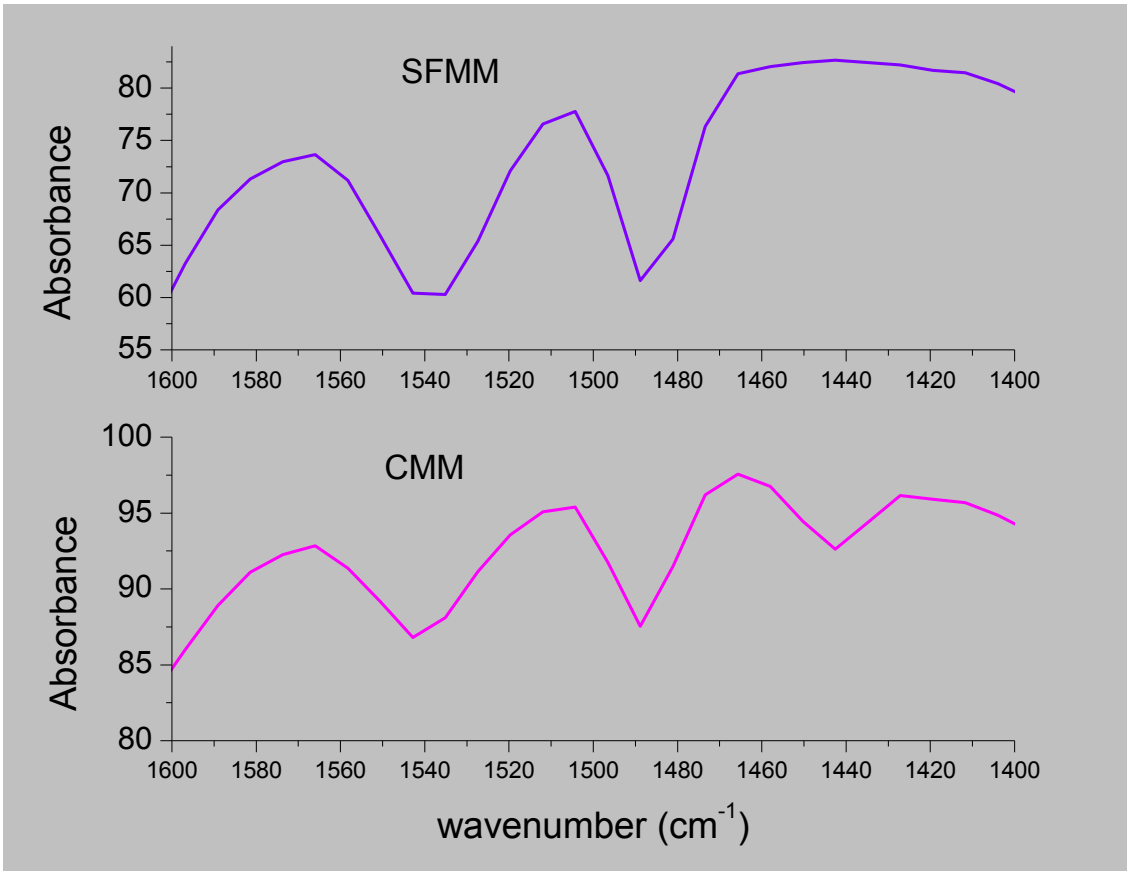

Figure 4.44: FT-IR Spectra of Adsorbed Pyridine on SFMM and CMM Catalysts

However, the intensity of this band has changed: it was 33% for CM whereas for CMM it was 20%. The number of acid sites on the modified catalysts was estimated from their IR spectra for adsorbed pyridine. The modified catalysts have increased concentrations of Brønsted acid sites than their counterparts (CM or SFM), as revealed by the py-IR analysis and shown in Figure 4.45. The SFMM had about 42mmol/g more Brønsted acid sites than the SFM but with fewer Lewis acid sites (12mmol/g).

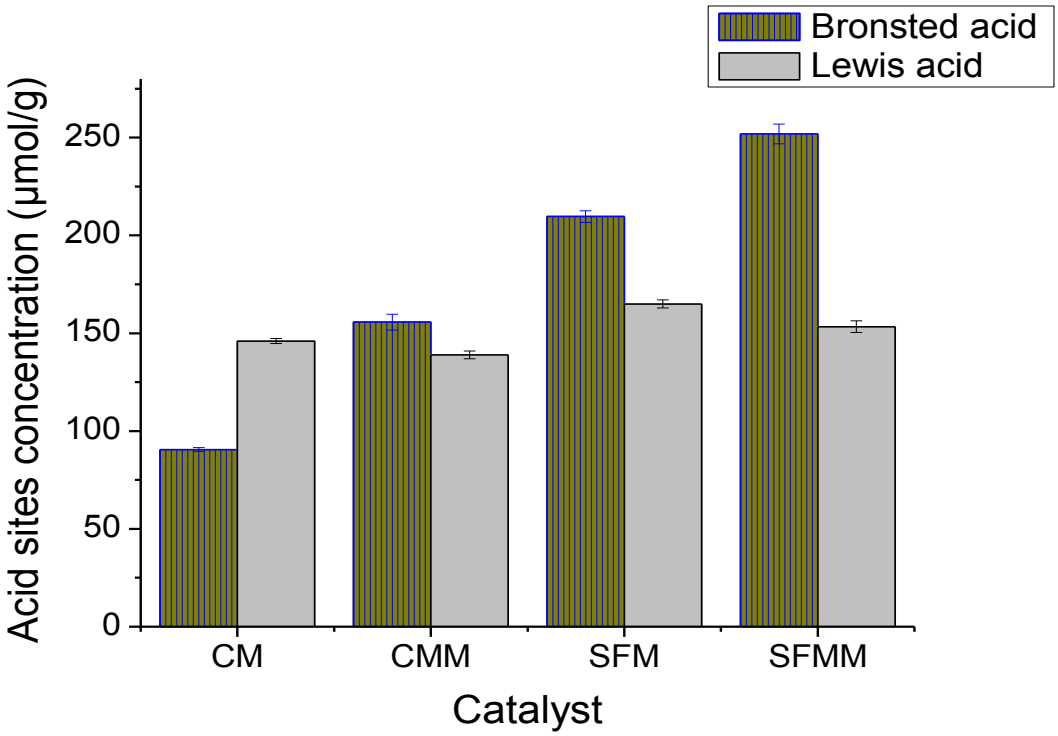

Figure 4.45: Comparison of Brønsted and Lewis Acid Sites Concentration on the Catalysts based on Method of Preparation

It is not surprising that the CMM had a reduced concentration of Lewis acid sites of 138.9mmol/g compared to CM having145.9mmol/g. This follows from the decreased intensity and area of the band at 1445cm^{-1} on CMM, corresponding to strong Lewis acid sites. The increased sulphate on the modified samples, as revealed by the IR spectra in section 4.2.1.2, was due to the presence of the meta-kaolin support on the catalysts allowing for more interaction between the pyridine and both types of acid site. Another observation is that the CMM and SFMM had a higher total acid concentration than their counterpart; CM and SFM. Higher Brønsted acid concentration was evident particularly the CMM, approximately 15% whereas SFMM had 5% (see Table 4.6).

Table 4.6: Brønsted and Lewis Acidity of the Meta-kaolin-supported Sulphated Zirconia Catalysts

Catalyst	Brønsted acid concentration (%)	Lewis acid concentration (%)
CM	38.3	61.7
CMM	52.8	47.2
SFM	56.8	43.2
SFMM	62.2	37.8

4.2.1.4 X-ray diffraction Pattern (XRPD) of CMM and SFMM

In Figure 4.46 the CMM catalyst exhibited tetragonal crystalline phase of zirconia, similar to that of the CM sample, and very low peak intensities of silicon oxide around 22-25^{o} 2θ. On the other hand, the X-ray diffraction pattern of SFMM showed a broad hump over the range 18-35^{o} corresponding to silicon oxide at lower angle and a reduced tetragonal peak at 30^{o}, broad peaks at 50^{o} and 60^{o} 2θ corresponding to zirconia. The broad hump indicates an extremely small crystallite size, which could be amorphous for the phases of the compound identified.

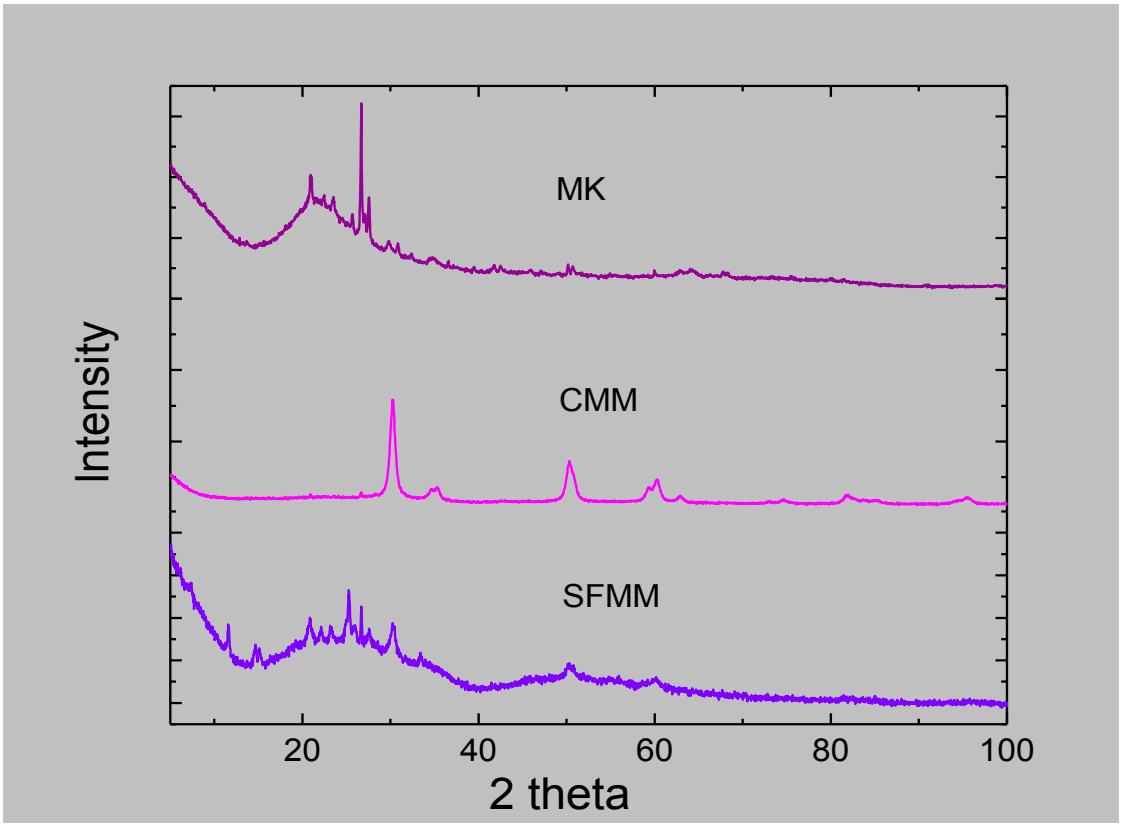

Figure 4.46: Comparison of XRPD Diffractograms of Metakaolin (MK) and Sulphated Zirconia doped with Metakaolin (CMM and SFMM) from Conventional and Solvent-free Methods

4.2.1.5 Physical properties of CMM and SFMM

Doping the samples with meta-kaolin increased the BET surface area of the modified catalysts. The surface area increased from 65m^2/g in CM to 83m^2/g in CMM. The SFMM sample had a relatively large surface area of 101m^2/g but this was lower than SFM and SFM* samples. The largest average crystallite size of 17.5nm was observed for the CM* catalyst, whereas the SFM had the lowest, at 3.4nm. The ratios of

SiO_2/Al_2O_3 and SO_4/Zr of the modified catalysts are shown in Table 4.7. The SFMM tends to have more silica and sulphate than the CMM. The EDX analyses of the samples indicated the presence of potassium

Table 4.7: Elemental Analysis and Textural Properties of Meta-kaolin-supported Sulphated Zirconia Catalysts

Catalyst	Si/Al	S/Zr	XRD pattern
CMM	8.8	0.3	T
SFMM	12.1	1.7	A

T is tetragonal, A is amorphous

The possible formulae for the kaolin-supported sulphated zirconia catalysts as deduced based on the elemental analyses are given in Table 4.8. However there were traces of potassium in the samples; 1.2 wt% and 1.01 wt% in CMM and SFMM respectively.

Table 4.8: Proposed Formulae for the Meta-kaolin-supported Sulphated Zirconia Catalysts

Catalyst	Formula
CMM	$2ZrSO_4.4ZrO_2.SiO_2.Al_2O_3$
SFMM	$6ZrSO_4.SiO_2SO_4.Al_2O_3.14SiO_2$

The SFMM had more sulphate bonded to zirconia and silicon oxide on the surface than CMM however, the increased acid concentration on the CMM than the CM is evident from the formula. This no doubt is expected to increase the catalytic activity of the catalysts.

4.3 Chloride Determination in All Solvent-free Samples

The solvent-free method involved the use of zirconium oxychloride ($ZrOCl_2.8H_2O$) as one of the reactants during the preparation. It therefore became necessary to determine the level of chloride in the catalysts in order to be sure of their safety in the application of biodiesel production. The determination was performed as described in section 3.2.6. The values of the chloride ions in mg/kg found in the solvent-free samples are quite negligible as revealed by the analysis and shown in Table 4.9.

Table 4.9: Chloride ion Content in the Solvent-free Catalysts

Catalyst	Concentration of Chloride ion (mg/kg)
SFM	0.2
SFM*	0.8
SFMM	0.8

The negligible values of chloride ion in the solvent-free method catalysts are indications that the method is not detrimental to the applicability of the catalysts.

4.4 Analysis of the Liquid Product

In this section the different analytical methods used in determining the activity of the catalysts are evaluated with regards to the procedure employed and the reproducibility of results.

4.4.1 Gas chromatography

The determination of methyl ester in the product mixture was carried out as described in section 3.4.1. A typical chromatogram from the ester GC analysis is shown in Appendix I. It shows traces of the different esters and the internal standard. Each of the peaks could be attributed to a different ester. These were identified by analysing various standards of pure esters and noting their retention times. The dominant methyl ester in the mixture depended on the catalyst used for the cracking. In the case of the conventional sulphated zirconia catalyst, the main methyl ester was methyl myristate, and others were methyl oleate and methyl linoleate as is evident on the chromatogram. For the solvent-free catalyst, methyl oleate was the main ester present in the product mixture as revealed on its chromatogram in Appendix I. With the solvent-free catalyst, the mixture was composed mostly of unsaturated methyl ester. However, the conventionally prepared catalyst produced mainly saturated methyl esters. The peak with an asterisk (*) is the trans form of the methyl oleate, as revealed by running the trans and cis standards on the GC (see Appendix I). The mass spectra of peaks at a retention time between 10.4-13.8 minutes corresponded to methyl ester as identified from the GC-MS and compared with the software library showed the trans and cis methyl oleate in the sample mixture. This showed the difference in the activity of the solvent-free and conventional catalysts. However, more information about the product

mixture was obtained by glyceride analysis using GC-MS. This allowed the quantification of the triglyceride, diglyceride, monoglyceride and glycerol contents, whereas only the ester content was given by the GC. The time required for sample preparation and analysis was shorter for the GC than the GC-MS. The analysis took 25 minutes for the GC and 45 minutes for the GC-MS.

4.4.2 Gas Chromatography/Mass Spectrometry (GC-MS)

Triglyceride, diglyceride and monoglyceride quantification was determined according to the procedure in section 3.4.2. A typical GC-MS chromatogram of a sample cracked by the solvent-free catalyst showing the composition of the mixture is shown in Appendix J. Matching the various peaks on the chromatograms with the software library on the GC-MS identified the closest compounds exhibiting the mass spectrum. A typical mass spectrum of the methyl ester peak from the GC-MS is also shown in the same Appendix J. To quantify the glyceride content in the product samples, calibration curves were determined for the triglyceride, diglyceride and monoglyceride components in the sample in the presence of internal standards 1 and 2. The glyceride GC was required in order to obtain the concentrations of the partial glycerides in the reaction product mixture, which were needed to determine the kinetics of the reaction. The calibration curves were determined from the reference solution. A typical chromatogram of the calibration standard solution as well as the calibration curves based on peak area resulting from the monoglyceride, diglyceride and triglyceride content in terms of area are shown in Appendix J respectively. The R^2 values for the mono-, di- and triglycerides are above those in the BS 14105:2003 specifications, which give an indication of the precision of the technique. The reproducibility of the analysis was checked by calculating the random error for the reference solutions of mono-, di- and triglycerides in three different runs and shown in Table 4.10.

Table 4.10: Random Error in the Results of Repeated Analysis of the Calibration Glycerides Samples using GC-MS

Standard	Mean	Standard deviation	Error (%)
Monoglyceride	2.12	0.028	1.32
Diglyceride	1.27	0.036	2.83
Triglyceride	2.58	0.057	2.20

For the analysis of glycerides, the use of an on-column injector on the GC-MS enhanced the reproducibility of the method (Schomburg *et al*., 1981). Therefore the data can be considered to be reliable and can be used in the study of the kinetics of the reaction. According to Schomburg *et al*. (1981); it is more suitable to operate with on-column rather than split injection. The on-column injector will not allow for "sample discrimination". Sample discrimination in GCs is when high boiling-point components in the sample injected are not volatilized and are preferentially carried away instead of entering the column. This tends to occur more with the split column. Calibration curves were also produced for the following methyl esters from their standards: palmitate, heptadecanoate, stearate, oleate and linoleate (see Appendix J).

The various peaks of methyl ester standard were calibration using GC-MS. However the GC-MS was not suitable for quantifying the methyl ester in the sample mixture because the esters peaks on the chromatogram overlapped, and it was therefore difficult to determine the area under each peak. For the case of accuracy and reproducibility therefore, the GC-MS was not used to quantity the methyl ester, but rather GC was used. The random error of the results for the total methyl ester content of the product mixture using the GC was obtained by repeated manual injection of the samples, and was calculated to be +/- 2 wt%. The low percentage error shows that the method is acceptable for quantifying the ester concentration in the product mixture.

4.5 Catalyst Screening

This section is subdivided into three sections which discuss the conversion of triglyceride, and the production of methyl ester and other products that were identified.

4.5.1 Triglyceride Conversion

The catalysts were screened in a batch reactor for their activity in the catalytic cracking of triglycerides, as described in section 3.3.1, with the aim of finding the most active catalysts and highest selectivities for fatty acid methyl ester. Table 4.11 gives a summary of the maximum conversions achieved by the solvent-free and conventional catalysts over three hours.

Table 4.11: Conversion in the Cracking of Rapeseed Oil with the Various Catalysts

Catalyst		Conversion
Solvent-free method	SFM	76 ± 3%
	SFM*	78 ± 4%
Conventional method	CM	62 ± 2%
	CM*	66 ± 2%

Clearly, the catalysts were generally active in converting triglycerides to the products, as shown in the conversion profile in Figure 4.47. The conversion profiles within the reaction time of three hours are similar in pattern; however, with different values along the reaction time.

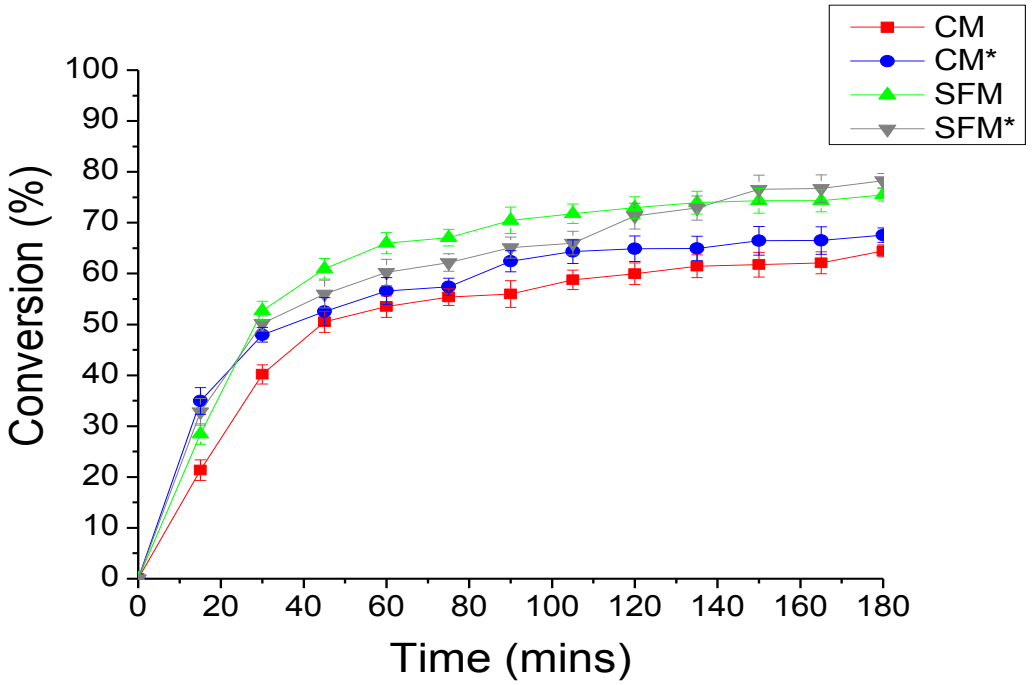

Figure 4.47: Conversion Profile of Triglycerides with the four different Catalysts

The SFM catalyst achieved 76% conversion of the triglycerides used. Although Garcia *et al*. (2008) reported 98% and 92% conversion with the SFM catalyst but it was in the transesterification of soybean oil in the presence of methanol and ethanol respectively. To the best of our knowledge the SFM catalyst has not been used in thermocatalytic cracking of triglycerides before now. Li *et al*. (2010) achieved rate of 95% using modified sulphated zirconia (doped with titanium oxide) catalyst. Similarly Sun *et al*. (2005) used the SFM catalyst in the esterification of cyclohexanol with acetic acid and

reported a rate of 80.4%. However, little is known about its use in thermocatalytic cracking. The conventional catalyst, CM, has found wide applications, particularly in the isomerization reaction of n-butane to iso-butane with various conversion rates depending on the reaction condition. However, Li *et al*. (2010) achieved 95% conversion in the esterification of free fatty acid. The SFM* and CM* are novel catalysts in terms of the $Zr(OH)_4/SO_4^{2-}$ ratio used during preparation and application.

4.5.2 Methyl Ester Production

The trend of methyl ester yield, as revealed in Figure 4.48, is quite different from the conversion pattern seen in Figure 4.47. Of all the catalysts, it was obvious that there was loss of methyl esters as the reaction progressed. However, this occurred at different time of the reaction and is discussed further in section 4.5.5.

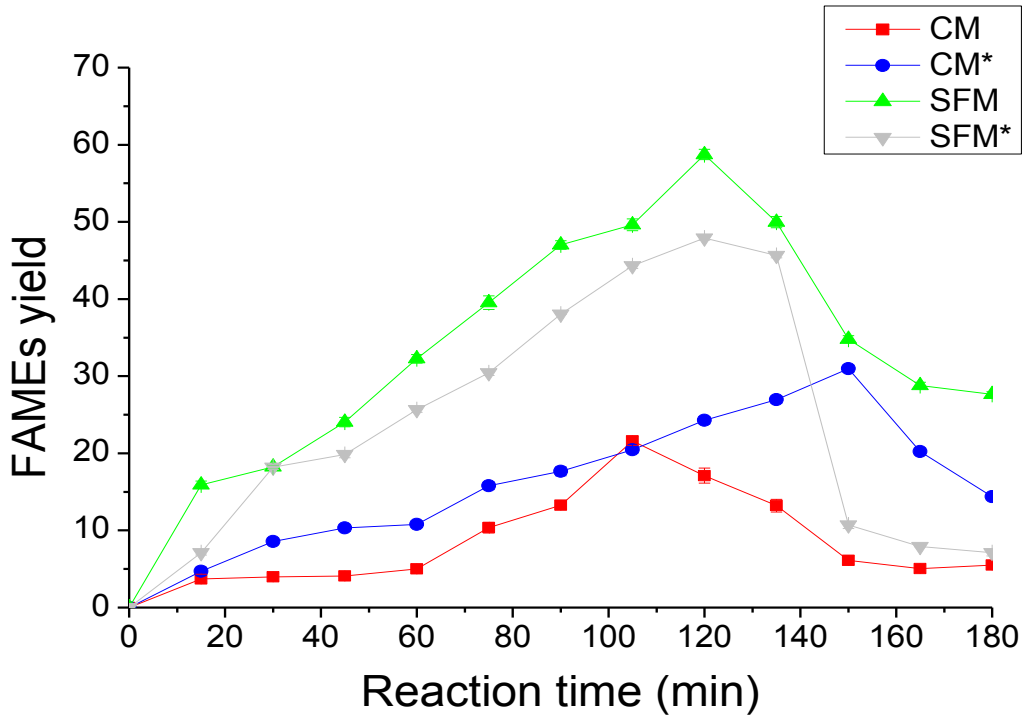

Figure 4.48: Methyl Ester Yields with Different Catalysts at 270°C within a Reaction Time of 3 hours

The solvent-free catalysts exhibited significantly higher maximum yields for methyl ester production than the conventional catalysts: at approximately 59% for SFM and 32% for the conventional catalyst (CM*) after 3 hours of the reaction. However, no previous study has revealed such a high yield of methyl esters from the direct cracking of triglycerides but with different yields of intermediate hydrocarbon fractions as

biofuels. Charusiri and Vitidsant (2005) recorded a rate of 24.5% as their highest yield of gasoline from spent vegetable oil over sulphated zirconia at high temperature (400-430^{o}C) and high pressure (10-30bars). There are many reports of the cracking of biomass/triglycerides to hydrocarbon fuels from using different types of catalysts, ranging from bio-gasoline to biodiesel, however, the yield has depended on the catalysts and operating conditions used. Some authors such as Twaiq *et al*. (1999), reported a rate of 28% of gasoline, Kubicka and Kaluza (2010) achieved 40% of n-heptadecane over NiMo/Al_2O_3 at 260^{o}C**,** Ooi *et al*. (2004) reported 44.4% of gasoline and Tamunaidu and Bhatia (2007) achieved 35% yield of gasoline fraction. However, Katikaneni *et al*. (1995b) reported a higher yield of 53% of hydrocarbons using a silica-alumina catalyst in the presence of steam at 550^{o}C. The differences in methyl ester profiles for each catalyst are due to the diverse properties of the catalysts, as described in section 4.1. The higher yields of methyl ester using the solvent-free catalysts are attributable to the higher concentration of Brønsted acid sites on the surface of the catalysts which is achieved through the method of preparation.

Surprisingly, although the CM* catalyst was prepared by the conventional method with a smaller amount of sulphuric acid (3.4ml/g of $Zr(OH)_4$ than CM (15ml/g of $Zr(OH)_4$), it exhibits a higher maximum FAME yield (31%) than its counterpart (22%). The difference is due to the presence of more Brønsted acid sites on the CM* catalyst than CM as shown in Figure 4.49. This occurred as a result of a more controlled ratio of $Zr(OH)_4/H_2SO_4$ used in the preparation of CM* rather than the conventional method. The pyridine-Brønsted integrated area was 68% of the total for CM* compared to 33% for the CM catalyst, as shown in Figure 4.49. This implies that Brønsted acid sites are more critical in the catalytic conversion of triglycerides to methyl esters. This is very clear in the comparison with the solvent-free catalysts with higher Brønsted acid sites and higher methyl ester yields. Generally the solvent-free catalysts have higher concentrations of acid sites. No doubt the Lewis acid sites are involved in the formation of other products, but its activity towards FAMEs in this reaction is lower as shown by the CM catalyst in Figure 4.49.

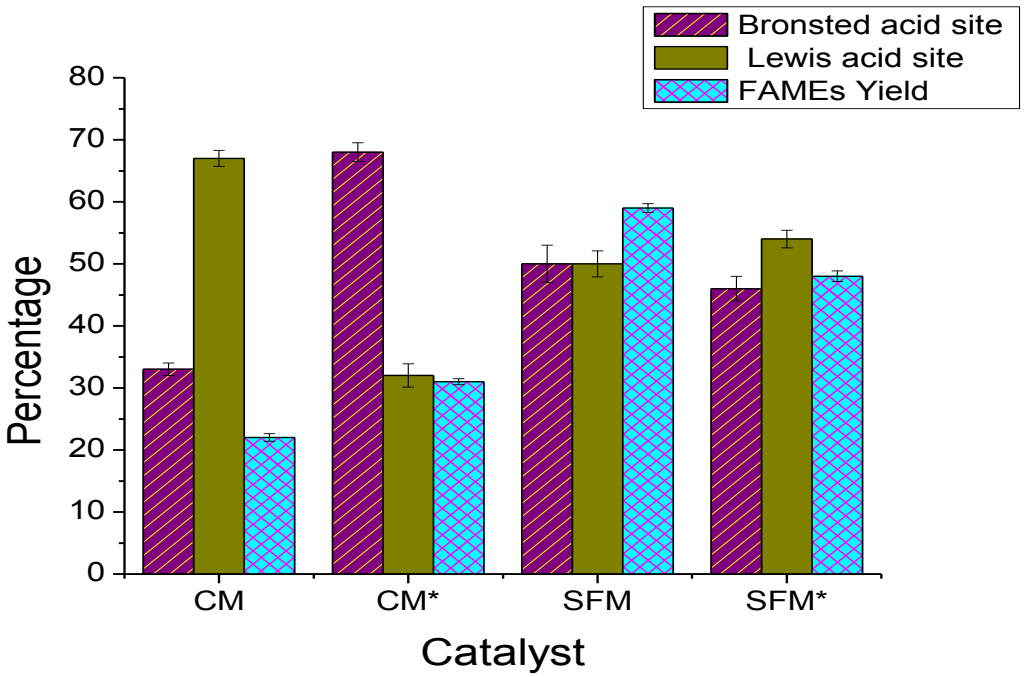

Figure 4.49: Percentages of FAME Yields Compared with the Brønsted and Lewis Acid Sites Concentration on the Catalysts

From the above Figure (Figure 4.49), it has been shown that the activity and selectivity for methyl ester depend on the Brønsted sites available on the catalyst. The CM*, SFM and SFM* had higher percentage of Brønsted sites then the CM, which followed the same trend with their percentage yield in methyl ester.

The drop in the yield of methyl ester after reaction times above 2h for the CM*, SFM and SFM* samples and above 1h 50min for the CM sample, as shown earlier in Figure 4.48, is due to the further breakdown of the methyl ester into other forms. Maki-Arvela *et al*. (2007) also reported the catalytic deoxygenation of esters over Pd supported on carbon in the presence of hydrogen to hydrocarbons fuels at 300-320°C and 6-17.5 bar. They observed that the catalytic transformation of methyl esters proceeded mainly via the decarbonylation of the esters into fatty acids, carbon-monoxide and alkanes. They achieved a selectivity of 46% of n-heptadecane at 300^{o}C. In another report, Kubickova *et al*. (2005) achieved 70% selectivity for n-heptadecane under the same reaction conditions; however, yield was not reported. The catalysts synthesized in this study were not just active for fatty acid methyl ester, but in addition exhibited some selectivity for esters depending on the type of bond present. Selectivity in the catalytic cracking of triglycerides to methyl esters was considered from two different angles under this study: (i) saturated and unsaturated methyl esters, and (ii) selectivity to individual methyl

esters composition. The solvent-free catalysts SFM and SFM* were more selective for unsaturated methyl esters at above 75% as shown in Figure 4.50.

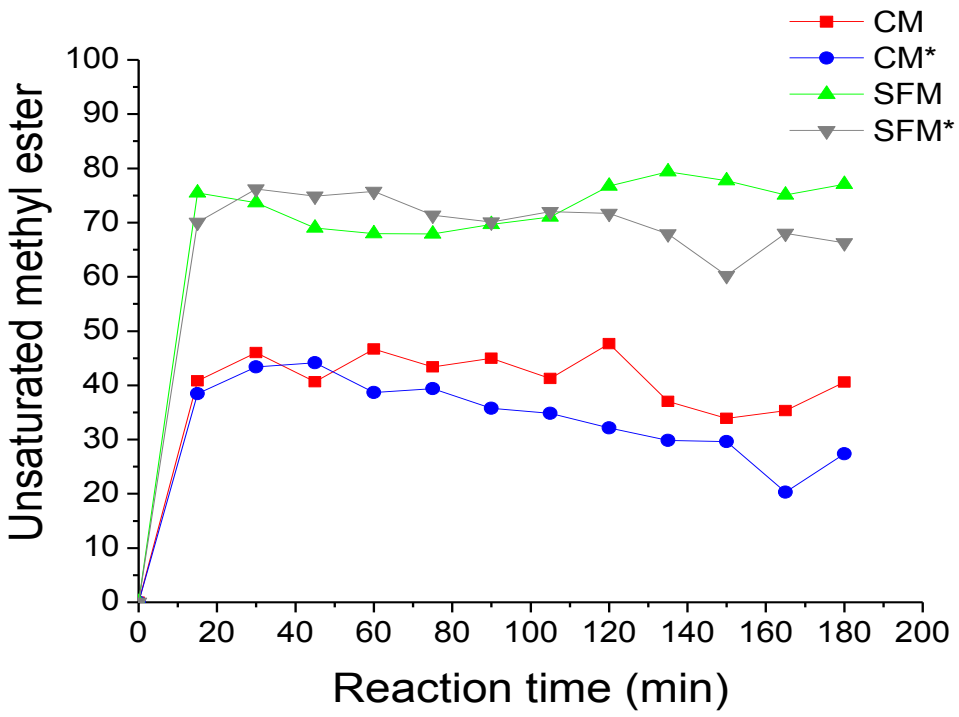

Figure 4.50: Catalysts Selectivity for Unsaturated Methyl Ester in the FAME product Mixture

On the contrary the conventional catalysts CM and CM* were more selective for saturated methyl esters, with CM* having a selectivity of approximately 68% after 2h of reaction.

4.5.3 Effect of Catalysts on the Chain Length of the Feed (Rapeseed Oil)

There was a substantial reduction in the percentage of oleic acid chain in the product sample compared to the feed. On the other hand there was an increase in the percentage of saturated acids compared to 7% in the feedstock as shown in Figure 4.51. This is clear evidence of the cracking of the triglyceride molecules, showing that the methyl esters produced by solvent-free catalysts comprised mainly of mono- and di-unsaturated esters. The catalytic activity of the catalysts is further demonstrated by a comparison of the carbon chain length composition of the feedstock with that of the methyl esters from the reaction product.

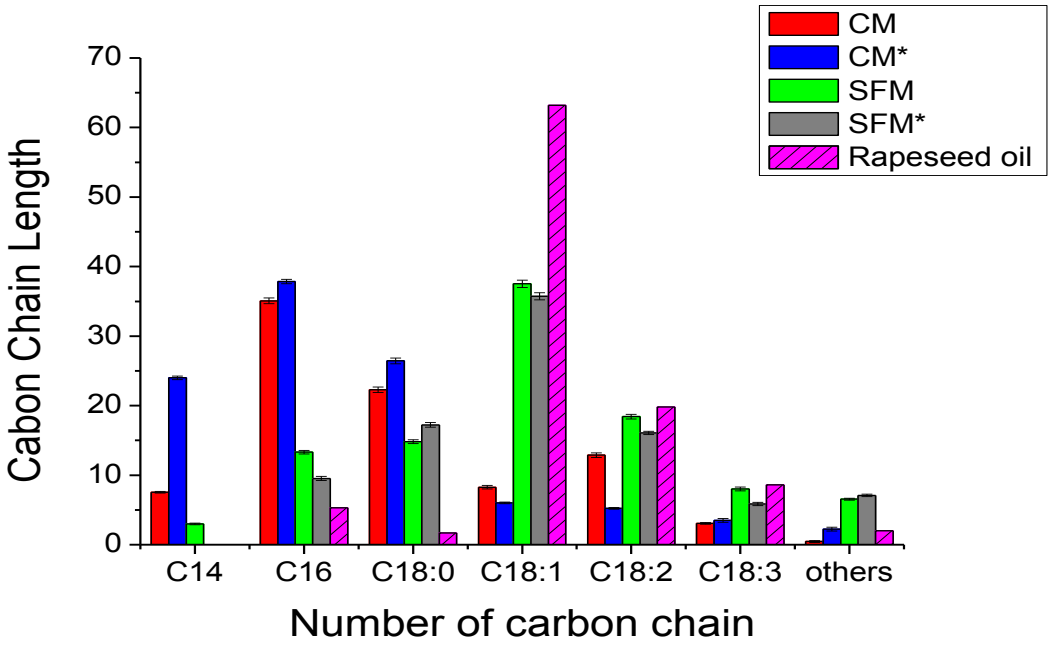

Figure 4.51: Percentages of Carbon Chain Length Distribution of Methyl Esters in the Product Compared with the Carbon Chain Length in the Feed (Rapeseed oil)

4.5.4 Effect of the Catalysts on Methyl Ester Chain Length

The average carbon chain length of methyl ester from each of the catalysts, as shown in Figure 4.52, further reveals that the CM and CM* were predominantly selective for saturated esters while the SFM and SFM* catalysts were selective for unsaturated methyl esters.

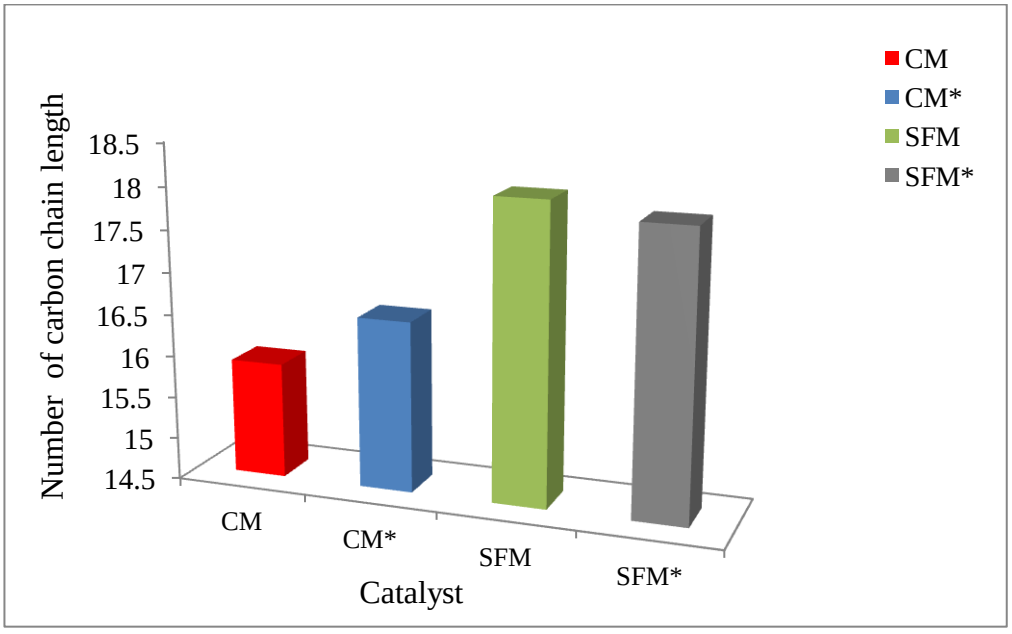

Figure 4.52: Overall Average Carbon Chain Length of Methyl Esters based on Catalyst

Furthermore, the carbon chain length distribution of the FAME composition after different reaction times clearly indicates the composition of the esters at each stage of the reaction. In Figure 4.53 and Figure 4.54 there is a trend of a decrease of $C_{18:1}$, which is the main component in the composition of the feed used for the reaction. There was single and double C-C bond cleavage of saturated and unsaturated chains, followed by C-H bonds which resulted in chain length reduction as shown in the product profile.

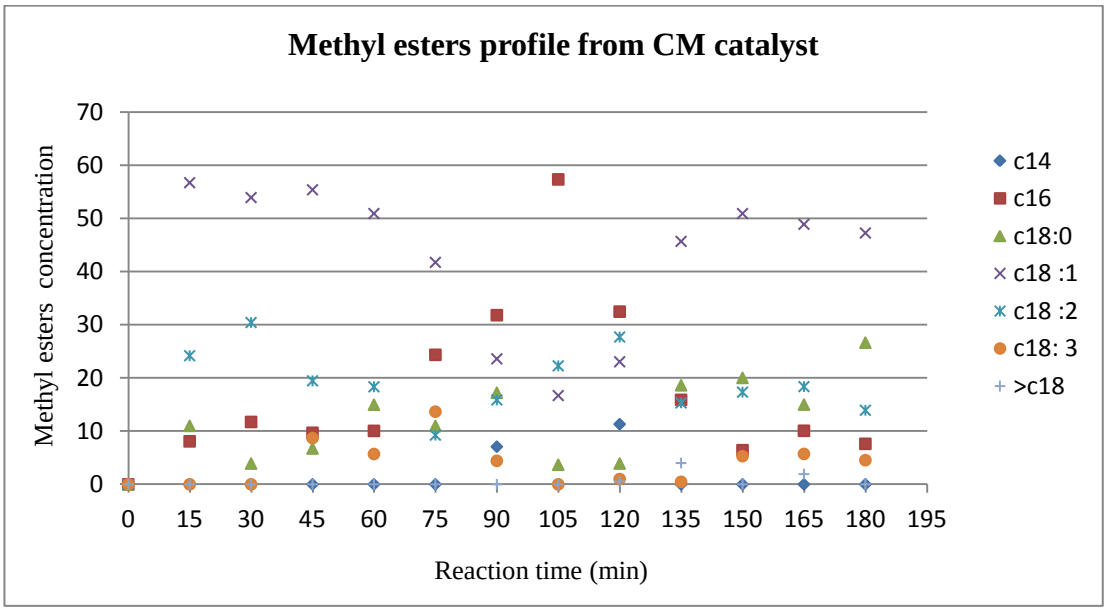

Figure 4.53: Selectivity of the CM catalyst to Different Methyl Esters at Different Time of the Reaction

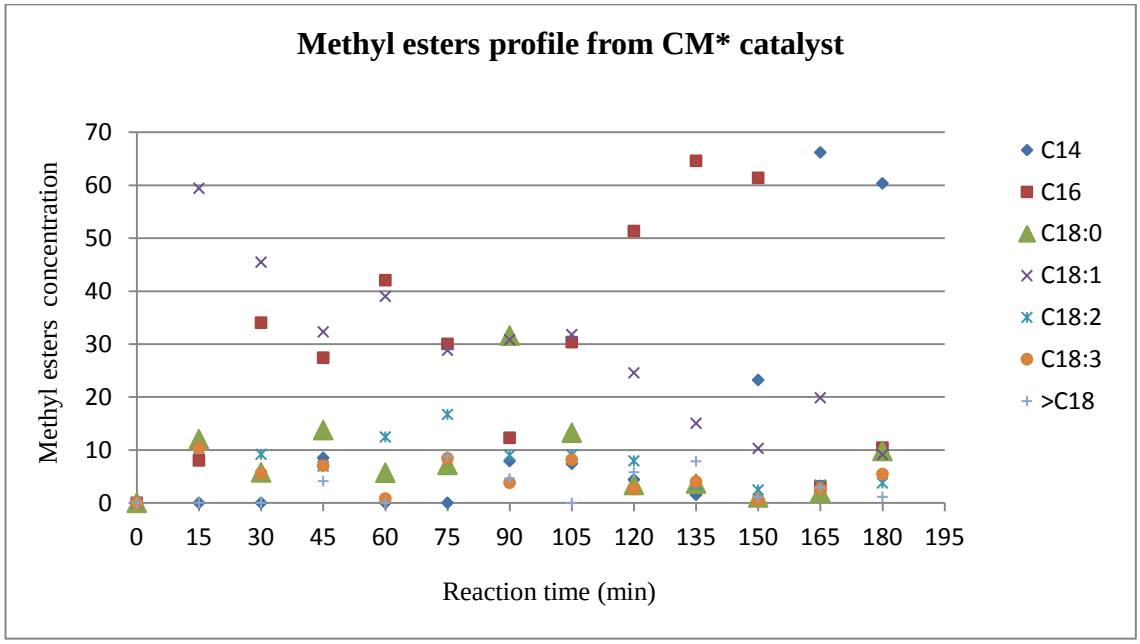

Figure 4.54: Selectivity of the CM* catalyst to Different Methyl Esters at Different Time of the Reaction

It is well established that radicals are very reactive. In addition to the cleavage of carbon bonds the solvent-free catalysts allowed for reactive radicals. With solvent-free catalysts, there is likelihood of most cleavage at the carbonyl-oxygen bonds. In addition, the availability of more Brønsted acid sites on the catalysts enhanced the different reaction of radicals as described by Vonghia *et al*. (1995a), producing a clearer and better distribution of methyl esters of lower molecular weight as shown in Figure 4.55 and Figure 4.56 than with the conventional catalysts.

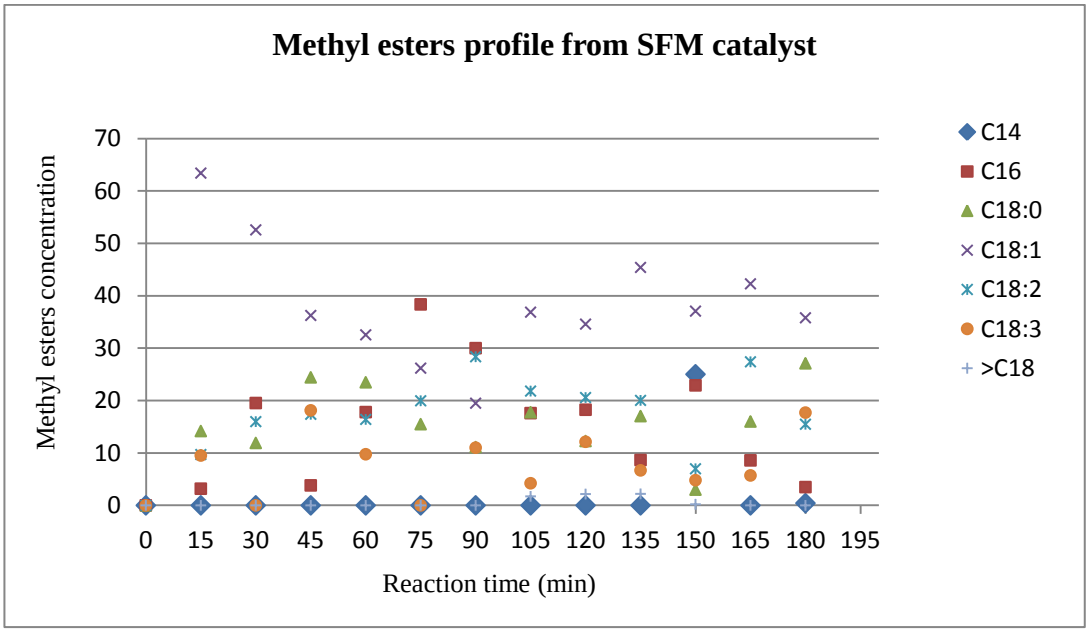

Figure 4.55: Selectivity of the SFM Catalysts to Different Methyl Esters at Different Time of the Reaction

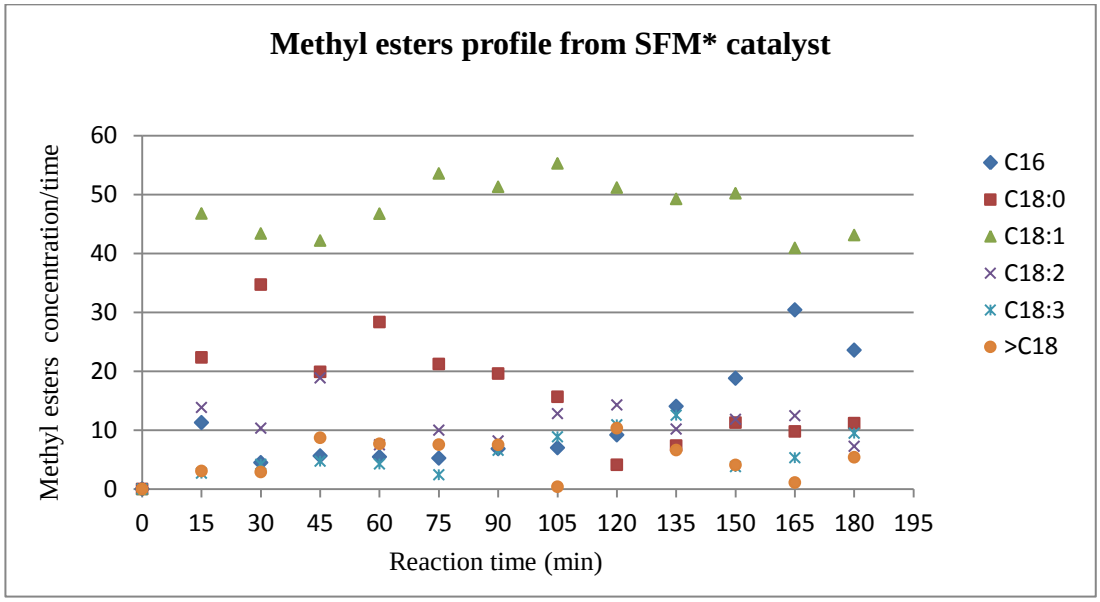

Figure 4.56: Selectivity of the SFM* Catalysts to Different Methyl Esters at Different Time of the Reaction

The significant differences in the distribution of the methyl esters between the two classes of sulphated zirconia catalysts prepared are due to the different concentrations and strengths of their Lewis and Brønsted acid sites. Although information from the literature concerning the reaction mechanism in the direct thermocatalytic cracking of rapeseed oil to methyl ester compared to other biofuels is scarce, the following reaction schemes in Figure 4.57 could be suggested:

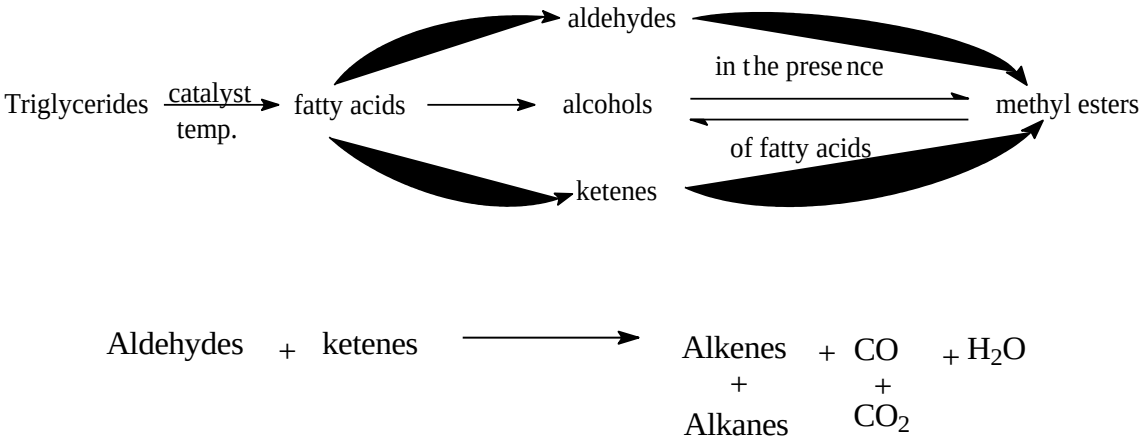

Figure 4.57: Proposed Mechanism for the Thermocatalytic Cracking of Rapeseed Oil to Methyl Esters by Thermocatalytic Cracking

The average carbon chain length distribution of each catalyst revealed the selectivity of each catalyst to the type of methyl esters produced with respect to reaction time. The distributions shown in Figure 4.58 further confirm the differences in selectivity to saturated and unsaturated methyl esters at every sampling point in the reaction.

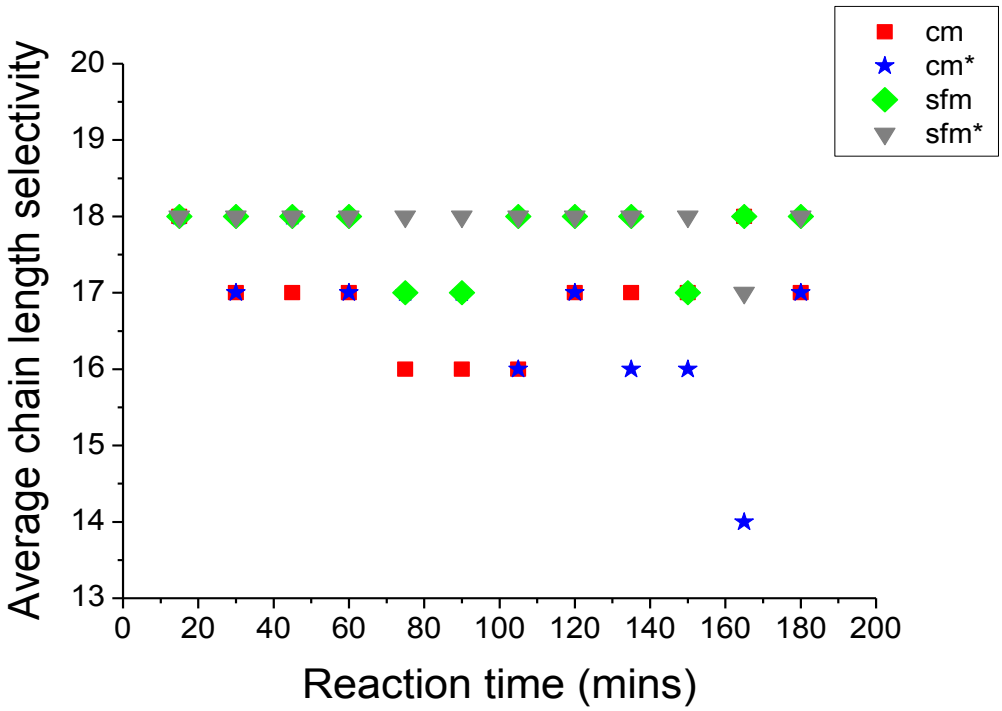

Figure 4.58: Average Carbon Chain Length of Methyl Esters in the Product Mixture at Various Reaction Times for Three Hours

The reaction is expected to begin with the thermal decomposition of triglycerides into fatty acids, which is a relatively rapid and temperature dependent process. With the presence of a catalyst with active acid sites, the fatty acid decomposes or cracked into alcohols, aldehydes and ketones most of which are present as free radicals that react in various ways (Dupain *et al*., 2007; Katikaneni *et al*., 1995a). The number of radicals that can form in the system is large because triglycerides are a complex and large molecules with many C-H and C-C bonds. The alcohols in the reaction medium undergo further reaction to produce methyl esters. The formation of esters by this mechanism is one of the reaction pathways described by Kubicka and Kaluza (2010) in deoxygenation of rapeseed oils to hydrocarbons in the presence of hydrogen. However, there must be high active acid site concentrations to favour the formation of esters, because the formation of alcohols, free fatty acids and methyl esters occurs simultaneously. The aldehydes, ketones and free fatty acids undergo further cracking and processes such as aromatization, alkylation, isomerisation, oligomerization, polymerization and condensation occur to form other hydrocarbons, of which some of those identified are discussed in section 4.5.5.

One striking observation is the presence of the peak for methyl heptadecanoate ($C_{17:0}$) in the GC chromatogram of the samples (see Appendix K) when it was analysed

without an internal standard. This was further confirmed by comparing the chromatogram for methyl heptadecanoate with that of the sample without the internal standard, as seen in same Appendix K. The peak at 11.18 minutes corresponded to the retention time of methyl heptadecanoate. Thus far no study has reported the production of methyl heptadecanoate from the cracking of vegetable oils.

4.5.5 Other Products

The product distributions shown in Figure 4.59 to Figure 4.62 reveal the presence of free fatty acid, diglycerides, other products and the change in the concentration of triglyceride in addition to methyl esters in the liquid product mixture. As earlier reported in section 4.5.2, there was some loss of methyl esters as the reaction progressed which were subsequently converted into hydrocarbons. The observed reaction follows well the findings of various studies (Kubicka and Kaluza, 2010; Osmont *et al*., 2007; Kubickova *et al*., 2005) of the decarboxylation of vegetable oils, fatty acids and esters to hydrocarbon fuels. There is a **c**lear correlation between later free fatty acid (FFA) formation and FAME loss. Except with the SFM and CM* catalysts, the higher the methyl ester loss the higher the free fatty acids formed. This is because the esters decomposed in the presence of radicals in the reaction mixture. As described by the mechanism shown in Figure 4.57, the formation of esters is a reversible reaction. Therefore, there must be a high active acid site concentration on the catalyst to favour the forward formation of methyl esters.

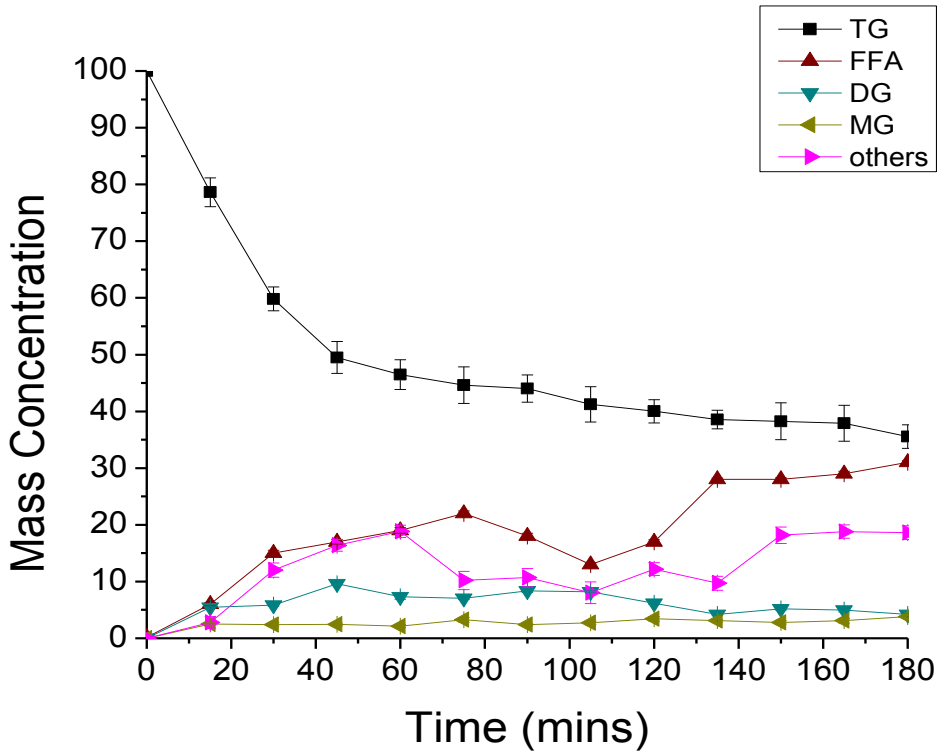

Figure 4.59: CM Catalysed Reaction Profile, 2wt% Catalyst at 270^{o}C, Indicating the Product Mixture at Different Reaction Time

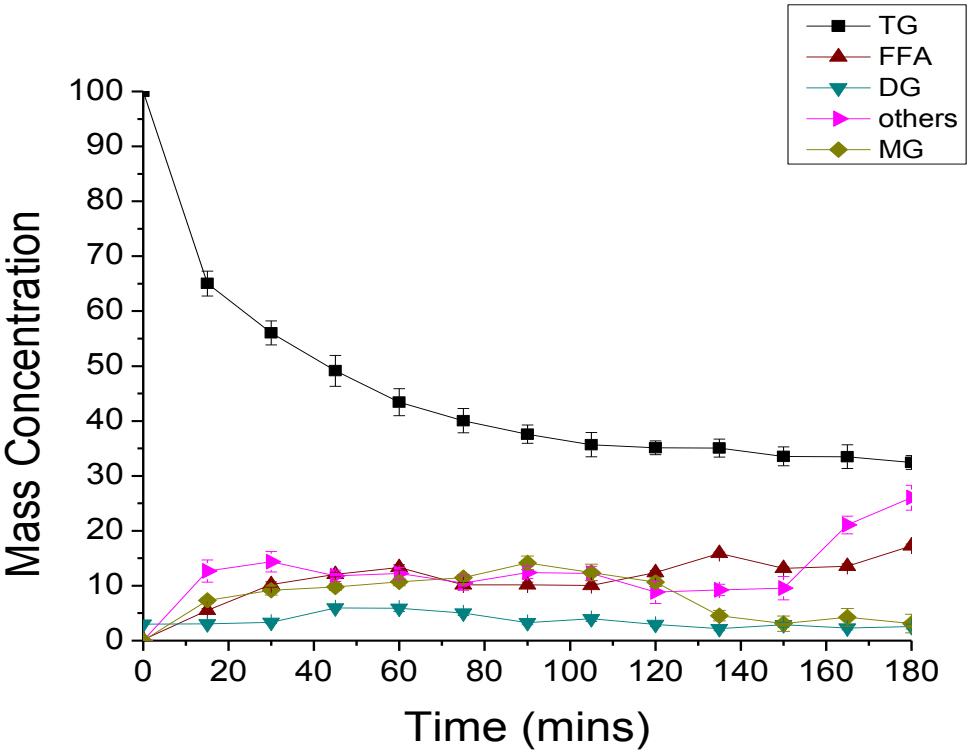

Figure 4.60: CM* Catalysed Reaction Profile, 2wt% Catalyst at 270^{o}C, Indicating the Product Mixture at Different Reaction Time

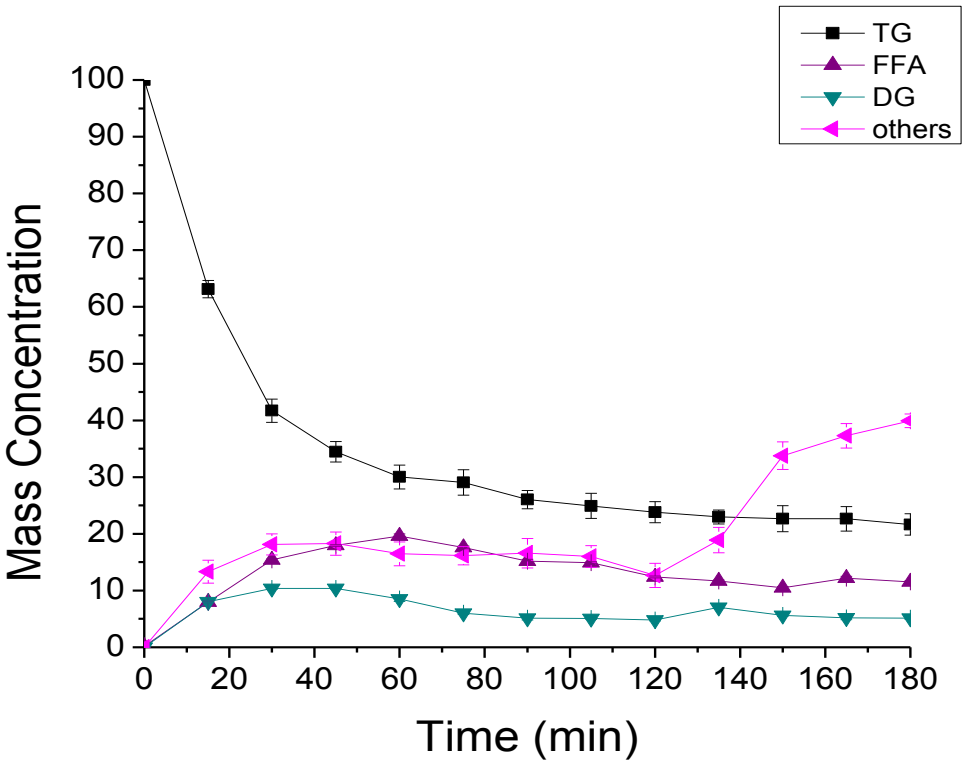

Figure 4.61: SFM Catalysed Reaction Profile, 2wt% Catalyst at 270^{o}C, Indicating the Product Mixture at Different Reaction Time

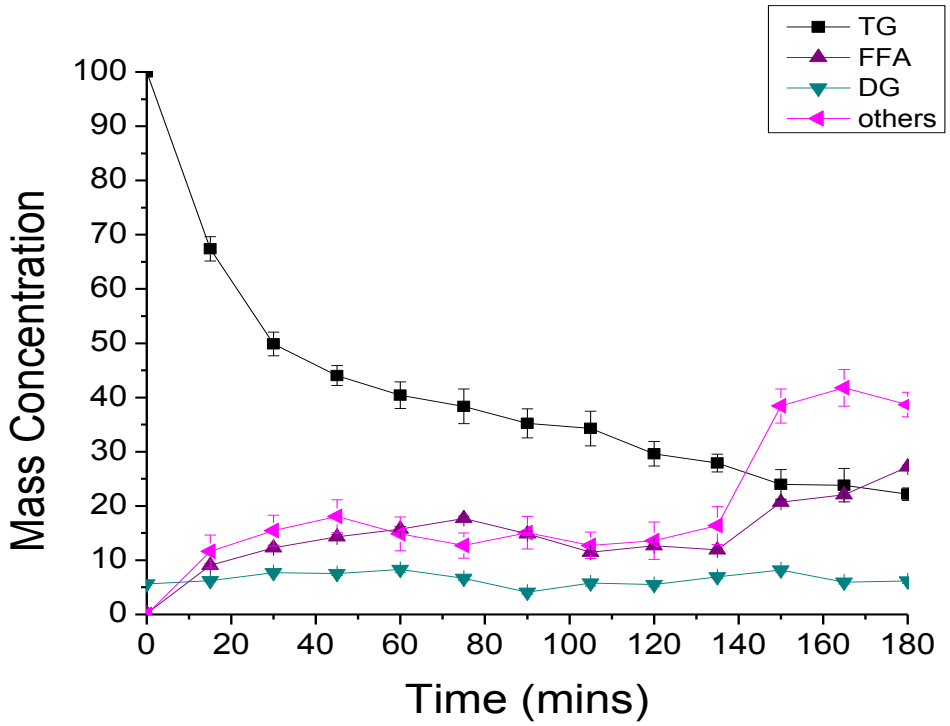

Figure 4.62: SFM* Catalysed Reaction Profile, 2wt% Catalyst at 270^{o}C, Indicating the Product Mixture at Different Reaction Time

These compounds were also identified by Idem *et al*. (1996) in the cracking of canola oil. Other products identified using GC-MS included ethyl iso–allocholate ($C_{26}H_{44}O_5$), an aldehyde E-14-Hexadecenal ($C_{16}H_{30}O$) and long chain unsaturated fatty acid alcohol (1-Heptatriacotanol, $C_{37}H_{76}O$). This work is the first to report such long chain unsaturated fatty acid alcohol from catalytic cracking of triglycerides. The presence of these products could be due to the several reactions such as isomerisation, elimination, reduction, aromatization, dehydration and disproportionation that occurred. This was earlier reported by Vonghia *et al*. (1995a) in the deoxygenation of triglycerides to aliphatic hydrocarbons (see Figure 2.11) to various alcohols, ketones and hydrocarbon products**.** In addition, monoglycerides were observed in the product streams from the conventional catalysts, but these were not evident in the product stream of solvent-free catalysts. The reaction scheme for methyl esters decomposition to other hydrocarbon products could be described as given in Figure 4.63. This agrees with the study of Maki-Arvela *et al*. (2007) in their study of catalytic deoxygenation of fatty acids and esters to n-heptadecane.

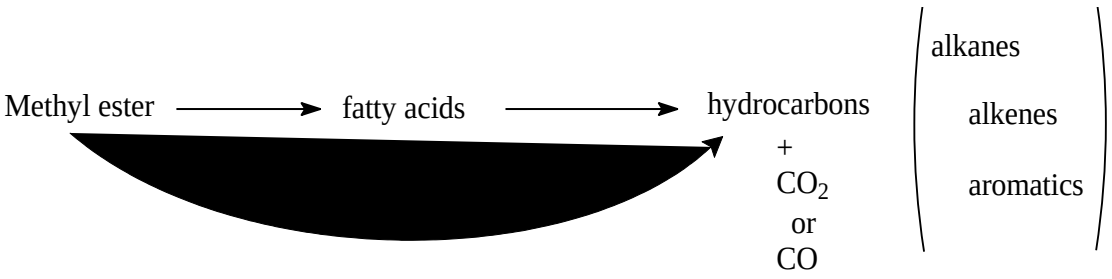

Figure 4.63: Reaction Scheme for Methyl Esters and Free Fatty Acids Decomposition

The gaseous products identified were methane, CO_2, and CO; however, these were not quantified. The amounts of water present in the product samples were at negligible concentrations which could not be detected even with Karl Fisher reagent.

It is evident from the present results that the production of methyl esters by the thermocatalytic cracking of rapeseed oil using sulphated zirconia catalyst is a selective reaction which depends on the active acid sites on the catalyst. The cracking of the triglycerides into methyl ester and other products in addition to carboxylic acids (FFAs) was clearly enhanced by the catalysts, because the thermal cracking of the same feedstock at the same temperature yielded only fatty acids without any methyl ester as revealed by the GC and GC-MS chromatograms.

4.6 Kinetics of the Reaction

The Arrhenius activation energies of the catalysts were determined using the procedure described in section 3.4.5. The reaction rate constant is related to the reaction temperature through the Arrhenius equation, so that the overall reaction activation energy can be calculated from Equation 4.1 using the reaction rate constant at different temperatures.

$$ln(k) = \frac{-E_a}{R}\frac{1}{T} + \ln(A) \qquad \text{Equation 4.1}$$

where:

A is the pre-exponential factor (the unit depends on the order of the reaction)

k is the rate constant (the unit depends on the order of the reaction)

E_a is the activation energy (kJ/mol)

R is the gas constant ($JK^{-1}mol^{-1}$)

T is the temperature of reaction (K)

The kinetic data for the reaction were obtained by thermogravimetric analysis (TGA) at isothermal reaction temperatures of 210°C, 240°C, 270°C and 300°C with 2wt% sulphated zirconia. The reaction rate was found to increase with increased temperature.

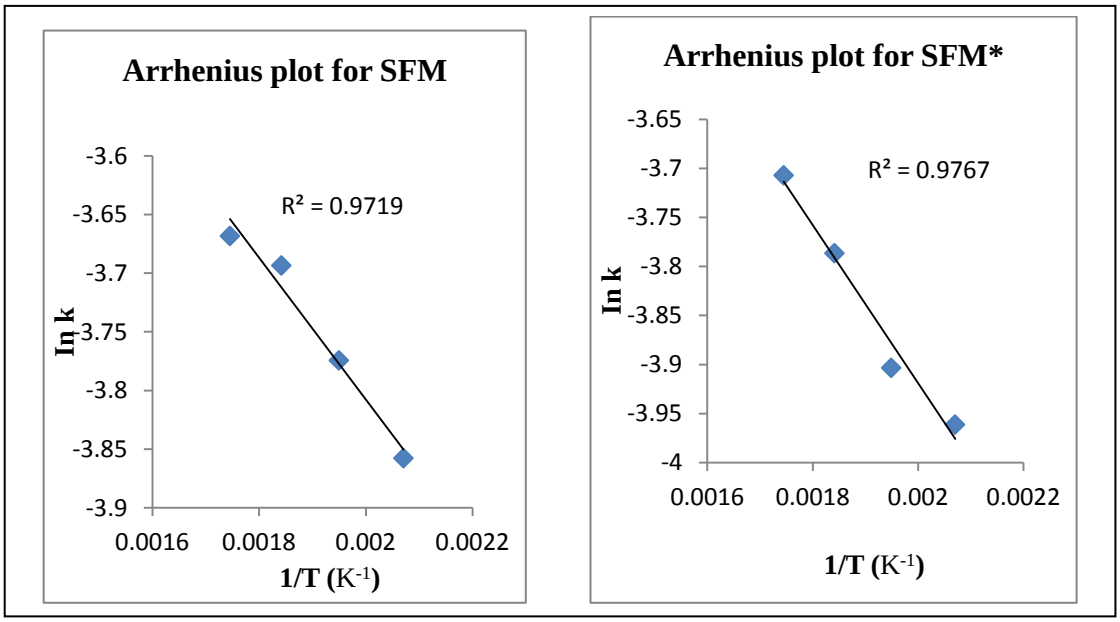

Figure 4.64: Arrhenius Plots for Triglyceride Cracking with SFM Catalysts

Activation energies of the catalysts were determined by reformulating Equation 4.1 and plotting lnk vs 1/T. Based on the Arrhenius activation energy plots in Figure 4.64 to

Figure 4.65 the activation energy (E_a) and the pre-exponential factor (A) were determined.

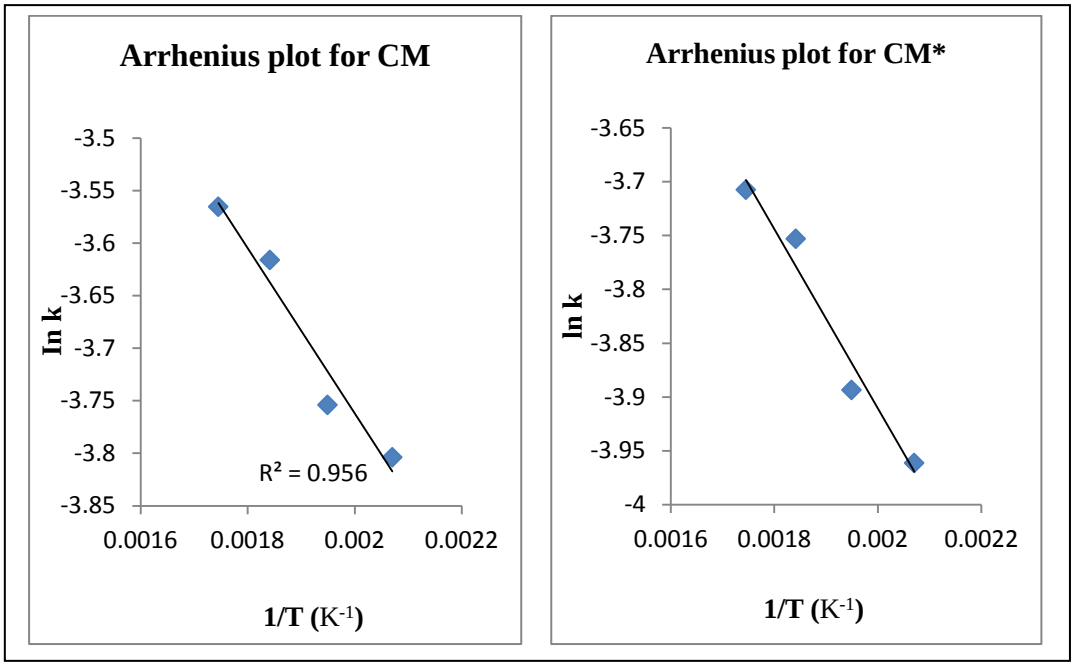

Figure 4.65: Arrhenius Plots for Triglyceride Cracking with CM Catalysts

The turnover frequency of the catalysts was determined using Equation 4.2. The turnover frequency (often designated TOF) is a measure of the catalytic activity of a catalyst in a reaction. It is simply the number of times that the overall catalytic reaction takes place per catalyst site per time for a fixed set of reaction conditions. The kinetic data and the turnover frequency for the catalysts are given in Table 4.12.

$$TOF = \frac{number\ of\ molecules\ of\ a\ given\ product}{(number\ of\ catalyst\ active\ sites) \times (time)} \qquad \text{Equation 4.2}$$

Table 4.12: Activation Energies and Catalytic Activities for the Catalytic Cracking of Triglyceride (rapeseed oil)

Catalyst	Activation energy (Ea) kJ/mol	TOF* (10^{-2} min^{-1})
CM	6.92± 2	2.33
CM*	6.71± 2	4.34
SFM	5.02± 2	7.41
SFM*	6.53± 2	6.22

* *Based on the number of acid sites measured by pyridine- DRIFTS analysis*

The solvent-free catalysts have higher turnover frequency (TOF) than the conventional, the SFM having the highest. However, and interestingly the CM* had nearly twice the turnover frequency of the CM catalyst. This is a clear indication that although the CM* was prepared in the same manner as the CM but the level of the Brønsted acid enhanced its catalytic reaction as shown by the turnover frequency. The catalysts were non-porous so there was no internal or external mass transfer. The high values of TOF obtained for the solvent-free catalysts further support the fact that, under the reaction conditions used, thermocatalytic cracking of triglycerides by the catalysts was kinetically controlled and no mass transfer limitations were present.

4.7 Catalysts Characterization and Their Catalytic Activity

Following the various characterization that were carried out on the catalysts the characterization results of XRD revealed the morphology of the conventional catalysts as crystalline and the solvent-free as amorphous. The FTIR identified their functional group as SO_4^{2-} and particularly the IR-py, showed the presence of both Lewis and Brønsted acid sites on the catalysts. The Lewis sites is an indication that the S=O bond was predominant and this was stronger in the conventionally prepared sulphated zirconia whereas, it was S-O bond in solvent-free catalysts implying Brønsted acid sites. The bisulphate anions were probably responsible for the high Lewis activity of sulphated zirconia from the conventional method of preparation. This is attributed to the inductive effect of these bisulphate groups which withdraw electron density from the three-coordinate zirconium cation through the bridging oxygen. The XPS technique which was used to investigate the chemistry at the surface of the catalysts revealed the SFM catalyst surface was purely sulphate bonded to zirconia whereas zirconium oxide was present on other catalysts in the following order: SFM*< CM* < CM. The catalyst with the highest zirconium oxide on its surface was found to be the CM (see Table 4.3). Whereas the catalysts from the solvent-free method were found to retain more sulphates; with both Lewis and Brønsted acid sites being present, although a Brønsted acid site was predominant. Further analysis of the XPS sulphur spectra of the catalysts revealed protonated sulphur species on the solvent-free samples. On the other hand, deprotonated sulphur species exists on the catalysts prepared by the conventional method; however, CM* sample showed less of the deprotonated sulphate species than CM sample.

From the conversion profile the catalysts were all active in catalytic cracking of triglycerides irrespective of the type and the amount of acid sites (Lewis or Brønsted) on the catalysts. The highest conversion was 78% by the solvent-free catalyst while the least was 62% by the conventional catalyst. However, the production of methyl ester (biodiesel) by these catalysts is quite different from the conversion. The solvent-free catalysts were more selective towards the production of methyl ester (59%) and more particularly towards unsaturated methyl ester. For the conventional catalysts, the methyl ester was of a lower yield (32%) and predominantly saturated. The differences in the reactivity and selectivity of these catalysts to producing methyl ester could be attributed to the difference in their morphology and acid sites concentration and its activity per site (as described in Table 4.12). The solvent-free catalysts were amorphous in nature; had more defects on the surface, and defects tend to be higher energy sites that are active for reaction and Brønsted-dominated. These imply more surface area and protonated sulphate available for the catalytic reaction. In other words more sulphate was on the surface of the catalysts. On the other hand, the conventional catalysts were Lewis-dominated and crystalline. Their crystallinity resulted in lesser surface area that is available for the catalytic reaction compared to their counterpart, the solvent-free catalysts. The Lewis acid sites and surface sulphate which was predominantly deprotonated were responsible for their selectivity for saturated methyl ester. There is a relationship between the number of Brønsted acid sites, its activity and the amount of methyl ester produced. This was particularly demonstrated between the conventionally synthesized sulphated zirconia catalysts. The XPS showed that the CM had more S=O than S-O bonds on its surface, explaining its Lewis acidity. Meanwhile, the CM* had higher percentage of sulphate-oxygen, indicating more S-O than S=O bonds, which led to its Brønsted acidity that resulted into higher yield of methyl ester (32%) compared to 21% for the CM. Notably, both the Lewis and the Brønsted acid sites were active for the catalytic conversion of triglycerides to methyl esters but the Brønsted acid sites was more active than Lewis acid sites for the selectivity of methyl ester. Particularly, higher concentration and higher activity per site are needed for unsaturated methyl ester production. The study has revealed the possibility of controlling the degree of saturation of the methyl ester product by catalyst design. The differences in the characterization of the catalysts help to explain the variation in the yield of methyl ester as well as the enhanced activity of the solvent-free catalysts cum selectivity.

4.8 Coke Deposition and Catalyst Regeneration

The coke deposited on the catalysts was determined as described in section 3.5.1. The coke deposition was presumably due to the adsorption of carbon and hydrocarbon molecules on the surface of the catalysts from the reaction mechanism. The results showed CM and SFM* had higher carbon weight deposit of 0.54g and 0.24g respectively than the SFM and CM*. The least amount of coke was recorded by SFM 0.23g and 0.34g for the CM* catalyst. The coke deposition could have caused the catalysts to deactivate after several hours of the reaction by covering the active sites on the catalysts. The results showed 17% of the catalyst weight as carbon deposited on the SFM and 25% on the CM* catalyst. The SFM* and CM had 31% and 40% weight of catalyst respectively.

4.8.1 Characterization of Regenerated Catalysts

In order to test whether or not the catalysts could be reused they were regenerated as described in section 3.5.3 and characterized. The XPS results for the regenerated catalysts revealed similar results as the EDX indicating lost of sulphur from the catalysts. The CM had zero percentage sulphur retention whereas the SFM had 98%. However, the SFM* lost a substantial amount of sulphur (20%). There was no change in the crystallographical pattern of the regenerated catalysts, the solvent-free catalysts were all amorphous and the conventional were crystalline.

4.8.1.1 Test of Leaching

A Leaching test was conducted as described in section 3.5.2 to determine whether or not the sulphate leached during the reaction. After the treatment the catalysts were subjected to FTIR and EDX analyses. The results in Figure 4.66 showed that the CM had lost all of the sulphate content (100%) after the reaction. Surprisingly, the CM* only lost 16% and the SFM* lost 18% whereas the SFM retained almost 100% of sulphur. The SFM experienced a loss of only 0.4%. This showed that the solvent-free method was appropriate in synthesizing an active catalyst that can be reused, although attention must be paid to the molar ratio of sulphate to zirconia. The presence of excess sulphate leaves some of the SO_4^{2-} ions that are not bonded to the zirconia which allows leaching to occur, particularly in CM and SFM* which both had a higher ratio of sulphate of 1:15 during the preparation. However, the addition of metakolin to the CM and SFM catalysts during preparation led to the improved retention of sulphur on the catalysts. This was particularly true for the CMM, which lost approximately 5.74% sulphur

compared to the CM which lost 100% after three hours of reaction. In other words, the bonds between the silicon and sulphate ions in the modified CM catalyst were strong enough to avoid the leaching of the sulphate during the reaction despite the preparation method used. In the case of the modified solvent-free catalyst (SFMM), there was only 0.5% sulphur loss. Generally, the solvent-free method has proved to be an effective method of synthesizing sulphated zirconia with higher activity and with little or no leaching during use.

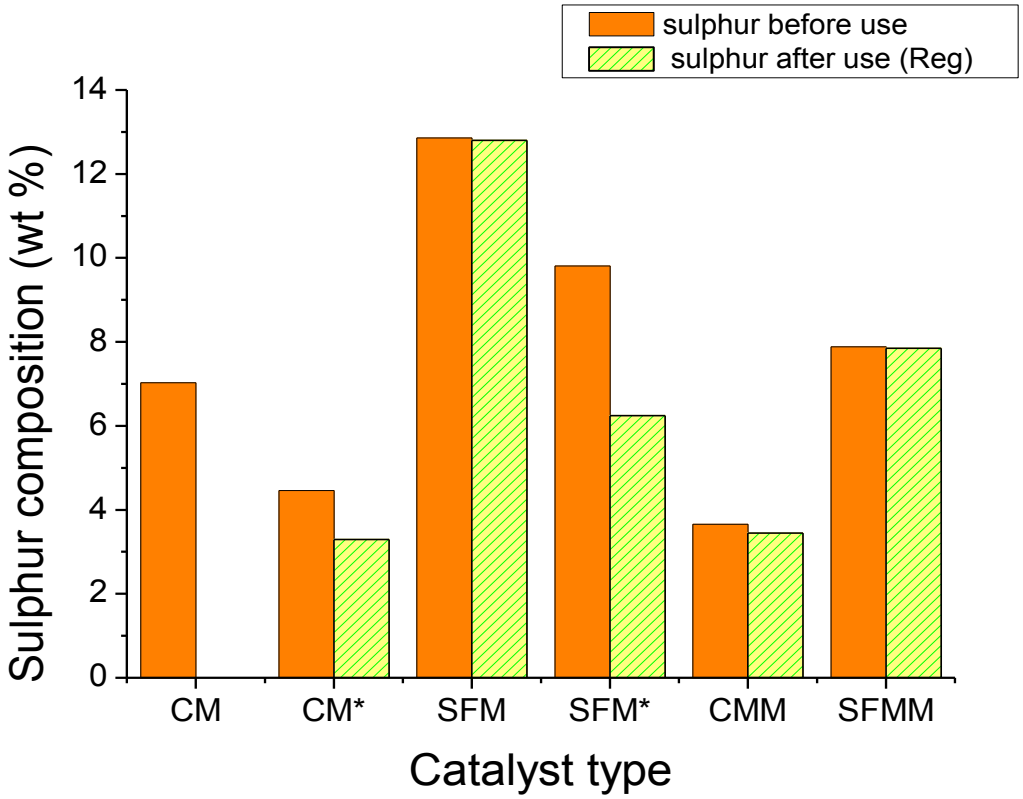

Figure 4.66: Comparison of Sulphur Content (wt %) in Catalyst Before reaction and After the Reaction.

The leaching observed was not due to the method of preparation, but rather the amount of sulphating agent used during the preparation as explained in section 4.1.2.3.

4.9 Varying the Reaction Conditions

Mass of catalysts and reaction temperature were varied. A limited set of reactions were conducted at lower and higher temperatures as reported in section 3.3.1 using a 100ml batch micro reactor (Parr Instrument Company; Model 5500). The temperatures tested were 210^{o}C, 240^{o}C and 300^{o}C. The reactor had no sampling port, so samples could not be collected at intervals as in the previous reactor used (HEL automate system; Model

4560). After each experiment it took the reactor 3½ hours to cool to room temperature before any sample could be taken. Another issue was the method of injecting the catalyst into the reactor. With the HEL automate system reactor, the catalyst was injected at the reaction temperature (isothermal reaction), but in the case of the Parr micro reactor the catalyst and the rapeseed oil were heated from room temperature to the reaction temperature. Although the temperature profiles shown in Figure 4.67 look the same, the reaction products are bound to be affected because of the difference in the time and temperature at which the catalyst was injected.

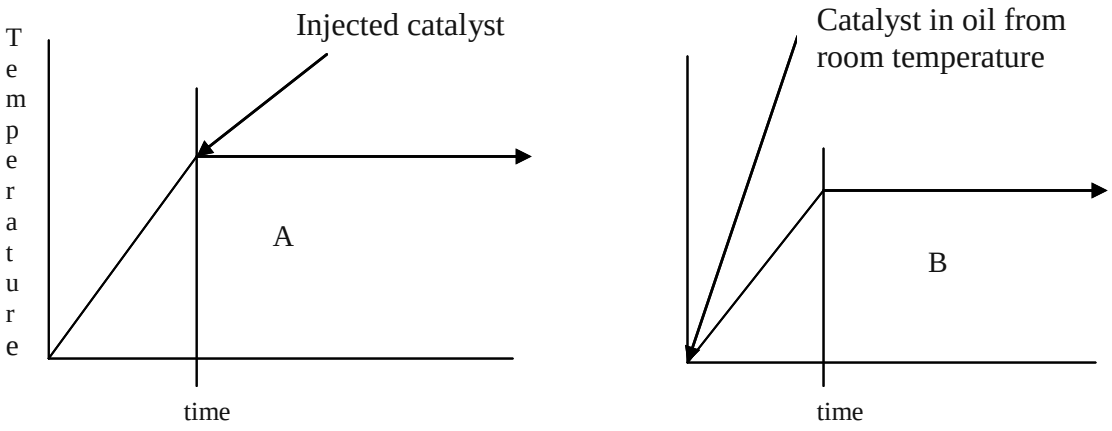

Figure 4.67: Temperature Profile for the Reactors

From Figure 4.67, A is the HEL automate system and B is the Parr micro reactor. Using a GC, no FAME was identified. This could be due to further reaction of the FAMEs to other biodiesel/hydrocarbon products, since it was not possible to monitor the progress of the reaction within the reactor. Even when a sampling port was attached to the reactor there was no FAME in the liquid samples. Probably because the catalysts were added to the feed at the beginning of the reaction and different reactions would have taken place in the reactor before the 3 hours sampling time.

4.10 Catalytic Activity of Doped Sulphated Zirconia with Metakaolin

The GC analysis of the liquid product from the modified catalysts had very small peaks of methyl ester on the chromatogram. However the GC-MS chromatograms indicated clear peaks assigned to methyl esters in addition to other products. It could be that the presence of potassium in the modified catalysts resulted to catalyst poison. Further work

is required on the pre-treatment of the kaolin and the application of these catalysts as well as product analysis.

Chapter 5: Conclusions and Further Work

5 Conclusions

In this study conventional wet-precipitation and solvent-free methods were used to synthesize sulphated zirconia catalysts with different molar ratios of the sulphating agent. Their activity for the direct catalytic cracking of rapeseed oil under similar reaction conditions of temperature and pressure in a batch reactor was evaluated. When the intrinsic catalytic activities of all of the catalysts were compared on a rate per site basis by turnover frequency (TOF), all of the catalysts exhibited catalytic activity, suggesting that they all have acid sites capable of effectively catalyzing triglyceride cracking. Differences in the reactivity of the catalysts to give the desired product were attributed to their Brønsted acid site concentrations. It has also been shown that the tetragonal phase of sulphated zirconia is not necessarily required for Brønsted acid site formation, in contrast to the findings of studies reviewed by Song and Sayari (1996). The solvent-free method is more economical since no waste is involved in the procedure.

5.1 Solvent-free Catalysts (SFM and SFM*)

Two catalysts prepared by the solvent-free method were SFM and SFM*. The difference is in the ratio of sulphating agent to the zirconia during preparation. The $Zr(OH)_4/SO_4^{2}$ ratios were 1:6 and 1:15 for SFM and SFM* respectively. These sulphated zirconia catalysts, calcined to 600^{o}C, were found to be amorphous in nature with higher surface area than those produced by conventional wet methods. Their acid sites were principally Brønsted in nature. XPS studies showed that they had higher percentages of sulphate-oxygen than oxide-oxygen. The SFM had 93% and the SFM* 81% of sulphate-oxygen on the surface of the catalyst. This indicated that most of the sulphate species bonded to zirconia is on the surface of the catalysts rather than within the bulk. This preparation method generated more S-O than S=O bonds on the surface of the catalysts, which led to higher Brønsted acidity. Both catalysts were active in the thermocatalytic cracking of triglycerides at 270^{o}C. In three hours the SFM* achieved 78% conversion of triglycerides and the SFM 76%. These catalysts were found not just to be active, but selectively active towards biodiesel (methyl esters) production. The maximum yields of methyl esters achieved by SFM and SFM* were 59% and 49% respectively after 2 hours of the reaction. There was a strong correlation between the

sulphate-oxygen level on the surface of the catalysts and their activity. The catalytically activity of sulphated zirconia has been shown in previous studies (Marcus *et al*., 2003; Zalewski *et al*., 1999) to be enhanced by the percentage of sulphate-oxygen on the catalyst. The catalysts can be regenerated after use; however, the SFM* catalyst was found to leach its active species into the reaction. Based on EDX analysis, there was a 20% loss of sulphur from the SFM* and 0% for the SFM. The XRD pattern of the regenerated catalysts was similar to that of the fresh catalysts, indicating that there was no phase change in the catalysts during the reaction. The higher conversion and yield of SFM is due to the greater amount of pure $Zr(SO_4)_2$ on the surface of this catalyst.

.

5.2 Conventional Wet-precipitated Catalysts (CM and CM*)

Based on the ratio of zirconia to sulphuric acid, two catalysts were prepared by conventionally wet-precipitated method. The catalyst with 1:6 ratio of $Zr(OH)_4/SO_4^{2}$ was designated as CM* and CM for 1:15. These catalysts were demonstrated to be predominantly crystalline (using XRPD). The CM was tetragonal in nature, while CM* exhibited monoclinic phase in addition to the tetragonal phase. Their crystallite sizes were found to be 10.5nm and 17.3nm for CM and CM* respectively. The CM was Lewis acid-dominated, whereas the CM* was Brønsted acidic. When sulphated with 15ml of H_2SO_4 per gram of $Zr(OH)_4$ during preparation, the CM catalyst was found by XPS analysis to exhibit 46% sulphate-oxygen on the surface. CM* was sulphated with only 3ml of H_2SO_4, yet exhibited 58% of surface sulphate-oxygen. This showed that the CM had more S=O than S-O bonds on its surface, explaining its Lewis acidity. This was not the case for the CM* because of the high percentage of sulphate-oxygen, indicating more S-O than S=O bonds, which led to its Brønsted acidity. XPS and EDX recorded higher sulphur retention of the CM* than the CM, yet more sulphuric acid was used for CM during preparation. This clearly showed that the use of a large excess of sulphuric acid during preparation had no positive impact on the amount of sulphate retained on the catalyst surface. Farcas¸iu *et al.* (1997) had reported that at higher sulphate loading the sulphate moves into the bulk phase of the catalyst rather than on the surface. However, both catalysts were catalytically active in the thermocatalytic cracking of triglycerides at 270^{o}C. The CM and CM* catalysts exhibited similar conversion rates of 62% and 66%, but different yields of methyl esters. The yield of methyl ester for the CM* catalyst was 32% whereas for the CM catalyst it was only 21%. Although CM* had fewer Brønsted sites more than its Lewis sites, its activity per site was higher than CM for the desired methyl ester product. The difference in methyl ester yield was due to

the higher activity of the Brønsted sites on the CM* catalyst. Therefore, increasing the amount of sulphuric acid in the wet precipitation method to increase activity was counterproductive, as it actually decreased activity towards the desired product. The XPS and EDX results for the regenerated CM and CM* catalysts revealed that CM catalyst suffered higher sulphur loss during the reaction. The CM completely lost its sulphate whereas CM* lost only 16% after the reaction. This means the catalytic activity of CM catalyst was affected during the reaction because of sulphate leaching rather than carbon deposition on the active sites.

5.3 Meta-kaolin-supported Sulphated Zirconia Catalysts

The addition of meta-kaolin support was found to improve the physiochemical properties of the modified sulphated zirconia catalysts. The properties include: surface area, higher S/Zr ratios and acid sites concentration, particularly the Brønsted acidity. These properties were higher than those of the unmodified sulphated zirconias (i. e. CM, CM*, SFM and SFM*). High BET surface area and homogeneity were achieved with the solvent-free method. However the presence of potassium from the meta-kaolin on the catalyst poisoned the modified catalysts, which had an effect on their catalytic activity and selectivity for methyl esters. Although the catalysts had higher concentrations of both Brønsted and Lewis acid sites, their GC chromatograms had very small peaks of methyl ester.

5.4 Summary

Comparing the amount of sulphate used in the preparations, the reduction in methyl ester yield observed with the conventional catalysts suggests that the solvent-free method facilitates a better interaction between the sulphate groups and zirconia cations. In all of the samples it is evident that there is a direct relationship between the number of Brønsted acid sites and the amount of sulphate retained on the catalysts. However, it is clear that both the Lewis and the Brønsted acid sites were active in the catalytic conversion of triglycerides, but the Brønsted acid sites had a more significant effect than the Lewis acid sites on the selectivity towards methyl ester production.

Another important observation is that the solvent-free sulphated zirconia exhibited higher selectivity for unsaturated methyl esters. Catalysts synthesized via the wet precipitation method produced a larger fraction of saturated methyl esters, albeit with a lower overall conversion to methyl ester. Hence, the research work has shown that

changing the method of catalyst preparation can change the selectivity to methyl ester and, within that, selectivity to degree of saturation. This opens up the possibility of controlling the degree of saturation of the methyl ester product by appropriate catalyst design, in order to produce more or less saturated fuels for different markets. In addition, methyl heptadecanoate, which is a commonly purchased internal standard for GC methyl ester analysis, was one of the various methyl esters identified in the product mixture from the direct cracking of the triglycerides. Another important industrial chemical identified is a long chain unsaturated fatty acid alcohol, 1-Heptatriacotanol ($C_{37}H_{76}O$). No previous study has reported the production of methyl heptadecanoate or the unsaturated fatty acid alcohol from the cracking of triglycerides.

If selectivity is to methyl esters only, regardless of the saturation of the product, the best catalyst is that with the most Brønsted acid sites, that is, a catalyst produced by the solvent-free production method. The distinct differences found in this study are indications that excess sulphate may not be necessary for the preparation of an active catalyst, but rather that the method used is critical. The activation energies are consistent and in a narrow range (5-7kJ/mol), indicating that these catalysts probably used sites with similar characteristics to carry out the reactions. The direct thermocatalytic cracking of triglycerides is thus a promising process for methyl ester (biodiesel) production, since the need for alcohol in the conventional transesterification process is entirely removed, and there are potential synergies with the cracking of oil. Using these catalysts high selectivity for methyl ester is possible and the degree of saturation of the methyl esters produced can be tuned.

5.5 Recommendation for Further Work

The use of crude oils is important if the cost of production is to be kept to a minimum, and so the catalysts should be tested with waste and non-edible oils. Information obtained from batch reactions of thermocatalytic cracking is fundamental in the development of a continuous process. Further research into reaction conditions and the use of a continuous process would be beneficial considering that conversions are reported to be high, up to 78% in $2^1/_2$ hours. Once the optimal conditions and reaction system have been identified at the batch level, it will be necessary to perform the reactions in a continuous reactor at various conditions in order to optimize the process.

Further investigation of the optimum reaction conditions to reduce the reaction time is required.

Alternative techniques for the separation of the product mixture into different fractions have not been investigated here. Although gas chromatography and gas chromatography/mass spectroscopy have proven to be the most effective methods to analyse the full spectrum of the product mixture, they are not the cost-effective techniques for separation. There may be a need to try techniques such as distillation, which could add significant effectiveness to the process by given different product range. Further processing of the downstream into various products and chemicals is recommended as this will add impetus to the entire process.

Further research on meta-kaolin-supported sulphated zirconia should be conducted to avoid the poisoning of catalysts by potassium. Potassium is soluble in water therefore it can simply be removed during the pre-treatment of the kaolin to meta-kaolin before using it as a support. Its hydroxide is an important industrial chemical and that can add value to the process. Unfortunately their catalytic activity yielded no good results because of the potassium therefore, their application in thermocatalytic cracking of triglycerides should be investigated.

At present, the understanding of the full mechanism of the reaction involved in the thermocatalytic cracking of triglycerides to produce methyl esters is underdeveloped, and there thus exists the need to refine knowledge of the process ranging, from fundamental catalytic chemistry to process optimization performing series of experiment at different temperature and catalyst ratio.

Conferences and Publications

Conferences

Eterigho, E. J., Lee, J. G. M. and Harvey, A. P. (2011) 'Synthesis, Characterization and Evaluation of two Forms of Sulphated Zirconia for Biofuel Production by Triglyceride Cracking *', Bioenergy III Conference: Present and New Perspectives on Biorefineries* Lanzarote, Canary Islands, May 22 - 27.

Eterigho, E. J., Lee, J. G. M. and Harvey, A. P. (2011) 'Evaluation of Catalytic Activity of Synthesized Sulphated Zirconia for Triglyceride Cracking *', 8th European Congress of Chemical Engineering.* Berlin, Germany, September 25 - 29.

Eterigho, E. J., Lee, J. G. M. and Harvey, A. P. (2011) 'Catalytic Cracking of Triglyceride by Sulphated Zirconia for Fatty Acid Methyl Ester with High Selectivity*', 2012 AIChE Annual Meeting.* Minneapolis, MN, United States, October 16-21, 2011.

Publications

Eterigho, E. J., Lee, J. G. M. and Harvey, A. P. (2011) 'Triglyceride cracking for biofuel production using a directly synthesised sulphated zirconia catalyst', *Bioresource Technology,* 102, (10), pp. 6313-6316.

Eterigho, E. J, Karen Wilson and Adam P. Harvey 'Enhanced Selectivity for Fatty Acid Methyl Ester Production from Triglycerides (Rapeseed Oil) Using Sulphated Zirconia' (Submitted for Publication)

Posters

Eterigho, E. J., Lee, J. G. M. and Harvey, A. P. 'Development of Sulphated Zirconia Catalyst for Biofuel by Triglyceride Cracking' (2009)

Eterigho, E. J., Lee, J. G. M. and Harvey, A. P. 'Direct Synthesis of Sulphated Zirconia for Triglyceride Cracking' (2009)

Eterigho, E. J., Lee, J. G. M. and Harvey, A. P. 'The Effect of Direct Synthesis on the Catalytic Activity of Sulphated Zirconia' (2010)

Eterigho, E. J., Lee, J. G. M. and Harvey, A. P. 'Development of Heterogeneous Catalyst for Triglyceride Cracking' (2010)

Eterigho, E. J., Lee, J. G. M. and Harvey, A. P. 'Synthesis of sulphated zirconia with improved catalytic properties for biodiesel production' (2011)

Award and Prize

The second best post graduate presenter at the 2010 conference on ‘catalyst preparation 4 the 21st century’ by the IChemE Catalysis Group, UK.

References

(2010) *BiofuelsDigest*. Available at: http://biofuelsdigest.com/bdigest/2010/12/03 (Accessed: 05/08/2011).

Adebanjo, A., Kulkarni, M. G., Dalai, A. K. and Bakhshi, N. N. (2007) 'Pyrolysis of waste fryer grease in a fixed-bed reactor', *Energy and Fuels,* 21, (2), pp. 828-835.

Adeeva, V., Dehaan, J. W., Janchen, J., Lei, G., D., S., V., , Vandeven, L. J. M., Sachder, W. M. H. and Vansanten, R. A. (1995) 'Acid Sites in Sulphated and Metal Promoted Zirconium Dioxide Catalysts', *Journal of Catalysis,* 151, (2), pp. 364-372.

Agarwal, A. K. (2007) 'Biofuels (alcohols and biodiesel) applications as fuels for internal combustion engines', *Progress in Energy and Combustion Science,* 33, (3), pp. 233-271.

Akkari, R., Ghorbel, A., Essayem, N. and Figueras, F. (2008) 'Sulphated zirconia grafted on a mesoporous silica aerogel: Influence of the preparation parameters on textural, structural and catalytic properties', *Microporous and Mesoporous Materials,* 111, (1-3), pp. 62-71.

Ali, Y. and Hanna, M. A. (1994) 'Alternative diesel fuels from vegetable oils', *Bioresource Technology,* 50, (2), pp. 153-163.

Arata, K. and Hino, M. (1990) 'Preparation of superacids by metal oxides and their catalytic action', *Materials Chemistry and Physics,* 26, (3-4), pp. 213-237.

Arumugam, S., Kien Yoo, C., Paolo, F., Francis, K., Sergey, Z. and Stanislav, M. (2009) 'Catalytic Applications in the Production of Biodiesel from Vegetable Oils', *ChemSusChem,* 2, (4), pp. 278-300.

Babou, F., Coudurier, G. and Vedrine, J. C. (1995) 'Acidic Properties of Sulphated Zirconia: An Infrared Spectroscopic Study', *Journal of Catalysis,* 152, (2), pp. 341-349.

Balat, M. (2008) 'Global trends on the processing of bio-fuels', *International Journal of Green Energy,* 5, (3), pp. 212-238.

Barnwal, B. K. and Sharma, M. P. (2005) 'Prospects of biodiesel production from vegetable oils in India', *Renewable and Sustainable Energy Reviews,* 9, (4), pp. 363-378.

Bartholomew, C. H. and Farrauto, R. J. (2006) *Fundamental of Industrial Catalytic Processes.*2nd ed United State: John Wiley and Sons, Inc.

Bear, I. J. and Mumme, W. G. (1970) 'The crystal chemistry of zirconium sulphates. Part VII. Structural relationships and transformations among the Zr(SO4)2-hydrates', *Journal of Solid State Chemistry,* 1, (3-4), pp. 497-505.

Billaud, F., Dominguez, V., Broutin, P. and Busson, C. (1995) 'Production of hydrocarbons by pyrolysis of methyl esters from rapeseed oil', *Journal of the American Oil Chemists' Society,* 72, (10), pp. 1149-1154.

Billaud, F., Tran Minh, A. K., Lozano, P. and Pioch, D. (2001) 'Catalytic cracking of octanoic acid', *Journal of Analytical and Applied Pyrolysis,* 58-59, pp. 605-616.

Canakci, M. and Van Gerpen, J. (1999) 'Biodiesel production via acid catalysis', *Transactions of the Asae,* 42, (5), pp. 1203-1210.

Charusiri, W. and Vitidsant, T. (2005) 'Kinetic study of used vegetable oil to liquid fuels over sulphated zirconia', *Energy and Fuels,* 19, (5), pp. 1783-1789.

Charusiri, W., Yongchareon, W. and Vitidsant, T. (2006) 'Conversion of used vegetable oils to liquid fuels and chemicals over HZSM-5, sulphated zirconia and hybrid catalysts', *Korean Journal of Chemical Engineering,* 23, (3), pp. 349-355.

Chen, F. R., Coudurier, G., Joly, J. F. and Vedrine, J. C. (1993) 'Superacid and Catalytic Properties of Sulphated Zirconia', *Journal of Catalysis,* 143, (2), pp. 616-626.

Chen, X. R., Ju, Y. H. and Mou, C. Y. (2007) 'Direct synthesis of mesoporous sulphated silica-zirconia catalysts with high catalytic activity for biodiesel via esterification', *Journal of Physical Chemistry C,* 111, (50), pp. 18731-18737.

Chew, T. L. and Bhatia, S. (2008) 'Catalytic processes towards the production of biofuels in a palm oil and oil palm biomass-based biorefinery', *Bioresource Technology,* 99, (17), pp. 7911-7922.

Clearfield, A., Serrette, G. P. D. and Khazi-Syed, A. H. (1994) 'Nature of hydrous zirconia and sulphated hydrous zirconia', *Catalysis Today,* 20, (2), pp. 295-312.

Corma, A. (1995) 'Inorganic Solid Acids and Their Use in Acid-Catalyzed Hydrocarbon Reactions', *Chemical Reviews,* 95, (3), pp. 559-614.

Corma, A. (1997) 'Solid acid catalysts', *Current Opinion in Solid State and Materials Science,* 2, (1), pp. 63-75.

Corma, A. and Garcia, H. (1997) 'Organic reactions catalyzed over solid acids', *Catalysis Today,* 38, (3), pp. 257-308.

Corma, A. and Garcia, H. (2003) 'Lewis Acids: From Conventional Homogeneous to Green Homogeneous and Heterogeneous Catalysis', *Chemical Reviews,* 103, (11), pp. 4307-4366.

Czernik, S. and Bridgwater, A. V. (2004) 'Overview of Applications of Biomass Fast Pyrolysis Oil', *Energy & Fuels,* 18, (2), pp. 590-598.

Dandik, L. and Aksoy, H. A. (1998) 'Pyrolysis of used sunflower oil in the presence of sodium carbonate by using fractionating pyrolysis reactor', *Fuel Processing Technology,* 57, (2), pp. 81-92.

Davis, B. H., Keogh, R. A. and Srinivasan, R. (1994) 'Sulphated zirconia as a hydrocarbon conversion catalyst', *Catalysis Today,* 20, (2), pp. 219-256.

De Hoffmann, E. and Stroobant, V. (2007) *Mass Spectroscopy: Principles and Applications* John Wiley & Sons Ltd.

Demirbas, A. (2003) 'Biodiesel fuels from vegetable oils via catalytic and non-catalytic supercritical alcohol transesterifications and other methods: A survey', *Energy Conversion and Management,* 44, (13), pp. 2093-2109.

Demirbas, A. (2005) 'Biodiesel production from vegetable oils via catalytic and non-catalytic supercritical methanol transesterification methods', *Progress in Energy and Combustion Science,* 31, (5-6), pp. 466-487.

Demirbas, A. (2006) 'Biodiesel production via non-catalytic SCF method and biodiesel fuel characteristics', *Energy Conversion and Management,* 47, (15-16), pp. 2271-2282.

Demirbas, A. (2007) 'Progress and recent trends in biofuels', *Progress in Energy and Combustion Science,* 33, (1), pp. 1-18.

Demirbas, A. (2008) 'Relationships derived from physical properties of vegetable oil and biodiesel fuels', *Fuel,* 87, (8-9), pp. 1743-1748.

Demirbas, A. (2009a) 'Progress and recent trends in biodiesel fuels', *Energy Conversion and Management,* 50, (1), pp. 14-34.

Demirbas, A. (2009b) 'Biodiesel from waste cooking oil via base-catalytic and supercritical methanol transesterification', *Energy Conversion and Management,* In Press, Corrected Proof.

Demirbas, M. F. and Balat, M. (2006) 'Recent advances on the production and utilization trends of bio-fuels: A global perspective', *Energy Conversion and Management,* 47, (15-16), pp. 2371-2381.

Dias, A., Lima, S., Pillinger, M. and Valente, A. (2007) 'Modified versions of sulphated zirconia as catalysts for the conversion of xylose to furfural', *Catalysis Letters,* 114, (3), pp. 151-160.

Dupain, X., Costa, D. J., Schaverien, C. J., Makkee, M. and Moulijn, J. A. (2007) 'Cracking of a rapeseed vegetable oil under realistic FCC conditions', *Applied Catalysis B: Environmental,* 72, (1-2), pp. 44-61.

Dupont, J., Suarez, P. A. Z., Meneghetti, M. R. and Meneghetti, S. M. P. (2009) 'Catalytic production of biodiesel and diesel-like hydrocarbons from triglycerides', *Energy & Environmental Science,* 2, (12), pp. 1258-1265.

Dutta, A. (2007) *BIO-energy, MDG's and Global Sustainabilty*. Available at: http://www.soi.wide.ad.jp/class/20070041/slides/07/index_13.html (Accessed: 27/05/09).

Farcas¸iu, D., Li, J. Q. and Cameron, S. (1997) 'Preparation of sulphated zirconia catalysts with improved control of sulfur content II. Effect of sulfur content on physical properties and catalytic activity', *Applied Catalysis A: General,* 154, (1-2), pp. 173-184.

Fukuda, H., Kondo, A. and Noda, H. (2001) 'Biodiesel fuel production by transesterification of oils', *Journal of Bioscience and Bioengineering,* 92, (5), pp. 405-416.

Garcia, C. M., Teixeira, S., Marciniuk, L. L. and Schuchardt, U. (2008) 'Transesterification of soybean oil catalyzed by sulphated zirconia', *Bioresource Technology,* 99, (14), pp. 6608-6613.

Gerpen, V. J., Shanks, B., Pruszko, R., Clements, D. and Knothe, G. (2004) *Biodiesel Production Technology*. Available at: http://www.nrel.gov/docs/fy04osti/36244.pdf (Accessed: 04/05/2011).

Goyal, H. B., Seal, D. and Saxena, R. C. (2008) 'Bio-fuels from thermochemical conversion of renewable resources: A review', *Renewable and Sustainable Energy Reviews,* 12, (2), pp. 504-517.

Gusmao, J., Brodzki, D., Djega-Mariadassou, G. and Frety, R. (1989) 'Utilization of vegetable oils as an alternative source for diesel-type fuel: hydrocracking on reduced Ni/SiO2 and sulphided Ni-Mo/γ-Al2O3', *Catalysis Today,* 5, (4), pp. 533-544.

Hino, M., Kobayashi, S. and Arata, K. (1979) 'Reactions of butane and isobutane catalyzed by zirconium oxide treated with sulfate ion. Solid superacid catalyst [7]', *Journal of the American Chemical Society,* 101, (21), pp. 6439-6441.

Hino, M., Kurashige, M., Matsuhashi, H. and Arata, K. (2006) 'The surface structure of sulphated zirconia: Studies of XPS and thermal analysis', *Thermochimica Acta,* 441, (1), pp. 35-41.

Huber, G. W. and Corma, A. (2007) 'Synergies between bio- and oil refineries for the production of fuels from biomass', *Angewandte Chemie - International Edition,* 46, (38), pp. 7184-7201.

Huber, G. W., Iborra, S. and Corma, A. (2006) 'Synthesis of Transportation Fuels from Biomass: Chemistry, Catalysts, and Engineering', *Chemical Reviews,* 106, (9), pp. 4044-4098.

Idem, R. O., Katikaneni, S. P. R. and Bakhshi, N. N. (1996) 'Thermal cracking of canola oil: Reaction products in the presence and absence of steam', *Energy and Fuels,* 10, (6), pp. 1150-1162.

Idem, R. O., Katikaneni, S. P. R. and Bakhshi, N. N. (1997) 'Catalytic conversion of canola oil to fuels and chemicals: Roles of catalyst acidity, basicity and shape selectivity on product distribution', *Fuel Processing Technology,* 51, (1-2), pp. 101-125.

IEA. (2007) *IEA World Energy Outlook 2007.* Paris: International Energy Agency

Katada, N., Endo, J. I., Notsu, K. I., Yasunobu, N., Naito, N. and Niwa, M. (2000) 'Superacidity and catalytic activity of sulphated zirconia', *Journal of Physical Chemistry B,* 104, (44), pp. 10321-10328.

Katada, N., Igi, H. and Kim, J.-H. (1997) 'Determination of the Acidic Properties of Zeolite by Theoretical Analysis of Temperature-Programmed Desorption of Ammonia Based on Adsorption Equilibrium', *The Journal of Physical Chemistry B,* 101, (31), pp. 5969-5977.

Katikaneni, S. P. R., Adjaye, J. D. and Bakhshi, N. N. (1995a) 'Catalytic conversion of canola oil to fuels and chemicals over various cracking catalysts', *Canadian Journal of Chemical Engineering,* 73, (4), pp. 484-497.

Katikaneni, S. P. R., Adjaye, J. D. and Bakhshi, N. N. (1995b) 'Studies on the catalytic conversion of canola oil to hydrocarbons: Influence of hybrid catalysts and steam', *Energy & Fuels,* 9, (4), pp. 599-609.

Katikaneni, S. P. R., Adjaye, J. D., Idem, R. O. and Bakhshi, N. N. (1996) 'Catalytic conversion of canola oil over potassium-impregnated HZSM-5 catalysts: C2-C4 olefin production and model reaction studies', *Industrial and Engineering Chemistry Research,* 35, (10), pp. 3332-3346.

Kirszensztejn, P., Przekop, R., Tolia,,ska, A. and MaaKowska, E. (2009) 'Pyrolytic and catalytic conversion of rape oil into aromatic and aliphatic fractions in a fixed bed reactor on Al2O3 and Al 2O3/B2O3 catalysts', *Chemical Papers,* 63, (2), pp. 226-232.

Kiss, A. A., Dimian, A. C. and Rothenberg, G. (2008) 'Biodiesel by catalytic reactive distillation powered by metal oxides', *Energy and Fuels*, 22, (1), pp. 598-604.

Konwer, D., Taylor, S., Gordon, B., Otvos, J. and Calvin, M. (1989) 'Liquid fuels fromMesua ferrea L. seed oil', *Journal of the American Oil Chemists' Society*, 66, (2), pp. 223-226.

Kubicka, D. and Kaluza, L. (2010) 'Deoxygenation of vegetable oils over sulfided Ni, Mo and NiMo catalysts', *Applied Catalysis A: General*, 372, (2), pp. 199-208.

Kubickova, I., Snare, M., Eränen, K., Maki-Arvela, P. and Murzin, D. Y. (2005) 'Hydrocarbons for diesel fuel via decarboxylation of vegetable oils', *Catalysis Today*, 106, (1-4), pp. 197-200.

Leng, T. Y., Mohamed, A. R. and Bhatia, S. (1999) 'Catalytic conversion of palm oil to fuels and chemicals', *Canadian Journal of Chemical Engineering*, 77, (1), pp. 156-162.

Li, M., Feng, Z., Xiong, G., Ying, P., Xin, Q. and Li, C. (2001) 'Phase Transformation in the Surface Region of Zirconia Detected by UV
Raman Spectroscopy', *Journal of Physical Chemistry B*, 105, pp. 8107-8111.

Li, Y., Zhang, X.-D., Sun, L., Zhang, J. and Xu, H.-P. (2010) 'Fatty acid methyl ester synthesis catalyzed by solid superacid catalyst /ZrO2-TiO2/La3+', *Applied Energy*, 87, (1), pp. 156-159.

Lotero, E., Liu, Y., Lopez, D. E., Suwannakarn, K., Bruce, D. A. and Goodwin, J. G. (2005) 'Synthesis of Biodiesel via Acid Catalysis', *Industrial & Engineering Chemistry Research*, 44, (14), pp. 5353-5363.

Lunsford, J. H., Sang, H., Campbell, S. M., Liang, C. H. and Anthony, R. G. (1994) 'An NMR study of acid sites on sulphated-zirconia catalysts using trimethylphosphine as a probe', *Catalysis Letters*, 27, (3), pp. 305-314.

Luque, R., Pinzi, S., Campelo, J. M., Ruiz, J. J., Lopez, I., Luna, D., Marinas, J. M., Romero, A. A., Dorado, M. P. and Shah, V. (2010) 'Prospects and Challenges Emerging Environmental Technologies, Volume II', in *Biofuels for Transport*. Springer Netherlands, pp. 171-210.

Ma, F. and Hanna, M. A. (1999) 'Biodiesel production: A review', *Bioresource Technology*, 70, (1), pp. 1-15.

Maher, K. D. and Bressler, D. C. (2007) 'Pyrolysis of triglyceride materials for the production of renewable fuels and chemicals', *Bioresource Technology*, 98, (12), pp. 2351-2368.

Maki-Arvela, P., Kubickova, I., Snare, M., Eranen, K. and Murzin, D. Y. (2007) 'Catalytic Deoxygenation of Fatty Acids and Their Derivatives', *Energy & Fuels*, 21, (1), pp. 30-41.

Marchetti, J. M., Miguel, V. U. and Errazu, A. F. (2007) 'Possible methods for biodiesel production', *Renewable and Sustainable Energy Reviews*, 11, (6), pp. 1300-1311.

Marcus, R., Diebold, U. and Gonzalez, R. D. (2003) 'The Locus of Sulfate Sites on Sulphated Zirconia', *Catalysis Letters*, 86, (4), pp. 151-156.

McIntosh, D. J. and Kydd, R. A. (2000) 'Tailoring the pore size of mesoporous sulphated zirconia', *Microporous and Mesoporous Materials*, 37, (3), pp. 281-289.

Meher, L. C., Vidya Sagar, D. and Naik, S. N. (2006) 'Technical aspects of biodiesel production by transesterification - A review', *Renewable and Sustainable Energy Reviews*, 10, (3), pp. 248-268.

Melada, S., Ardizzone, S. A. and Bianchi, C. L. (2004) 'Sulphated zirconia by sol-gel route. The effects of the preparative variables', *Microporous and Mesoporous Materials*, 73, (3), pp. 203-209.

Melero, J. A., Clavero, M. M., Calleja, G., GarciÌ • a, A., Miravalles, R. n. and Galindo, T. (2009) 'Production of Biofuels via the Catalytic Cracking of Mixtures of Crude Vegetable Oils and Nonedible Animal Fats with Vacuum Gas Oil', *Energy & Fuels*, 24, (1), pp. 707-717.

Meng, X., Xu, C., Gao, J. and Li, L. (2005) 'Studies on catalytic pyrolysis of heavy oils: Reaction behaviors and mechanistic pathways', *Applied Catalysis A: General*, 294, (2), pp. 168-176.

Miller, D. J. and Jackson, J. E. (2004) *Catalysis for Biorenewables Conversion*. Available at: www.egr.msu.edu/apps/nsfworkshop (Accessed: 09/02/2011).

Mittelbach, M. and Remschmidt, C. (2006) *Biodiesel, the Comprehensive Handbook.* Martin Mittelbach.

Morterra, C., Cerrato, G. and Bolis, V. (1993a) 'Lewis and Brønsted acidity at the surface of sulfate-doped ZrO2 catalysts', *Catalysis Today*, 17, (3), pp. 505-515.

Morterra, C., Cerrato, G., Emanuel, C. and Bolis, V. (1993b) 'On the Surface Acidity of Some Sulfate-Doped ZrO2 Catalysts', *Journal of Catalysis*, 142, (2), pp. 349-367.

Moulder, J. F., Chastain, J., Stickle, W. F., Sobol, P. E. and Bomben, K. D. (1995) *Handbook of x-ray photoelectron spectroscopy: a reference book of standard spectra for identification and interpretation of XPS data.* Physical Electronics.

Nascimento, P., Akratopoulou, C., Oszagyan, M., Coudurier, G., Travers, C., Joly, J. F., Vedrine, J. C., L. Guczi, F. S. and P, T. (1993) 'ZrO2-SO42-Catalysts. Nature and Stability of Acid Sites Responsible for n-Butane Isomerization', in *Studies in Surface Science and Catalysis.* Vol. Volume 75 Elsevier, pp. 1185-1197.

Nijhuis, T. A., Beers, A. E. W., Kapteijn, F. and Moulijn, J. A. (2002) 'Water removal by reactive stripping for a solid-acid catalyzed esterification in a monolithic reactor', *Chemical Engineering Science*, 57, (9), pp. 1627-1632.

Olszak-Humienik, M. (2001) 'On the thermal stability of some ammonium salts', *Thermochimica Acta*, 378, pp. 107-112.

Ooi, Y. S., Zakaria, R., Mohamed, A. R. and Bhatia, S. (2004) 'Catalytic conversion of palm oil-based fatty acid mixture to liquid fuel', *Biomass and Bioenergy*, 27, (5), pp. 477-484.

Ooi, Y. S., Zakaria, R., Mohamed, A. R. and Bhatia, S. (2005) 'Catalytic conversion of fatty acids mixture to liquid fuel and chemicals over composite microporous/mesoporous catalysts', *Energy and Fuels*, 19, (3), pp. 736-743.

Osmont, A., Catoire, L., Gokalp, I. and Swihart, M. T. (2007) 'Thermochemistry of C-C and C-H Bond Breaking in Fatty Acid Methyl Esters', *Energy & Fuels*, 21, (4), pp. 2027-2032.

Parvulescu, V., Coman, S., Grange, P. and Parvulescu, V. I. (1999) 'Preparation and characterization of sulphated zirconia catalysts obtained via various procedures', *Applied Catalysis A: General*, 176, (1), pp. 27-43.

Permsubscul, A., Vitidsant, T. and Damronglerd, S. (2007) 'Catalytic cracking reaction of used lubricating oil to liquid fuels catalyzed by sulphated zirconia', *Korean Journal of Chemical Engineering*, 24, (1), pp. 37-43.

Pickett, J. (2008) 'Sustainable biofuels: prospects and challenges', in *Policy document 01/08.* The Royal Society, pp. 3-90.

Poynter, W. G. and Barrlos, R. J. (1994) 'Coulometric Karl Fischer titration simplifies water content testing', *Oil and Gas Journal*, 92, (15), pp. 53-56.

Prichard, E. and Stuart, B. (2003) *Gas Chromatography.* Royal Society of Chemistry.

Puppan, D. (2002) 'Environmental Evaluation of Biofuel', *Periodica Polytechnica* 10, pp. 95–116.

Rattanaphra, D., Harvey, A. and Srinophakun, P. (2010) 'Simultaneous Conversion of Triglyceride/Free Fatty Acid Mixtures into Biodiesel Using Sulphated Zirconia', *Topics in Catalysis*, 53, (11), pp. 773-782.

Rbitz, W. K. (2001) *New Trends in Developing Biodiesel World-wide*. Available at: http://www3.sympatico.ca/ufp/BiodieselWorldwide.pdf (Accessed: 12/06/2010).

Reddy, B. M., Sreekanth, P. M. and Lakshmanan, P. (2005) 'Sulphated zirconia as an efficient catalyst for organic synthesis and transformation reactions', *Journal of Molecular Catalysis A: Chemical*, 237, (1-2), pp. 93-100.

Great Britain. Parliament. (2007) *Mitigation. Contribution of Working Group III to the Fourth Assessment Report of the Intergovernmental Panel on ClimateChange* Cambridge University Press, Cambridge, United Kingdom and New York, NY, USA.
.

Rosenberg, D. J. and Anderson, J. A. (2002) 'On determination of acid site densities on sulphated oxides', *Catalysis Letters*, 83, (1-2), pp. 59-63.

Rosenberg, D. J., Bachiller-Baeza, B. n., Dines, T. J. and Anderson, J. A. (2003) 'Nature of Surface Sulfate Species and the Generation of Active Sites on Silicaâˆ’Zirconia Mixed-Oxide Catalysts', *The Journal of Physical Chemistry B*, 107, (27), pp. 6526-6534.

Schomburg, G., Husmann, H. and Rittmann, R. (1981) '(on-column) sampling into glass capillary columns : Comparative investigations on split, splitless and on-column sampling', *Journal of Chromatography A*, 204, (0), pp. 85-96.

Schuchardt, U., Sercheli, R. and Vargas, R. M. (1998) 'Transesterification of vegetable oils: A review', *Journal of the Brazilian Chemical Society*, 9, (3), pp. 199-210.

Sharma, Y. C., Singh, B. and Upadhyay, S. N. (2008) 'Advancements in development and characterization of biodiesel: A review', *Fuel*, 87, (12), pp. 2355-2373.

Smith, B., Greenwell, H. C. and Whiting, A. (2009) 'Catalytic upgrading of tri-glycerides and fatty acids to transport biofuels', *Energy & Environmental Science*, pp. -.

Song, X. and Sayari, A. (1996) 'Sulphated zirconia-based strong solid-acid catalysts: Recent progress', *Catalysis Reviews - Science and Engineering*, 38, (3), pp. 329-412.

Srinivasan, R., Keogh, R. A., Milburn, D. R. and Davis, B. H. (1995) 'Sulphated Zirconia Catalysts: Characterization by TGA/DTA Mass Spectrometry', *Journal of Catalysis*, 153, (1), pp. 123-130.

Srivastava, A. and Prasad, R. (2000) 'Triglycerides-based diesel fuels', *Renewable and Sustainable Energy Reviews*, 4, (2), pp. 111-133.

Stokes, D. J. (2008) *Principles and Practice of Variable Pressure/Environmental Scanning Electron* John Wiley & Sons Ltd.

Suarez, P. A. Z. (2006) *Alternative fuels from the thermo- catalytic cracking of triglycerides*. Available at: www.nist.gov/oiaa/Suarez.pdf (Accessed: 01/05/09).

Sun, Y., Ma, S., Du, Y., Yuan, L., Wang, S., Yang, J., Deng, F. and Xiao, F. S. (2005) 'Solvent-free preparation of nanosized sulphated zirconia with brønsted acidic sites from a simple calcination', *Journal of Physical Chemistry B*, 109, (7), pp. 2567-2572.

Sun, Y., Yuan, L., Ma, S., Han, Y., Zhao, L., Wang, W., Chen, C. L. and Xiao, F. S. (2004) 'Improved catalytic activity and stability of mesostructured sulphated zirconia by Al promoter', *Applied Catalysis A: General*, 268, (1-2), pp. 17-24.

Tamunaidu, P. and Bhatia, S. (2007) 'Catalytic cracking of palm oil for the production of biofuels: Optimization studies', *Bioresource Technology*, 98, (18), pp. 3593-3601.

Tanabe, K. and Yamaguchi, T. (1994) 'Acid-base bifunctional catalysis by ZrO2 and its mixed oxides', *Catalysis Today*, 20, (2), pp. 185-197.

Taufiqurrahmi, N. and Bhatia, S. (2011) 'Catalytic cracking of edible and non-edible oils for the production of biofuels', *Energy & Environmental Science*, 4, (4), pp. 1087-1112.

Thomas, J. M. and Thomas, W. J. (2005) *Principles and Practice of Heterogeneous Catalysis*.Third Reprint ed Weinheim (Germany): VCH Publishers Inc., New York, NY (USA).

Tian, H., Li, C., Yang, C. and Shan, H. (2008a) 'Alternative Processing Technology for Converting Vegetable Oils and Animal Fats to Clean Fuels and Light Olefins', *Chinese Journal of Chemical Engineering*, 16, (3), pp. 394-400.

Tian, H., Li, C., Yang, C. and Shan, H. (2008b) 'Alternative Processing Technology for Converting Vegetable Oils and Animal Fats to Clean Fuels and Light Olefins* * Supported by the Major Research Plan of PetroChina Company Limited (07-03D-01-01-02-02)', *Chinese Journal of Chemical Engineering*, 16, (3), pp. 394-400.

Twaiq, F. A., Zabidi, N. A. M. and Bhatia, S. (1999) 'Catalytic conversion of palm oil to hydrocarbons: Performance of various zeolite catalysts', *Industrial and Engineering Chemistry Research*, 38, (9), pp. 3230-3237.

Twaiq, F. A. A., Mohamad, A. R. and Bhatia, S. (2004) 'Performance of composite catalysts in palm oil cracking for the production of liquid fuels and chemicals', *Fuel Processing Technology*, 85, (11), pp. 1283-1300.

USDA (2011) *Foreign Agricultural Service: production, supply and distribution.* Available at: http://www.fas.usda.gov/psdonline/psdQuery.aspx (Accessed: 10/02/12).

Vasudevan, P. T. and Briggs, M. (2008) 'Biodiesel production - Current state of the art and challenges', *Journal of Industrial Microbiology and Biotechnology*, 35, (5), pp. 421-430.

Vonghia, E., Boocock, D. G. B., Konar, S. K. and Leung, A. (1995a) 'Pathways for the deoxygenation of triglycerides to aliphatic hydrocarbons over activated alumina', *Energy & Fuels*, 9, (6), pp. 1090-1096.

Vonghia, E., Boocock, D. G. B., Konar, S. K. and Leung, A. (1995b) 'Pathways for the Deoxygenation of Triglycerides to Aliphatic Hydrocarbons over Activated Alumina', *Energy & Fuels*, 9, pp. 1090-1096.

Wagner, C. D., Naumkin, A. V., Kraut-Vass, A., Allison, J. W., Powell, C. J. and Rumble, J. R. (2000) *NIST X-ray Photoelectron Spectroscopy Database* Available at: http://srdata.nist.gov/xps/Default.aspx (Accessed: 02/02/11).

Waqif, M., Bachelier, J., Saur, O. and Lavalley, J.-C. (1992) 'Acidic properties and stability of sulfate-promoted metal oxides', *Journal of Molecular Catalysis*, 72, (1), pp. 127-138.

Ward, D. A. and Ko, E. I. (1994) 'One-Step Synthesis and Characterization of Zirconia-Sulfate Aerogels as Solid Superacids', *Journal of Catalysis*, 150, (1), pp. 18-33.

Weisz, P. B., Haag, W. O. and Rodewald, P. G. (1979) 'Catalytic Production of High-Grade Fuel (Gasoline) from Biomass Compounds by Shape-Selective Catalysis', *Science*, 206, (4414), pp. 57-58.

Yadav, G. and Nair, J. (1999a) 'Selectivity engineering in the nitration of chlorobenzene using eclectically engineered sulphated zirconia and carbon molecular sieve catalysts', *Catalysis Letters*, 62, (1), pp. 49-52.

Yadav, G. D. and Murkute, A. D. (2004) 'Preparation of a novel catalyst UDCaT-5: Enhancement in activity of acid-treated zirconia - Effect of treatment with chlorosulfonic acid vis-Ã -vis sulfuric acid', *Journal of Catalysis*, 224, (1), pp. 218-223.

Yadav, G. D. and Nair, J. J. (1999b) 'Sulphated zirconia and its modified versions as promising catalysts for industrial processes', *Microporous and Mesoporous Materials*, 33, (1-3), pp. 1-48.

Yamaguchi, T. (1990) 'Recent progress in solid superacid', *Applied Catalysis*, 61, (1), pp. 1-25.

Yamaguchi, T., Jin, T., Ishida, T. and Tanabe, K. (1987) 'Structural identification of acid sites of sulfur-promoted solid super acid and construction of its structure on silica support', *Materials Chemistry and Physics*, 17, (1-2), pp. 3-19.

Yamaguchi, T., Jin, T. and Tanabe, K. (1986) 'Structure of acid sites on sulfur-promoted iron oxide', *The Journal of Physical Chemistry*, 90, (14), pp. 3148-3152.

Yi, N., Cao, Y., Feng, W.-L., Dai, W.-L. and Fan, K.-N. (2005) 'Synthesis and characterization of thermally stable mesostructured sulphated zirconia by a novel sulfate-assisted alcohothermal route', *Catalysis Letters*, 99, (1), pp. 73-78.

Yilmaz, V. T., Cbudak, H. and Olmez, H. (1994) 'Thermal behaviour and kinetic analysis of the thermogravimetric data of double ammonium sulphate hexahydrate salts of Mn(II), Fe(II), Co(II), Ni(II) and Cu(II)', *Thermochimica Acta*, 244, pp. 85-92.

Zabeti, M., Wan Daud, W. M. A. and Aroua, M. K. (2009) 'Activity of solid catalysts for biodiesel production: A review', *Fuel Processing Technology*, 90, (6), pp. 770-777.

Zaher, F. A. and Taman, A. R. (1993) 'Thermally decomposed cottonseed oil as a diesel engine fuel', *Energy Sources*, 15, (3), pp. 499-504.

Zalewski, D. J., Alerasool, S. and Doolin, P. K. (1999) 'Characterization of catalytically active sulphated zirconia', *Catalysis Today*, 53, (3), pp. 419-432.

Zhao, E., Isaev, Y., Sklyarov, A. and Fripiat, J. J. (1999) 'Acid centers in sulphated, phosphated and/or aluminated zirconias', *Catalysis Letters*, 60, (4), pp. 173-181.

Zhou, Z., Zhang, Y., Tierney, J. W. and Wender, I. (2003) 'Hybrid zirconia catalysts for conversion of Fischer-Tropsch waxy products to transportation fuels', *Fuel Processing Technology*, 83, (1-3 SPEC.), pp. 67-80.

Zhu, G., Wang, C., Zhang, Y., Guo, N., Zhao, Y., Wang, R., Qiu, S., Wei, Y. and Baughman, R. H. (2004) 'Highly effective sulphated zirconia nanocatalysts grown out of colloidal silica at high temperature', *Chemistry - A European Journal*, 10, (19), pp. 4750-4754.

Zinoviev, S., Arumugam, S. and Miertus, S. (2007) *Biofuel Production Technologies*. Available at: http://www.fao.org/uploads/media/0706_ICS_UNIDO_-_Bio-fuels.pdf (Accessed: 11/08/11).

Appendices

Name and formula

Reference code: 01-080-0965

ICSD name: Zirconium Oxide

Empirical formula: O_2Zr
Chemical formula: ZrO_2

Crystallographic parameters

Crystal system: Tetragonal
Space group: P42/nmc
Space group number: 137

a (Å): 3.5925
b (Å): 3.5925
c (Å): 5.1837
Alpha (°): 90.0000
Beta (°): 90.0000
Gamma (°): 90.0000

Calculated density (g/cm^3): 6.12
Volume of cell (10^6 pm^3): 66.90
Z: 2.00

RIR: 10.18

Subfiles and Quality

Subfiles: Inorganic
Alloy, metal or intermetalic
Corrosion
Modelled additional pattern
Quality: Calculated (C)

Comments

ICSD collection code: 068781

References

Primary reference: *Calculated from ICSD using POWD-12++*, (1997)
Structure: Howard, C.J., Kisi, E.H., Roberts, R.B., Hill, R.J., *J. Am. Ceram. Soc.* **73**, 2828, (1990)

Peak list

No.	h	k	l	d [Å]	2Theta[deg]	I [%]
1	1	0	1	2.95272	30.244	100.0
2	0	0	2	2.59185	34.579	8.1
3	1	1	0	2.54028	35.304	12.7
4	1	0	2	2.10192	42.997	1.2
5	1	1	2	1.81421	50.250	33.2
6	2	0	0	1.79625	50.788	17.4
7	2	0	1	1.69724	53.983	0.1

8	1	0	3	1.55715	59.298	11.5
9	2	1	1	1.53460	60.259	21.8
10	2	0	2	1.47636	62.900	5.3
11	2	1	2	1.36554	68.680	0.3
12	0	0	4	1.29593	72.940	1.7
13	2	2	0	1.27014	74.669	4.1
14	1	0	4	1.21904	78.379	0.2
15	2	1	3	1.17659	81.792	7.6
16	3	0	1	1.16677	82.630	3.7
17	1	1	4	1.15439	83.715	2.8
18	2	2	2	1.14055	84.967	2.1
19	3	1	0	1.13605	85.383	1.9

Stick Pattern

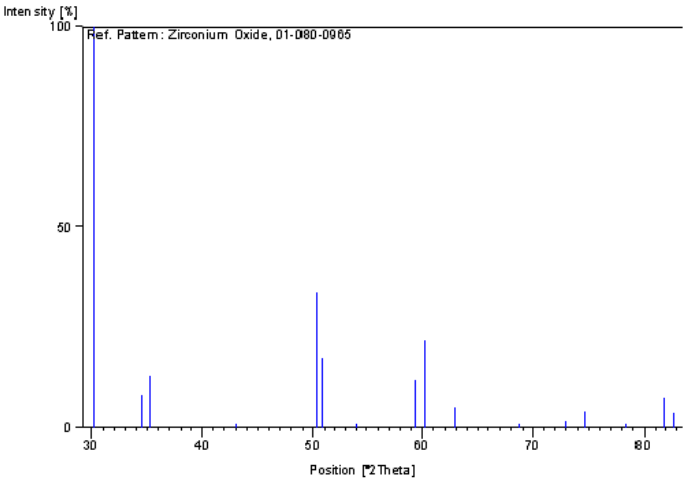

Name and formula

Reference code:	01-078-0047
ICSD name:	Zirconium Oxide
Empirical formula:	O_2Zr
Chemical formula:	ZrO_2

Crystallographic parameters

Crystal system:	Monoclinic
Space group:	P21/c
Space group number:	14
a (Å):	5.1507
b (Å):	5.2028
c (Å):	5.3156
Alpha (°):	90.0000
Beta (°):	99.1960
Gamma (°):	90.0000
Calculated density (g/cm^3):	5.82
Volume of cell (10^6 pm^3):	140.62
Z:	4.00
RIR:	3.52

Subfiles and Quality

Subfiles:	Inorganic Alloy, metal or intermetalic Corrosion Modelled additional pattern
Quality:	Calculated (C)

Comments

ICSD collection code:	060900
Test from ICSD:	No R value given.

References

Primary reference:	*Calculated from ICSD using POWD-12++*, (1997)
Structure:	Hann, R.E., Suitch, P.R., Pentecost, J.L., *J. Am. Ceram. Soc.* **68**, 285, (1985)

Peak list

No.	h	k	l	d [A]	2Theta[deg]	I [%]
1	1	0	0	5.08450	17.428	6.8
2	0	1	1	3.69456	24.068	17.6
3	1	1	0	3.63639	24.459	11.7
4	-1	1	1	3.16287	28.192	100.0
5	1	1	1	2.84069	31.467	63.0
6	0	0	2	2.62364	34.147	16.9

7	0	2	0	2.60140	34.448	10.6
8	2	0	0	2.54225	35.276	11.9
9	-1	0	2	2.50003	35.891	2.4
10	0	2	1	2.33070	38.598	3.9
11	2	1	0	2.28415	39.417	0.7
12	-1	1	2	2.25338	39.978	0.3
13	-2	1	1	2.21389	40.723	8.0
14	1	0	2	2.19308	41.127	3.4
15	-1	2	1	2.17809	41.422	2.9
16	1	2	1	2.06394	43.828	0.1
17	1	1	2	2.02089	44.812	3.8
18	2	1	1	1.99173	45.505	4.2
19	-2	1	2	1.86009	48.928	1.2
20	0	2	2	1.84728	49.290	9.1
21	2	2	0	1.81819	50.132	11.0
22	-1	2	2	1.80256	50.597	5.8
23	-2	2	1	1.78215	51.218	2.6
24	2	0	2	1.69535	54.048	5.0
25	1	2	2	1.67674	54.697	0.3
26	0	1	3	1.65791	55.371	3.8
27	-1	1	3	1.65170	55.598	3.0
28	0	3	1	1.64666	55.783	1.6
29	1	3	0	1.64141	55.977	2.9
30	3	1	0	1.61070	57.141	3.1
31	-1	3	1	1.59010	57.951	1.9
32	-2	2	2	1.58143	58.299	1.4
33	1	3	1	1.54402	59.854	3.0
34	-3	0	2	1.54023	60.016	3.7
35	1	1	3	1.51025	61.334	1.8
36	-2	1	3	1.49628	61.970	1.9
37	3	1	1	1.47871	62.789	2.9
38	0	2	3	1.45150	64.104	0.4
39	-1	2	3	1.44733	64.311	0.7
40	2	3	0	1.43266	65.050	0.2
41	-1	3	2	1.42497	65.445	0.6
42	2	2	2	1.42035	65.685	1.7
43	1	3	2	1.36033	68.980	0.5
44	1	2	3	1.34931	69.624	0.2
45	-2	2	3	1.33932	70.219	0.1
46	-3	2	2	1.32535	71.071	0.4
47	-1	0	4	1.32237	71.255	0.9
48	0	0	4	1.31182	71.917	0.2
49	-2	3	2	1.30793	72.164	0.3
50	2	1	3	1.30070	72.629	0.3
51	-3	1	3	1.28658	73.556	0.1
52	0	1	4	1.27113	74.601	0.3
53	0	4	1	1.26249	75.200	0.7
54	1	4	0	1.26012	75.366	0.4
55	-2	0	4	1.25001	76.083	0.1
56	-4	1	1	1.24587	76.382	0.4
57	-1	4	1	1.23645	77.070	0.1
58	4	1	0	1.23481	77.191	0.1
59	0	3	3	1.23152	77.436	0.2
60	-1	3	3	1.22897	77.627	0.1
61	1	0	4	1.22379	78.017	0.2
62	-2	1	4	1.21543	78.657	0.1
63	3	3	0	1.21213	78.913	0.3
64	2	2	3	1.19417	80.339	0.1
65	1	1	4	1.19074	80.618	0.1
66	-3	2	3	1.18266	81.284	0.1

Time: 11:59:26 Date: 25/06/2010 File: EE_CM_2_140610

67	-1	2	4	1.17881	81.605	0.2
68	0	2	4	1.17132	82.239	0.1
69	1	3	3	1.16724	82.589	0.2
70	4	1	1	1.16241	83.008	0.1
71	-2	3	3	1.16075	83.153	0.3
72	2	4	0	1.15794	83.400	0.2
73	3	3	1	1.15249	83.884	0.2
74	-2	4	1	1.14847	84.245	0.2
75	4	2	0	1.14208	84.826	0.2
76	-3	0	4	1.12832	86.109	0.1
77	-2	2	4	1.12669	86.264	0.1
78	1	4	2	1.11874	87.030	0.1
79	2	4	1	1.11381	87.512	0.2
80	1	2	4	1.10738	88.151	0.2
81	3	1	3	1.10447	88.444	0.3
82	2	0	4	1.09654	89.253	0.1
83	-4	1	3	1.09177	89.748	0.2

Stick Pattern

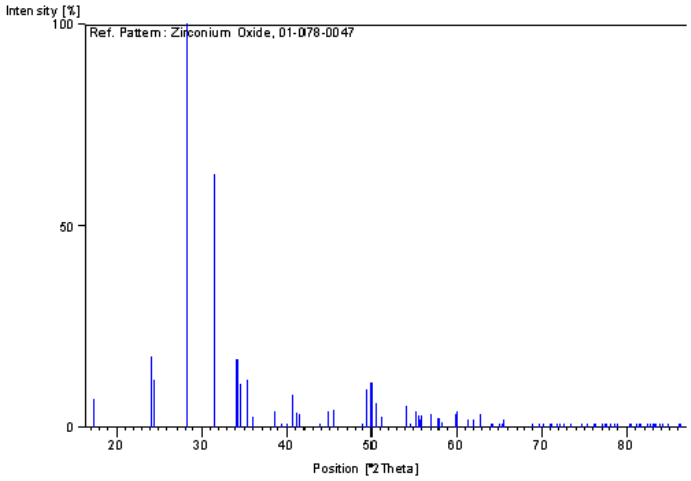

Surface Area Report

BET Surface area 65.263 sq.m/g

Slope 0.065920
Intercept 0.000770
C_value 86.648
Monolayer Volume 14.9948 cc/g (STP)
Correlation Coefficient 0.99998

One Point BET Surface Area (Ps/Po=0.3) 63.552 sq.m/g

Analysis Data

Ps/Po	BET Function	Vads cc/g(STP)
0.0536	0.004271	13.270
0.0582	0.004584	13.470
0.0632	0.004927	13.682
0.0695	0.005359	13.943
0.0796	0.006036	14.325
0.1000	0.007392	15.033
0.1196	0.008681	15.655
0.1381	0.009883	16.209
0.1582	0.011199	16.782
0.1784	0.012519	17.351
0.1984	0.013831	17.898

Interpolated Data

Ps/Po	BET Function	Vads cc/g(STP)
0.0500	0.004066	12.945
0.0800	0.006043	14.389
0.1200	0.008680	15.710
0.1600	0.011317	16.831
0.2000	0.013954	17.916

EDX Spectra of the Catalysts

SFM

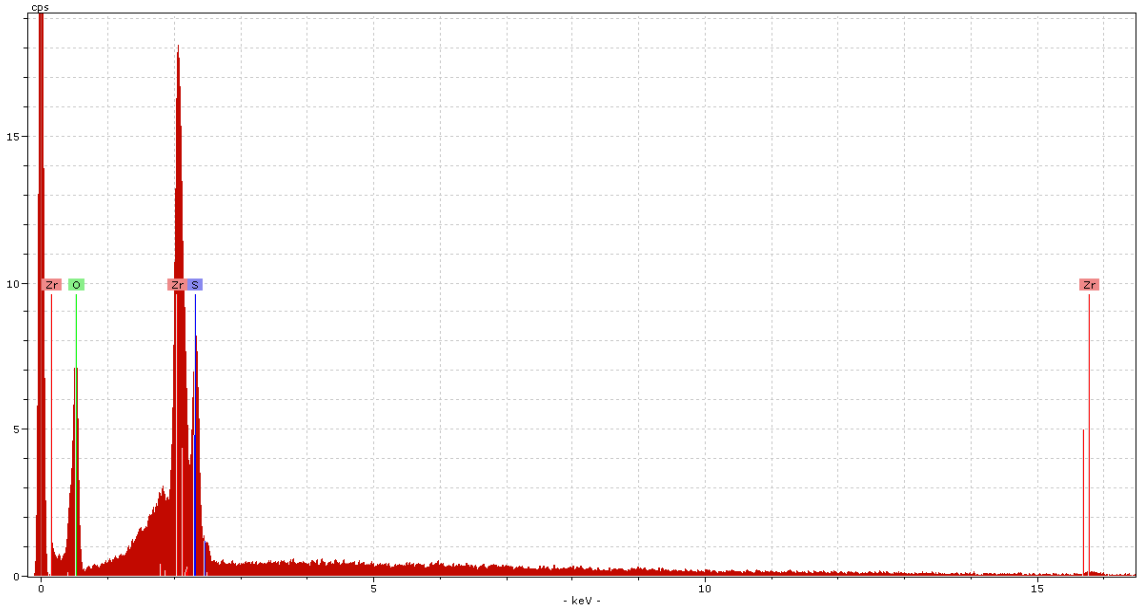

EDX Spectra of SFM Catalyst indicating the Various Elements

SFM*

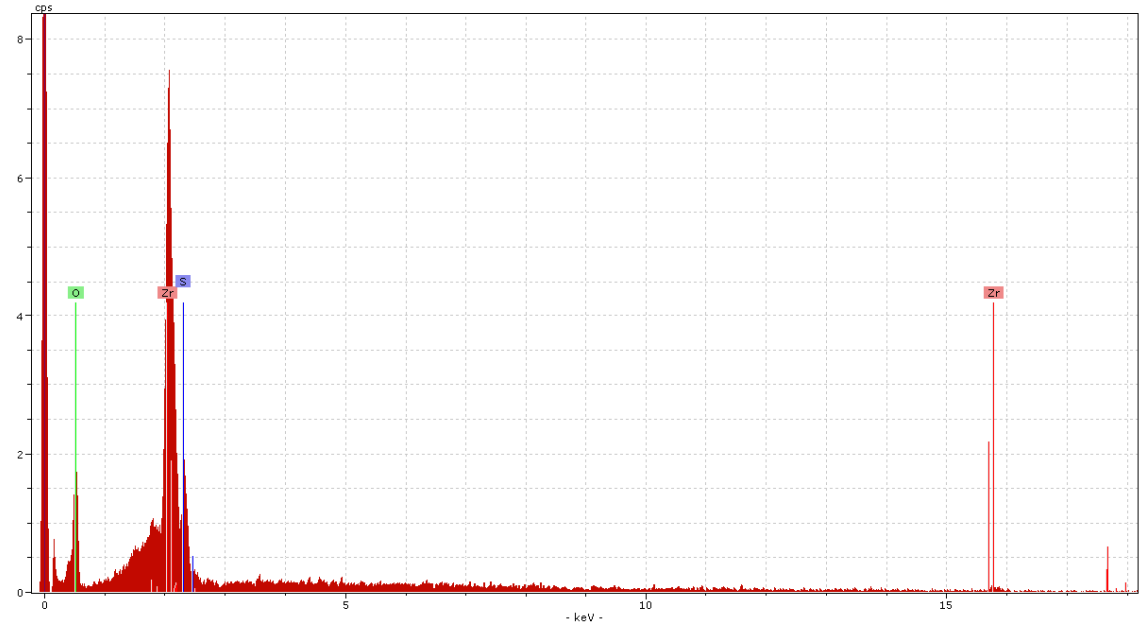

EDX Spectra of SFM Catalyst indicating the Various Elements

CM

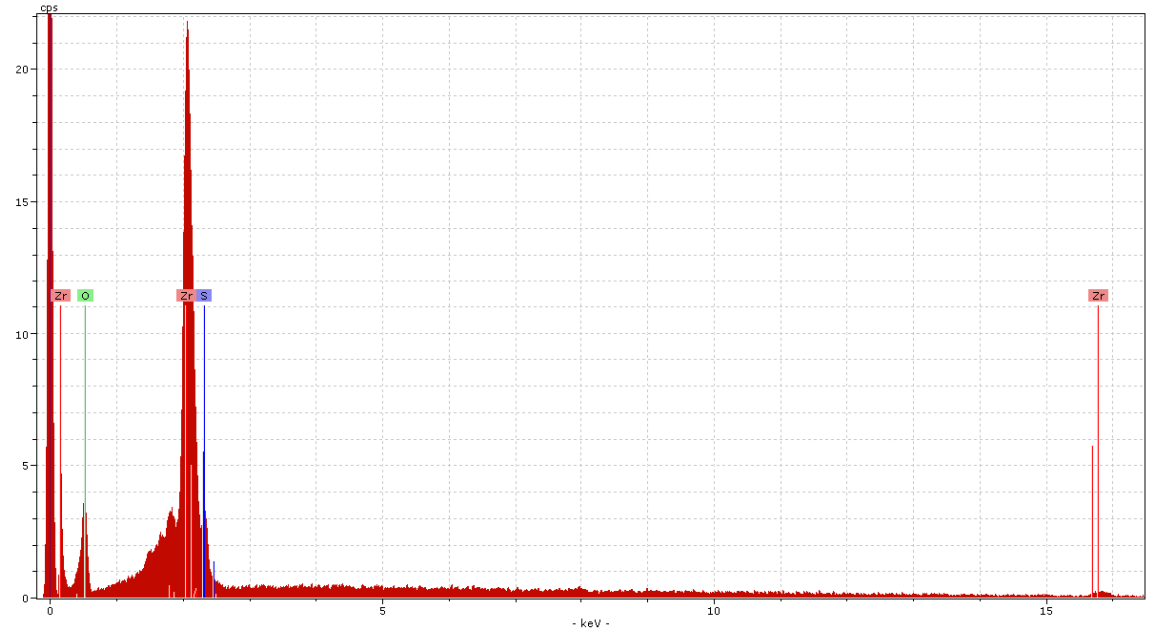

EDX Spectra of CM Catalyst indicating the Various Elements

CM*

EDX Spectra of CM* Catalyst indicating the Various Elements

EDX Spectra of Modified Catalysts

Kaolin

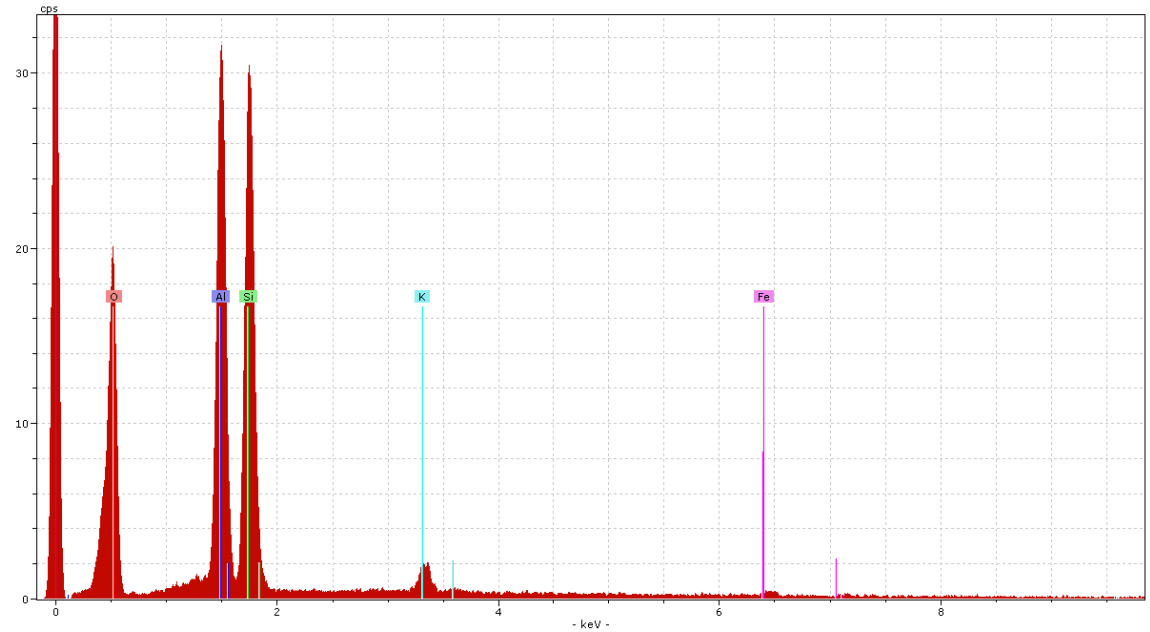

EDX Spectra of Kaolin Catalyst indicating the Various Elements

MK (Metakaolin)

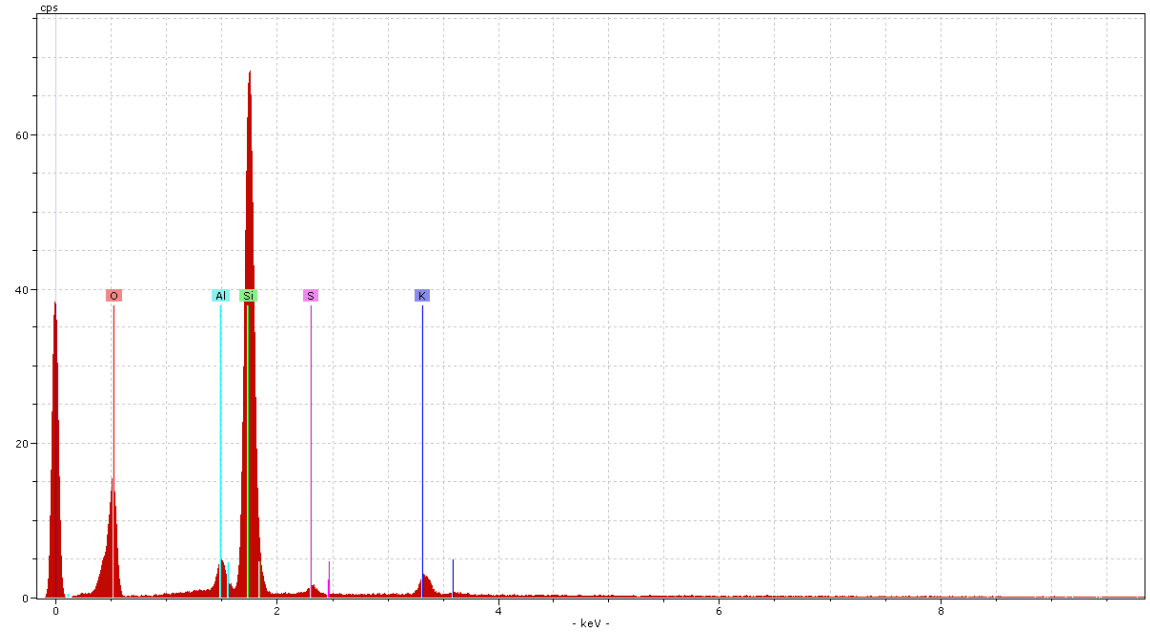

EDX Spectra of Matakaolin (MK) Catalyst indicating the Various Elements

NCM

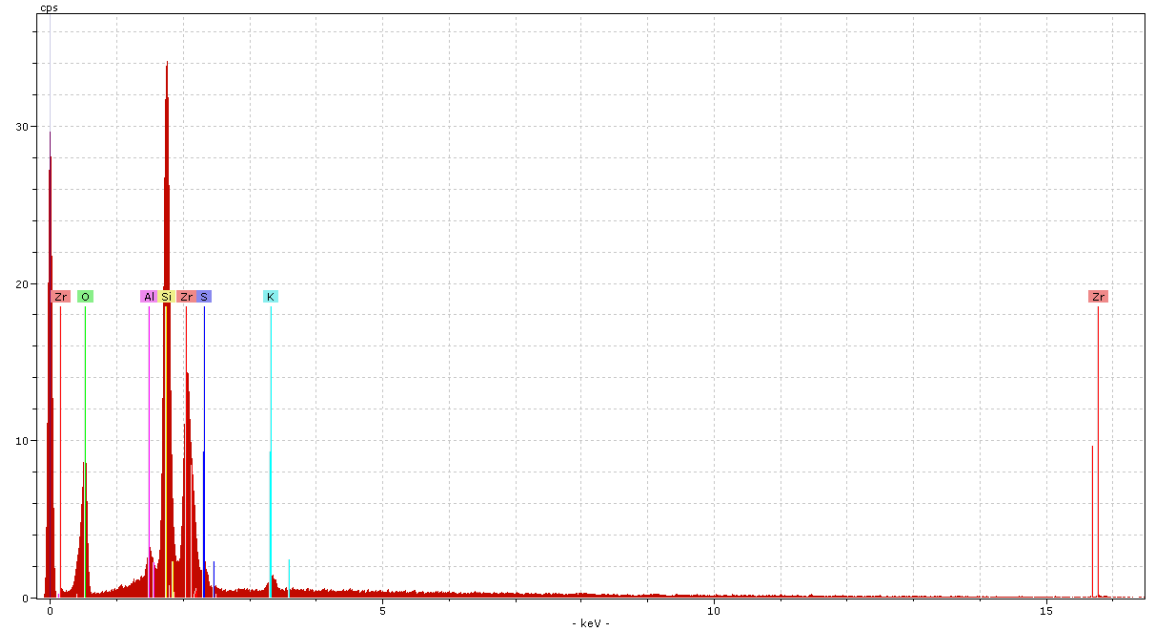

EDX Spectra of NCM Catalyst indicating the Various Elements

NSFM

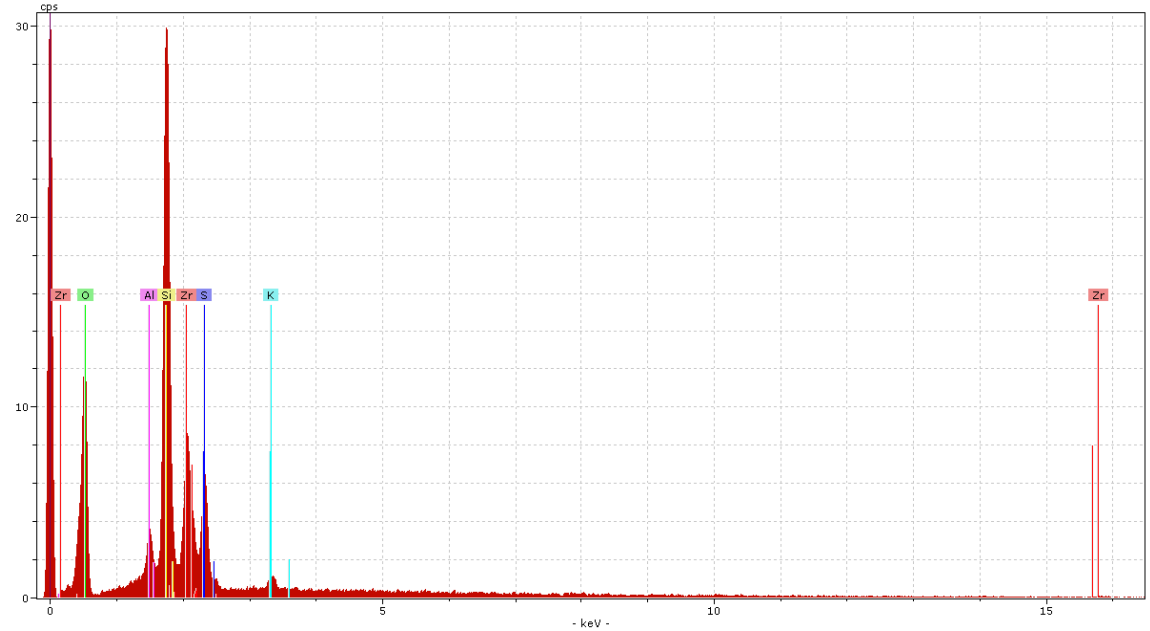

EDX Spectra of NSFM Catalyst indicating the Various Elements

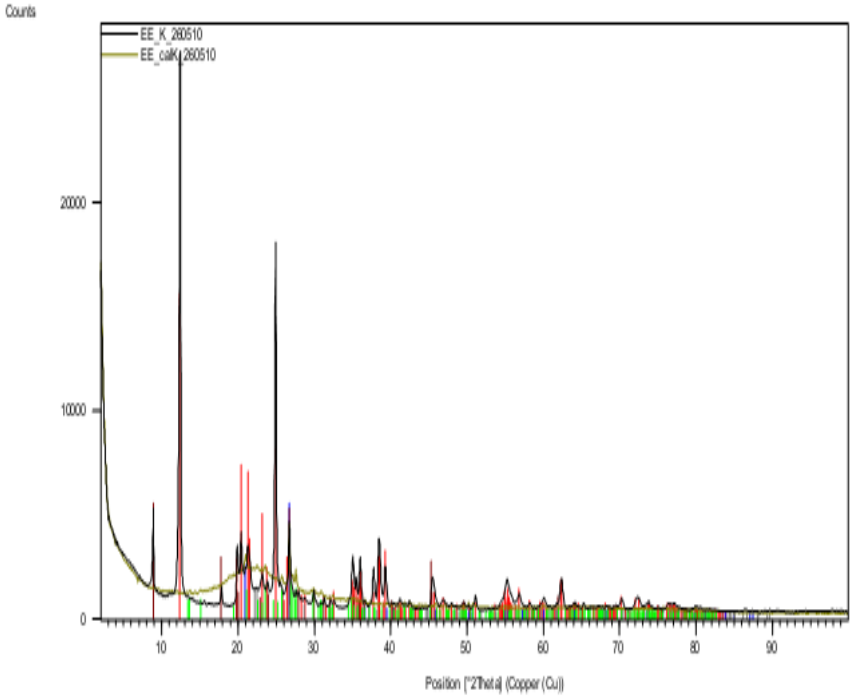
Counts
EE_K_260510
EE_calK_260510
20000
10000
0
10
20
30
40
50
60
70
80
90
Position [°2Theta] (Copper (Cu))

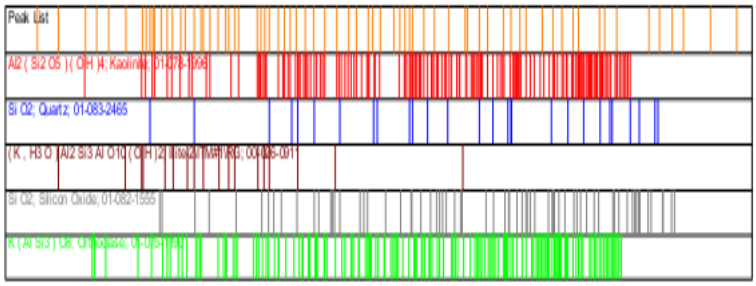
Peak List
Al2 (Si2 O5) (OH)4; Kaolinite; 01-078-1996
Si O2; Quartz; 01-083-2465
Si O2; Silicon Oxide; 01-082-1555

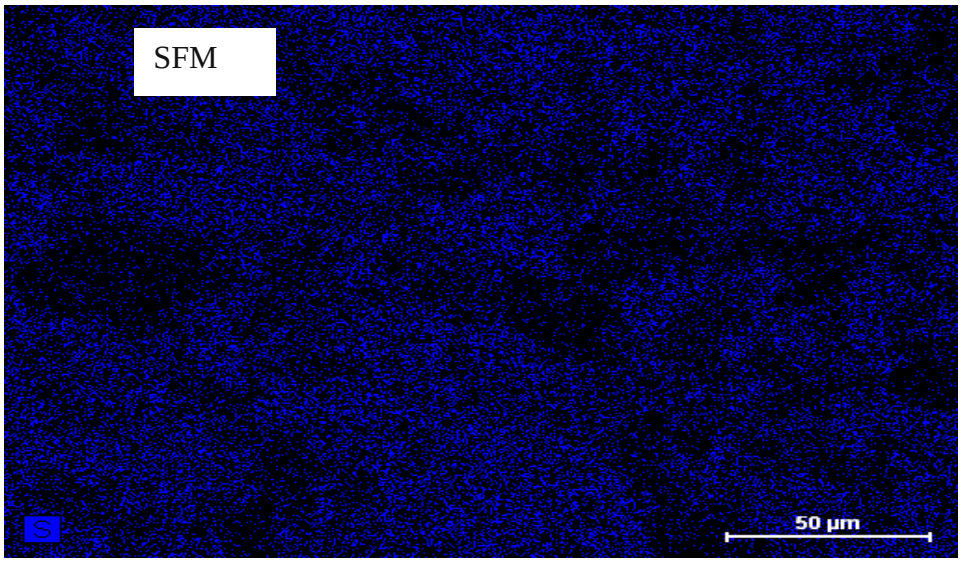

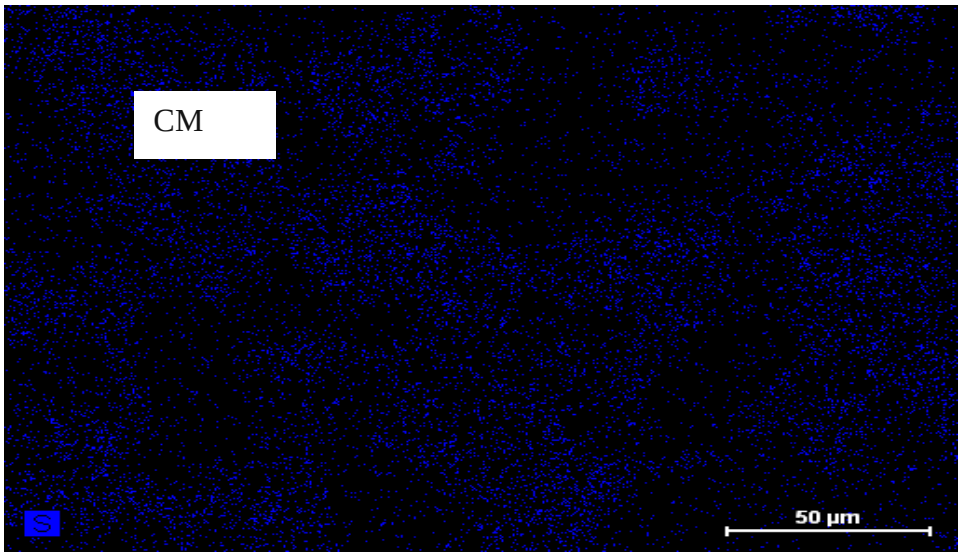

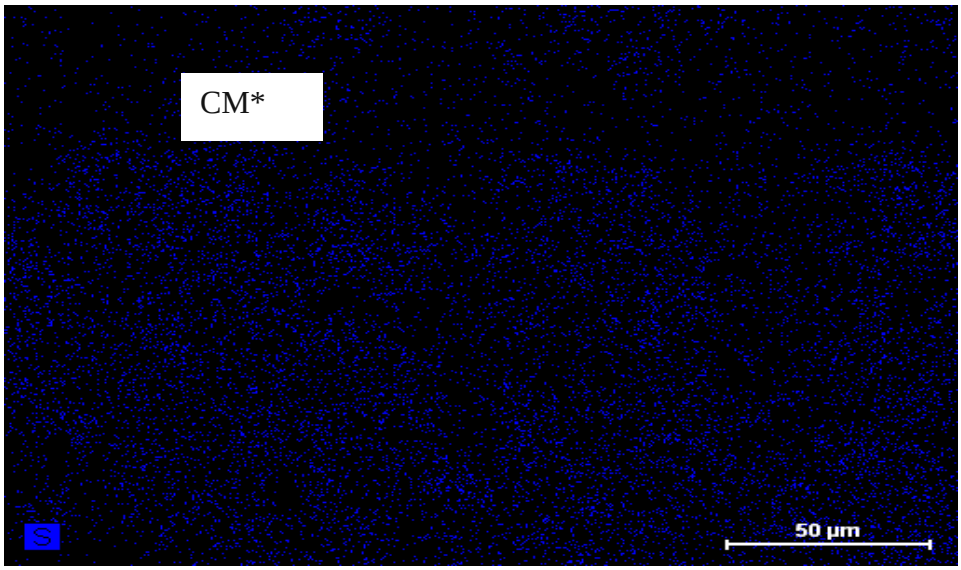

The Spotted Blue on the Maps is the Indication of the Presence of Sulphur Distribution on the Catalysts

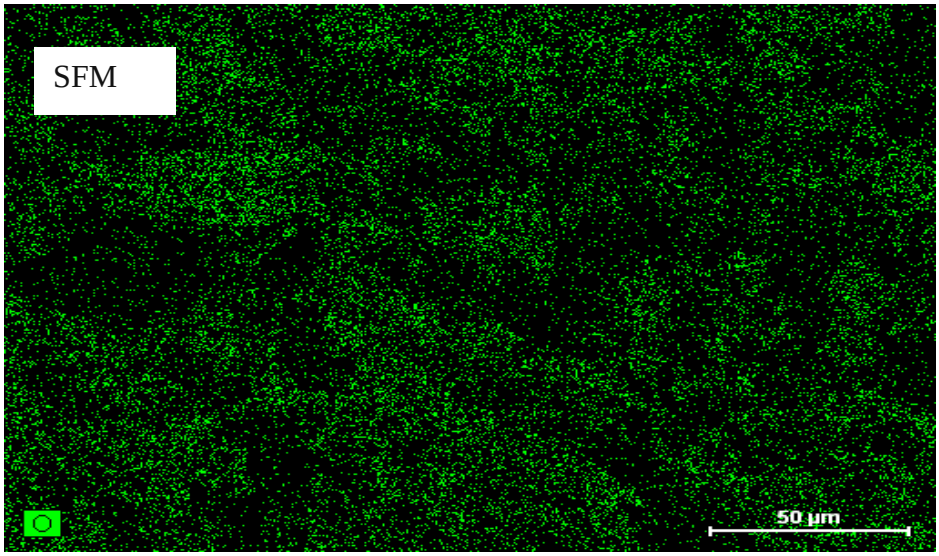

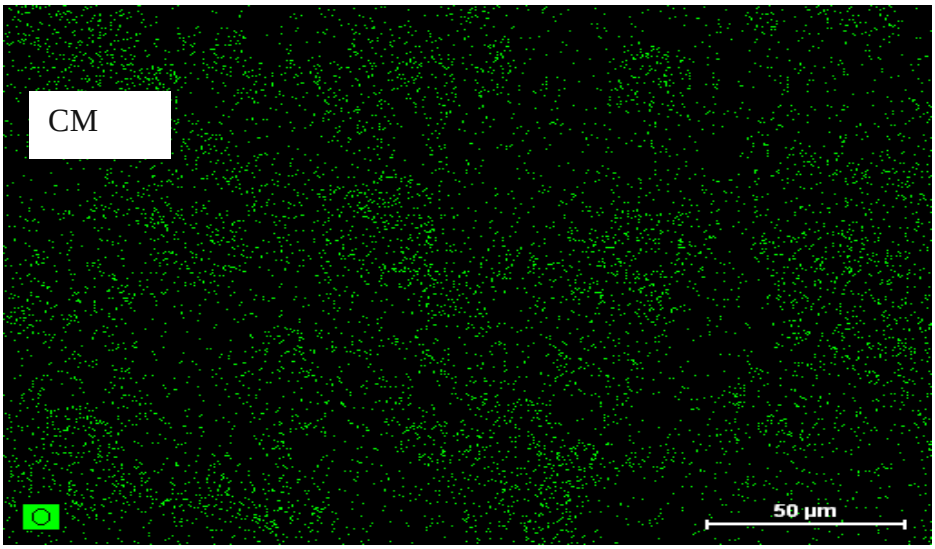

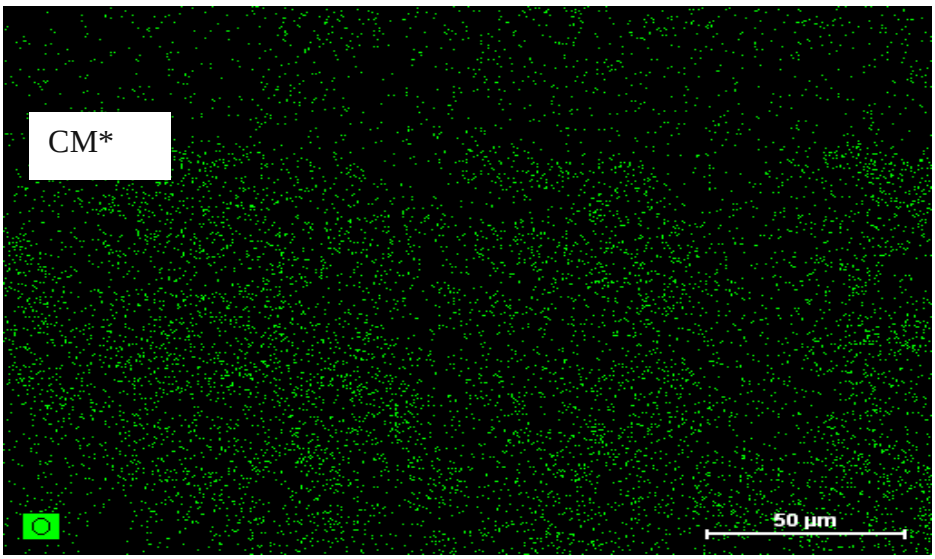

The Spotted Green on the Maps is the Indication of the Presence of Oxygen Distribution on the Catalysts

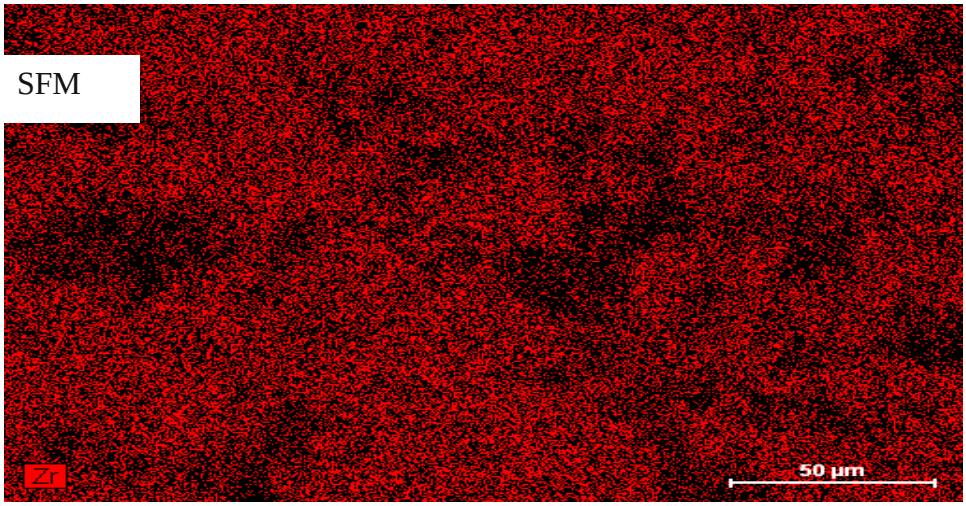

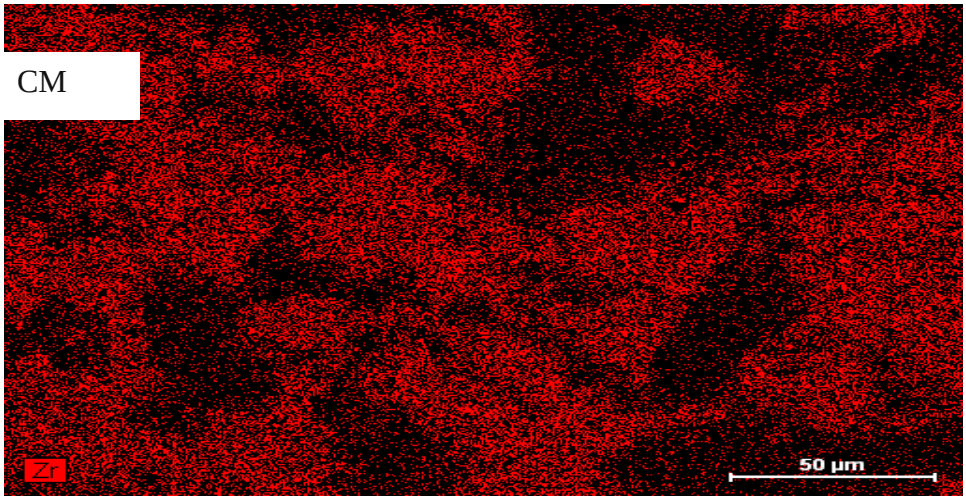

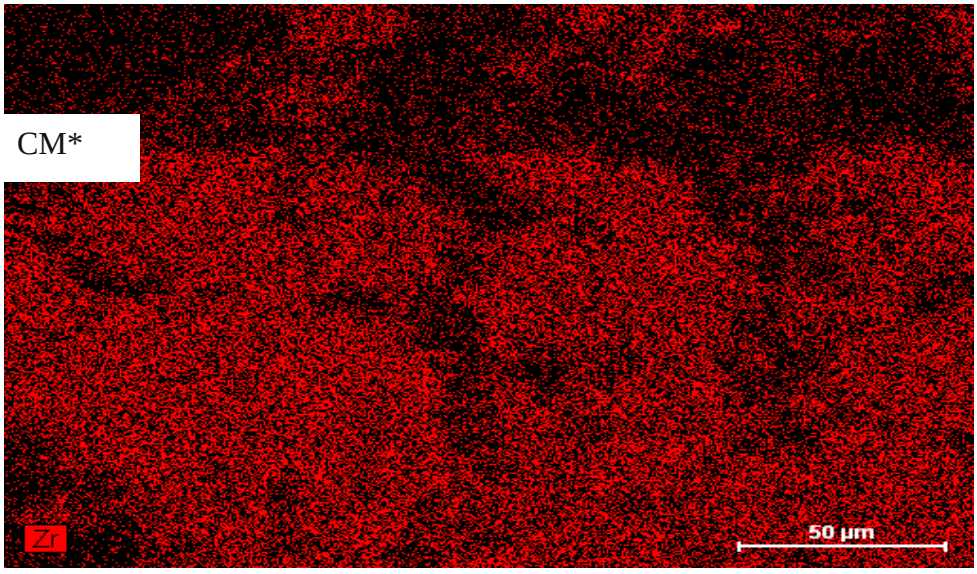

The Spotted Red on the Maps is the Indication of the Presence of Zirconia Distribution on the Catalysts

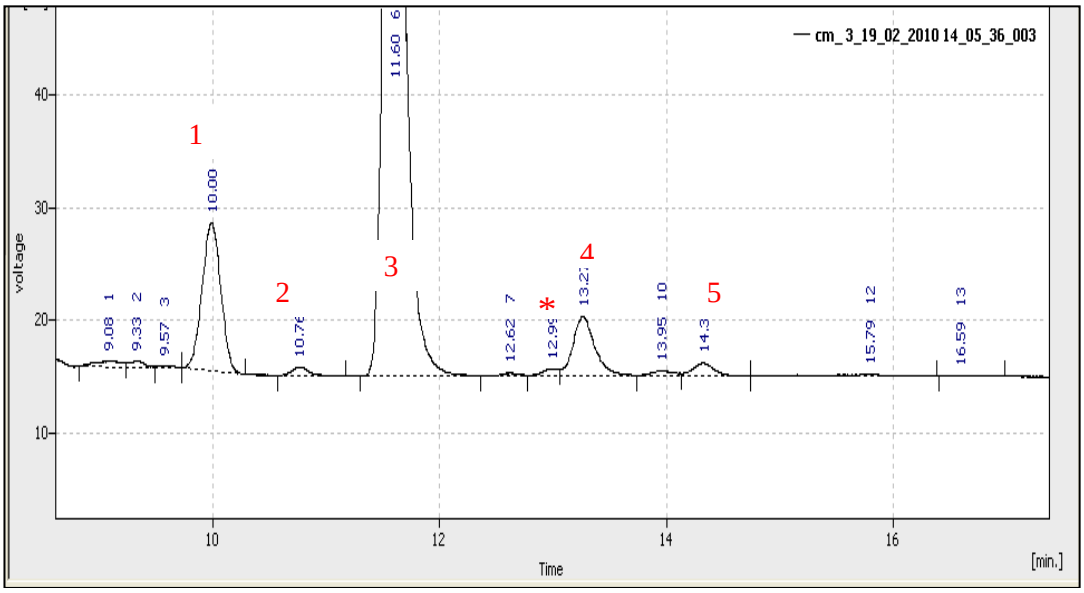

A Typical GC Trace from the Ester Analysis of the Product Mixture using Conventional Catalyst

The 1st peak is methyl myristate, 2nd peak methyl palmitate, 3rd peak methyl heptadecanoate, * peak methyl stearate, 4th peak methyl oleate, and 5th peak methyl linoleate.

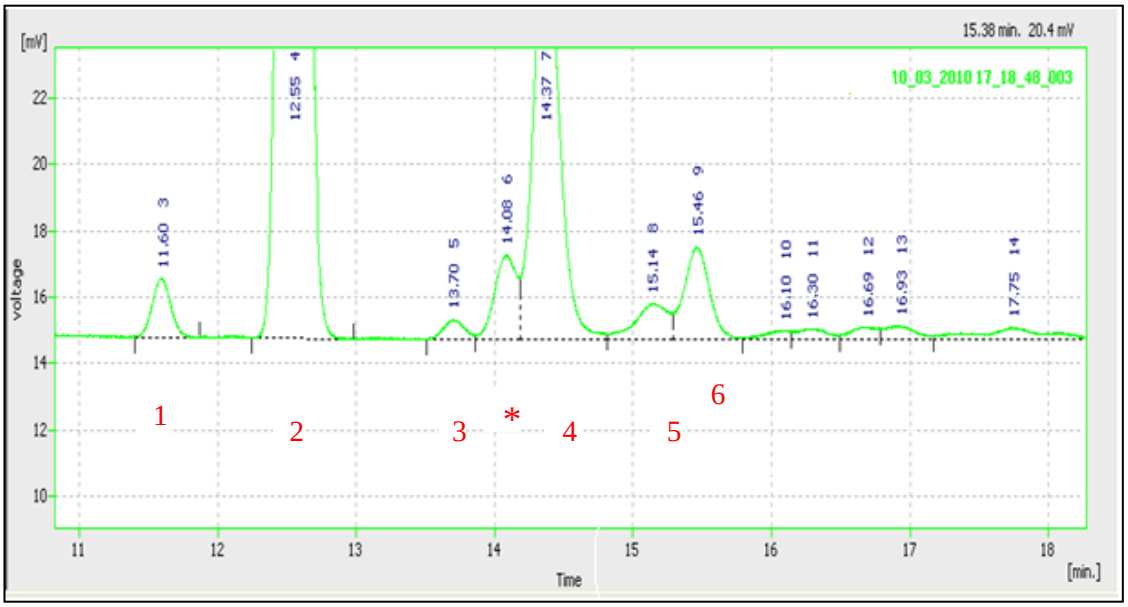

A Typical GC Trace in the Ester Analysis of the Product Mixture using Solvent-free Catalyst

The 1st peak is methyl palmitate, 2nd peak methyl heptadecanoate, 3rd peak methyl stearate, 4th peak methyl oleate (* peak trans-oleate), 5th peak methyl linoleate and 6th peak methyl linolenate

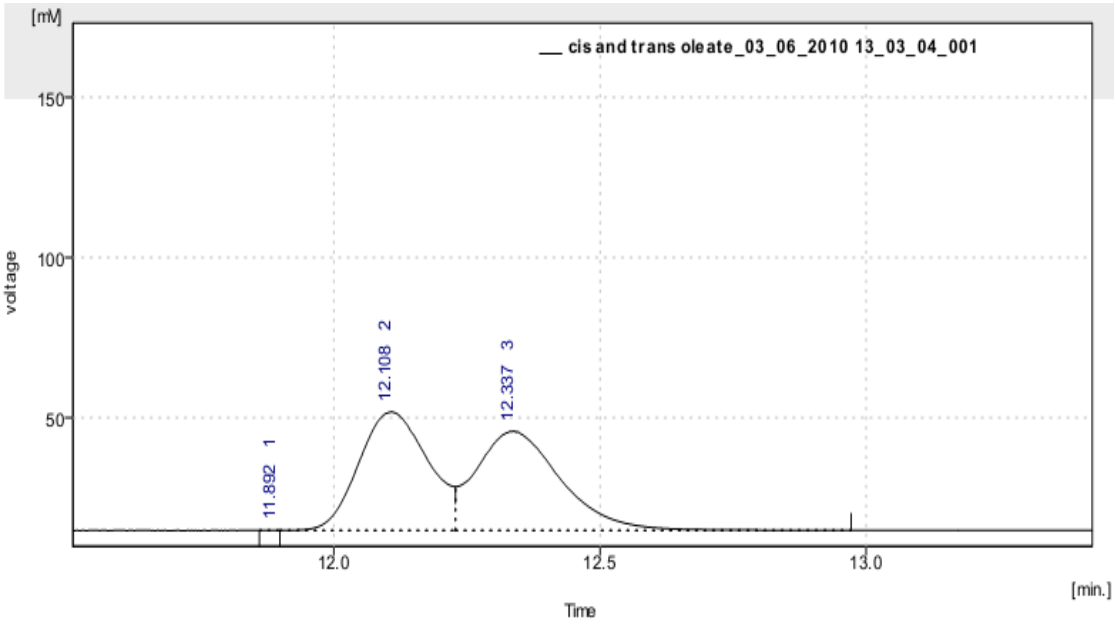

The Gas Chromatogram of Standard Methyl Oleate for the Determination of Trans and Cis Methyl Oleate in the Sample Mixture

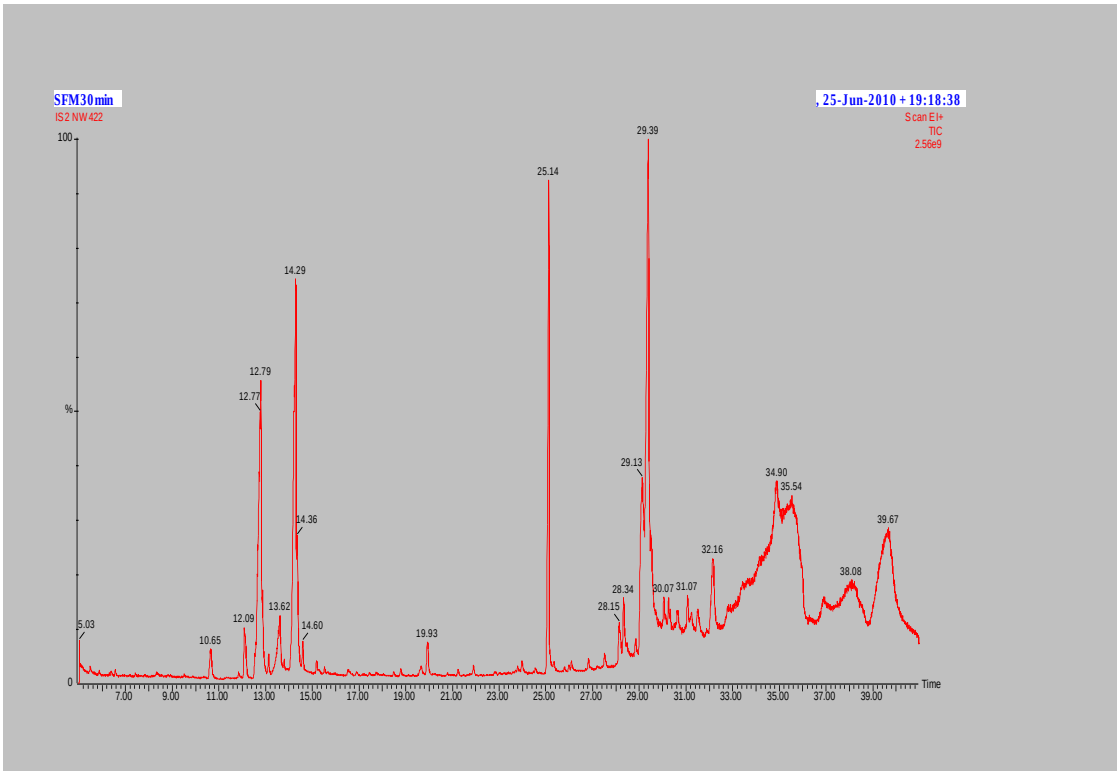

A Typical GC Chromatogram of the Product Mixture from GC-MS Analysis revealing the various compounds in the sample

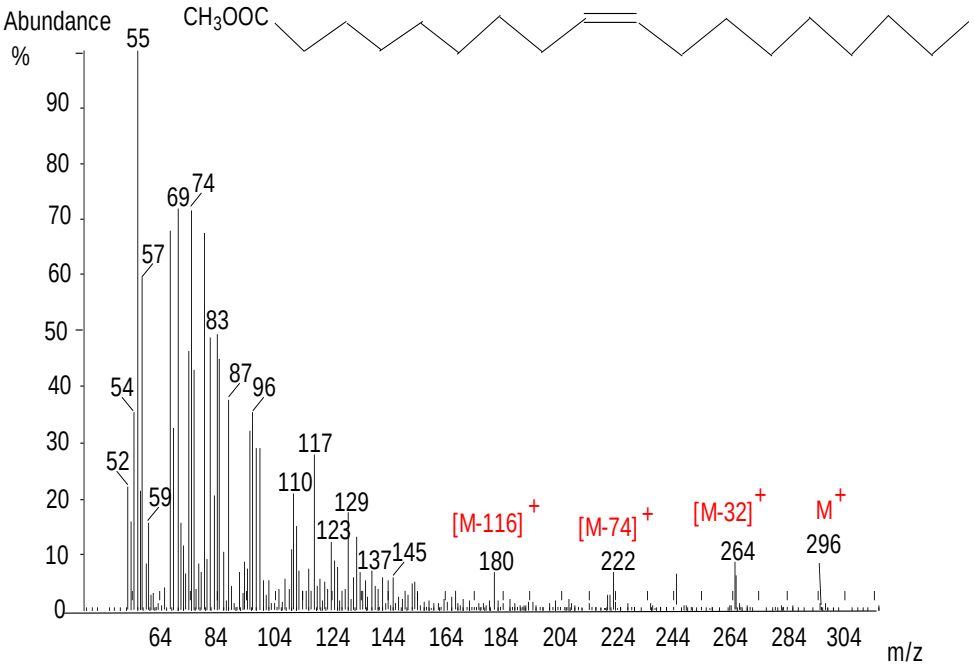

Mass Spectrum of Methyl Ester from the GC-MS

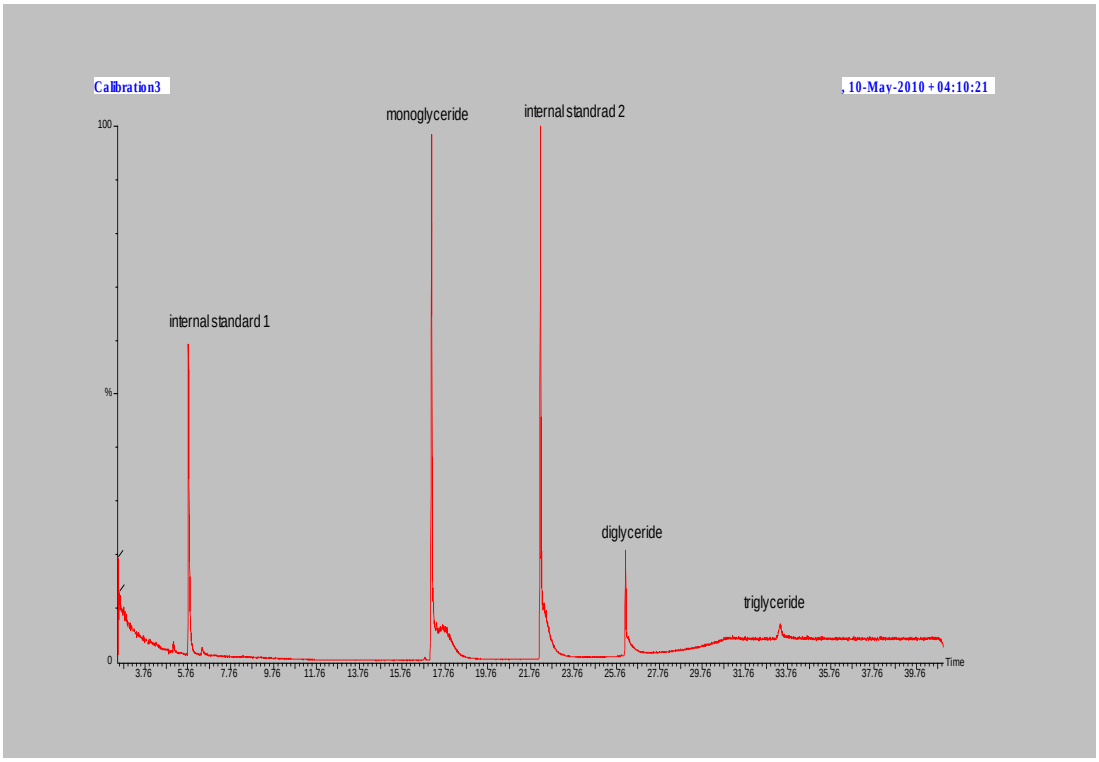

A GC Chromatogram for Reference Glycerides Analysis from GC-MS used for calibration

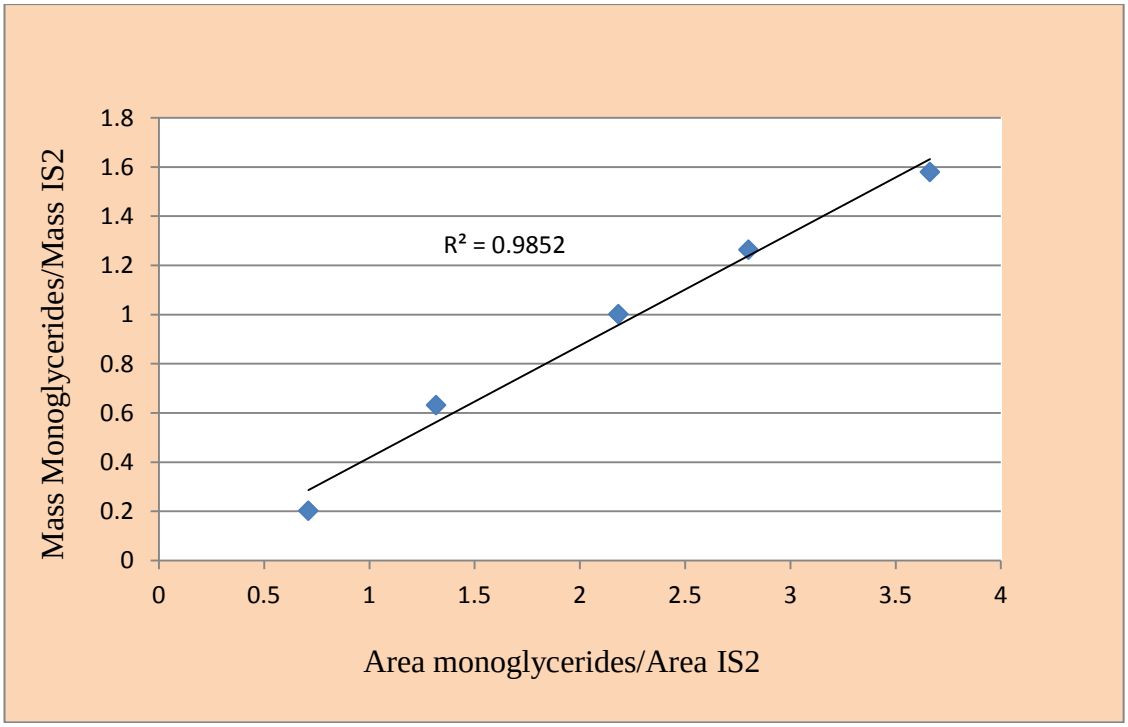

Calibration Curve for Monoglyceride from the Reference samples for GC-MS Analysis

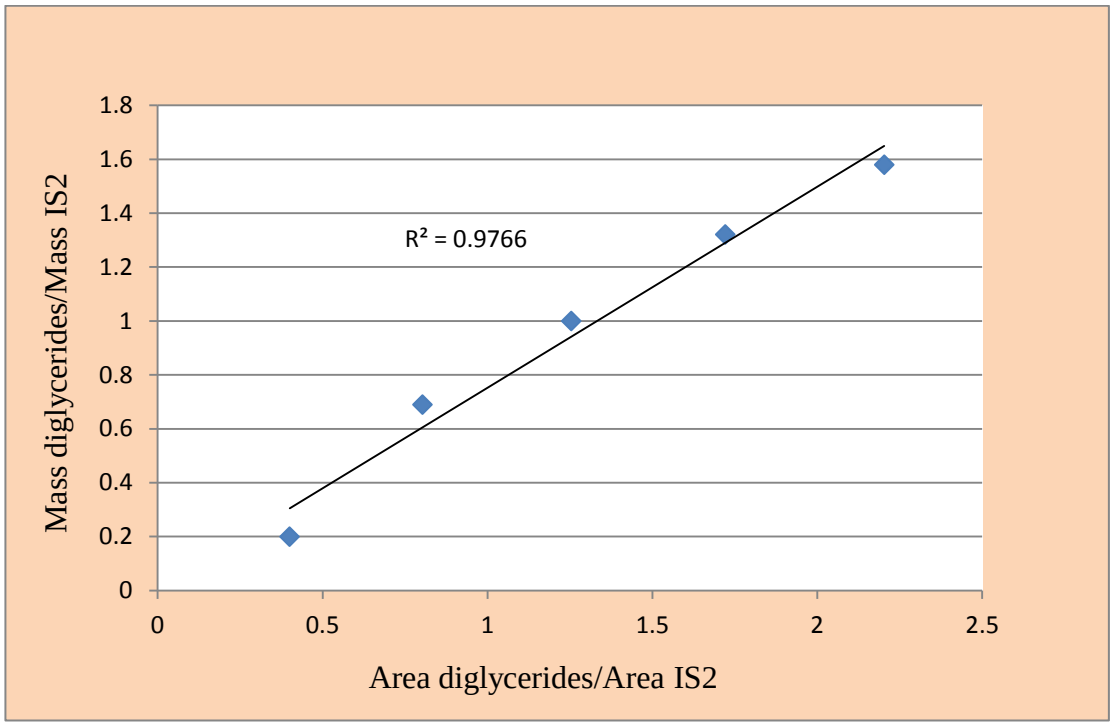

Calibration Curve for Diglyceride from the Reference samples for GC-MS Analysis

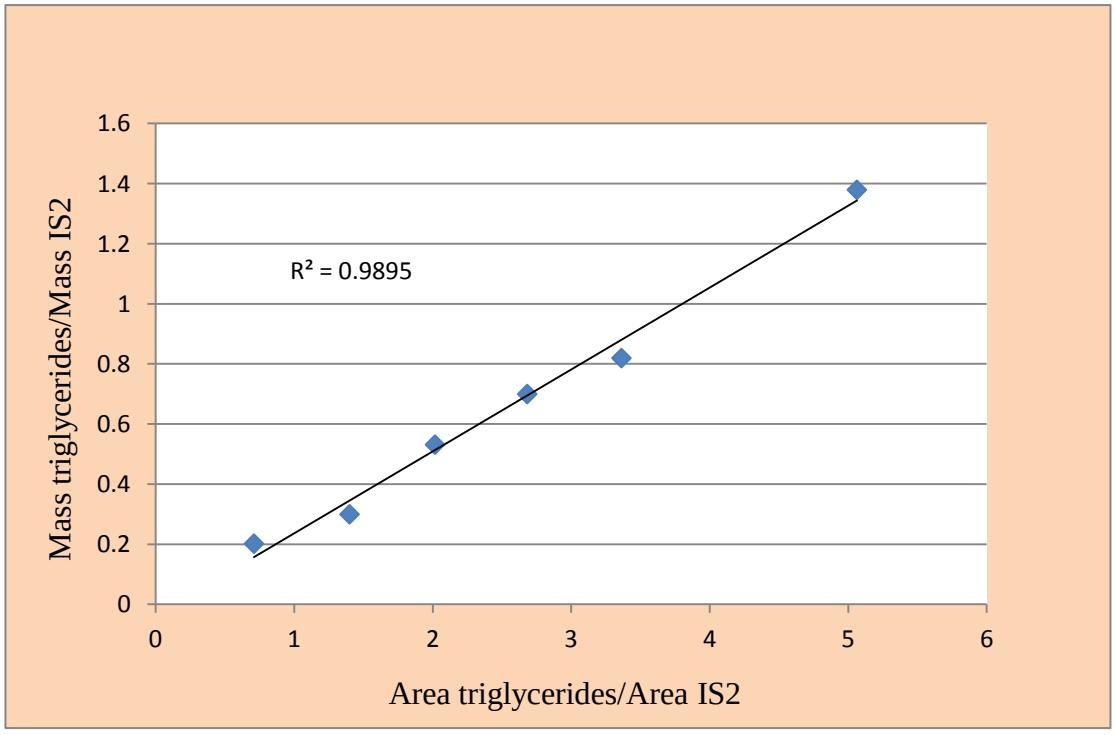

Calibration Curve for Triglyceride from the Reference samples for GC-MS Analysis

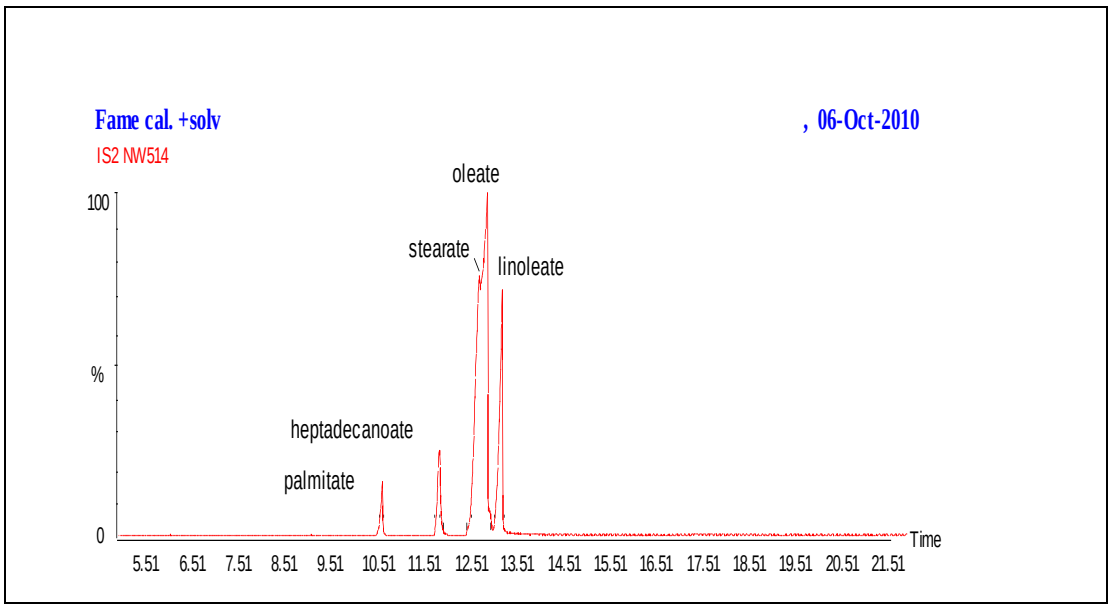

GC Chromatogram for Standard Methyl Esters Analysis from GC-MS used for the Calibration of Methyl Esters in the Sample

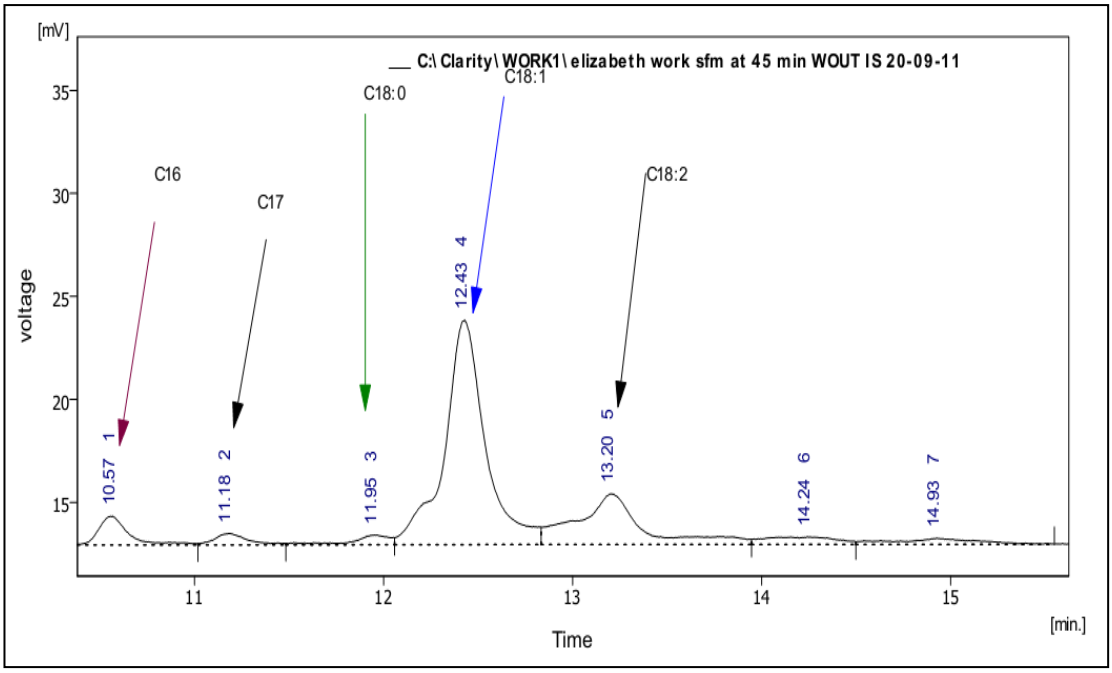

GC Chromatogram of Sample from the thermocracking analysed without Internal Standard, C_{17} (methyl heptadecanoate) but the chromatogram indicated the presence of methyl heptadecanoate (C_{17})

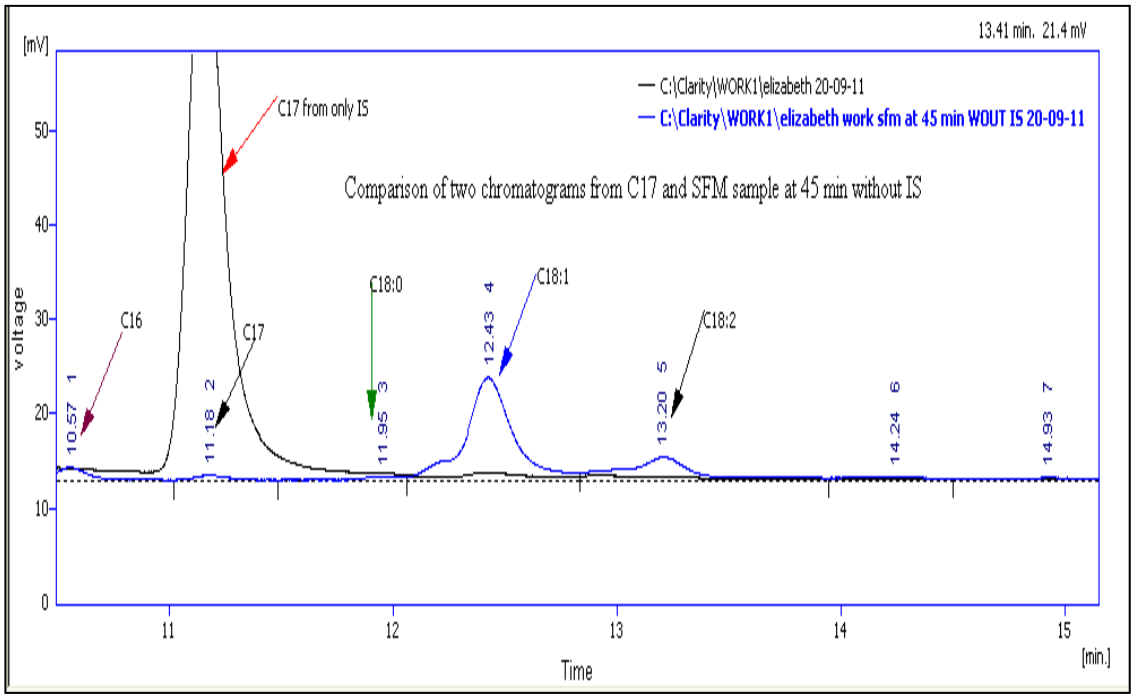

Comparing the GC Chromatograms of Internal Standard and Sample without Internal Standard for the Confirming of the C17 Peak